SYNTHESIS OF MESOPOROUS SILICA PARTICLES BY CONTROLLING THE CTABr-PLURONIC ASSEMBLY

A THESIS

SUBMITTED TO THE DEPARTMENT OF CHEMISTRY

AND THE INSTITUTE OF ENGINEERING AND SCIENCES

OF BİLKENT UNIVERSITY

IN PARTIAL FULFILLMENT OF THE REQUIREMENTS

FOR THE DEGREE OF

MASTER OF SCIENCE

By

ALTUĞ SÜLEYMAN POYRAZ

July 2009

I certify that I have read this thesis and that in my opinion is it is fully adequate, in scope and quality, as a thesis of the degree of Master in Science

……..

Prof. Dr. Ömer Dağ (Supervisor)

I certify that I have read this thesis and that in my opinion is it is fully adequate, in scope and quality, as a thesis of the degree of Master in Science

……..

Prof. Dr. Şefik Süzer

I certify that I have read this thesis and that in my opinion is it is fully adequate, in scope and quality, as a thesis of the degree of Master in Science

……..

Assoc. Prof. Dr. Margarita Kantcheva

I certify that I have read this thesis and that in my opinion is it is fully adequate, in scope and quality, as a thesis of the degree of Master in Science

……..

Assoc. Prof. Dr. Ayşen Yılmaz

I certify that I have read this thesis and that in my opinion is it is fully adequate, in scope and quality, as a thesis of the degree of Master in Science

……..

Assist. Prof. Dr. Emrah Özensoy

Approved for the Institute of Engineering and Sciences

……..

Prof. Dr. Mehmet Baray

Director of Institute of Engineering and Science

ABSTRACT

SYNTHESIS OF MESOPOROUS SILICA PARTICLES BY CONTROLLING THE CTABr-PLURONIC ASSEMBLY

ALTUĞ SÜLEYMAN POYRAZ

M.S. in Chemistry

Supervisor: Prof. Dr. Ömer Dağ

July, 2009

In the synthesis of mesoporous silica materials, self-assembly of a charged surfactant (cetyltrimethylammoniumbromide, CTABr) and a pluronic (PEO_x-PPO_y-PEO_x where PEO is CH_2CH_2O and PPO is $CH(CH_3)CH_2O$) into micelles have key. By controlling the hydrophilic-hydrophobic character of the CTABr-Pluronic micelles, mesoporous silica particles can be synthesized with different morphologies (sphere, wormlike, crystal-like etc.). The particles generally have 2D hexagonal mesostructure with a high surface area (as high as 800 m^2/g). Shape of the micelles as well as the morphology of the particles depend on the hydrophobic nature of the pluronic surfactant and the CTABr amount. The CTABr amount is carefully adjusted to control the morphology and structural order of the particles. The self-assembly of the CTABr-Pluronic micelles and silica species

has been achieved by adjusting pH of the synthesis medium to 1.0 in order to produce mesoporous particles with a distinct morphology and mesostructure.

Nature of the CTABr-Pluronic micelles can be influenced by adding organic and inorganic additives to the reaction media. The effect of the lyotropic (F^-, SO_4^{2-} and Cl^- etc.) and hydrotropic (NO_3^-, SCN^- etc.) anions on the micellization of P85 has been first investigated in the aquoues media using UV-Vis Spectroscopy and ethyl orange dye. Then these inorganics and organic (Benzene) additives, in the synthesis of mesoporous silica, have been used to control the micellization of the CTABr-P123 couples as well as the morphology and the pore structure of the silica particles. Highly ordered particles with larger pores and various pore structures have been synthesized using lyotropic anions in the CTABr-P123 system. Furthermore, the hydrotropic anions control the CTABr content of the CTABr-P123 micelles. Increasing CTABr amount in the CTABr-P123 micelles decreases the wall thickness of the silica particles. The hydrophobic character of the micelles can also be enhanced by adding water insoluble organic additives (benzene). The silica particles, synthesized using CTABr-P123-Benzene system, are well structured, where the higher order X-ray diffraction lines can also be observed.

Finally, the catalytic role of F^- ions on the polymerization of the silica has been studied in the CTABr-Pluronic system. Addition of F^- ion to the reaction medium speeds up the formation process and producing spherical and uniform mesoporous particles less than 20 minutes. The effect of each of the reaction component, F^- ion, CTABr and P123 molecules, to the assembly rate has also been investigated by determining the turbidity

point (due to the formation of silica particles) of the solutions. A correlation between the particle size and reaction rate has also been brought out.

The mesoporous silica particles synthesized in this thesis have been characterized using PXRD, FT-IR and Raman Spectroscopy, SEM, TEM and N_2 sorption measurements.

Keywords: Mesoporous Silica Particles, Micellization, Pluronic, CTABr, Hydrotropic, Lyotropic, Morphology, Spherical Particles, Wormlike particles Crystallike Particles.

ÖZET

CTABr-PLURONİC SİSTEMİNİN KONTROLÜYLE MEZOGÖZENEKLİ SİLİKA PARÇACIKLARININ SENTEZLENMESİ

ALTUĞ SÜLEYMAN POYRAZ

Kimya Yüksek Lisans Tezi

Danışman: Prof. Dr. Ömer Dağ

Temmuz, 2009

Mezogözenekli silika parçacıkların sentezlenmesinde iyonik yüzeyaktif (Cetyltrimethylammoniumbromide, CTABr) ve pluronic (PEO_x-PPO_y-PEO_x PEO CH_2CH_2O ve PPO $CH(CH_3)CH_2O$ dur) tipi yüzeyaktiflerin birlikte misel oluşturmaları önemli bir rol oynar. Oluşan CTABr-Pluronic miselrinin hidrofilik-hidrofobik karakterinin kontrol edilmesiyle çeşitli morfolojilerde mezogözenekli silika parçacıklar sentezlenebilir (küresel, solucanımsı, kristalimsi vb.). Bu parçacıklar genelde 2B (iki boyutlu) altıgen mezoyapıda olup çok yüksek yüzey alanlarına sahip olabilirler (800 m^2/g a kadar). Oluşan miselrin şekilleri ve dolayısıyla oluşan parçacıkların morfolojileri pluronic yüzeyaktiflerin hidrofobik doğasına ve miselrdeki CTABr yüzeyaktiflerinin miktarına bağlıdır. Parçacıkların morfoloji ve yapısal düzenliliklerini kontrol etmek için misellerdeki CTABr

miktarı dikkatlice ayarlandı. Belirli morfolojilerde ve mezodüzenlilikte silika parçacıklar elde etmek için CTABr-Pluronic miselrinin silika parçacıklarıyla kendi kendine biraraya gelmesi sentez pH değerinin 1.0 a ayarlanmasıyla gerçekleştirildi.

CTABr-Pluronic miselrinin doğası bazı anorganik tuzlar ve organik moleküllerin tepkime ortamına eklenmesiyle etkilenebilir. P85 yüzeyaktifinin miselşmesine lyotropic (F^-, SO_4^{2-} ve Cl^- vb.) ve hydrotropic (NO_3^-, SCN^- vb.) anyonlarının etkisi UV-Vis Spektroskopi ve Ethyl Orange indikatörü kullanılarak incelenmiştir. Daha sonra bu anorganik tuzlar ve organik moleküller mezogözenekli silika parçacık sentezinde kullanılarak CTABr-P123 ikilisi miselri kontrol edilerek silika parçacıkların morfolojileri ve gözenek yapıları kontrol edilmiştir. Lyotropic anyonlarının kullanılmasıyla CTABr-P123 sisteminde yüksek düzenlilikte ve daha büyük gözenekli silika parçacıklar sentezlenmiştir. Ayrıca hydrotropic anyonların CTABr-P123 miselrindeki CTABr miktarını arttırdığı tespit edilmiştir. Miseldeki CTABr miktarının arttırılmasıyla sentezlenen malzemedeki gözenekler arası duvar kalınlığının düştüğü gözlenmiştir. Miselin hidrofobik karakteri suda çözünmeyen organik moleküllerin (benzen) sentez ortamına eklenmesiyle de kontrol edilebilir. Organik moleküllerin kulanılmasıyla oluşturulan mezogözenekli silika parçacıkların oldukça düzenli olduğuna x-ışını kırınım desenlerinde gözlenen yüksek düzenli düzlemlere ait kırılımların gözlenmesiyle karar verilmiştir.

Son olarak, F^- iyonunun silika polimerleşmesindeki katalitik rolü CTABr-P123 sistemi kullanılarak çalışılmıştır. F^- iyonunun eklenmesi parçacık oluşumunu hızlandırarak aynı boyutlarda ve küresel mezogözenekli silika parçacıkların 20 dakika gibi kısa bir sürede sentezlenmesini sağlamıştır. Ayrıca her bileşen miktarının (CTABr, P123 ve F^-

iyonu) parçacık oluşma hızına etkisi, bulanıklaşma zamanları belirlenerek gösterilmiştir. Bu ölçümler sonucunda oluşan parçacıkların boyutlarıyla bulanıklaşma değerleri arasındaki ilişki tespit edilmiştir.

Sentezlenen mezogözenekli silika parçacıkların karakterizasyonu X-Işını Kırınım, FT-IR ve Raman Spektroskopisi, SEM ve TEM görüntüleme ve N_2 sorpsiyon teknikleriyle gerçekleştirilmiştir.

Anahtar Kelimeler: Mezogözenekli Silika Parçacıklar, Miselşme, Pluronic, CTABr, Hidrotropik, Liyotropik, Morfoloji, Küresel Parçacıklar, Solucanımsı Parçacıklar, Kristalimsi Parçacıklar.

ACKNOWLEDGEMENTS

At the end of my long educational life in Bilkent University, I would espress my deepest thankfulness to Prof. Ömer Dağ for his supervison and guidence through my scientific studies and discussions in scientific ethics for last four years. During these short four years, I have learned a lot about chemistry and patience in scientific work from him.

I would thank to previous and current Dağ's group members; Faik Demirörs, Yaşar Akdoğan, Yurdanur Türker and special thanks to Cemal Albayrak, Halil Ibrahim Okur and my eccentric friend Mustafa Sayın.

I will always remember my friends Ahmet Keleş, Pınar Cönger, İlknur Tunç, Fahri Alkan, Hacı Osman Güvenç, Alper Kılıklı in Bilkent University.

I would also thank to Emre Tanır for his help in TEM images and TUBITAK for financial support during my master degree.

Finally, I would thank to my family for their endless moral and financial support during my past and future education life .

TABLE OF CONTENTS

LIST OF TABLES

LIST OF FIGURES

1. Introduction

1.1. Mesoporous Silica Particles

The synthesis of first ordered mesoporous silica particles by the Mobil Company in 1992 has opened new and highly promising research area for scientists in almost all fields of Chemistry [1]. During 17 years, first efforts were on synthesizing different mesostructured materials with various mesophases, morphology and pore structure. On the other hand, in recent years, the efforts have turned into investigation for possible applications in different areas and understanding the formation mechanism of these materials. This 17 years of work can be classified under three main subgroup, see **Scheme 1.1**.

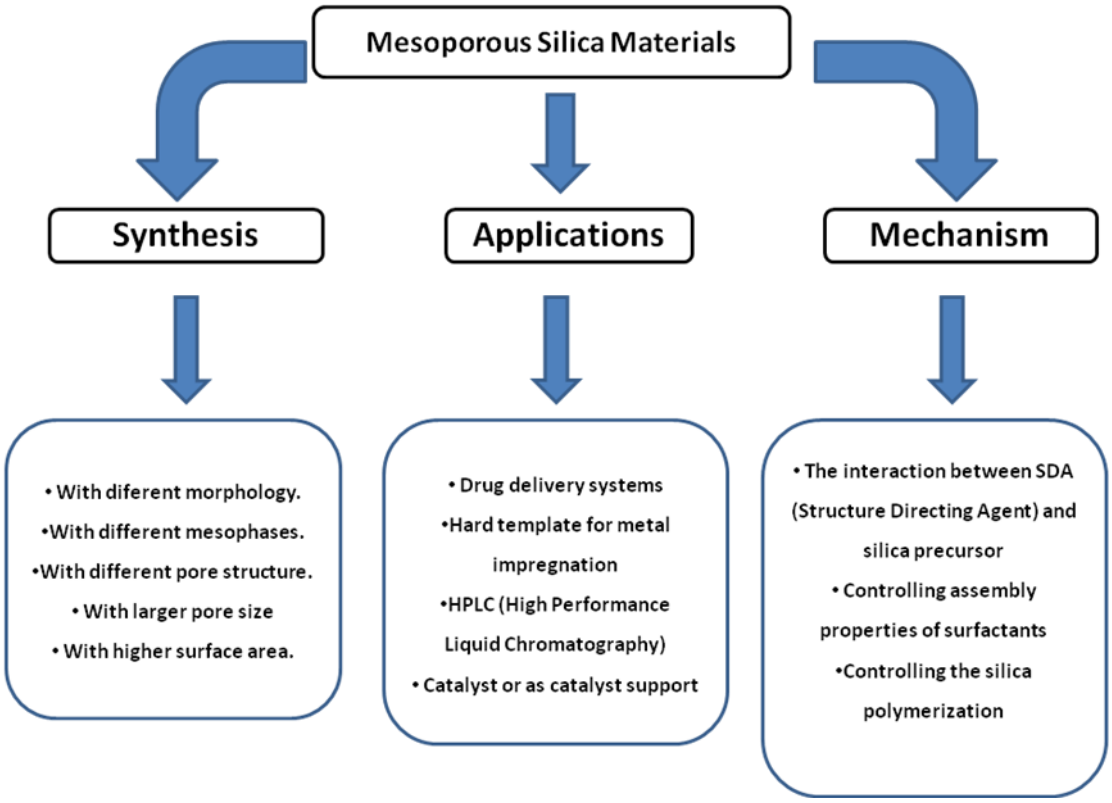

Scheme 1.1: The summary of work in synthesizing mesoporous silica particles in last 17 years.

1.1.1. Historical Background of Mesoporous Silica Particles

The development of first mesoporous silica particles, which are named as MCM (Mobil Crystalline Material) [1,2] , evoked a remarkeble interest about these newly developed materials. The different mesostructured versions of these materials were named as MCM-41 (hexagonal), MCM-48 (cubic) and MCM-50 (lamellar) [3]. The MSU-X (Michigan State University) and SBA (Santa Barbara) are the other two famous classes of these materials [2]. Ordered mesoporous silica particles have been synthesized in various morphologies, such as spheres [4,5], crystal like [6,7], wormlike [8,5], ropelike [8-10], hollow spheres [11], gyroid [8,9] and toroids etc. [8,12]. The morphology, monodispersity and pore structure are the three important parameters in many possible applications, like drug delivery systems, photonic crystals, chromatography and catalysis [4,9,13-17]. The essential step, in the formation of all these mesoporous particles, is the surfactant aggregation into the micelles. That is why this field is also so called as the micelle templated structures (MTS) [11]. The structure directing agents, so called surfactants, can be classified in two main groups. The first type is charged surfactants and the other one is neutral surfactants. Table 1 illustrates some of the most common surfactants used in the synthesis of mesostructured materials. Tergitol [11,14, 18], Triton [2] and TCI [7] are the other famous surfactants, which are also widely used in the synthesis of mesoporous silica particles. The obtained mesostructures depend on the surfactant type, modification of the reaction conditions, inorganic additives and usage of cosolvent [6,19-22]. The above mentioned factors cause a drastic change in the assembly and micellization properties of the surfactants.

Ionic Surfactants	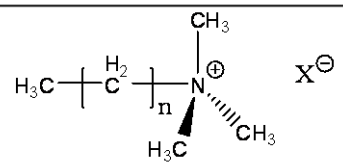	CnTAX
		CTABr, CTACl
	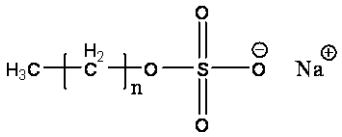	SDS
Nonionic Surfactants	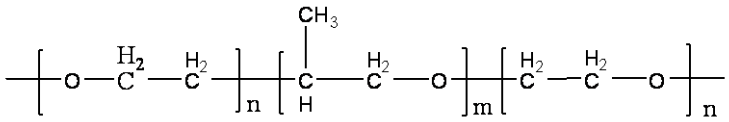	Pluronic ®
		P123, F127, L64, P85 etc.
	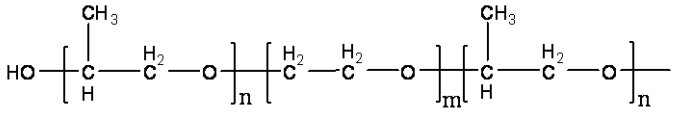	Pluronic® R
		Pluronic 25R5, Pluronic 17R2 etc.
	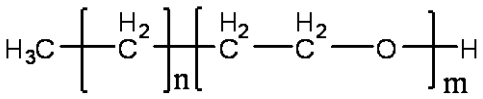	Brij
		Brij 56,
	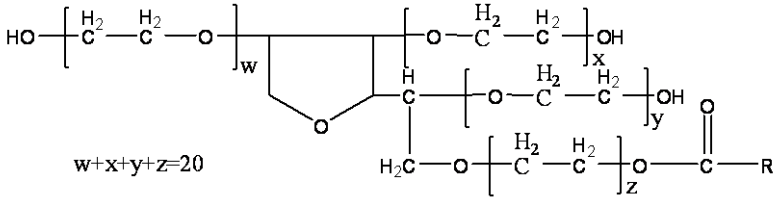	Tween
		Tween 20

Table 1.1: Classical commercial surfactants.

1.1.2. The Pore Structure:

Pore structure of these materials is another important property, which is widely investigated. This is, because, it determines suitablity of the materials in many applications, such as controlled drug release, nano-wire production, synthesis of nano-sized metal oxide, surface modification and HPLC (High Performance Liquid Chromatography) [17,23-28] etc. For the mesoporous silica particles, N_2 adsorption is the most widely used technique for determination of the mesopore properties [29-32]. The other adsorbates, used in characterization of mesopores are argon, krypton,

xenon, oxygen and carbon dioxide (for porous organic molecules) [29,33]. However, N_2 is the most common adsorbate among others for the surface area determination of the silica particles. For surface area calculations the BET (Brunauer-Emmett-Teller) equation is widely employed [34-37]. This equation is quite aplicable for silica surfaces, since the adsorption of N_2 on silica surfaces is highly energetic (exothermic) and usage of the BET equation, which ignores adsorbate-adsorbate interaction, does not bring a significant error [29]. The only encountered problem with the BET equation is the calculation of the surface area of mesoporous materials having fair amount of micropores together with mesopores. The existance and volume of the micropores can be determined from the N_2 adsorption isotherm by simply drawing a t-plot and α-plot by using FHH (Frenkel-Halsey Hill) and Harkins-Jura equations [29,34,38-42]. The t-plot should pass throug the origin, any upward deviation indicates existence of mesopores, any downward deviation indicates the existence of micropores and a downward followed by an upward deviation indicates the existance of both micro- and mesopores together [34,38,39,40,41,42] (see **Figure 1.1**). The mesoporous materials typically have type IV isotherm with a hysteresis. Note also that the mesoporous silica particles, with smaller pore size, corresponding to small P/P_o do not show any hysteresis [29,37]. The hysteresis of an isotherm of mesoporous material generally gives information about the pore structure and can be classified in four groups [29]. The average pore size is an another important parameter that can generally be obtained by using BJH (Barrett, Joyner and Halenda) theorem for both adsorption and desorption isotherms of the mesoporous silica particles [29,34,40].

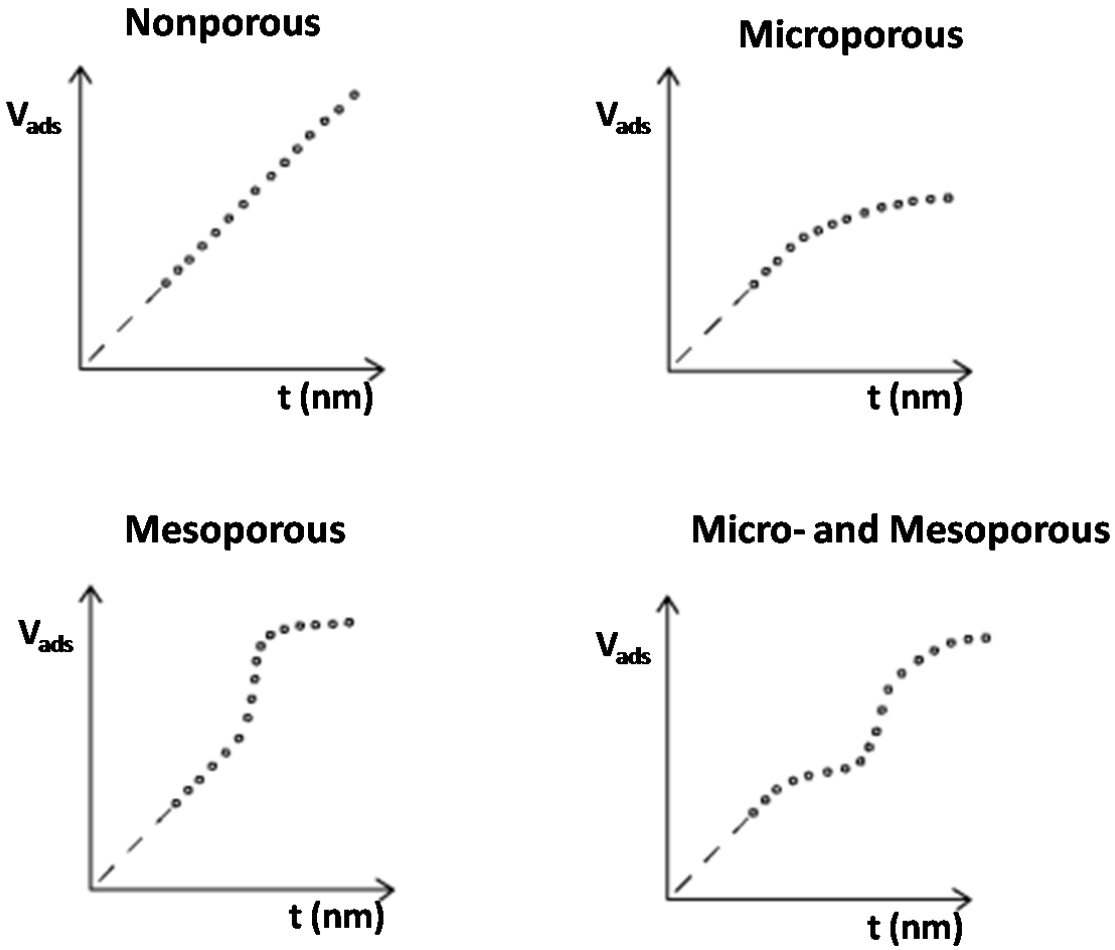

Figure 1.1: The t-plots of nonporous, microporous, mesoporous and micro-mesoporous materials.

The N_2 adsorption measurement has been widely used in determining the pore structure, surface area, pore diameter and wall thickness of mesoporous silica particles. **Table 1.2** summarizes nitrogen adsorption measurements of some common mesoporous silica particles[2,4,13,14,18,43-46]. One obvious result could be deduced from the **Table 1.2** is the wall thickness and pore size differences between the particles synthesized using cationic surfactant (MCM type) and the one synthesized by non-ionic surfactants. The higher surface area for the MCM type materials could be attributed to thinner wall when compared to the ones synthesizd by non-ionic

surfactants. In spite of the fact that the thicker wall causes a decrease in surface area per gram, however the thicker wall serves termal and physical stablity to mesoporous materials [30]. It is generally beleived that repulsive interaction between the PEO (poly (ethyleneoxide)) chains (forms the corona of a micelle) is the reason of the thicker wall formation [47,48]. Almost all of the non-ionic surfactants have poly (ethylene oxide) group as the hydrophilic side [49]. The existance of PEO groups is also important for the micropore formation. Because the hydrated PEO float freely in water and are covered by monomeric silica particles in solution [30,31,35,38]. Consequently, the resulting mesoporous material might also contain the micropores. This situation is illustrated in **Figure 1.2**. Notice that the existance of PEO groups not only causes the formation of micropores, but also leads to the formation of interconnecting channels between the two mesopores [47,31,37].

	Surface Area (m^2/g)	**Average Pore Diameter (nm)**	**Wall Thickness (nm)**	**References**
SBA 15	**930 - 600**	**8.5 - 4.5**	**7.0 - 2.0**	**43,44,45**
SBA 16	**1000 - 750**	**7.0 - 5.4**	**5.0 – 7.0**	**44,45**
MCM 41	**1400 - 800**	**3.7 - 1.3**	**~1.0**	**4,13,46**
MSU-X	**1100 - 600**	**5.0 - 2.5**	**1.0 – 2.5**	**2,14,18**

Table 1.2: Typical surface area, pore diameter and wall thickness of common mesoporous materials.

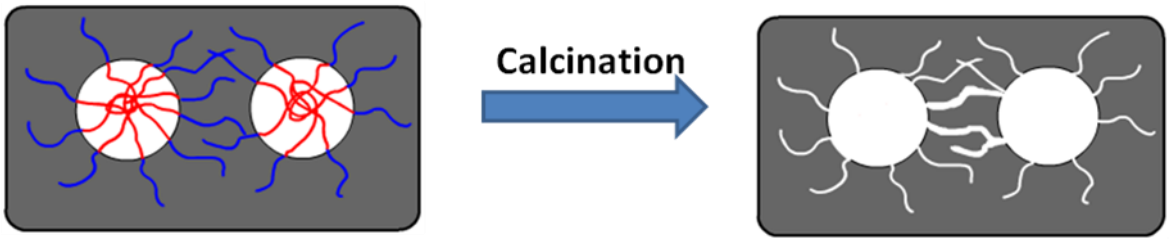

Figure 1.2: Schematic representation of micropore and interconnecting channel formation.

1.1.3. Possible Applications of Mesoporous Silica Materials:

Although the synthesis of mesoporous silica materials is a newly developing field, there has been conducted many investigations regarding possible applications of these materials. Some interesting properties like tunable wall thickness, having different pore systems (micro-meso and meso-macro) in one material and having highly active silanol groups on internal surfaces are the uppermost properties. One of the simplest applications is the use of mesoporous silica materials as hard templates for obtaining nano-sized metals and some metal oxides; because, in solution phase metal ions can easily be inserted into the pore channels and then be converted into metals and metal oxides [23,25,50,51]. There are numerous strategies for the encapsulation of nano-sized metal clusters into the mesopores. Some of the strategies are ion exhange, incipient wetness impregnation, in situ encapsulation, chemical vapor deposition, organmometallic methodologies and surface functionalization by organic molecules [52]. The impregnation of metal ions is very important in order to synthesize metal nanoparticles, that show intresting magnetic, electrical, optical properties and some catalytic activity different from their bulk [24, 49,50, 53-55].

The mesoporous silica has also been investigated for its usage as stationary phase in HPLC (High Performance Liquid Chromatography) [56]. The silica used in traditional chromatography generally have low surface area (less than $500m^2/g$) [26,31,37]. On the other hand, mesoporous silica materials might have a surface area as high as ~1500 m^2/g [31,37]. The morphology of the silica particles is crucial, since packing efficiency is another important parameter to construct a chromatography column [11,26,27,57].

Among all other possible applications, controlled drug delivery systems by using mesoporous materials is the most promising one. The efforts on drug delivery systems can be defined as having a system, which transporsts the desired drug to target part of the body by providing a controlled release. First of all, biodegradable amorphous silica is a perfect candidate for drug delivery systems, since for these systems biodegrability and biocompatibility are the fundamental requirements [28]. Its degredation product is orthosilicic acid and it can be easily eliminated in urine [58]. Experiments done on mices showed that mices can clear orthosilicic acid in couple of weeks [58]. Moreover, mesopores serve a perfect environment for insoluble drugs [28,58].

It is possible to talk about the effect of different properties of mesoporous materials on serving a controlled release individually. The first parameter is the drug loading, it can be easily done by loading in solution or by internal surface modification [28,59,60]. It is not hard to guess that there should be an inverse relation between pore size and drug release rate. However, this is not the only parameter that effects the drug release rate. The order and type of mesostructure is also crucial in drug release rate [60]. For example, For simply calcined samples that are compared

for the drug release rate. the following trend was observed: MCM-41>SBA-15>MCM-48>HMS [28]. The morphology is another parameter which has a remarkable effect in drug release rate. It has been shown that wormlike particles with tubular and wormhole pore structure has a smaller drug release rate than mesoporous silica particles with spherical morphology [17,59]. In addition, it has been also achieved that drug encapsulated mesoporous material which are sensitive to environment about the drug release rate [61].

Despite the above mentioned applications are the most popular ones, they are not the only possibilities. Yano et al. investigated the fabrication of colloidal crystal film from monodispersed mesoporous silica spheres [13,15]. By changing the size of synthesized monodispersed mesoporous silica spheres, it is possible to fabricate colloidal crystal films and artificial opals with different refractive indexes [15,62]. It is also possible to control packing of monodispersed mesoporous silica spheres by using different sedementation methods [16]. So far, face centered cubic (fcc) and hexagonal close packing have been achived by using different sedementation methods [16].

1.2. Mesoporous Silica Particles Based on Pluronic Surfactants.

Among the other surfactants, which are also used as structure directing agents, the pluronic surfactants have a special importance. Because, they are non-toxic, cheap and have excellent aggregation properties [63-65]. These surfactants are triblock co-polymers, with a relatively hydrophobic group poly(propylene oxide) (PPO) at the middle and relativly hydrophilic poly(ethylene oxide) (PEO) head groups at both ends of the polymer (PEO_x-PPO_y-PEO_x) (See **Table 1.1**). These surfactants are commercially available and have various trade names like Poloxamers (ICI) and

Pluronics (BASF) etc. [66,67,68,69,70] in the trade names, where the capital letters L, P and F refers to liquid, paste and flake form of the block co-polymer, respectively [71]. **Table 1.3** shows some of the physical properties of pluronics, which are widely used as structure directing agents in the synthesis of mesostructured silica particles.

Polymer	MW (g/mol)	Number of PO units	Number of EO units	Polymer	MW (g/mol)	Number of PO units	Number of EO units
L 64	2900	306	26	P103	4950	60	34
P65	3400	29	36	P104	5900	61	54
F68	8400	29	152	P105	6500	56	74
P84	4200	43	38	F108	14600	50	264
P85	4600	40	52	P123	5750	69	38
F88	11400	39	206	F127	12600	65	200

Table 1.3: Properties of some widely used Pluronic surfactants.

By the help of easily tunable hydrophilic-hydrophobic character of the pluronic surfactants, the mesostructured silica particles with different morphologies (sphere, rodlike, crystal like, gyroid) [5,72,73] and different mesostructures (2D-hexagonal (p6m), Cubic (Fm3m, Im3m, Ia3d) and lamellar) [5,49,74,75] have been synthesized. Two important family of these particles are the MSU and SBA [20,43,73,76]. In the SBA type particles, a cationic surfactant is involved as a co-surfactant. In this type of materials pluronic surfactants and CTMABr form charged micelles cooperatively. In the synthesis of the MSU type materials F^- ion is used as a catalyst [76]. Generally, the synthesis media of pluronic surfactant based mesostructured particles is quite acidic(pH< 2), which is the isoelectric point of silica.

One of the typical characteristics of the mesoporous materials synthesized using the pluronic type surfactants is the thick walls. The typical wall thickness is around 3 to 5 nm. The formation of thick walls could be attributed to the repulsive interaction between the corona (see text later) parts of the adjacent micelles. Simply, the corona part consist of hydrated units and the interaction between these hydrated units is repulsive [77]. On the other hand, the hydrated PEO units have a good hydrogen bonding interaction with the monemeric silica particles, so the repulsive interaction is reduced to some extent and the gap between the adjacent micelles are filled with amorphous silica [75,78]. See **Figure 1.3.**

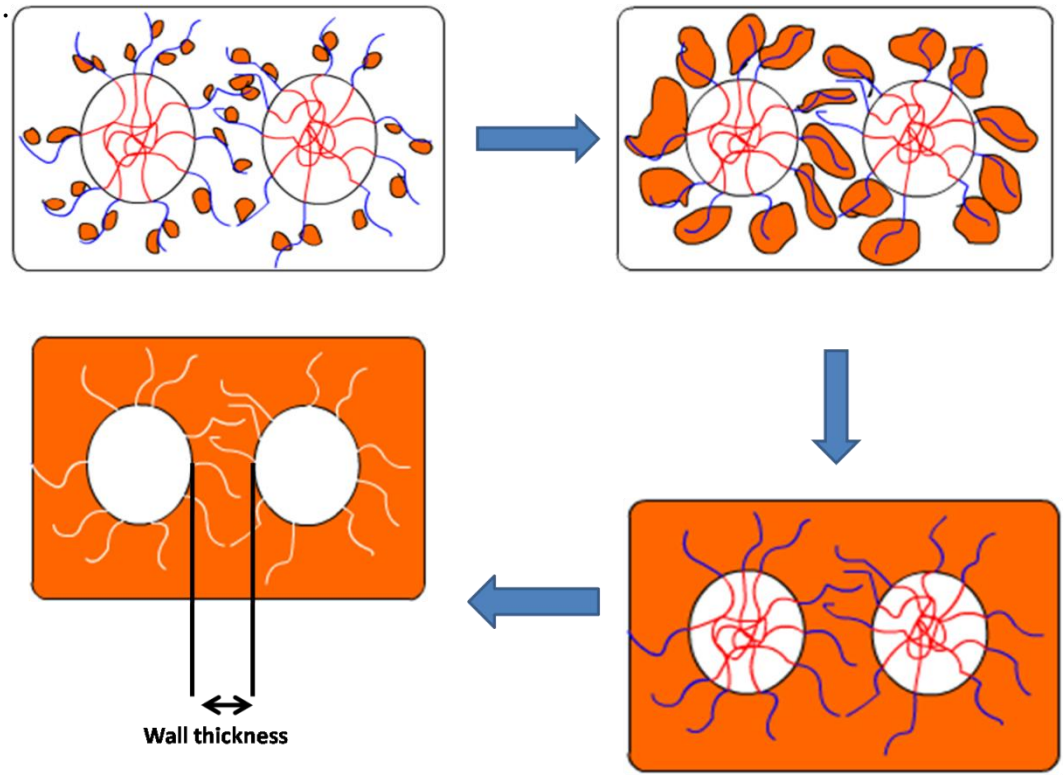

Figure 1.3: Interaction between micelle and silica monomers.

The synthesis of pluronic surfactant based mesoporous silica particles has been widely studied and well established in many aspects. Many structural properties of these materials have been improved by both organic and inorganic additives. The

generally used organic additives are TMB (trimethyl benzene), benzene, buthanol, alkanes and cyclohexane. The main goal is to change the morphology and tune the pore size [5,19,44,74,79-81] by means of changing micellization properties, which will be discussed in the following chapter. The hydrophobic micelle core is an appropriate environment for mainly water insoluble organic additives [71,82]. Moreover, once the organic additives penetrate into the micelles they increase the hydrophobic character of the micelles and swell the micelle [44,74,79-81]. Increasing hydrophobic character of the micelles results with a change in the geometry of the micelles from sphere to wormlike [5]. A similar geometry change has been observed upon addition of alkali salts of anions from the Hofmeister's series to the aquous surfactant solution [5,6,43,49,73]. The effect of the additives on the micellization and assembly of pluronic type surfactants will be discussed in the following chapters. Li et al. investigated the role of KCl on pore structure of the mesoporous silica particles [43]. Zhao et al. observed a remarkable impact of Cl^- and SO_4^{2-} ions on both morphology and mesostructure of the mesoporous silica particles [6,73]. Beyond the pore structure and morphology, added salts also affect the wall thickness by enhancing dehydration of the PEO units in corono region of the micelle [19]. The ultimate effect of the organic and inorganic additives is to change the hydrophilic-hydrophobic character of the pluronic surfactants. It necessarly means that the control of the hydrophilic and hydrophobic balance of the micelle. For instance, aggregation behaviour of a more hydrophobic surfactant can be simulated by decreasing the solubility of a pluronic by the additives or by increasing the temperature of the media. Because, the pluronic surfactant micellization is highly temperature dependent [63,66,67,83], the synthesis at high temperatures mimics the effect of both inorganic and organic additives.

1.3. Silica Polymerization:

The well known silicon chemistry serves great oppurtunities for the synthesis of mesoporous silica particles. Controlling the hydrolysis and condensation reactions by means of controlling acidity, using catalyst and careful temperature adjustment of the reaction environment, serves a great conrol on the order, size and morphology of synthesized mesoporous silica particles [84-88]. The individual steps in silica polymerization and the mesoporous particle formation are followed by in situ and time resolved measurements [85]. The polymerization of silica has been widely investigated by using TEM, XRD, NMR, FT-IR and Raman Spectroscopic techniques [84,85,89-91]. Specifically, spectroscopic techniques (FT-IR and Raman) are generally used to investigate the individual steps in silica polymerization, especially for hydrolysis step [85,91]. As an another spectroscopic technique, ^{29}Si-NMR is very helpful for deciding the degree of silica polymerization [90]. It might also give an evidence about the micropores in some circumstances. Different form the spectroscopic techniques, TEM and XRD are used to follow the improvement of order and formation of the mesostructured particles [78,85]. They also give information about the level of the silica polymerization to some extent.

The silica polymerization under dilute conditions starts with a rapid hydrolysis (depending on the size of alkoxide unit) and followed by a condensation reaction. According to Scherer and Brinker, the silica polymerization should be investigated in three different pH regions, below 2.0, between 2.0 and 7.0 and above 7.0 (**Figure 1.4**). Below pH2, the silica particles are positively charged. The pH2 is also known as the isoelectric point of silica in which electrical mobility of silica particles is zero [89]. In this pH range, the silica particles can be polymerized in a controlled way. The

formation of metastable silica particles and a controlled polymerization process are desired conditions for obtaining an highly ordered mesoporous silica particles. Above pH2, the silica particles are negatively charged and an increase in pH (until pH7) accelerates the rate of the silica condensation reaction. The reason is increasing the concentration of OH^- ions with increasing pH. The OH^- ion makes a similar catalytic effect like F^-, in the silica polymerization [89]. The F^- ion is a well known catalyst for both hydrolysis and condensation reactions of silica [86-89,92,93]. Above pH7, the silica condensation takes place with the same mechanism as of previous pH region. However, all the silica particles are ionized and this forms a repulsive interaction between these particles. This causes addition of these monomeric silica particles to higly condensed bigger particles rather than aggregation of individual smaller particles.

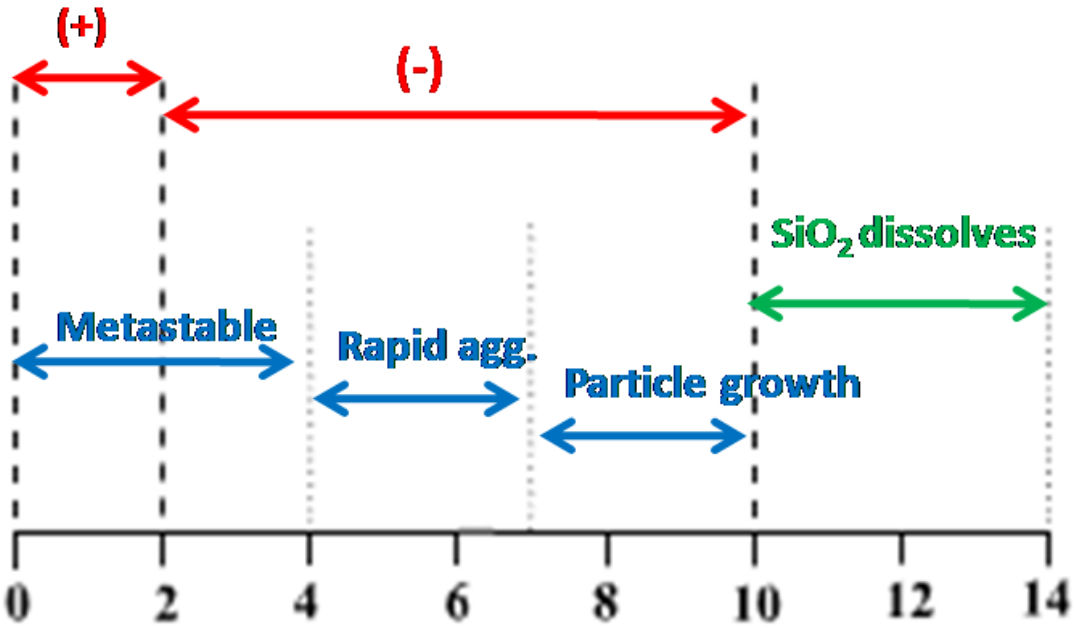

Figure 1.4: pH effect on aquous silica solutions.

The polymerization of silicon alkoxides in dilute solutions always start with a rapid hydrolysis reaction, that it is completed in couple of minutes [85,94]. The hydrolysis rate depends on the length of the alkoxide chain. Increasing alkoxide size reduces hydrolysis rate. One of the outcome of hydrolysis reaction is the alcohols of the alkoxide units of the silica source. Of course, the condensation of silica at various pH conditions is not the only mechanism of silicon alkoxides polymerization in water. In absence of a catalyst, like F^- or OH^-, alcohol and water condensation reactions also occur, unless the hydrolysis reaction is complete. In other words, when the rate of the hydrolysis reaction is comparable with other condensation reaction rates, these condensation rates also become important in the silica polymerization. **Figure 1.5** illustrates the hydrolysis and condensation reactions at different acidity conditions.

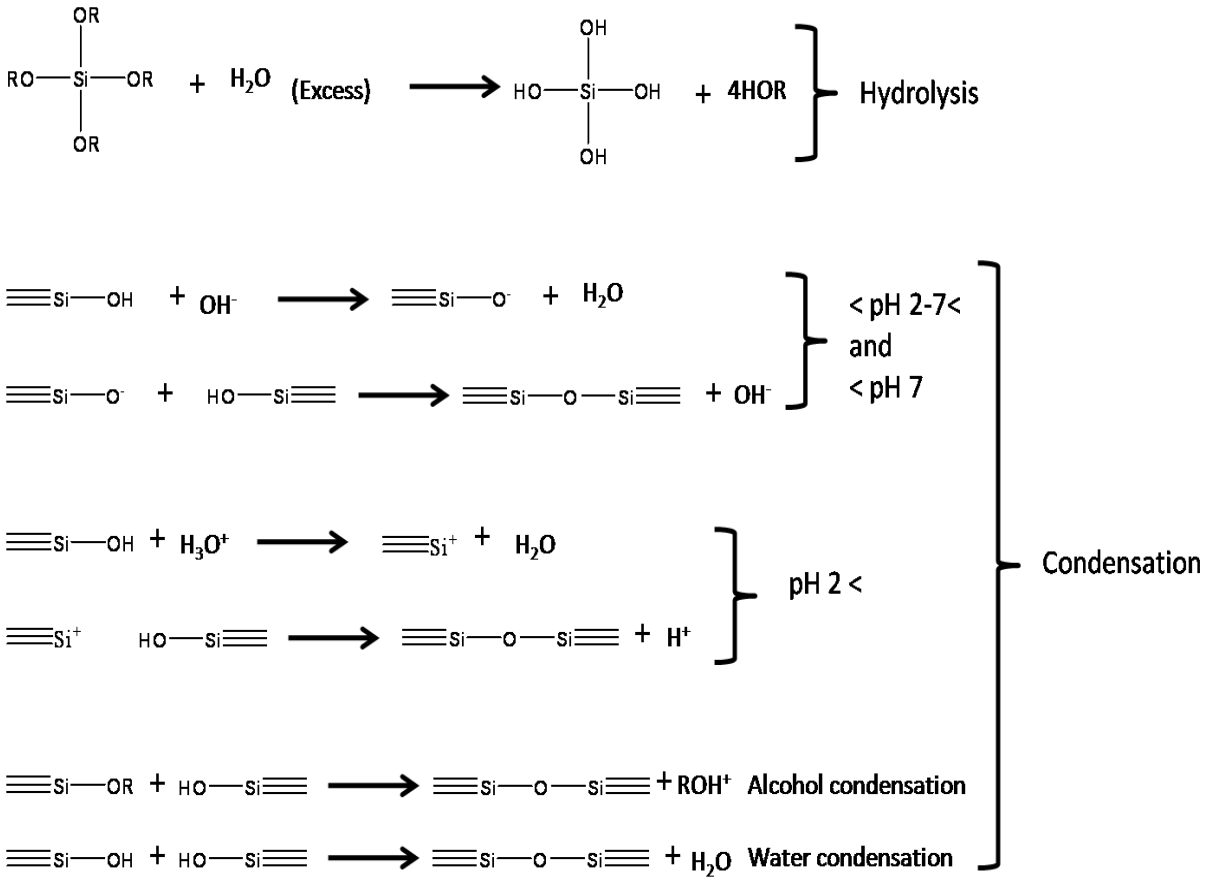

Figure 15: Hydrolysis and condensation reactions of silica alkoxides at different conditions [89].

1.4. Micellization

Roughly, micelle can be described as the assembly of amphiphilic surfactants by the solubility difference of its hydrophilic and hydrophobic parts in water. The concept of micelle was first described in 1930s by Herman (Parafin-Chain Salts: A study in micelle formation, Herman and Cie, Paris, 1936) [60,95]. Relatively hydrophobic part accomodates at the centre (core) of the micelle to keep itself away from the water, on the other hand the relatively hydrophilic parts surrounds the core of the micelle and forms namely corona part of the micelle. **Figure 1.6** describes the core, corona and hydrodynamic radius concepts. The hydrodynamic radius can be

described as hard sphere interaction distance [96,97] and it depends on the dilution of micellar solution. The hydrodynamic distance is almost equal to size of the micelle at concentrated solutions and in the liquid crystalline mesophases.

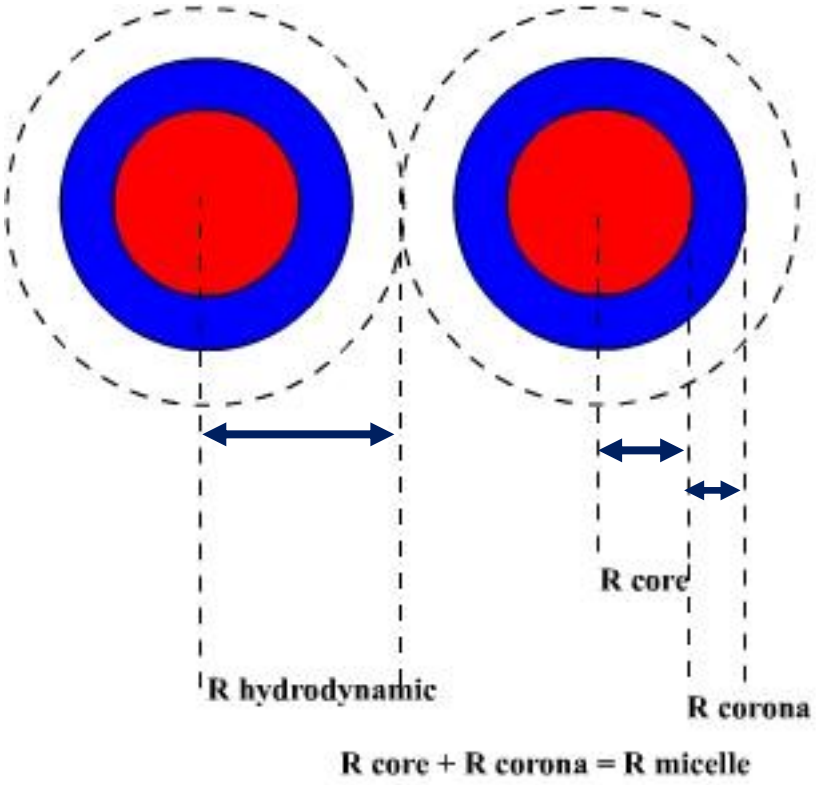

Figure 1.6: Basic concepts of micelle.

The micellization of various surfactants have been videly investigated by both experimentally (NMR, Dynamic and Static Light Scattering, Neutron Scattering, Differantial Scaning Calorimetry, Flourescence Spectroscopy, UV-Vis Spectroscopy, Gel permeation Spectroscopy, fixed interference method (FIM) etc.) and theorotically [63,65,96-103]. The reason of this great interest on micellization and aggregation of surfactants is the role of surfactants as structure directing agents in many mesostructured and mesoporous materials.

Besides the well known spherical shape of micelle, egg shape and elongated micelles also exist [63,104-106]. The change of aggregation type depends on the surfactant type and reaction environment. Surfactants with higher hydrophobic character are easily packed in an elongated form when compared to surfactants with lower hydrophobic character. Moreover, any parameter (temperature, concentration, ions etc.) that decreases the surfactant solubility promotes the formation of elongated micelles [64,67-69,107]. One step furher is the formation of bilayer surfactant assembly. **Figure 1.7** illustrates different type of surfactant assembly into different shapes. With decreasing surfactant solubility, the first effect observed is an increase in average number of surfactants in the micelle, which is known as aggregation number (N_{agg}) [105]. A further decrease in solubility causes a shape transformation [105]. An increase in aggregation number causes a gradual increase in micelle size (especially at R_{core}). Simply, shape of micelles starts with the most efficient packing (sphere) and ultimate point is bilayer assembly of surfactants. This bilayer assembly is the key step in vesicle formation that will be mentioned in the following chapters [108,109].

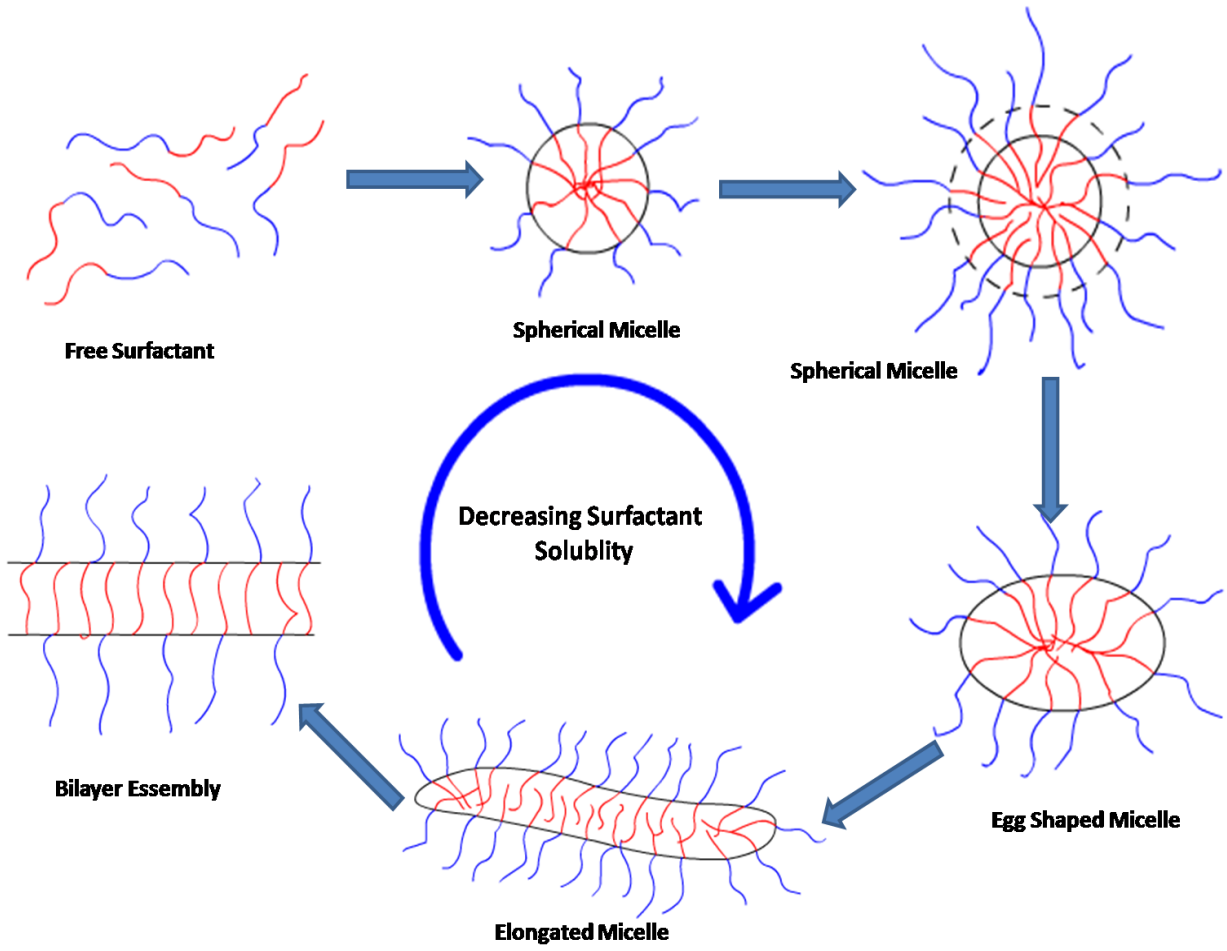

Figure 1.7: Change in micelle shape upon decreasing surfactant solubility.

The transition from spherical micelles to elongated micelles and finally bilayered structure (disc like micelle) can be explained by packing parameter, which is obtained by making very simple geometric calculations (**see Figure 1.8**). For illustration, packing parameter calculation for a spherical micelle is given below, the other two packing parameters (P) for elongated micelle and vesicle could be calculated in a similar way:

The volume (V) and surface area (S) of a spherical micelle with aggregation number N, can be given as;

$$V = N \times V_c = {}^{4}/_{3} \times \pi \times r^3 \qquad \{1\}$$

$$S = 4 \times \pi \times r^2 \qquad \{2\}$$

Where V_c is the volume of hydrophobic part of the surfactant and r is the radius of the core. Then surface area per surfactant "a" is given by (see **Figure 1.8**);

$$a = \frac{4 \times \pi \times r^2}{N} \qquad \{3\}$$

Use equation 3 in 1 to obtain;

$$a = \frac{3 \times V_c}{r} \qquad \{4\}$$

In this step, a new parameter (optimum surface area "a_o") is involved. Simply, a_o is determined by calculating the head group interactions [48]. In detail, a_o is a thermodynamic parameter and can be estimated if one knows interfacial interaction parameter and head group repulsion parameter [48]. If we divide both side with optimum surface area for each surfactant "a_o";

$$\frac{a}{a_0} = \frac{3 \times V_c}{r \times a_0} \qquad \{5\}$$

This equation can be written by using " ℓ ", which is critical chain length and it is equal to the chain length of the hydrophobic part of the surfactant. Note that core radius can not be bigger than ℓ.

$$\frac{a}{a_0} = \frac{3 \times \ell}{r} \times \frac{V_c}{a_0 \times \ell} \qquad \{6\}$$

For an optimum spherical packing of surfactants "a" has to be smaller or equal to "a_o". Because, "a" can not be bigger than "a_o", if one wants to pack surfactants in a spherical geometry. Obviously, radius of a spherical micelle can not be bigger than the chain length of the surfactant ($\ell \leq r$). This makes the first term in equation {6}

smaller than 3, necessarly the second term V_c / (a_o × ℓ) (P) has to be smaller than 1 / 3.

When the packing parameter (P) is smaller than 1/3, the resulted micelles are spherical and they form cubic mesophase. If P is between 1/2 and 1/3, the micelles are elongated and these micelles form hexagonal mesophase (2D Hexagonal). If P is 1/2 < P < 1 the micelles are namely disc like and these type of micelles are responsible in formation of vesicles and lamellar mesophase [110-112].

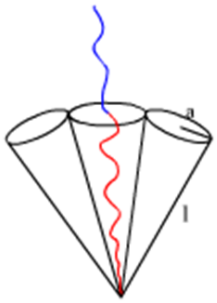

Shape of Micelle	P (packing parameter)
Sphere	< 1/3
Elongated	1/3 < P < 1/2
Bilayer	1/2 < P < 1

Figure 1.8: A Schamatic diagram of a surfactant in a micelle and the packing parameter for various micelle types.

Apart from packing properties of surfactants, as micelles, there are some other parameters, which is used to describe their assembly properties. The most common ones are critical micelle concentration (CMC), critical micelle temperature (CMT) and cloudy point (CP). The CMC can be described as the minumum surfactant concentration in a given temperature to form uniform micelles in solution. Similarly, the CMT is the minimum temperature for a given surfactant concentration in order to observe micellization [60,63,66-68,107]. The last one is a controversial concept, since it could be described in different ways depending on the measurement type [83,107]. However, simply cloudy point can be described as the point in which surfactant is no longer soluble in both as free surfactant and in micelle form. It is possible to reach the

cloudy point in either using excess surfactant in solution or increasing temperature far above to the CMT [69]. It is also possible to use salts to decrease the surfactant solubility [68,107,113,114]. The CMC, CMT and CP points of almost all commercially available surfactants are known and exist in the literature, therefore these database forms a wide perspective for new research activities in terms of both investigating their assembly properties and their usage as structure directing agent in many systems.

1.4.1. Micellization of Pluronic Surfactants:

The pluronic surfactants are three block co polymers that contains PPO group at the middle as the relatively hydrophobic part and two blocks of PEO groups at both ends. The most important feature of these polymers is their highly temperature dependent micellization properties. The relatively hydrophobic part (poly (propylene oxide)) easily dehydrates at room temperature and assemble to form the core of the micelle [63,65]. This temperature can be as low as 20^{o}C. Below this temperature, the micelle formation is rarely observed, if a high surfactant concentration is not reached [63,65,77]. On the other hand, PEO units of the pluronics remains hydrophilic upto 80^{o}C. Therefore, size of the pluronic micelle gradually increases from 20^{o} up to ~60^{o}C and then the size of the micelle decreases due to the dehydration of PEO groups. This trend continues until the CP is reached in which the pluronic surfactant is no longer soluble [65,67,77]. A temperature increase of the media decreases the surfactant solubility, and forces surfactants for a more effective packing. Therefore, the number of surfactants inside the micelle increases in order to pack itself more effectively [96,115,116]. The decrease of the micelle size above 60^{o}C can be atributed to conformational changes in the PEO units in the corona by loosing water

and becoming less hydrophilic. The aggregation of pluronics into the micelles is illustrated in **Figure 1.9**. Note that the CMC, CMT and CP of micelles highly depend on the hydrophobic character of the surfactant, however overall trends in the assembly process are more or less the same [63,67,69].

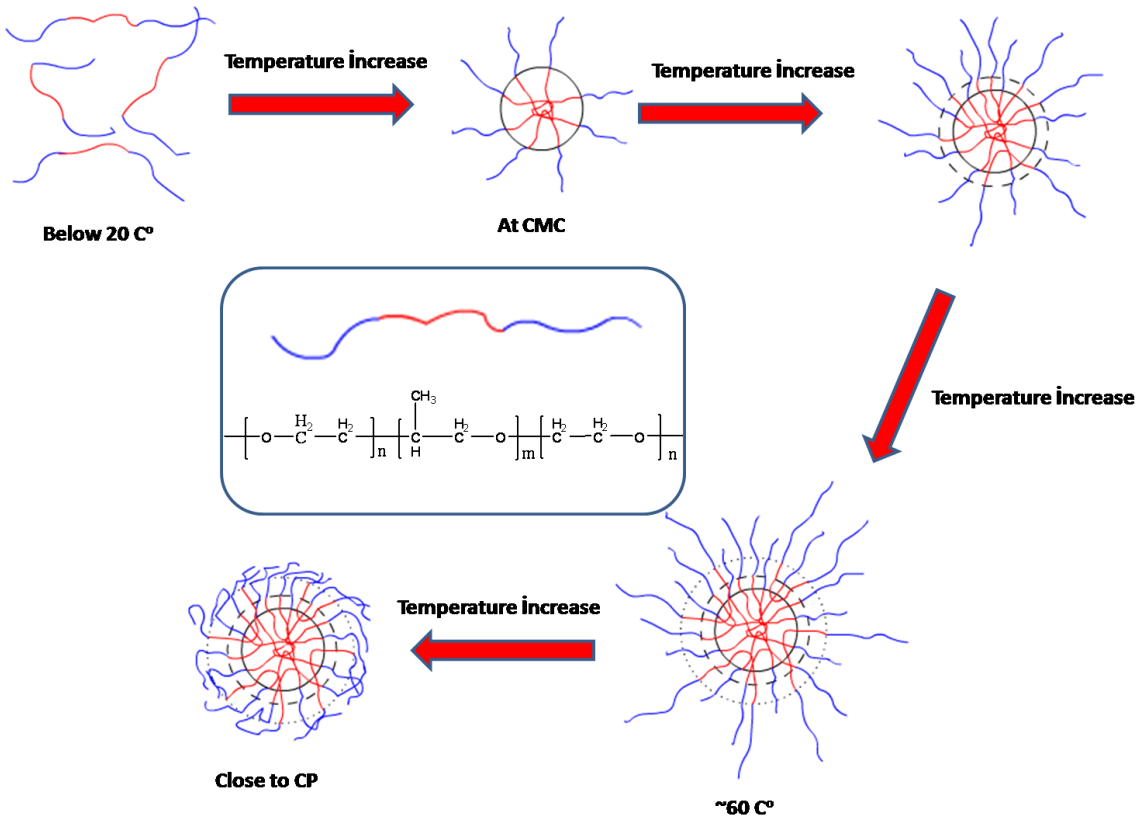

Figure 1.9: Temperature dependent micellization of Pluronic type surfactants.

Temperature basicly controls the hydration of the hydrophilic and hydrophobic blocks of the surfactants. The same impact could be created by using salts of the Hofmeister's series [64,68,99,104,107,117]. Franz Hofmeister, Professor of Pharmacology at the University of Prague, published seven papers describing the effect of anions on the protein precipitation during 1880s [113]. These seven paper series were collected in the name of " About the science of the effect of the salts"

[113,114]. Original papers are in German, Kuntz et al. translated his most famous first two publications to English. These salts can be collected under two main groups. In salt-surfactant system, the solubility of surfactants decreases while going to lyotropic (Kosmotropic) ions. On the other hand, the surfactant becomes more hydrophilic while going towards to more hydrotropic (Chaotropic) ions [113,114,118]. **Figure 1.10** gives the Hofmeisters' series for both anions and cations.

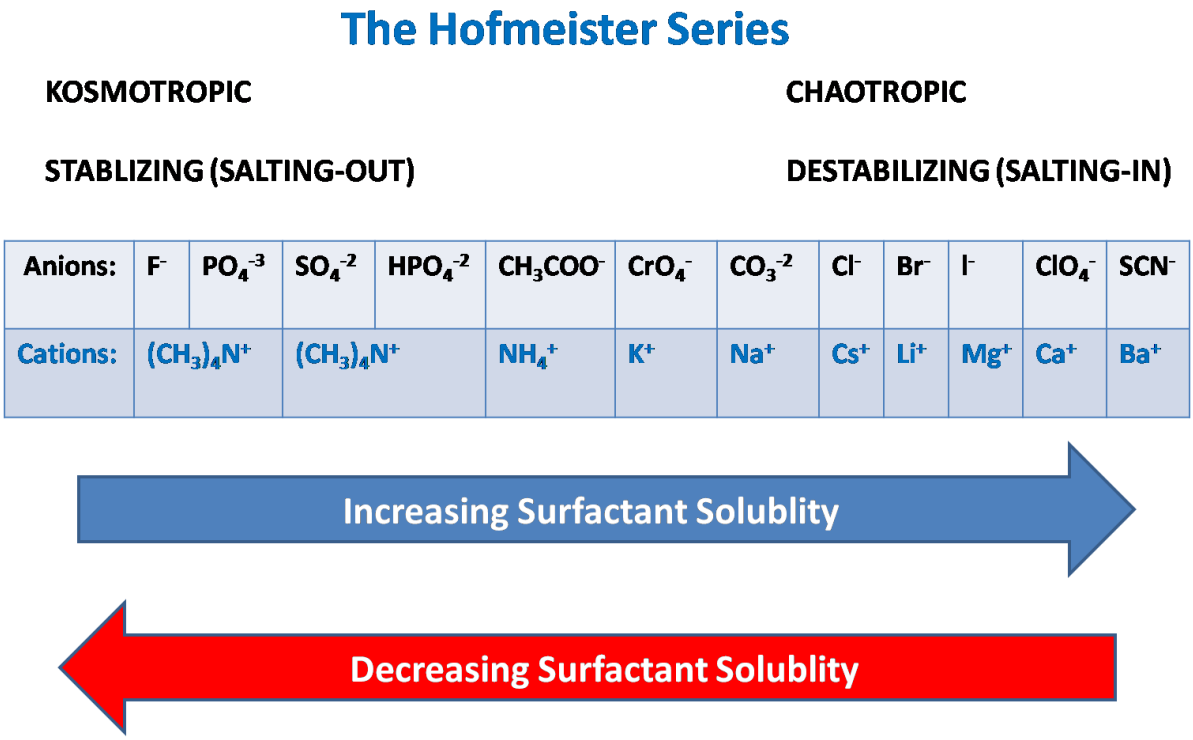

Figure 1.10: Anions and cations in the Hofmeisters' Series.

The lyotropic ions has very smilar effect like increasing temperature, these anions decreases the CMC, CMT and CP of the surfactant. Strength of the effect depends on the type of anion and its concentration [63,64,68,70,99,104,107,113,114,

118]. Moreover, it has been shown that usage of these lyotropic anions manupulates the type of aggregation and shape of the micelles [49,104].

The temperature and usage of salts are not the only parameters that control the pluronic surfactant micellization. The water free environment of the core of micelle is a suitable environment for non-polar solvent accomodation [71,82,119]. Nagarjan et al. investigated the solublization capacity of organic molecules in the pluronic micelle core and suggested that Benzene is the best nonpolar solute in terms of solublization in the core of pluronic micelles [71,82]. Another conclusion, he had reached is the solublization capacity of aromatic compounds in the pluronic micelle core is higher than non-aromatic hydrocarbons and other cyclic compounds [71,82]. The presence of nonpolar solutes strengthen the hydrophobic interaction of pluronic surfactants and swell the micelle [82,119]. The nonpolar solvents is widely used in the synthesis of mesoporous silica materials in order to enlarge the pore of the mesoporous material. These pore swelling agents also increase the order of formed silica particles [3,9,44,49,74]. The most widely used swelling agents are the TMB (Trimethyl Benzene) and TIPB (Triisopropyl Benzene) [49,74].

The overall trend in micellization of pluronic surfactants can be summarized in the following way: 1) in a given temperature, surfactants with higher molecular weight form micelle at lower concentrations, 2) surfactants with higher number of PPO units have lower CMC, 3) the PEO groups have secondary importance in the micellization properties of the pluronic surfactants [67]. Note that the micellization of pluronic surfactants is an endothermic process and the free energy change is a CMC dependent parameter [66,67]. The required energy can be attributed to the dehydration of the PPO block [120].

1.4.2. CTA^+ Micellization:

Like pluronic surfactants, positively charged CTABr surfactant has interesting assembly properties (for the molecular structure of CTMABr see **Table 1.1**). The alkyl chain of these surfactants forms the hydrophobic core and its chain length affects the CMC. With increasing hydrophobic alkyl group chain length, the CMC decreases [121]. Like pluronic surfactants, the micellization of cationic surfactants is also temperature dependent, where the CMC decreases with increasing temperature due to dehydration of the hydrophilic head group [121]. The cationic surfactants can also form aggregates in different shapes (spherical and rodlike micelles and vesicles) depending on the surfactant concentration, temperature and the type of counter anion [122]. The widely used counter anions are Br^-, Cl^- and I^-. However, the solubility of cationic surfactants decrease when the hydrotropic anions are used as the counter anion. When compared to lyotropic anions, hydrotropic anions are more effective to decrease the effective head group area of the cationic surfactant [123,124]. Because, hydrotropic anions binds more strongly to the positively charged head group of the surfactant [123]. That is why the cationic surfactant with hydrotropic counter anion has higher micelle aggregation number [124]. The hydrotropic anions reduces repulsive interaction of head group and decreases curvature (see **Figure 1.11**).

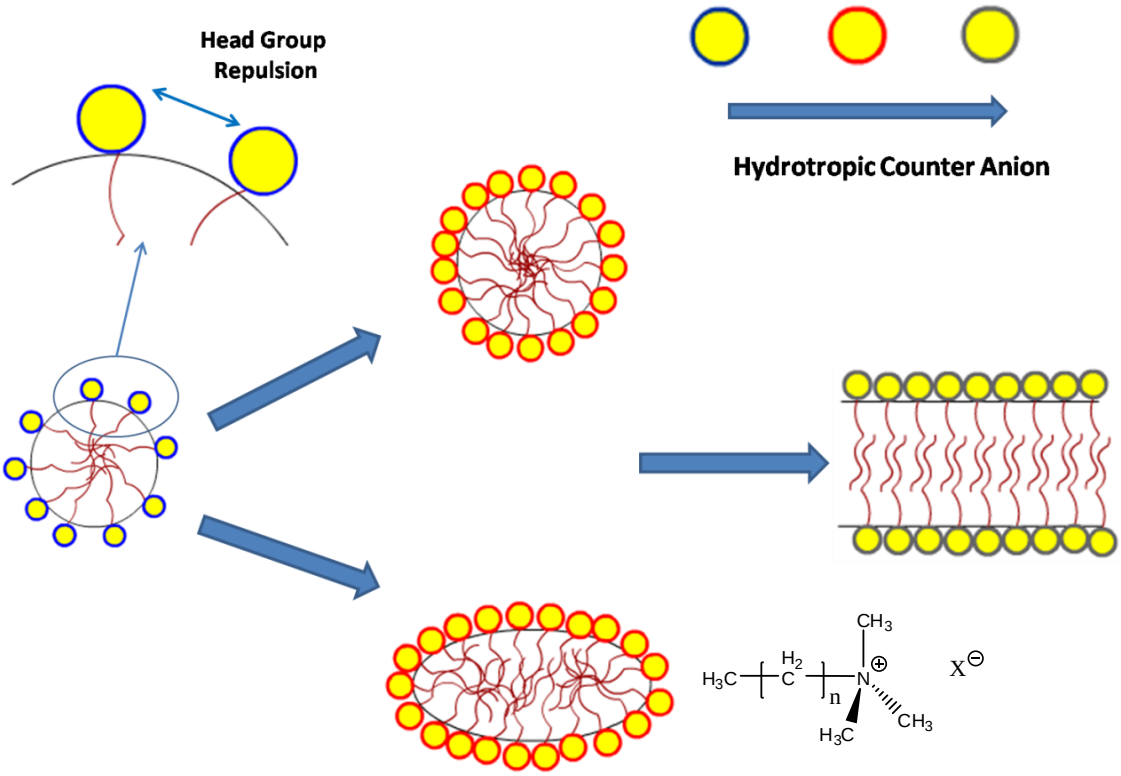

Figure 1.11: Micellization of cationic surfactants with different counter anion.

1.4.3. Cooparative Assembly of CTA^+ - Pluronic Surfactants:

The overall effect of CTA^+ on the pluronic surfactant is an increase in pluronic surfactant solubility. It increases the CP, CMC and CMT of the pluronic surfactants [120]. Different from SDS (sodium dodecyl sulphates, see **Table 1.1**), the CTA^+ interacts better with pluronic surfactants, which have higher hydrophobic content [125-127]. The binding of CTA^+ into the pluronic micelles starts at very low concentrations, however the SDS does not penetrate into the pluronic micelles until reaching a critical concentration [127,128]. The binding of charged surfactants to the pluronic micelles is an exothermic process and has a negative enthalpy value [120,127,129]. The micelle size and pluronic surfactant aggregation number decreases until the CTA^+ concentration reaches a critical concentration. Moreover, the micelles become positively charged and they stand at an equilibrium distance

from each other. When a high CTA^+ concentration is reached, the CTA^+ starts to break down the pluronic micelles and forms its' own micelles [120,127,128,130]. Entire process can be summarized in the following figure (**Figure 1.12**).

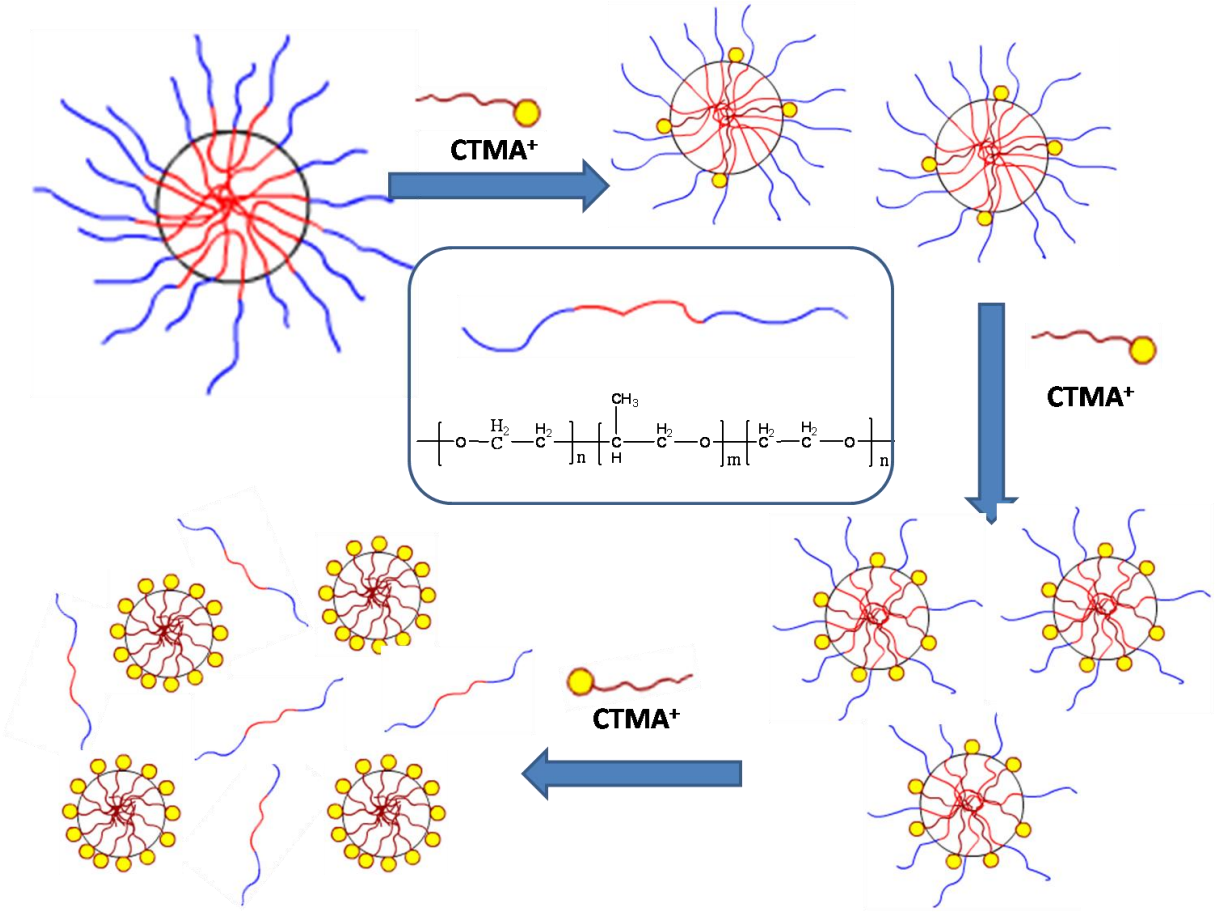

Figure 1.12: CTA^+ - Pluronic Surfactant Interaction.

1.5. Micelle Aggregation and Mesostructure Formation.

The micelle formation is a necessary step in the formation of a mesostructure silica materials, however in order to get a higly ordered particles, the micelle aggregation and interaction with monomeric silica particles are equally important [22,131]. The monomeric silica particles assemble with individual or poorley ordered micelles in aquous media to form final mesoporous particles (see **Figure 1.2**). In most cases, it is possible to estimate type of mesostructure by theorotical calculations

[101]. The micelles are generally assumed as hard spheres (hard sphere model) and their assembly is directed by the magnitude of the repulsive and attractive forces. 2D hexagonal packing is the most widely encountered type of mesostructure. As stated before, the 2D hexagonal mesostructure is obtained by the assembly of elongated micelles, in which the hydrophobic interaction is already high. That is why the hexagonal packing is the second most effective packing (first one is lamellar structure). Increasing repulsive force between the micelles causes a change in the mesostructure and forces the micelles to pack in a less effective way, which is cubic packing (FCC or BCC). Note that, assembly of the pluronic surfactants with higher hydrophilic character bring out a cubic mesostructure, whereas the surfactants with higher hydrophobic character produces a 2D hexagonal or lamellar mesostructure [6,20,21,75].

The relatively hydrophilic PEO groups on pluronic surfactant has a good interaction with silica species [78,132]. This interaction could also influence the shape of the micelle [78]. Interaction between PEO groups and silica species can be seen as the reason of choosing PEO as the hydrophilic part of the non-ionic surfactants in most systems [49]. The repulsive interaction between hydrated PEO groups of the micelles is reduced by the silica species and coperative assembly is achieved [133]. When the repulsion is reduced by the silanol groups, the hydrophobic attraction between the micelles becomes dominant. The surrounded micelles assemble together in a controlled way to form mesostructured silica materials [132,133]. During the assembly, first a poorly ordered liquid crystal phase occurs [78]. The highly ordered mesostructured particles are obtained after the complete silica polymerization (after a plausible aging time).

2. Experimental:

2.1. Materials:

All chemicals were used as received without further purification. A list of chemicals used in this work are tabulated in Table 4. The Pluronic surfactants (P65, P85, P103 and P123) are donated by the BASF Company.

Surfactants:	Company	M.W. (g/mol)	Molecular Formula
CTMABr	**Aldrich**	**364.46**	**$CH_3(CH_2)_{15}N(CH_3)_3Br$**
P65	**BASF**	**3400**	**$EO_{20}PO_{30}EO_{20}$**
P85	**BASF**	**4600**	**$EO_{27}PO_{33}EO_{27}$**
P103	**BASF**	**4950**	**$EO_{17}PO_{55}EO_{17}$**
P123	**BASF**	**5750**	**$EO_{20}PO_{70}EO_{20}$**
F68	**Sigma**	**8400**	**$EO_{80}PO_{27}EO_{80}$**
F127	**Sigma**	**12600**	**$EO_{106}PO_{70}EO_{106}$**

Salts:	Company	M.W. (g/mol)	Molecular Formula
Sodium Nitrate	**Panreac**	**84.99**	**$NaNO_3$**
Sodium Sulphate	**Carlo Erba**	**142.84**	**Na_2SO_4**
Sodium Flouride	**Merck**	**41.99**	**NaF**
Potassium Chloride	**Merck**	**74.55**	**KCl**
Potassium Bromide	**Merck**	**119.01**	**KBr**
Potassium Iodide	**Merck**	**166.00**	**KI**
Potassium Thiocyanate	**Merck**	**97.18**	**KSCN**

Other Chemicals:	Company	M.W. (g/mol)	Prutiy (%)
TMOS (Tetramethyl Orthosilicate)	**Aldrich**	**152.22**	**98**
Benzene	**Riedel-de Haen**	**78.11**	**98**
Cyclohexane	**Riedel-de Haen**	**84.16**	**99.5**
Ethyl Orange	**Aldrich**	**355.39**	**90**
HCl	**Riedel-de Haen**	**36.46**	**37**

2.2. Synthesis

2.2.1. The Critical Micelle Concentration (CMC) and The Critical Micelle Temperature (CMT) Determination

Various amount of P85 (0.1 to 12 w/v%) was dissolved in ~10^{-6} M solution of Ethyl Orange. The UV-Vis Spectra of the prepared ethyl orange solutions were recorded in 350- 700 nm range in order to determine the CMC. The spectra of pre-prepared solutions were also collected at four different temperatures (25^0, 30^0, 35^0 and 40^0C) in order to determine the CMT at a given concentration. The same measurements were also performed in presence of different salt (KSCN, KI, NaF, KBr, KI, Na_2SO_4 and $NaNO_3$) concentrations (0.1 M, 0.2 M, 0.5 M and 1.0 M).

2.2.2. Turbidity Point Measurements

Different amounts of pluronic surfactants (P65, P103 and P123), CTMABr and NaF were dissolved in 100 ml of distilled water and 1.2 ml 37% HCl solution (~pH 1). The resulting clear solutions were used for the Turbidity Point (TP) measurements. 2 ml TMOS (13.2×10^{-3} mol) was added to the above solutions under vigorous stirring at room temperature (RT). The solution becomes turbit that was

determined using a kronometer (see **Figure 2.1**). These measurements were done in a wide concentration range (of Pluronic, CTMABr and NaF) and keeping the water, HCl and TMOS amount constant. The effect of the quantity of these three components on the TP was determined individually by changing the amount of one component and keeping the other two constant at each time. The used concentration range for three varied components are given in **Table 1. 2**.

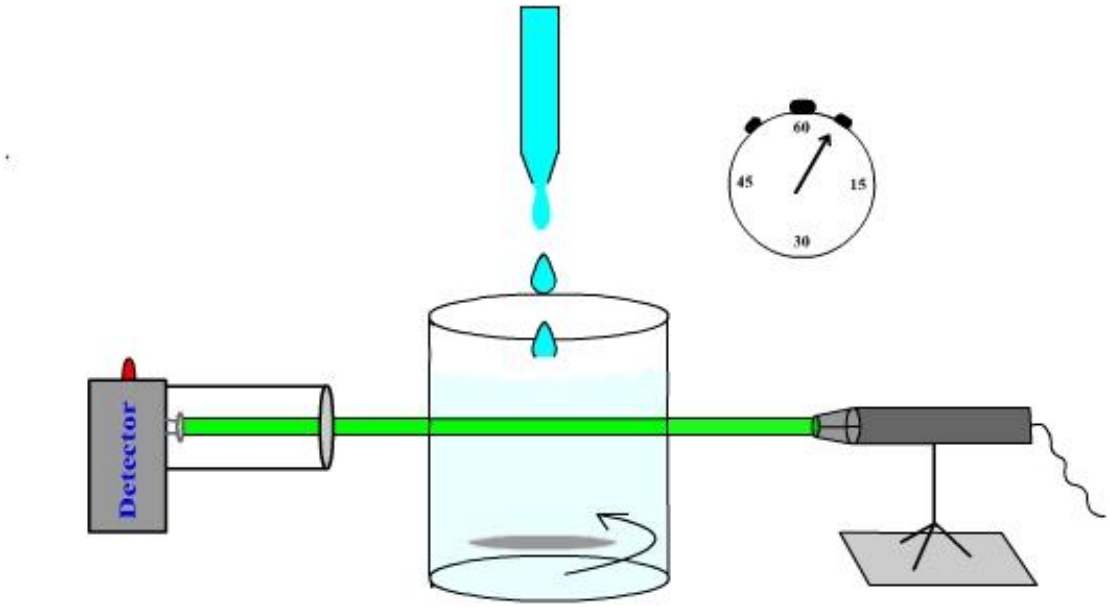

Figure 2.1: Schematic description of the Turbidity Point Measurement Aparatus.

	Surfactant Concentration ($\times 10^{-5}$ M)	CTMABr Concentration($\times 10^{-4}$ M)	NaF Concentration ($\times 10^{-4}$ M)
P65	**0.06 – 0.6**	**0 – 6**	**0 – 14**
P103	**0.06 – 0.4**	**0 – 4**	**0 – 10**
P123	**0.3 – 2.8**	**0 – 5.4**	**0 – 14**

Table 2.1: Concentration intervals used for turbidity point measurements.

2.2.3. Synthesis of Mesoporous Silica Particles

Two surfactants (Pluronic and CTMABr), in different CTMABr/ Pluronic ratios (between 0 and 12), were dissolved in a 100 ml aquous solution of HCl, where pH is 1.0 (1.2 ml 37%HCl in 100 mlwater). After a clear solution is obtained, 2.5 ml TMOS ($1.64\times10^{2-}$ mol) was added under vigorous stirring at RT. The resulting clear solution was put directly into a plastic bottles, which was kept in a 95^0C oven for five days. Then, the precipitate was filtered and washed three times with 50 ml portions of distilled water and then dried in 60^0C oven for three days. The dried samples were calcined with rapid calcination method in air at 600^0C for four hours [93]. In a typical synthesis, the mole ratios of used chemicals are P123:CTMABr:HCl:H_2O:TMOS - 1:4:56:21735:65. The same experiments were also done in the presence of different alkali salts (KCl, KBr, Na_2SO_4 and $NaNO_3$) in a wide concentration range (between 0.2 and 1.0 M) and organic additives (Benzene and Cyclohexane) in a $1.7\times10^{2-}$ – $9\times10^{2-}$ mol interval. The usage of additives does not change the procedure. All the additives were added and dissolved before TMOS addition step.

2.2.4. The Room Temperature Synthesis of Mesoporous Silica Particles

Two surfactants (Pluronic and CTMABr) in different CTMABr/ Pluronic ratios (between 0 and 12) and various amount of NaF (between 0 and 5×10^{-3} mol) were dissolved in a 100 ml aquous solution of HCl where pH is 1.0 (1.2 ml 37% HCl in 100 ml water). The resulting clear solution was mixed in a sonicator where 2.5 ml TMOS ($1.64\times10^{2-}$ mol) was added under constant stirring at desired temperatures (25, 35, 40, 45 and 55^0C). The solution was kept for 40 minutes in sonicator under constant stirring after addition of TMOS. Then, the precipitate was filtered and washed three times with 50 ml portions of distilled water and then dried in a 60^0C

oven for three days. The dried samples were calcined using a rapid calcination method in air at 600^0C for four hours (66). In a typical synthesis, the mole ratios of the chemicals are P123:CTMABr:HCl:H_2O:TMOS:NaF - 1:5:82:31928:94:11.

2.3. Instrumentation

2.3.1. Powder X-Ray Diffraction (PXRD) Patterns

The PXRD patterns were collected using Rigaku Miniflex diffractometer using a high power CuK_α source operating at 30kV/15 mA. The PXRD patterns of both assynthesized and calcined powder samples are prepared on metal powder holder and collected in 0.9-8 (2θ) range with a 1.0^o /minute scan rate.

2.3.2. Fourier Transform Infrared (FT-IR) Spectra

The FT-IR spectra were collected using Bruker Tensor 27 model FTIR spectrometer, that uses a DigiTectTM DLATGS detector. The resolution of measurements were 4 cm^{-1} and 128 scans were collected in absorbance mode for each powder sample in 400-4000 cm^{-1} range. The FT-IR spectra samples were prepared as KBr pellets.

2.3.3. The Raman Spectra

The micro-Raman spectra were recorded on a LabRam Model confocal Raman microscope with a 300 mm focal length. The spectrometer is equipped with MPC 6000 DPSS laser power supply with a 532nm green laser. The signal collected was transmitted through a fiber optic cable into a spectrometer with a 600 g/mm grating. The spectra were collected by placing and flattenning powder samples on

microscope slides and manually placing the probe tip near the desired point on the powder sample. The liquid samples were measured in a quartz liquid cell.

2.3.4. The UV-Visible Absorption Spectra

The UV-Vis Spectra were recorded using a Varian Cary 5 double beam spectrophotometer with a 200 nm/min scanning speed and a resolution of 2 nm over a wavelength range of 350 to 700nm. The liquid samples (including Ethyl Orange) were measured in plastic cells in visible region.

2.3.5. The Scanning Electron Microscope (SEM) Images

The SEM images were recorded using ZEISS EVO-40. The samples were prepared on aluminium sample holders by carefully dispersing powder samples with the help of acetone. The images were recorder at 15 kV (EHT) operating voltage and at around 1.900 A filament current.

2.3.6. The Transmittance Electron Microscope (TEM) Images

The TEM images were recorded on a FEI Technai G2 F30 at an operating voltage of 200 kV. The calcined powder samples were grinded in a mortar, then dispersed in 5 ml of acetone using sonicator for 5 minutes . One drop of the dispersed acetone solution was put on a TEM grid and dried on hot-plate.

2.3.7. The N_2 Sorption Measurements:

The N_2 (77.4 K) adsorption/desorption measurements were performed with a TriStar 3000 automated gas adsorption analyzer (Micrometrics) in a relative pressure range, P/P_0, from 0.01 to 0.99. To provide high accuracy and precision in the determination of P/P_0 , the saturation pressure P_0 was measured in every 120 min

intervals. The powder samples was dehydrated under (~10^{-2} torr) vacuum for 4 hours at 400^0C before measurements in order to remove adsorbed water and volatile species in the pores.

The N_2 (77.4 K) adsorption/desorption measurements of the samples synthesized at RT were performed with a Autosorb-1-C/MS (Quantachrome) in METU Central Laboratory. The calcined powder samples were heated to 250^0C with a 1^oC/min heating rate under vacuum and kept at that temperature for 3 hours before measurements in order to remove adsorbed water and volatile species in the pores.

2.3.8. The Turbidity Point (TP) Measurements

The TPs were determined as the point in which the solution is no longer transparent to green laser. All the measurements were conducted at 25^0C (± 3^0C). The exact TP is determined with an aparatus, which includes a photocell. **Figure 2.1** shows the experimental set up for the TP measurements.

3. Results and Discussion:

3.1. Micellization of Pluronic Surfactants

A prefered solubility of dye molecules in the hydrophobic core of a micelle can be used to investigate the micellization of the pluronic surfactants. Fluorescence and UV-Vis Spectroscopic techniques have been used for this purpose [63,68,107]. Two major adventages of these techniques, compared to other widely used techniques (NMR, SANS, DLS, SLS etc.), are short measurement times, easy and fast sample preperation. The commonly used dye molecules for this purpose are pyrene, methyl orange (MO) and ethyl orange (EO). The absorption spectra of these molecules depend on the polarity of the environment, which is also known as solvent effect [98-101]. We have used ethyl orange as a micelle indicator, which is a well known acid-base indicator. **Figure 3.1.1** shows the absorption spectra at two different pH (1.0 and 5.5) and a photograph of EO solutions at these two pH values. Interestingly, at acidic conditions EO does not respond to the polarity of the environment. Therefore, all the UV-Vis measurements were performed at pH 5.5, which is the pH of distilled water.

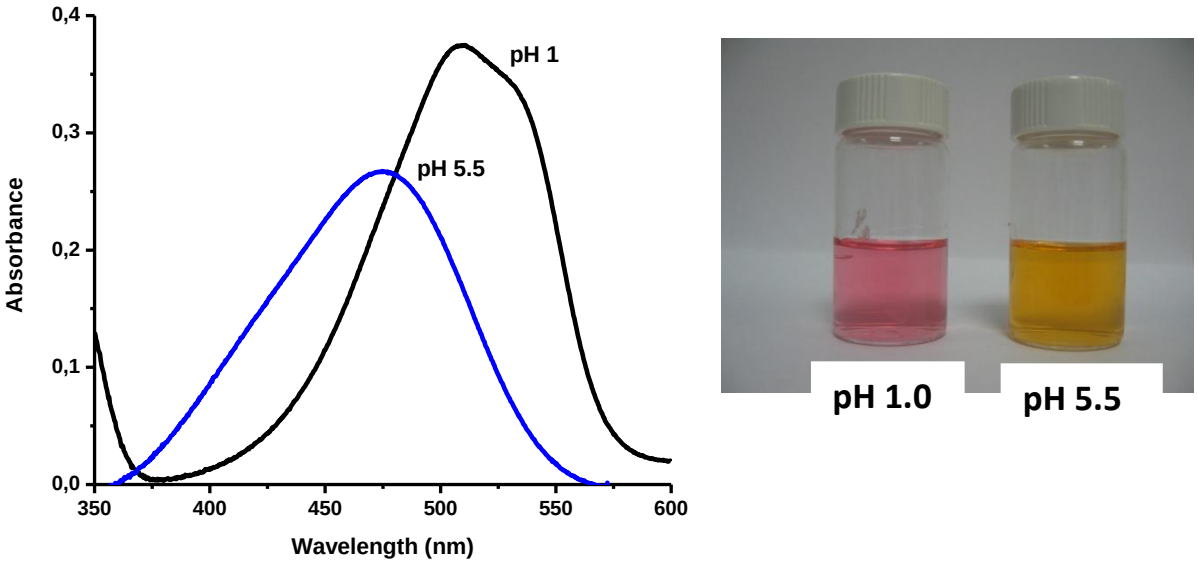

Figure 3.1.1: the UV-VIS absorption spectra and photograph of EO solutions in two different pH (pH 1 and pH 5.5).

Ethyl Orange has two absorption bands, both belongs to $\pi_1 \rightarrow \pi_1^*$ transitions of the azo moiety. The low energy absorption is attributed to hydrogen bonding interaction between the solvent and the azo nitrogen of EO. This absorption is not observed if the solvent and EO does not have any hydrogen bonding interaction with the solvent [118,134]. Intensity of the high energy transition increases, if the EO is in a hydrophobic environment (such as the core of a micelle). In the presence of micelles in water, the EO molecules penetrate into the micelle, where the absorption spectrum change. This change is very sharp and can be observed visually (**Figure 3.1.2)**. The EO solutions have the same color (orange), when EO is in the micelle and in propanol. Propanol has been used as the organic solvent to mimic the hydrophobic core of the micelle. Note that propanol and poly (propylene oxide) units have the same chemical structure. Similarly, the color of EO is the same when it is in water

and aquous surfactant solution in the absence of micelles. Therefore, the EO dye can be used to investigate the micellization properties of the pluronic surfactants in different environments (see text later) using UV-Vis absorption spectroscopy.

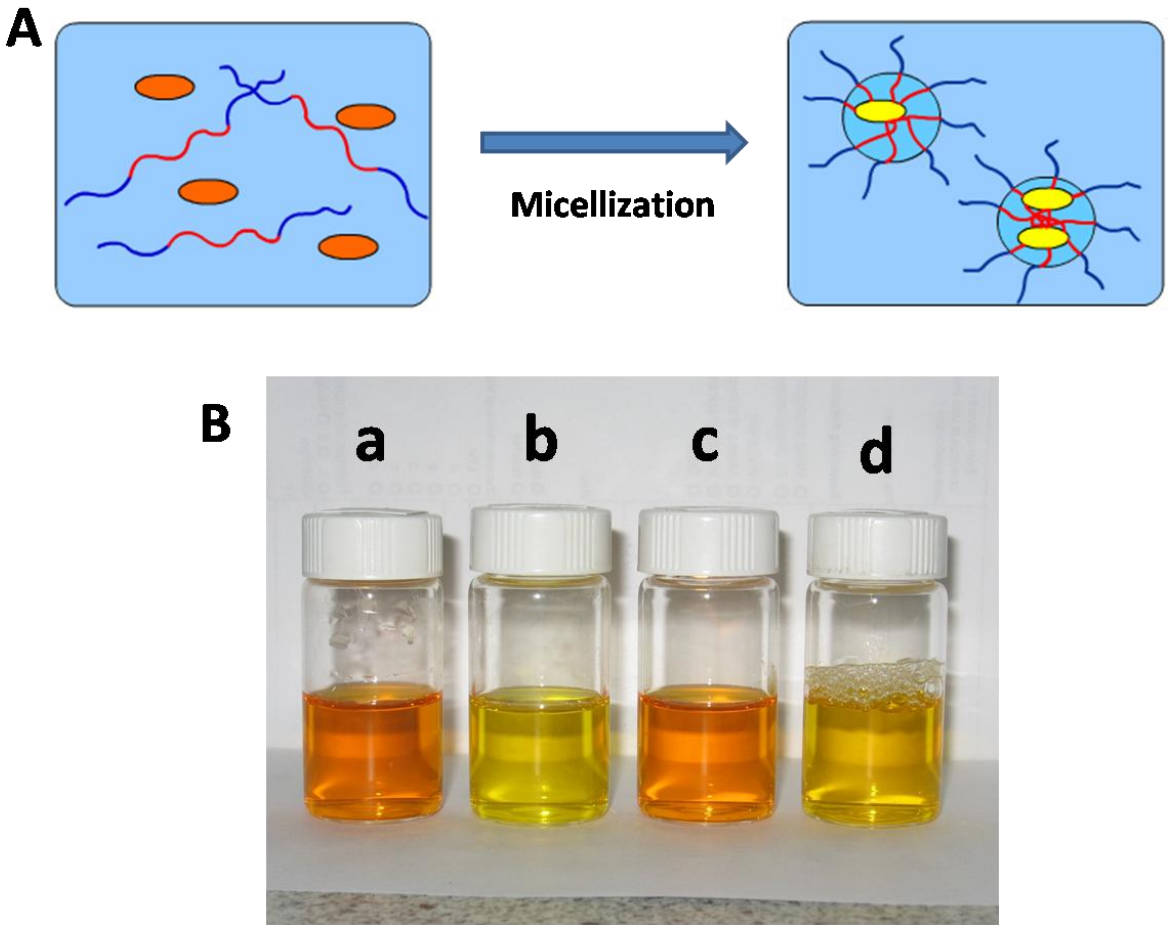

Figure 3.1.2: A) The behaviour of EO in aqueous surfactant solution. B) Photograph of EO solutions a) in water, b) in propanol, c) in aqueous surfactant solution (no micelle) and d) in aqueous surfactant solution (micelle exists).

The micellization of the pluronic surfactants can be determined by three different ways using the UV-Vis Spectra of the EO solutions. First and the simplest method is to follow the λ_{max} of the resulting peak. For the second and third methods, the UV-Vis absorption peaks need to be deconvoluted. The deconvolution process

producing two peaks (at 430 and 480 nm). The second method compares the ratio of absorbance of these two peaks. The third method compares the shifts of the individual deconvoluted signals. Because, besides a change in the absorbance of these signals, they also shift to higher energy in non-polar solvents (~10 nm). In this thesis, we have followed the changes in λ_{max}. The P85 ($EO_{38}PO_{43}EO_{38}$) is used as the pluronic surfactant in order to determine the effect of the additives and temperature on the micellization properties of the pluronic surfactants. Because, the micellization of P85 has been widely investigated in the literature [67,100,116]. The CMC of P85 is high enough to easily observe the changes in the assembly process. **Figure 3.1.3** displays the UV-Vis spectra of different amounts of P85 in the EO solutions, (~10^{-6} M) at 25^{o}C. Note that the concentration of the EO solution was kept very low in order to keep its effect, on the micellization of P85, negligible and make sure most of the dye molecules stay in the core of the micelles in the solution. Notice that, at higher concentrations of EO, it might behave like an organic additive and affects the micellization of the pluronic surfactant [119]. In order to determine the CMC clearly, the λ_{max} values were used and plotted vs log (w/v%) of P85**.** **Figure 3.1.4** shows λ_{max} vs log (w/v%) plot and the CMC of P85 at 25^{o}C. The CMC of P85 at RT is 4 w/v%, which is consistent with the literature values [67].

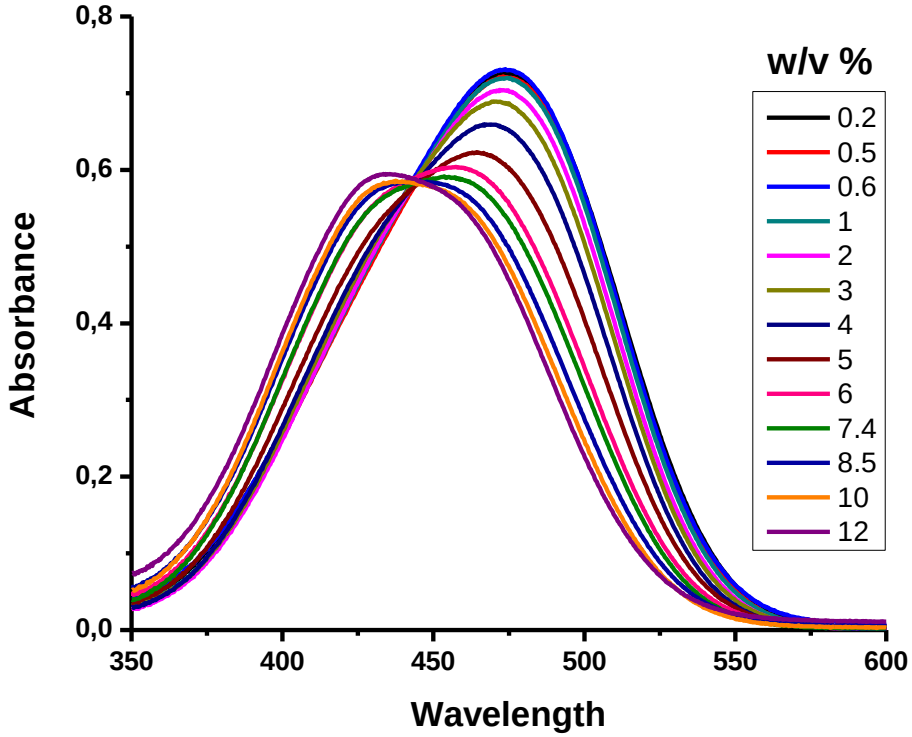

Figure 3.1.3: The UV-Vis spectra of different amounts of P85 (w/v%) in EO solutions.

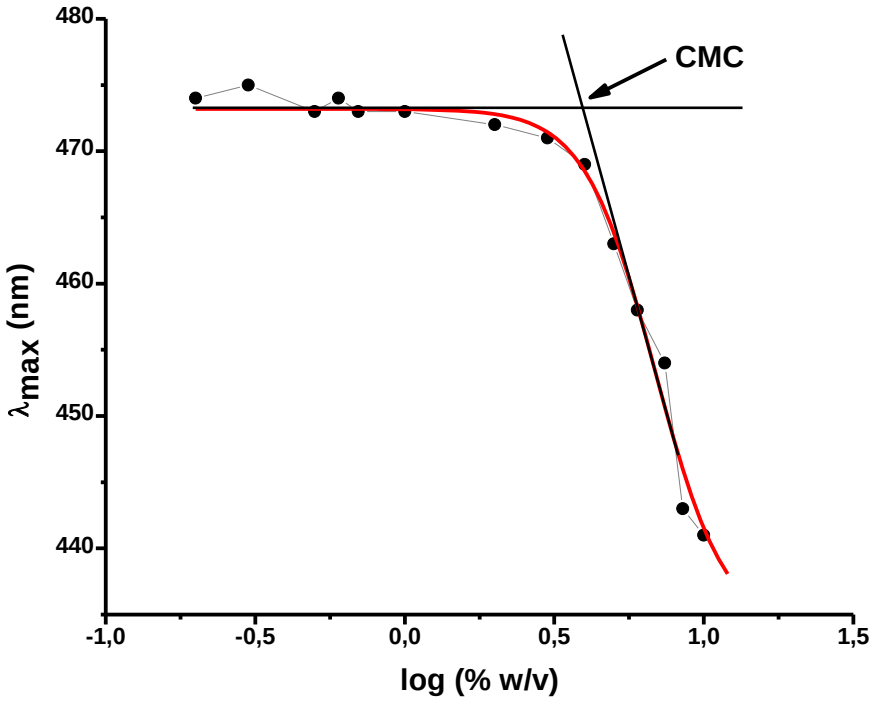

Figure 3.1.4: The λ_{max} vs. log P85concentration plot at 25 ^{o}C.

Micellization of the pluronic surfactants is a highly temperature dependent process [65,69,96,107,120] (**Figure 3.1.5**). The CMC decreases rapidly with increasing temperature, for example a 5°C increase in solution temperature can cause a ten fold decrease in the CMC of P85 (25°C to 30°C). Moreover, it is also true that a temperature increase causes a change in the micelle shape [105,106]. By increasing temperature, the λ_{max} decreases rapidly and approaches to its value in propanol. This can be interpreted as a change in hydrophobic character of the micelle. The micelle core gets dehydrated by taking more surfactant into the micelle and removing some water from the core or the corona (**Figure 1.7**). A size and geometry change of the micelles can also be expected, since the surfactants prefers to pack in a more effective way in order to keep water away from itself. Note also that the spectra of the aquous solution of EO, in these temperature interval, does not change.

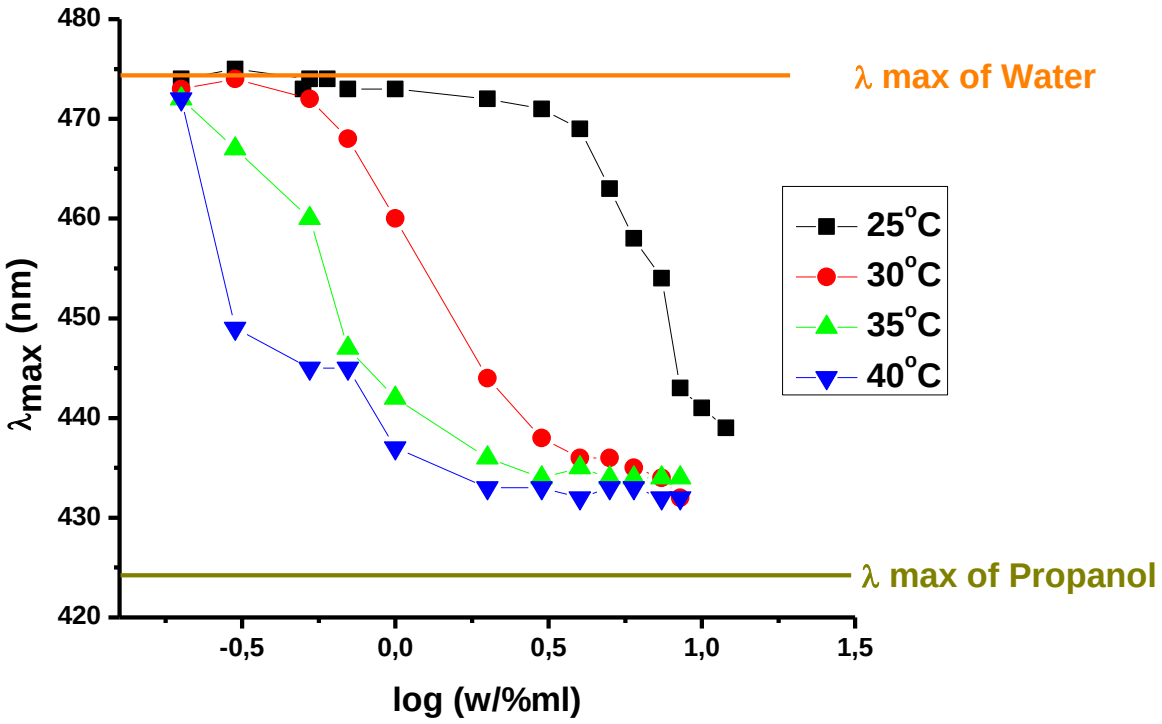

Figure 3.1.5: The λ_{max} vs. log P85concentration plot at ■ 25 °C, ● 30 °C, ▲ 35 °C and ▼40 °C.

Despite the fact that the micellization of the pluronic surfactants is very rapid and gives a quick respond to environmental conditions (temperature and additives), the micelles are quite stable in the solution and decomposition (di-micellization) of the surfactants takes several minutes. When the surfactant molecules are packed into the micelles, it is dificult to break them into individual surfactant molecules. **Figure 3.1.6** shows the changes in the UV-VIS spectra of 2 w/v% P85 (at 40^{o}C) with time (the spectra were recorded at RT). Notice that the peak at 432 nm gives no response for a while, then slowly shifts to 465 nm (RT value). Remember that the P85 molecules are in the micelle form at 40^{o}C and floats as individual molecules in water at 25^{o}C. This observation shows that as long as the micelles exist, the EO prefers to be in the core of the micelle and when the micelles are broken into molecules, the EO molecules sense the aquous media. The di-micellization starts roughly after six minutes so as the change of λ_{max} (**Figure 3.1.7**) for given temperature and concentration. This property of the micelles makes measurements easier at different temperatures. Therefore, solution can be heated to desired temperature, but the measurements can be done at RT for that desired temperature.

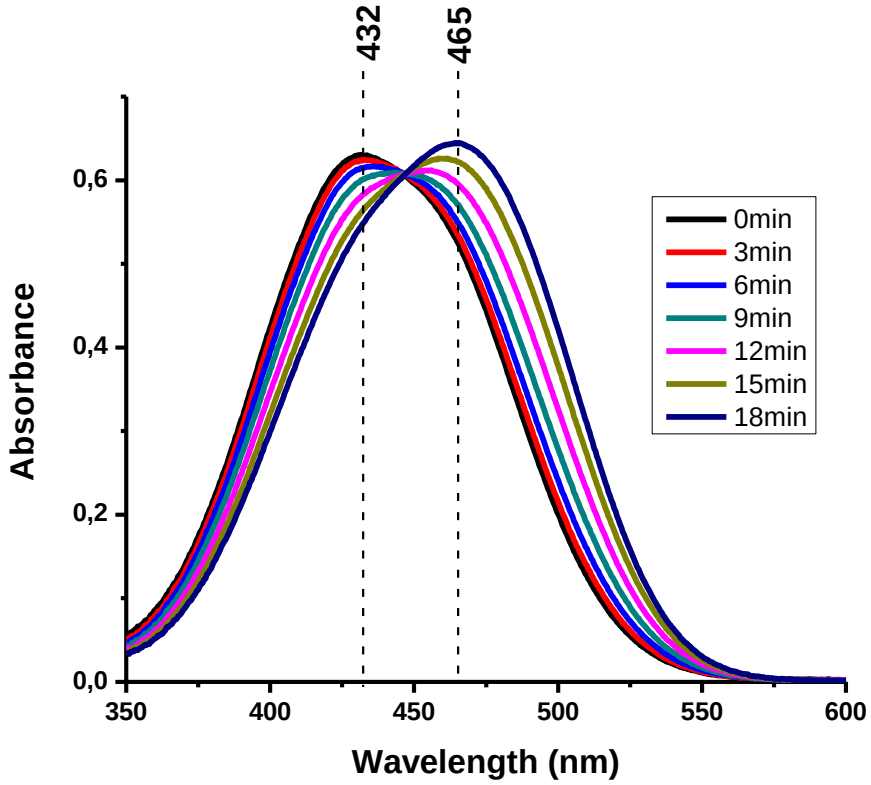

Figure 3.1.6: The UV-VIS spectra changes of the 2 w/v% P85 and ~10^{-6} M EO solution which is heated to 40°C for 3 hours and then kept at RT during the measurements.

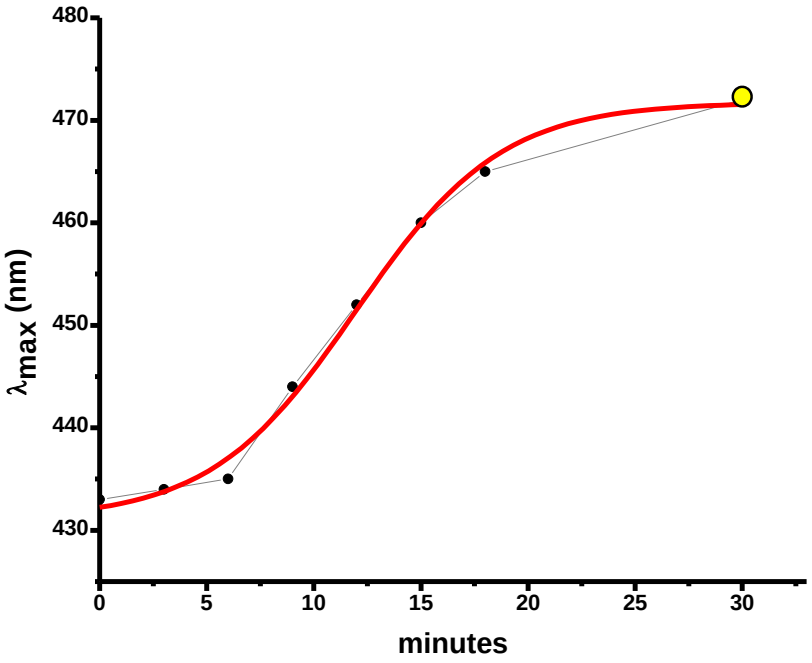

Figure 3.1.7: The plot of λ_{max} obtained from the spectra in **Figure 3.1.6** versus time at which the spectra were collected.

The anions of the alkali salts of the Hoffmeister series have a remarkable effect on the solubility and the micellization properties of the pluronic surfactants. A change in the solubility of pluronics not only affects the aggregation properties of the surfactants but also affects the pore structure, order and morphology of final mesostructured silica particles, if they are used in the synthesis media of mesoporous silica. The effects of anions on the pluronic surfactants can be classified in three groups. The first group is highly lyotropic anions, like F^- and SO_4^{-2}. These anions are very effective in terms of decreasing solubility even at very low concentrations. **Figure 3.1.8** and **Figure 3.1.9** show the changes in the CMC of P85 at various F^- and SO_4^{-2} concentrations, respectively. Note that, with increasing anion concentration, the micellization starts at lower concentrations and the λ_{max} reaches the plateau (432 nm) again at lower concentrations. The lyotropic anions have effects very similar to temperature changes (see **Figure 3.1.5**). At higher anion concentrations (F^- and SO_4^{-2}), the P85 is either in its cloudy point or insoluble in water.

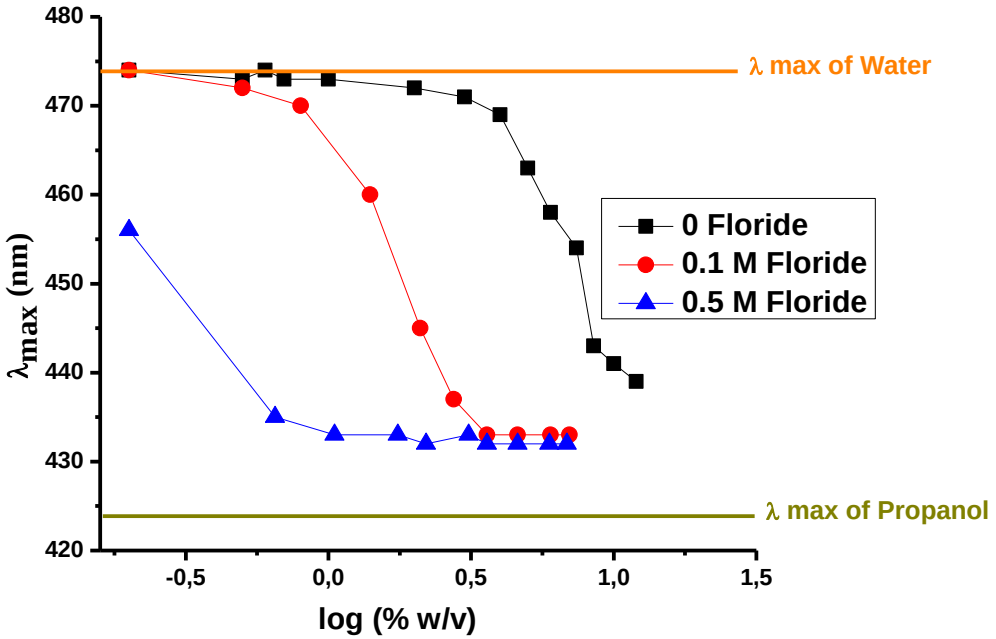

Figure 3.1.8: The λ_{max} of EO vs log P85concentration plot at ■ no ion, ● 0.1 M F^- and ▲ 0.5 M F^-.

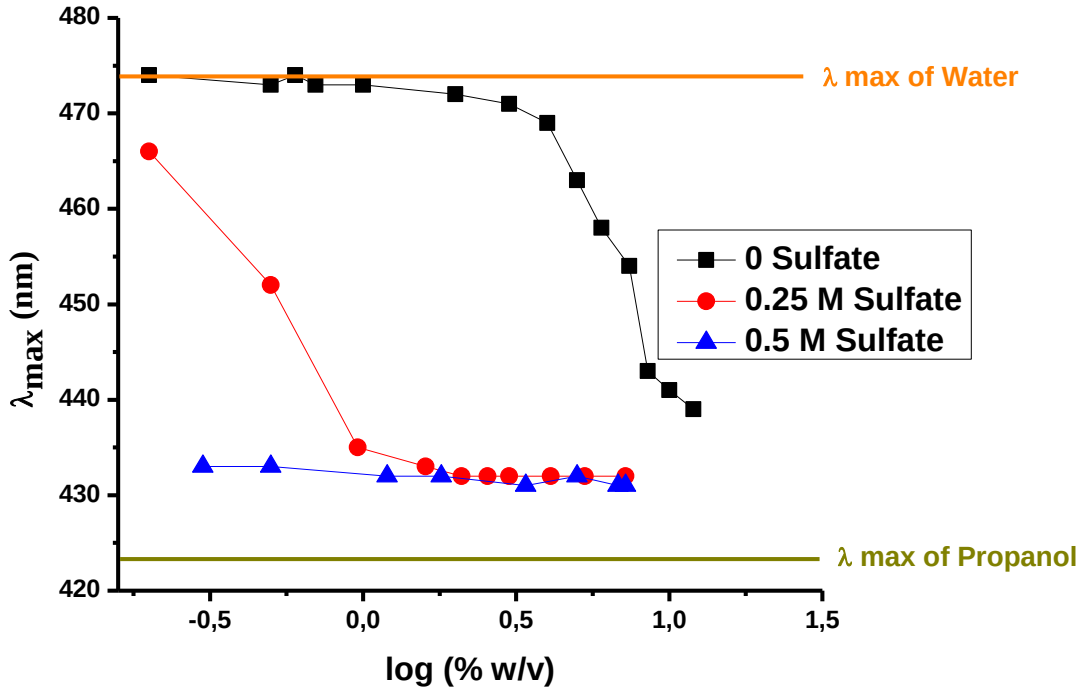

Figure 3.1.9: The λ_{max} of EO vs log P85 concentration plot at ■ no ion, ●0.25 M SO_4^{-2} and ▲ 0.5 M SO_4^{-2}.

The anions, like NO_3^- and I^- are in the second group and are not as effective as the lyotropic anions in decreasing solubility of the pluronic surfactant. These anions have no significant effect at low concentrations, however they decrease the solubility of the pluronic surfactants at higher concentrations (**Figure 3.1.10**). The last group of anions are the hydrotropic anions like SCN^-. These anions increases the solubility of the surfactant. Increasing salt concentration of these anions, results with an increase in the CMC (**Figure 3.1.11**). Moreover, in the presence of hydrotropic anions, the core of the micelles are more hydrated than the core of the micelles formed in presence of a lyotropic anion or at high temperatures. Note also that the EO solutions do not respond to the addition of salts. The only change is observed if EO is in a polar or non-polar environment, like aquous media and apolar core of a micelle.

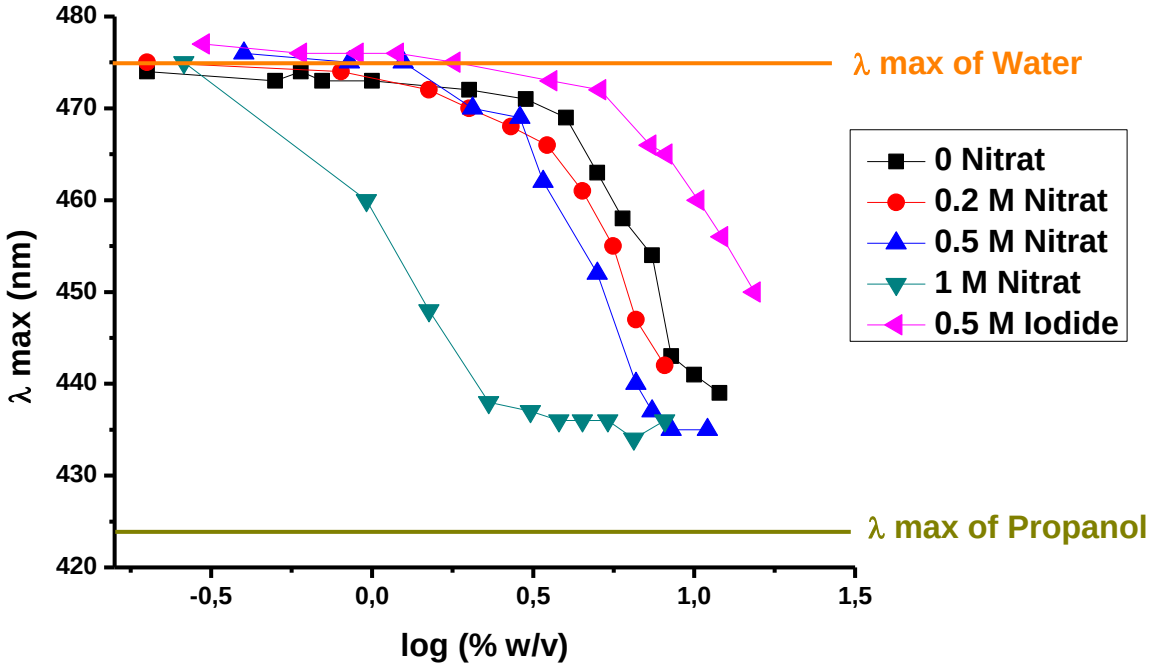

Figure 3.1.10: The λ_{max} of EO vs log concentration plot of P85 in the presence of ■ no ion, ● 0.2 M NO_3^-, ▲ 0.5 M NO_3^-, ▼1.0 M NO_3^- and ◄ 0.5 M I^-.

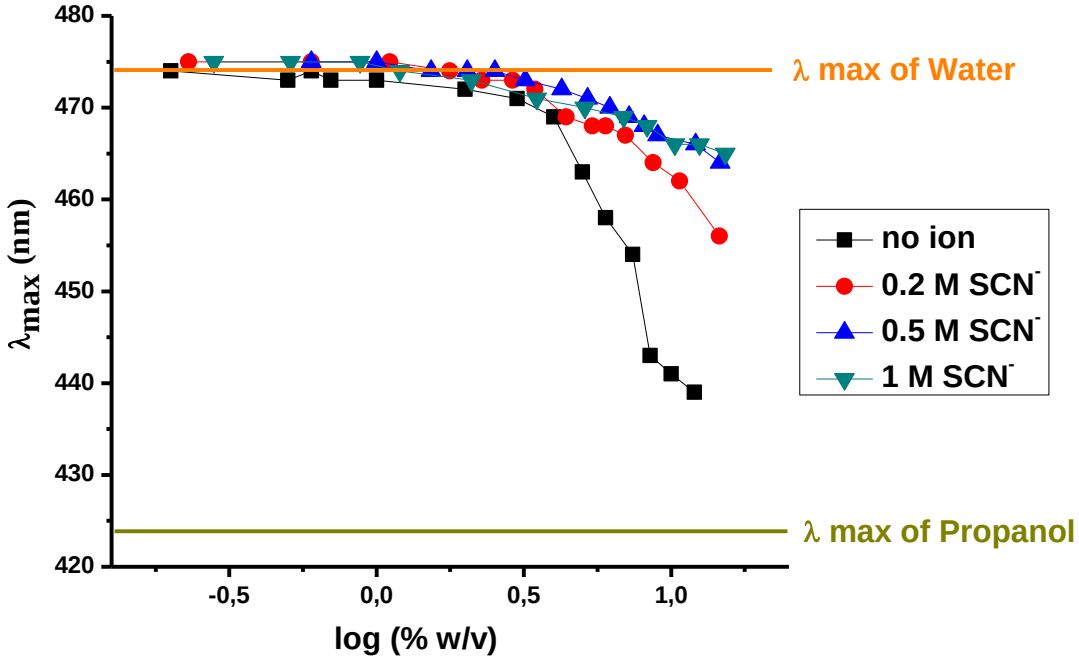

Figure 3.1.11: The λ_{max} vs of EO log P85concentration plot in the presence of ■ no ion, ● 0.2 M SCN^-, ▲0.5 M SCN^- and ▼1.0 M SCN^-.

Figure 3.1.12 shows the overall picture, which is a true representation of the Hofmeister series. In summary, the lyotropic anions decrease the solubility of the surfactant and CMC. In addition, for a given surfactant solution, the formed micelles have dehydrated core region that necessarily means an increase in the aggregation number of surfactant in the micelles. The anions, in the middle region of the series like NO_3^- and I^- (see **Figure 1.10**) do not have any significant effect on the micellization of the pluronic surfactants at low concentrations. However, they show a lyotropic character when they are used in high concentrations. The hydrotropic anions, increases the surfactant solubility at all concentrations and its effect on the solubility of surfactants increases with increasing salt concentrations.

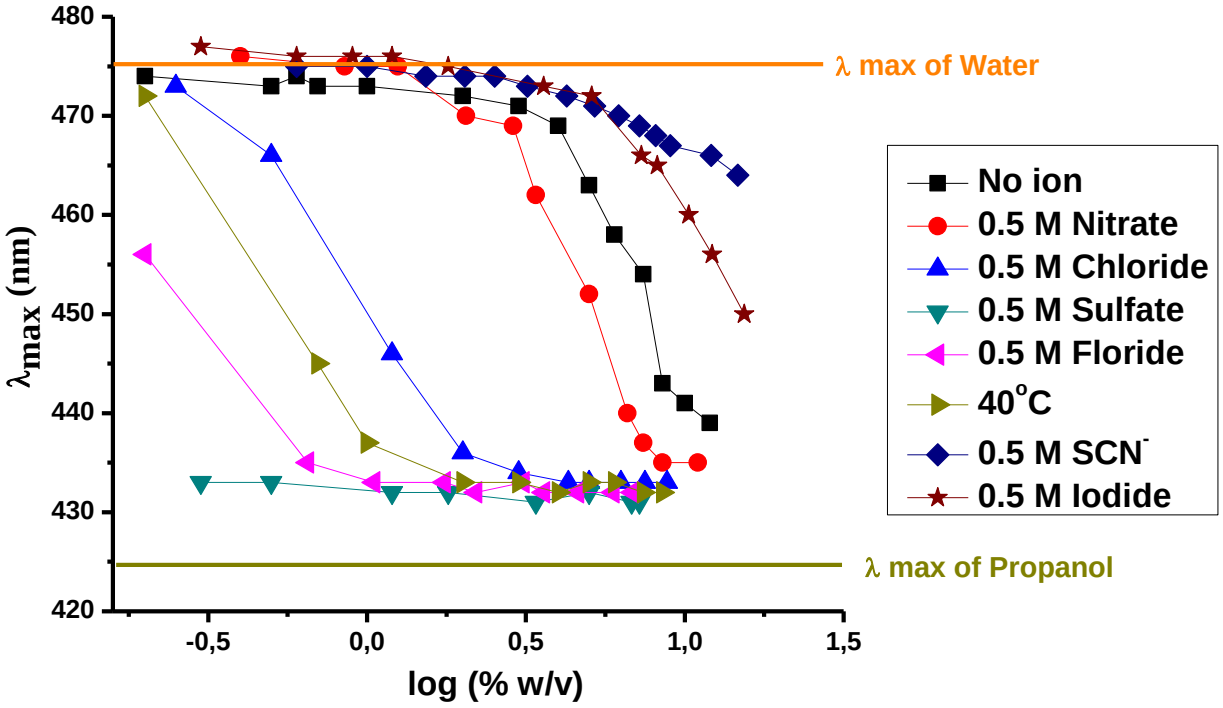

Figure 3.1.12: The λ_{max} of EO vs log P85 concentration plot in the presence of ■ no ion, ● 0.5 M NO_3^-, ▲ 0.5 M Cl^-, ▼0.5 M SO_4^{2-}, ◄ 0.5 M F^-, ►40°C, ♦ 0.5 M SCN^- and 0.5 M I^-.

All the plots converge to 432 nm at the end of micellization process; this is the position of the first signal when any spectrum is deconvoluted. Another comparison can be made by taking the absorbance ratio of the two signals after deconvolution. When this comparison is done, it can be clearly seen that the core of the micelles, in the presence of lyotropic anions or at high temperatures, is much drier (dehydrated). On the other hand, when hydrotropic anions are used, the core of the micelles is more hydrated. The most plausible explanation is the penetration of hydrotropic anions with water towards the core. Thus, they carry water to the core of the micelles, wet and increase the solubility of surfactants in aqueous media.

3.2. The Role of CTABr on the Mesoporous Silica Particle Formation:

The ambiguity in the cooparative micellization of the pluronic surfactants and CTABr arises form the difficulty in making measurements at high temperatures (95^{o}C). Therefore, the role of the CTABr on the formation of the pluronic based mesoporous silica particles is still not clear. It has been mentioned before that they micellize together at low temperatures. The CTAB-P123 system has been used to investigate the role of CTABr on the mesoporous particles. The CTAB/P123 ratio was varied between 0.0 and 10.0. In the absence of CTABr (CTAB/P123 ratio is 0.0), one obtains disordred silica particles without any distinct morphology (**Figure 3.2.1**). With increasing CTABr amount, first particles seem to be more rounded with a wormlike morphology. A transition, at around a CTAB/P123 mole ratio of 3.0, is observed, in which the wormlike and spherical particles coexist. When the CTAB/P123 mole ratio reaches to 4.0, all the particles are in a spherical morphology. A further increase in the CTABr amount does not affect the morphology of the formed particles. However, at higher CTAB/P123 ratio (higher than 4.0), a thin mesostructured silica film formation has also been observed in the air-water interface. The thickness of the film depends on the amont of extra CTABr. **Figure 3.2.2** shows the SEM image and PXRD pattern of the mesostructured film samples. Note that the unit cell of the film is too low to be originated from the CTAB/P123 couple. Note also that the FT-IR spectrum of the film sample resembles the spectrum of the mesostructured film synthesized by using only CTABr (**Figure 3.2.3**). Therefore, we conclude that CTABr is involved in the formation of mesostructured silica particles and changes its morphology up to a critical concentration (CTAB/P123 ratio is 4.0) and the excess CTABr goes to the air-water interface and forms mesostructured films.

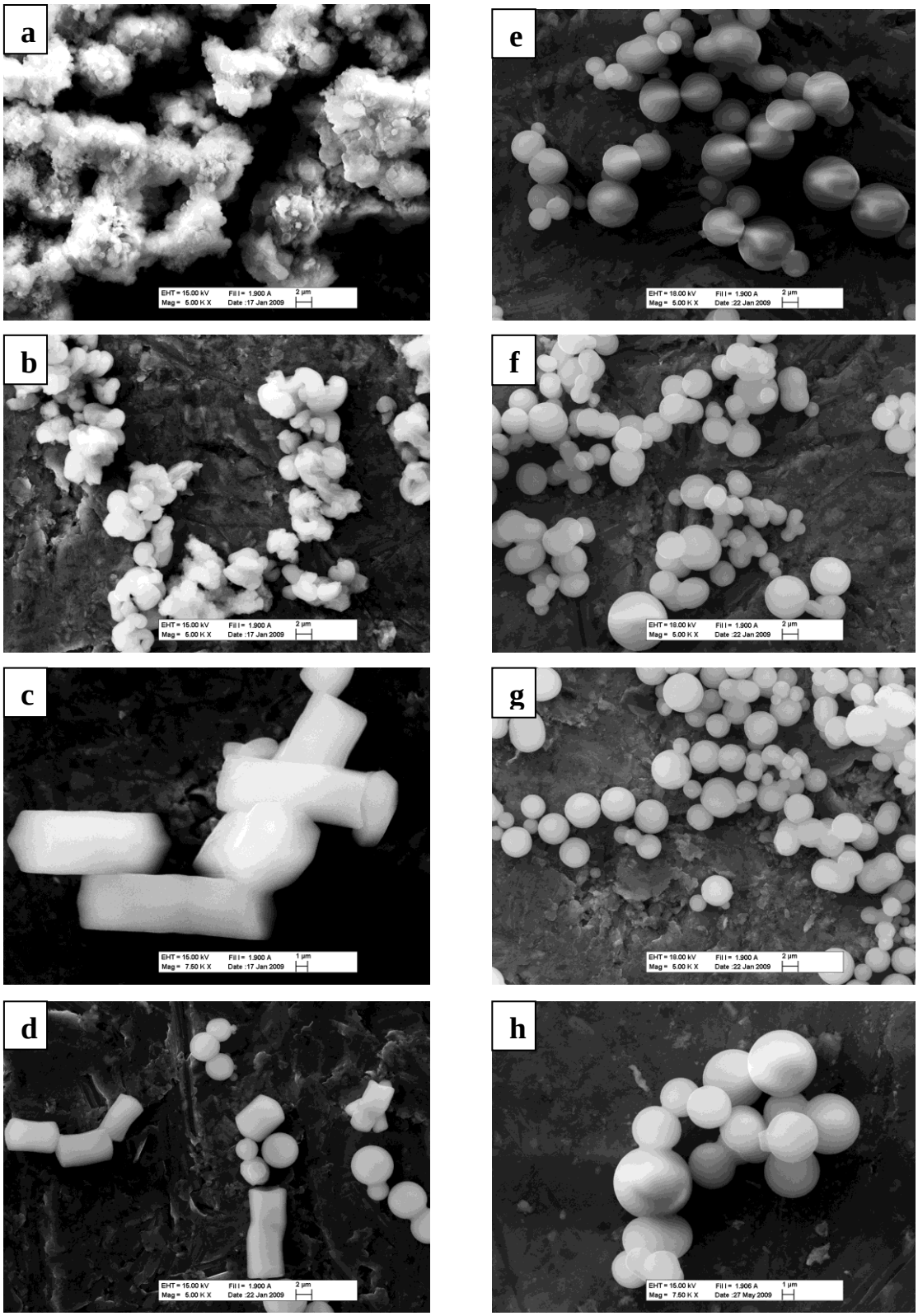

Figure 3.2.1: The SEM images of the mesostructured silica particles obtained from the CTAB-P123 systems with a CTAB/P123 mole ratio of (a) 0.0, (b) 1.0, (c) 2.0, (d) 3.0, (e) 4.0, (f) 5.0, (g) 6.0, and (h) 10.0.

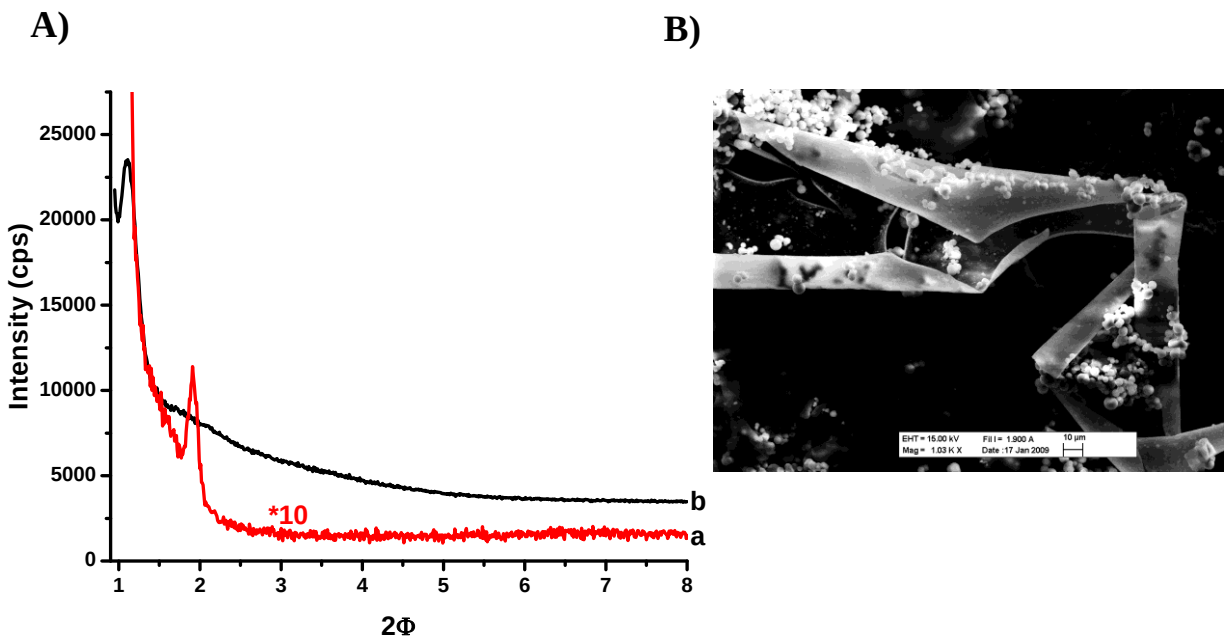

Figure 3.2.2: A) The PXRD pattern of the mesostructured silica film (a) and (b) powder particles obtained from the CTAB-P123 system with a CTAB/P123 mole ratio of 4.0. B) The SEM image of the mesostructured silica film.

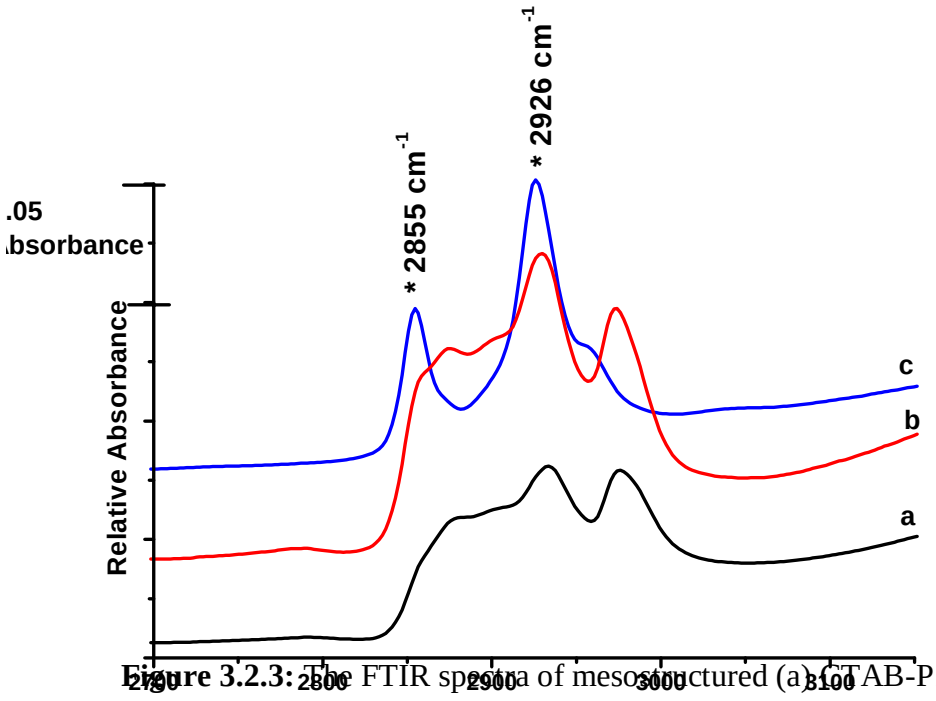

Figure 3.2.3: The FTIR spectra of mesostructured (a) CTAB-P123-SiO_2 particles, (b) silica film and (c) CTABr-SiO_2 particles.

The structure of the silica particles was determined using PXRD. In the absence of CTABr, one obtains disordered particles. Increasing CTABr amount step by step increases the order and a 2D Hexagonal mesostructure is observed up to a CTAB/P123 mole ratio of 3.0 and then a reduction in the unit cell is observed (**Figure 3.2.4**). The unit cell parameter **a** shifts to 9.2 nm and then to 9.6 nm by increasing the CTABr/P123 mole ratio to 6.0 and then to 10.0, respectively (See **Figure 3.2.4-d,e**). The inset in **Figure 3.2.4** clearly shows the (110), (200), (210) and (220) lines of the 2D hexagonal mesostructure. The typical unit cell parameter is in 9-10 nm range. Despite the fact that CTABr is essential in order to synthesize ordered mesostructured particles with distinct morphology. However, there is no direct relation between the CTABr amount and the BET surface area of the particles (**Table 3.2.1**). The mesoporous particles with high surface area (563.2 m^2/g) can also be synthesized using P123 without CTABr. However, there is a remarkable difference between the BET surface area of particles from the CTABr free system (CTABr/P123 mole ratio of 0) and the particles from the CTABr-P123 system (CTABr/P123 mole ratio of 1,2,3,4,5,6 and 10), which can be explained by the accessibility of the mesopores. In the absence of CTABr, the particles are disordered and probably some of the mesopores are closed. The CTABr molecules help forming ordered silica particles (~10 μm).

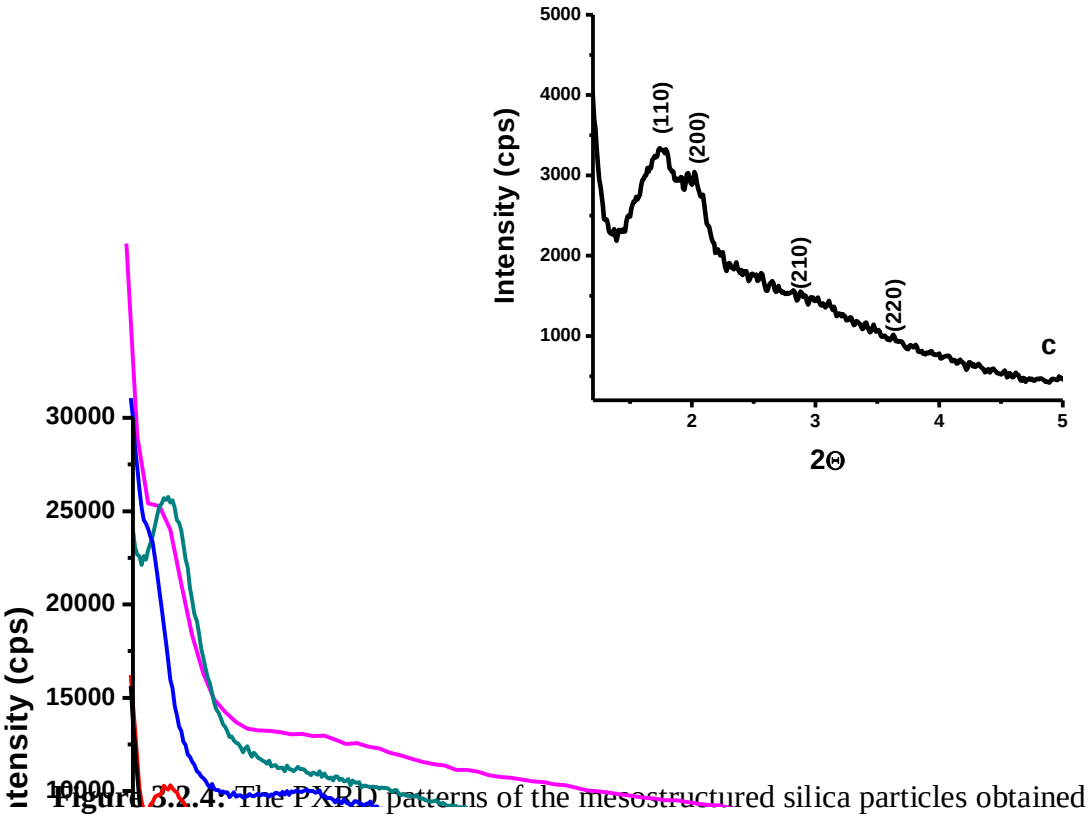

Figure 3.2.4: The PXRD patterns of the mesostructured silica particles obtained from CTABr-P123 systems with a CTABr/P123 mole ratio of (a) 0.0, (b) 1.0, (c) 3.0, (d) 6.0 and (e) 10.0.

CTMABr/ P123 (mole ratio)	BET surface area (m^2/g)	d_{100} (nm)	Pore diameter 2r (nm)	Wall thickness, t^a (nm)
0:1	**563**	----------	**14.8**	----------
1:1	**616**	----------	**6.9**	----------
2:1	**683**	**8.0**	**4.9**	**4.4**
3:1	**690**	**8.7**	**5.9**	**4.1**
4:1	**685**	**8.1**	**4.1**	**5.2**
5:1	**689**	**8.0**	**4.2**	**5.0**
6:1	**723**	**8.0**	**4.5**	**4.7**
10:1	**697**	**8.3**	**4.4**	**5.2**

[a] The wall thickness t is obtained by deducing the pore diameter (2r) from the unitcell a_o ($a_o = (2/\sqrt{3})d_{100}$), namely, t= a_o 2-r.

[b] Pore diameter is calculated from the adsorption branch of the isotherm by BJH method.

Table 3.2.1: The structural parameters of the silica particles obtained from the CTABr-P123 system with different CTABr/P123 mole ratios.

Figure 3.2.5 displays the N_2 sorption isotherms and pore size distributions of the samples investigated from the CTABr-P123 system. All the samples have type IV isotherm except, the samples prepared using 0.0 and 1.0 CTABr/P123 mole ratios. At low CTABr/P123 mole ratios (0.0 and 0.1), the silica particles are disordered and show very little mesoporosity (see **Figure 3.2.5**) and display type II isotherms. The samples having type II isotherms are propably non-porous or macroporous [29]. However, the high surface area rules out the non-porosity (**Table 3.2.1**). In the absence of CTABr, most of the P123 micelles are aggregated without any order and

silica species coat these disordered P123 micelles in the solution, therefore the silica materials with low CTAB/P123 mole ratio show very broad pore size distribution (**Figure 3.2.6**). Starting with 2:1 CTAB/P123 mole ratio, the isotherms turn to type IV, which is very characterstic for mesoporous materials. The desorption branch of an isotherm generally gives information about the pore structure [29,135-137]. The desorption branch generally shows hysteresis because of the late evaporation of N_2 from the pore surface (capillary condensation). At low CTABr/ P123 mole ratios (0.0 and 1.0), desorption branch of the isotherms show type III hysteresis, which generally indicates a slit-like pore structure [29]. Above 1.0 CTABr/P123 mole ratio, all the particles show type I hysteresis indicating a regular, spherical and an open pore structure [29,135].

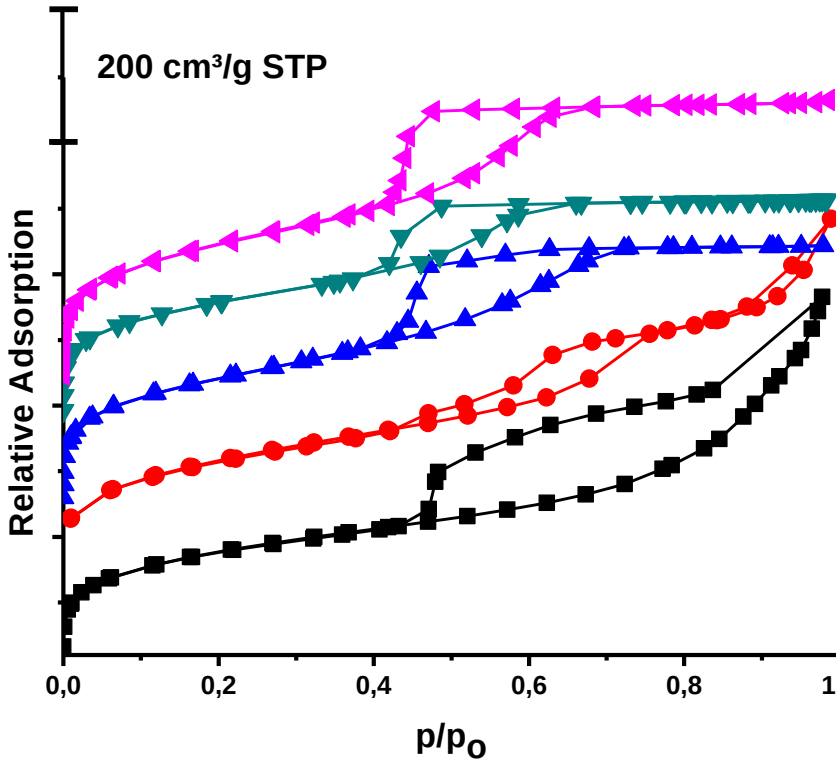

Figure 3.2.5: The N_2 adsorption-desorption isotherms at 77K for CTAB-P123 system in different CTAB/P123 mole ratios, ■ 0:1, ● 1:1, ▲ 2:1, ▼4:1 and ◄ 6:1.

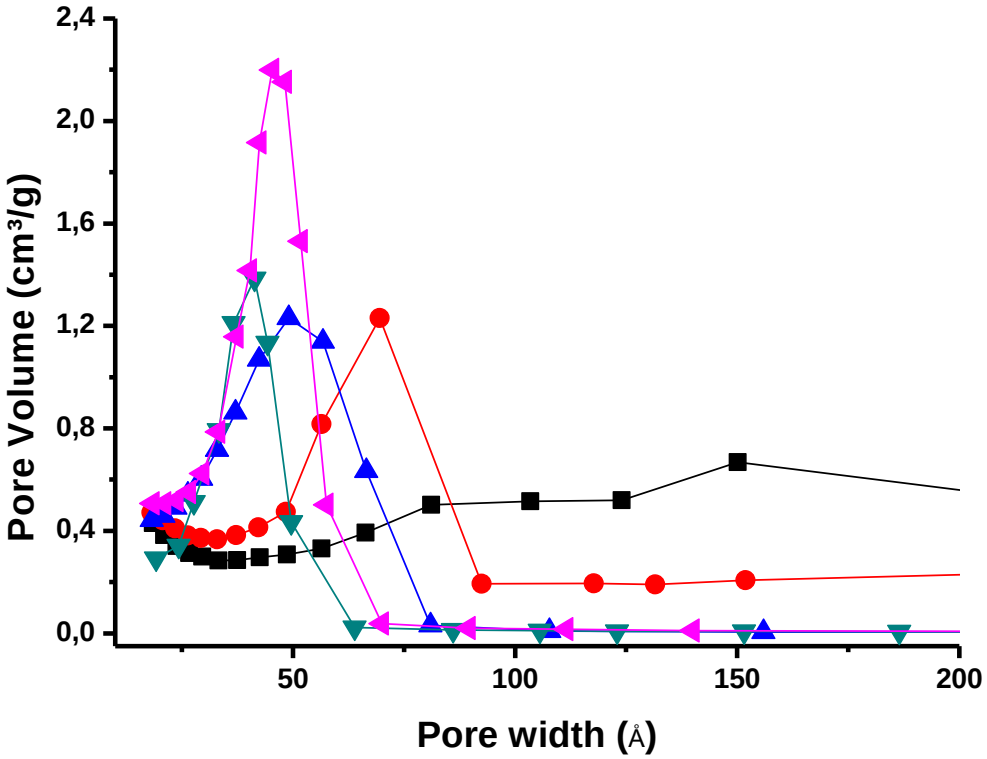

Figure 3.2.6: The BJH Adsorption pore size distribution (diameter) for CTAB-P123 system in different CTAB/P123 mole ratios, ■ 0:1, ● 1:1, ▲ 2:1, ▼4:1 and ◄ 6:1.

As stated before, CTABr has a key role in the micellization and aggregation of the micelles of P123. In the absence of CTABr, the silica particles have very broad pore size distribution (**Figure 3.2.6**) and an irregular pore structure. **Figure 3.2.6** clearly show that there is no regular pore in absence of CTABr, and regular and much uniform pore size distribution can be obtained by increasing CTABr/P123 mole ratio. Notice also that the pore size gets uniform and narrower with increasing CTABr in the reaction media, see **Figure 3.2.6**. CTABr breaks the aggregated P123 domains and help them to disperse into the solution as individual micelles. A very narrow pore size distribution can be interpreted as the formation of one type of micelle in the solution. One important question is the high surface area of the particles with low CTAB/P123 mole ratio **(Table 3.2.1)**. T-plot might help to understand the reasons

behind such a high surface area for these particles. This method is generally employed for determination of the micropores in a mesoporous system [31,36,37,39,135]. **Figure 3.2.7** shows the t-plots of the mesosturctured silica particles in different CTAB/P123 mole ratios. In pure P123 system, the t-plot shows only a downward deviation from the lineatity (from the solid line passing through the origin) is observed, indicating micropores without any mesopores. Note that the t-plot does not give information about the very large pores (macropores). However, N_2 adsorption-desorption isotherms (see **Figure 3.2.5**) of CTABr free sytem shows adsorption in macroporous range. Therefore, in the absence of CTABr micropores and macropores exist together. When the CTABr/P123 mole ratio is 1.0, the t-plot shows a downward deviation from the linearity followed by an upward deviation. A downward and following upward deviations from the linearity indicate two pore systems in the particles. Moreover, N_2 adsorption-desorption isotherms (see **Figure 3.2.5**) shows a small adsorption at macroporous range, so the particles synthesized from CTABr/P123 mole ratio of 1.0 has three pore structure together; micropore, mesopore and macropore. A further increase in the CTABr/P123 mole ratio causes almost disappearance of the downward deviation and a sharper upward deviation indicating that the particles have mainly mesopore and a little amount of micropores. The little microporosity originates from the interwall micropores, which are formed by the coverage of hydrated poly (ethylene oxide) groups by silica species. Note that these particles also have no adsorption at macroporous range (see **Figure 3.2.5**). That means when the CTABr/P123 mole ratio is higher than 2.0, the particles have mainly mesopores, little amount of micropores and no macropores.

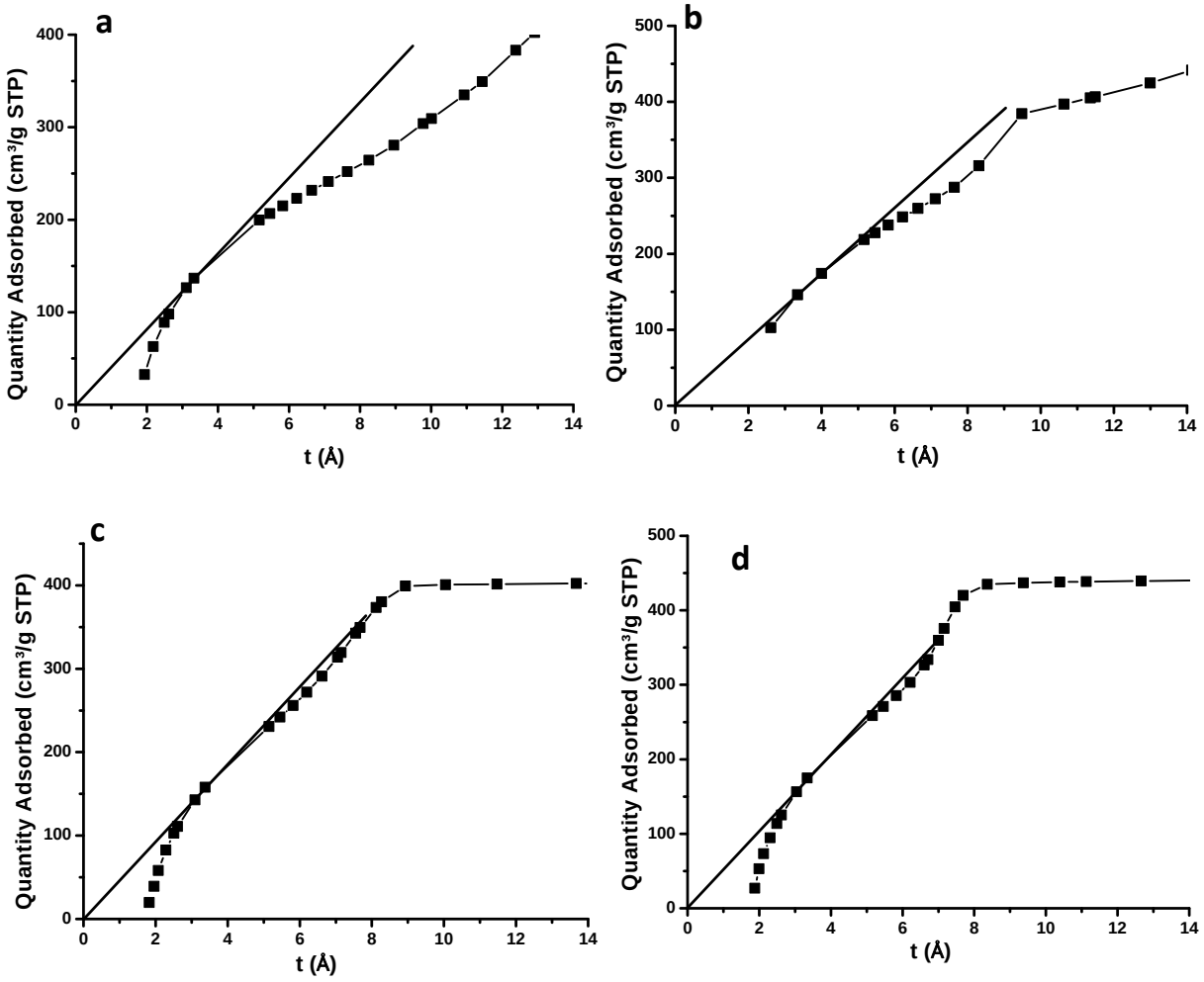

Figure 3.2.7: The t-plots for the N_2 adsorption isotherms at 77K for CTABr-P123 system at different CTABr/P123 mole ratios, a) 0.0, b) 1.0, c) 2.0, and d) 6.0.

As seen from the PXRD patterns and isotherms of the silica particles obtained from the CTABr-P123 system in different CTABr amounts, CTABr exist as a co-surfactant in the P123 micelles and helps these micelles aggregate in a controlled way. The amount of CTABr in the formed silica particles can also be determined spectroscopically. The characteristic υ-CH stretching modes of P123 and CTABr are given in **Table 3.2.2** [118,138-143]. With increasing CTABr amount in the silica particles, signals at 2930 cm^{-1} and 2860 cm^{-1} get more intense, which originate from

CTABr (**Figure 3.2.8**). Note that the spectrum does not change above CTABr/P123 mole ratio of 4.0. It means that the CTABr-P123 system is saturated at around CTABr/P123 mole ratio of 4.0, see **Figure 3.2.8**.

Pluronic Surfactant	**Infrared Spectroscopy (cm^{-1})**	**Raman Spectroscopy (cm^{-1})**
Symmetric C-H stretching of CH_2	**2868**	**2950**
Antisymmetric C-H stretching of CH_2	**2933 (PPO)**	**2875 (PPO)**
Antisymmetric C-H stretching of CH_2	**2948 (PEO)**	**2885 (PEO)**
Symmetric C-H stretching of CH_3	**2900**	**2935**
Antisymmetric C-H stretching of CH_3	**2980**	**2970**
CTMABr	**Infrared Spectroscopy (cm^{-1})**	**Raman Spectroscopy (cm^{-1})**
Symmetric C-H stretching of CH_2	**2850**	**2846**
Antisymmetric C-H stretching of CH_2	**2920**	**2885**
Symmetric C-H stretching of CH_3	**2872**	
Antisymmetric C-H stretching of CH_3	**2940 ($C-CH_3$)**	
Antisymmetric C-H stretching of CH_3	**2960 ($N-CH_3$)**	

Table 3.2.2: Characteristic FT-IR and Raman υC-H stretching frequencies of P123 and CTABr [118,138-143].

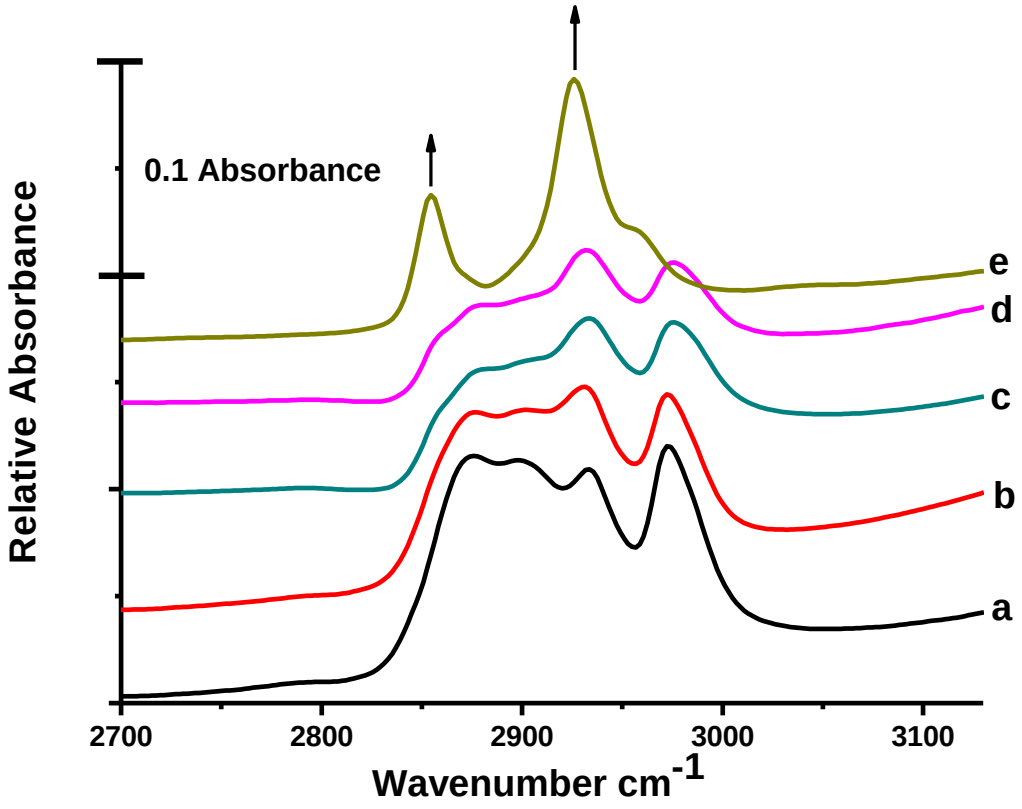

Figure 3.2.8: The FT-IR spectra of the mesostructured silica particles obtained the from CTABr-P123-SiO_2 systems with a CTABr/P123 ratio of (a) 0.0, (b) 1.0, (c) 4.0, (d) 10.0 and (e) CTAB-SiO_2.

3.3. The Role of Pluronic Surfactant on the Morphology of the Mesoporous Silica Particles:

By using a similar procedure mesostructured silica spheres, wormlike particles and single crystals were synthesized using P65, P85, P103 and F127 tri-block copolymers together with a cationic surfactant (CTABr). For all type of pluronic surfactants a wide range of CTABr concentration was tested (CTABr/Pluronic mole ratio is between 0.0 and 6.0). The resulting morphologies out of these experiments were tabulated in **Table 3.3.1**. A generalization can be made from the **Table 3.3.1** is that certain amount of CTABr is needed in order to obtain one type of morphology from the CTABr-Pluronic systems. The largest surfactant, F127, requires the highest amount of CTABr (CTABr/F127 mole ratio is 5) to obtain its final morphology, single crystals. General trend in the morphology is; disordered-wormlike-sphere-single crystal by increasing CTABr/Pluronic in the synthesis medium. The pluronic surfactant (no CTABr) is used at above its cloudy point (CP) at synthesis temperature (95^{o}C), therefore the formed particles are disordered and do not have regular pore size and pore structure. Under above conditions, there is no micellization of the pluronics. When CTABr is used as a co-surfactant, it increases the solubility of the pluronic surfactants and enhances the micellization (most propably elongated micelles at initial concentrations). These micelles form either egg shaped or wormlike particles depending on the CTABr amount (first elongated and then egg shaped), then with increasing CTABr concentration wormlike and spherical micelles are also formed. A further increase in the amount of CTABr causes the formation of spherical micelles and their controlled assembly results single crystal morphology.

Pluronics:	CTAB/ Pluronic (mol ratio)	Morphology:
P65 $EO_{20}PO_{30}EO_{20}$	0.0 – 2.0	Disordered
	2.0 – 4.0	Sphere
	4.0 – 6.0	Sphere + Films
P85 $EO_{27}PO_{33}EO_{27}$	0.0 – 1.0	Disordered
	1.0 – 2.0	Wormlike
	2.0 – 4.0	Sphere
	4.0 – 6.0	Sphere + Films
P103 $EO_{17}PO_{55}EO_{17}$	0.0 – 1.0	Disordered
	1.0 – 2.0	Wormlike
	2.0 – 3.0	Sphere + Wormlike
	3.0 – 4.0	Sphere
	4.0 – 6.0	Sphere + Films
P123 $EO_{20}PO_{70}EO_{20}$	0.0 - 2.0	Disordered
	2.0 – 3.0	Wormlike
	3.0 – 4.0	Sphere + Wormlike
	4.0 – 5.0	Sphere
	5.0 – 10.0	Sphere + Films
F127 $EO_{106}PO_{70}EO_{106}$	0.0 – 2.0	Disordered
	2.0 – 4.0	Sphere
	4.0 – 5.0	Rhombododecahedron + Sphere
	5.0 – 6.0	Rhombododecahedron

Table 3.3.1: The morphology of CTABr-Pluronic-SiO_2 at various CTABr/Pluronic mole ratios.

Figure 3.3.1 shows the SEM images of a series of samples obtained from the CTABr-Pluronic systems. The trend in the morphology follows the hydrophilicity of the used pluronic surfactant. The most hydrophilic surfactant (F127) forms mesoporous spheres at low CTABr concentrations (CTAB/F127 mole ratio 2.0 – 4.0) and forms single crystals at higher CTABr concentrations (CTABr/F127 mole ratio above 4.0. The same situation is valid for other surfactants, which form wormlike particles at low CTAB/Pluronic surfactants and forms spherical particles at high CTAB/Pluronic mole ratios. However, relatively more hydrophobic surfactants, like P103 and P123, require more CTABr in order to form spherical particles than the relatively more hydrophilic pluronic surfactants, such as P65 and P85. In other words, the hydrophobic character of the pluronic surfactant determines the amount of required CTABr in order to obtain a desired morphology. Remember that CTABr is not only required for changing the morphology of the formed mesostructured silica particles but it is also necessary to synthesize higly ordered mesoporous silica particles. The most remarkable effect of the CTABr is on the structural order of the formed mesoporous materials. In the absence of CTABr, it is not possible to synthesize ordered particles using pluronics. One of the major problems is the synthesis temperature. At 95^{o}C both poly (propylene oxide) and poly (ethylene oxide) groups are dehydrated [63,65,67,155]**.** The pluronic surfactants are above their cloudy point and insoluble in water at this temperature.

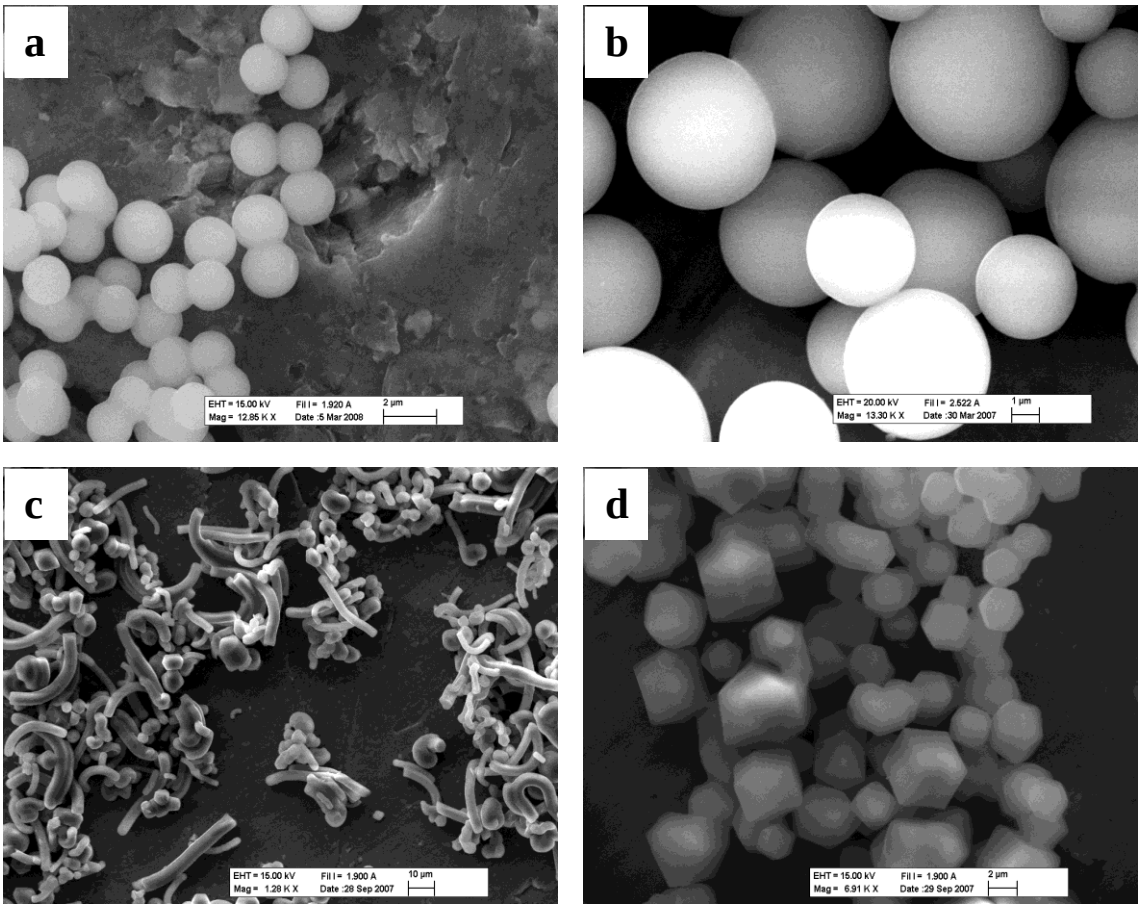

Figure 3.3.1: The SEM images of the mesostructured silica obtained from CTABr-Pluronic systems (a) CTABr/P65 system with a mole ratio 4.0, (b) CTABr/P85 system with a mole ratio 4.0, (c) CTABr/P103 system with a mole ratio 2.0 and (d) CTAB/F127 system with a mole ratio 5.0.

All mesoporous particles show 2D Hexagonal mesostructure except CTAB-F127 system. **Figure 3.3.2** shows the PXRD patterns of the as-synthesized mesostructured particles. Since the diffraction lines are not well resolved in CTABr-F127 system, it is not possible to determine the structure type. However, generally mesoporous particles synthesized using F127 show cubic mesostructure with a much larger unit cells [19,20,79,144]. The major diffraction lines are at lower angles and we could not observe them using our XRD set up (lower than 0.8, 2Θ). However, the samples prepared using P65, P85 and P103 display characteristic (100), (110) and (200) lines of the 2D hexagonal structure (**Figure 3.3.2**).

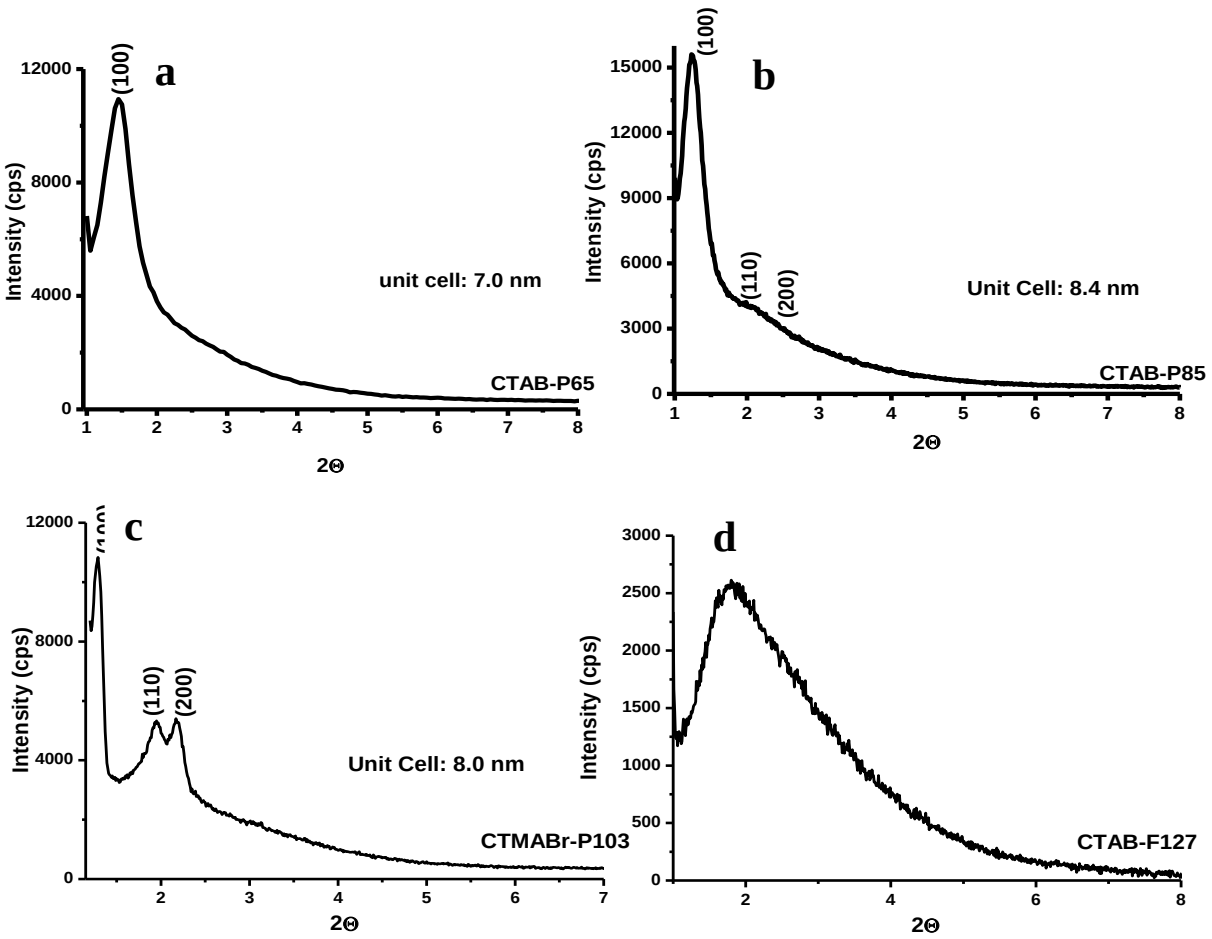

Figure 3.3.2: The PXRD patterns of the mesostructured silica particles obtained from the CTABr-Pluronic systems; (a) CTABr/P65 system with a mole ratio of 4.0, (b) CTABr/P85 system with a mole ratio of 4.0, (c) CTABr/P103 system with a mole ratio 2.0 and (d) CTABr/F127 system with a mole ratio of 5.0.

3.4. The Effect of Additives on the Synthesis of Mesoporous Silica Particles:

Both organic and inorganic additives have a significant impact on the assembly properties of pluronic and cationic surfactants. Influencing micellization properties of the pluronics also affects the meso-order of the mesoporous silica particles. The additives used in this work can be classified in two main groups; one is organic additives (Cyclohexane and Benzene) and the other is alkali metal salts of the anions from the Hofmeister series. The anions used in this work can be classified in four main groups; the first one is fluoride, which accelerates the silica polymerization and can be used to obtain uniform mesoporous particles at room temperature and in very short synthesis time. Despite fluoride ion is highly lyotropic anion and decreases the surfactant solubility, it was used in very low concentrations, where the effect of F^- ion on the surfactant assembly properties is negligible. The mesoporus materials synthesized using F^- will be discussed in the next chapter. The second anion used is the sulphate ion; it decreases the solubility of pluronics, as discussed before. The third anion is nitrate; it has almost no effect on the pluronic micellization, but it affects the assembly properties of the CTABr by interacting with the positively charged head group. The last anion tested is chloride, which affects both P123 and CTABr. Its effect is more like the combination of sulphate and nitrate. Benzene was used as the organic additive and it dissolves in the core and dehydrate corona of formed micelles and swells the micelles as a result the pore size of mesoporous materials. Moreover, it increases the order of mesoporous silica particles.

3.4.1. The effect of Sulphate:

The sulphate ions decrease the solubility of the pluronics and cause a more effective packing of these surfactants (see **Chapter 1**). A more effective packing means an increase in aggregation number with a geomertry change of the micelles (either a size or a shape change). When the surfactants are packed in a more effective way, the core of the micelle gets dehydrated in which the hydrophobic interaction gets stronger. This interaction causes the formation of more ordered mesoporous materials. **Figure 3.4.1** shows the PXRD patterns of the mesoporous silica particles synthesized using different SO_4^{2-} concentrations. In the absence of SO_4^{2-}, the particles display one sharp diffraction line due to (100) planes and the other lines (110 and 200) generally appear together as a broad peak. At low CTABr/P123 mole ratios (3.0 and 4.0), besides a very high diffraction intensity of (100) plane, the other diffraction lines ((110) and (200)) are also better resolved (**Figure 3.4.1-a,b**). Moreover, for the CTABr/P123 mole ratio of 3.0 and 0.5 M SO_4^{2-} concentration, diffraction lines originating from (210) and (300) planes are also observed (**Figure 3.4.1-a inset**).

Despite the fact that SO_4^{2-} ion helps the formation of more ordered particles at high CTABr/P123 mole ratio (6.0), increase in order is not that high when compared to particles synthesized at lower CTABr/P123 mole ratios **(Figure 3.4.1-c)**. First three diffraction lines ((100), (110) and (200)) are again well resolved, but they are broader and have lower intensity when compared to diffraction lines obtained from the particles synthesized at lower CTABr/P123 mole ratios. Lower order of these particles can be explained by high CTABr concentration. More hydrophobic core and larger micelles of P123 formed by sulphate addition can accommodate more CTABr molecules than sulphate free system and a CTABr rich micelle is more positively

charged. The charge repulsion between these micelles might decrease the order during the assembly process. However, excess CTABr molecules does not stay in the pluronic micelles during the entire synthesis process and leaves the micelle, because the FTIR and Raman spectra of these materials do not show any significant change originating from additional CTABr molecule, which is in the micelle at the beginning of the reaction. Moreover, for these samples an excess film formation is also observed (like CTABr-P123 system with mole ratio of 6.0). The likely explanation can be the number of CTABr molecules is high at the beginning of the assembly process (between the micelles and silica species) but the number decreases during the synthesis. Remember that, excess CTABr forms mesostructured film on the water-air interface and these films were collected before filtering process.

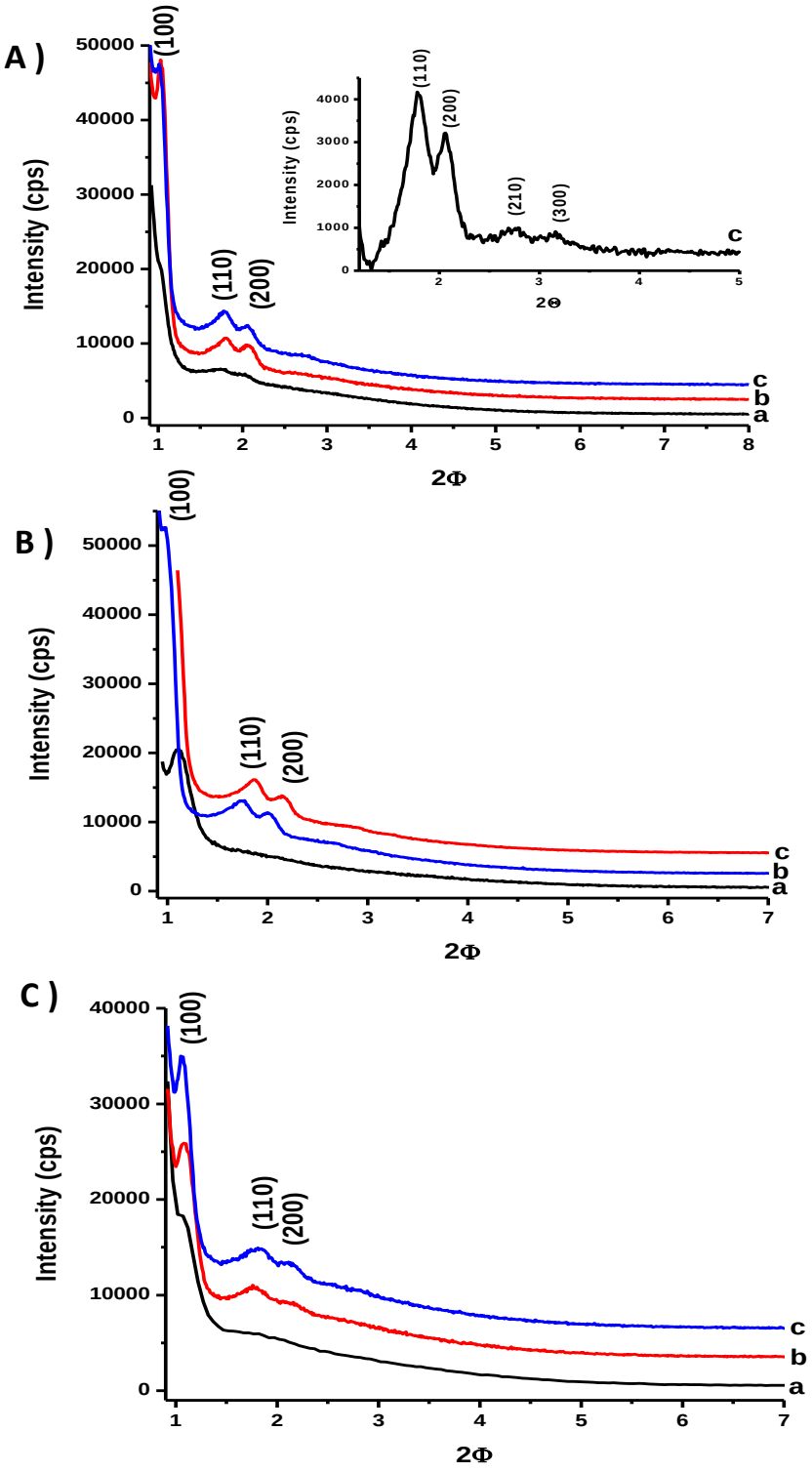

Figure 3.4.1: The PXRD patterns of the mesostructured silica obtained from the CTABr-P123 systems using at different CTABr/P123 mole ratios and at different SO_4^{2-} concentrations A) CTABr/P123 mole ratio of 3.0 (a) 0.0 M, (b) 0.25 M, (c) 0.5 M SO_4^{2-}, B) CTABr/P123 mole ratio of 4.0 (a) 0.0 M, (b) 0.25 M, (c) 0.5 M SO_4^{2-} and C) CTABr/P123 mole ratio of 6.0 (a) 0.0 M, (b) 0.25 M, (c) 0.5 M SO_4^{2-}.

The improved diffraction patterns with sulphate addition can be attributed to formation of better ordered particles with a long range order. The TEM images shown in **Figure 3.4.2** also prove this conclusion**.** A long range order in a meso scale can be clearly seen in these images. The spacing between the lines is around 9 nm, which is also consistant with the d-spacing measured by XRD. The darker parts in the images are the amorphous silica walls and the lighter parts shows the pore channels, where the channel structure is characteristic for 2D hexagonal mesoporous materials.

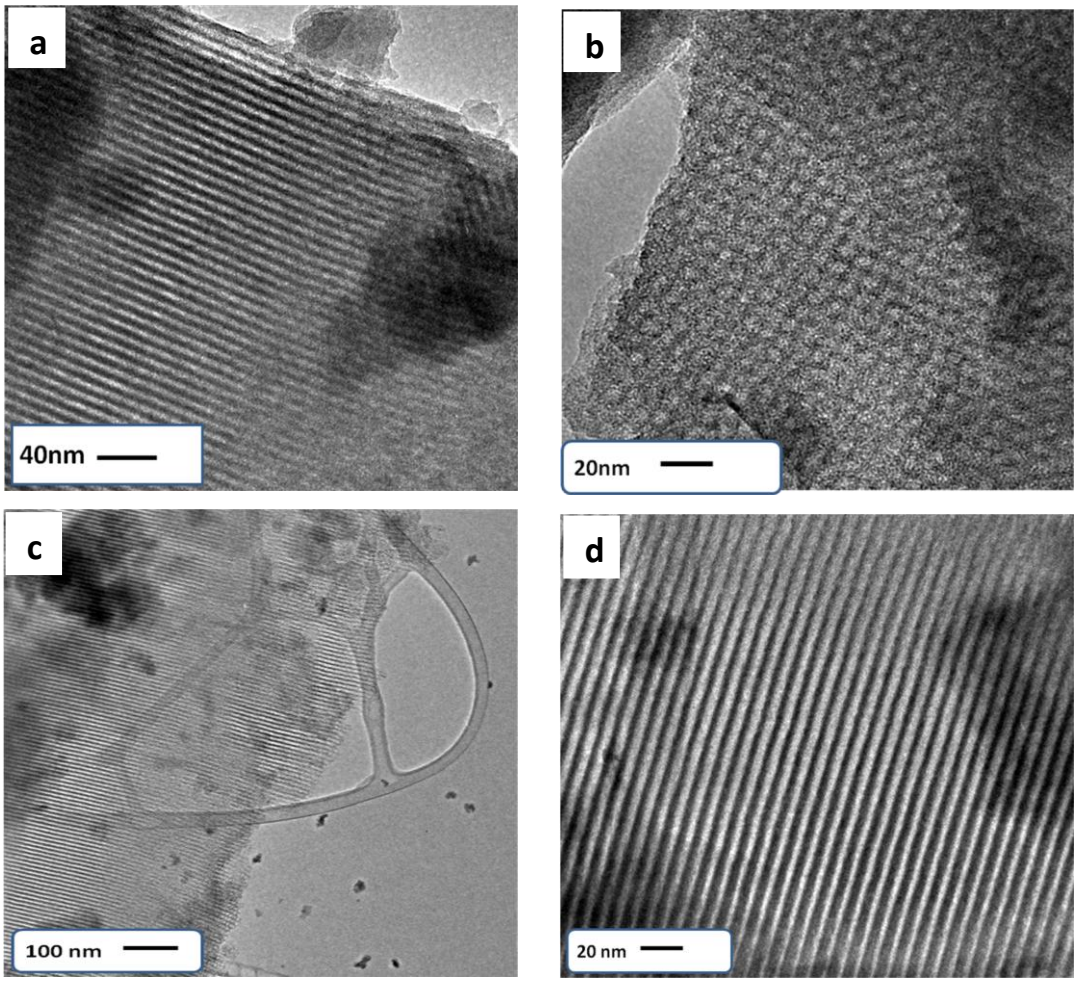

Figure 3.4.2: The TEM images of the mesostructured silica particles obtained from the CTABr-Pluronic-SO_4^{2-} systems, SO_4^{2-} ion concentration is 0.5M and the CTABr/P123 mole ratios of; (a), (b) 4.0 and (c), (d) 6.0.

The stronger hydrophobic interactions in the core of the micelles results in better ordered pore structure. Of course, these stronger interactions can also influence the morphology of the silica particles. **Figure 3.4.3** shows the SEM images of the particles obtained from the CTABr-P123-SO_4^{2-} system, at different CTABr/P123 mole ratios and SO_4^{2-} concentrations. Remember that the CTABr/P123 mole ratio of 3.0 (no sulphate) forms mainly spherical particals (minor wormlike morphology) and above this ratio all particles are spherical (see **Figure 3.2.1**). When the SO_4^{2-} ions are used, the particles are wormlike, even in the presence of 0.25 M SO_4^{2-}, and longer wormlike particles are observed, when the SO_4^{2-} concentration is 0.5 M for the same CTABr/P123 mole ratio of 3.0. Under these conditions, rarely spherical particles are observed. At a CTABr/P123 mole ratio is 4.0, most of the particles are wormlike and small fractions remain spherical, but not perfect spheres. However, in the absence of SO_4^{2-}, for the same CTABr/P123 mole ratio, all the particles have a perfect spherical morphology. At higher CTABr concentrations (CTABr/P123 mole ratio of 6.0), the particles are spherical (with cornered surfaces rather than smooth surfaces). Higher SO_4^{2-} concentrations were also tested (1 M and 2M); where it is not possible to dissolve the pluronic surfactants. Because the lyotropic anions especially sulphate and flouride sharply decrease the CMC and CMT of pluronic surfactants. The solution becomes cloudy at high sulphate concentrations (0.25 M and 0.5 M), indicating that the P123 molecules aggregate into much larger particles. On the other hand at high SO_4^{2-} concentrations, the CTABr surfactatant is completely soluble, upon addition of CTABr to above cloudy solution, the solution becomes clear, indicating that the P123 aggregates break down to micelles and to molecular species.

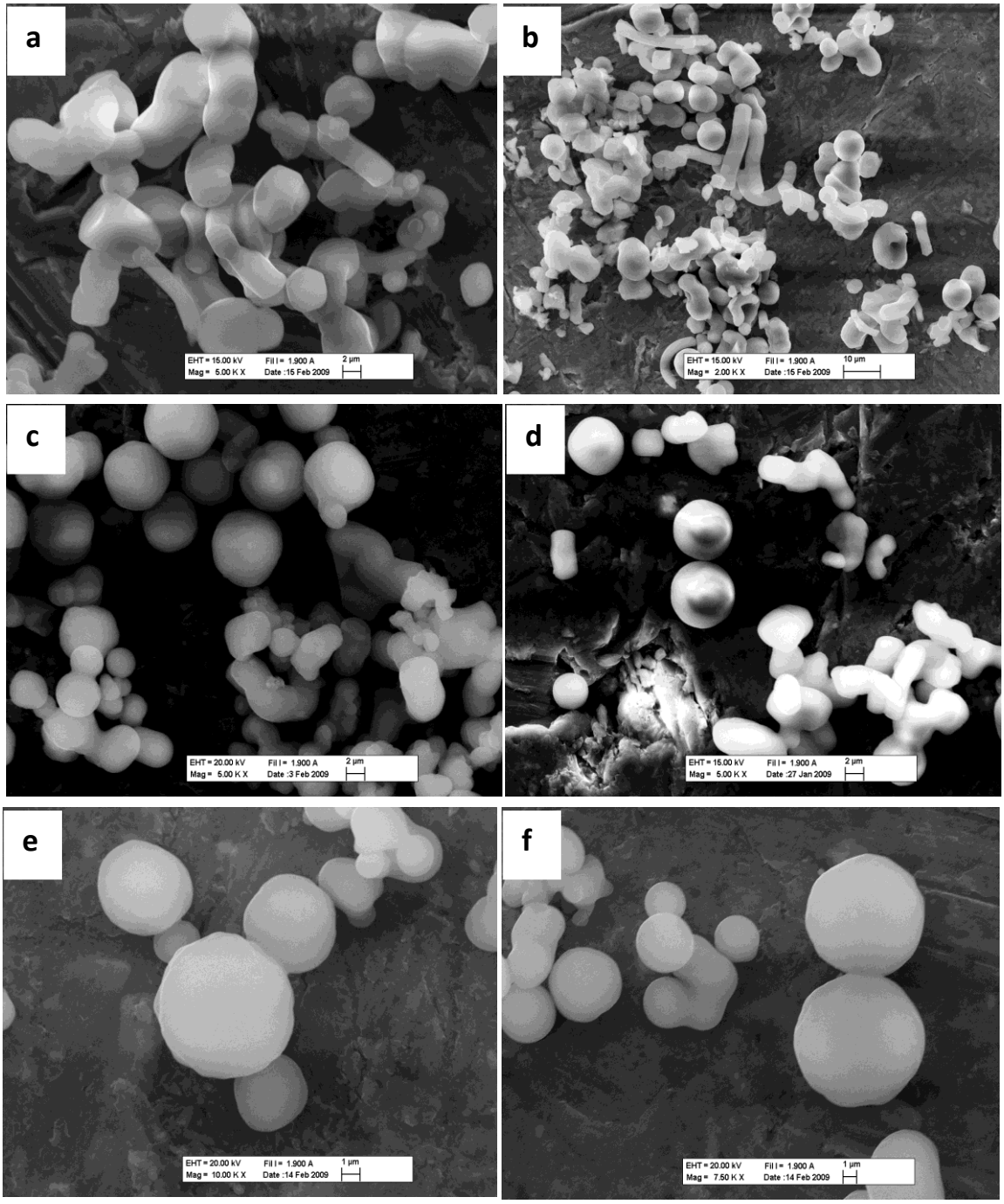

Figure 3.4.3: The SEM images of the CTABr-P123-SO_4^{2-} system; for the CTABr/P123 mole ratio of 3.0 and the SO_4^{2-} concentration of (a) 0.25M and (b) 0.5 M, the CTABr/P123 mole ratio of 4.0 and the SO_4^{2-} concentration of (c) 0.25M and (d) 0.5 M and the CTABr/P123 mole ratio of 6.0 and the SO_4^{2-}concentration of (e) 0.25M and (f) 0.5 M.

As mentioned before, addition of sulphate decreases the solubility of P123, however, increases the aggregation number of the micelle. One would expect a pore size expansion of the synthesized mesoporous silica particles. **Table 3.4.1** summarizes the N_2 adsorption-desorption measurements of particles from the CTABr-P123-SO_4^{2-} system. The general trend is an increase in pore size with increasing SO_4^{2-} ion concentration. On the other hand, the surface area decreases with increasing SO_4^{2-} concentration. Since the amount of silica source used is the same in all the samples and the aggregation number is increasing with the SO_4^{2-} ion concentration. It means that there is a decrease in the number of micelles in the solution, therefore the excess silica must form a significant amount of non porous silica, which may correlate the measured low surface area. The non-porous silica might cover either surfaces of formed particles or might be inside the pore and causes pore blocking effect (see below). Another important information that can be obtained from **Table 3.4.1** is a decrease in the wall thickness (t) with increasing SO_4^{2-} concentration. It is well known that the shell thickness of the micelle decreases with increasing aggregation number. The wall thickness is the sum of the shell thickness of adjacent micelles and the distance between them. When the aggregation number is increased, the inner parts of the shell, which are formed by very tighlt, packed poly (ethylene oxide) groups and where the rigid part can be considered as a part of the core, because this region is also more dehydrated than the upper parts of the shell. Assuming the distances between the micelles are constant, a decrease in the wall thickness can be attributed to shirinkage of the shell. This is is illustrated in **Figure 3.4.4**.

CTAB/P123 mole ratio	Na_2SO_4 concentration (M)	BET surface area (m^2/g)	d100 (nm)	BJH pore size distribution [a](2r)	Wall thickness t [b] (nm)
3:1	0	690	8.8	5.9	4.3
	0.25	683	8.6	6.9	3.0
	0.50	630	8.7	6.6	3.4
4:1	0	685	7.9	4.1	5.0
	0.25	528	9.3	5.7	5.0
	0.50	672	8.2	7.0	2.5
6:1	0	723	8.4	4.6	4.7
	0.25	674	8.1	5.5	3.8
	0.50	644	8.3	6.0	3.6

[a] Pore diameter is calculated from the adsorption branch of the isotherm using BJH method.

[b] The wall thickness (t) is obtained by deducing the pore diameter (2r) from the unitcell a_o ($a_o = (2/\sqrt{3})d_{100}$), namely, $t = a_o$ 2-r.

Table 3.4.1: The structural parameters of the mesoporous silica particles, obtained from the CTABr-P123-SO_4^{2-} system with different CTABr/P123 mole ratios and with different SO_4^{2-} concentrations.

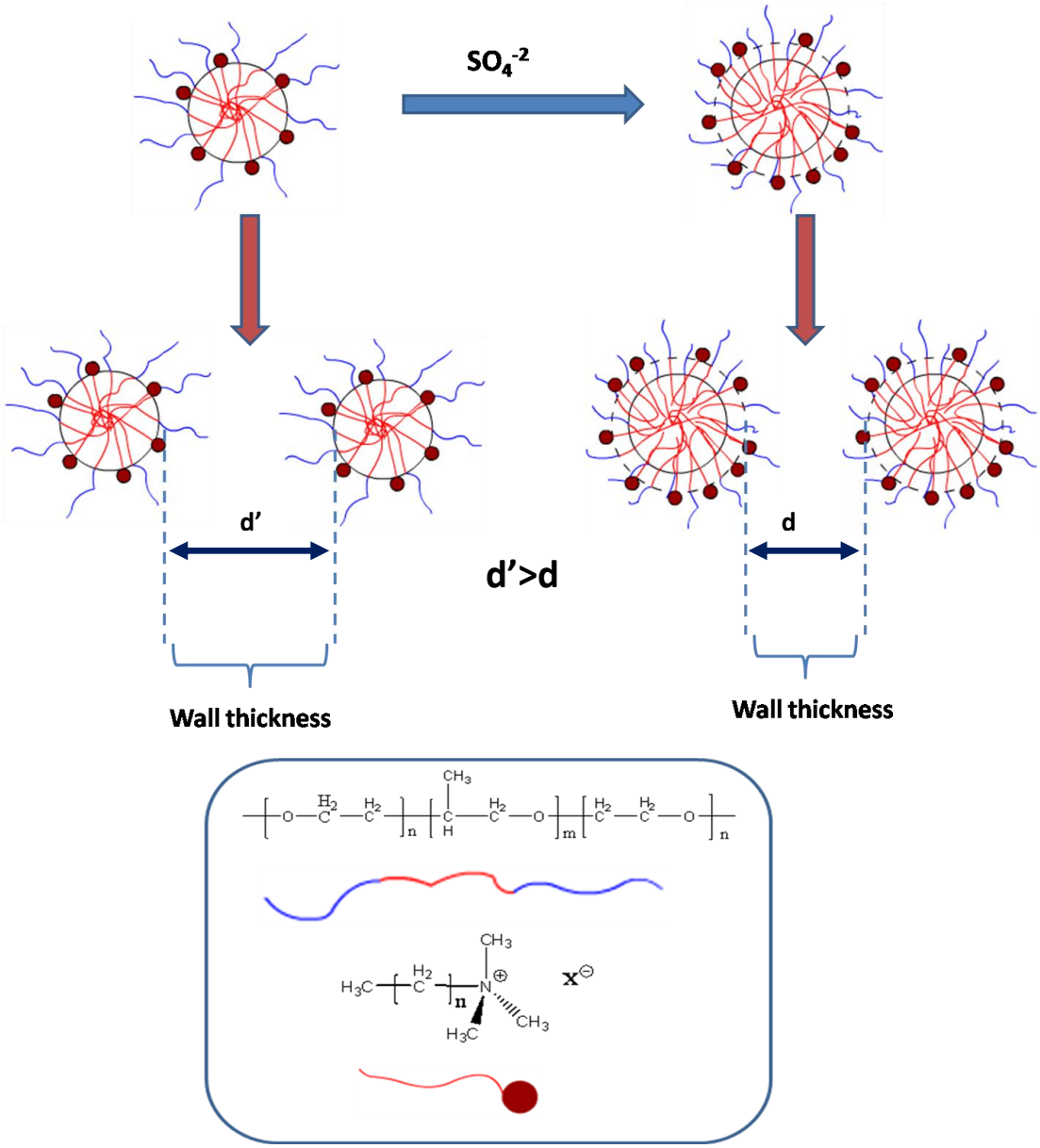

Figure 3.4.4: A schematic representation of the wall thickness change upon SO_4^{2-} addition.

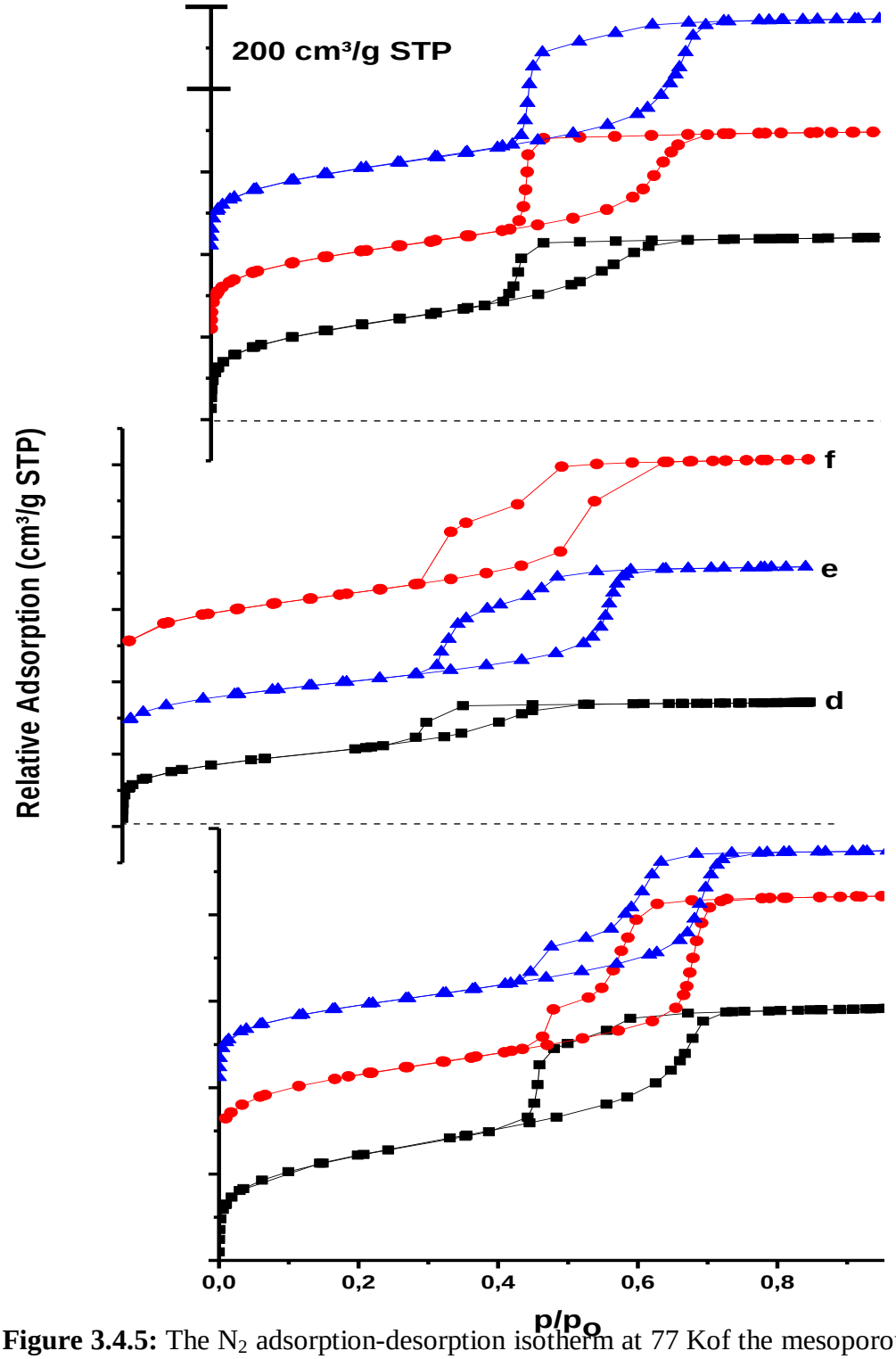

Figure 3.4.5: The N_2 adsorption-desorption isotherm at 77 Kof the mesoporous silica particles obtained from the CTABr-P123-SO_4^{2-} system. For the CTABr/P123 mole ratio of 3.0, the SO_4^{2-} ion concentration of (a) 0.0, (b) 0.25 M and (c) 0.5 M, for the CTABr/P123 mole ratio of 4.0, the SO_4^{2-} ion concentration of (d) 0.0, (e) 0.25 M and (f) 0.5 M and for the CTABr/P123 mole ratio of 6.0, the SO_4^{2-} ion concentration of (g) 0.0, (h) 0.25 M and (i) 0.5 M.

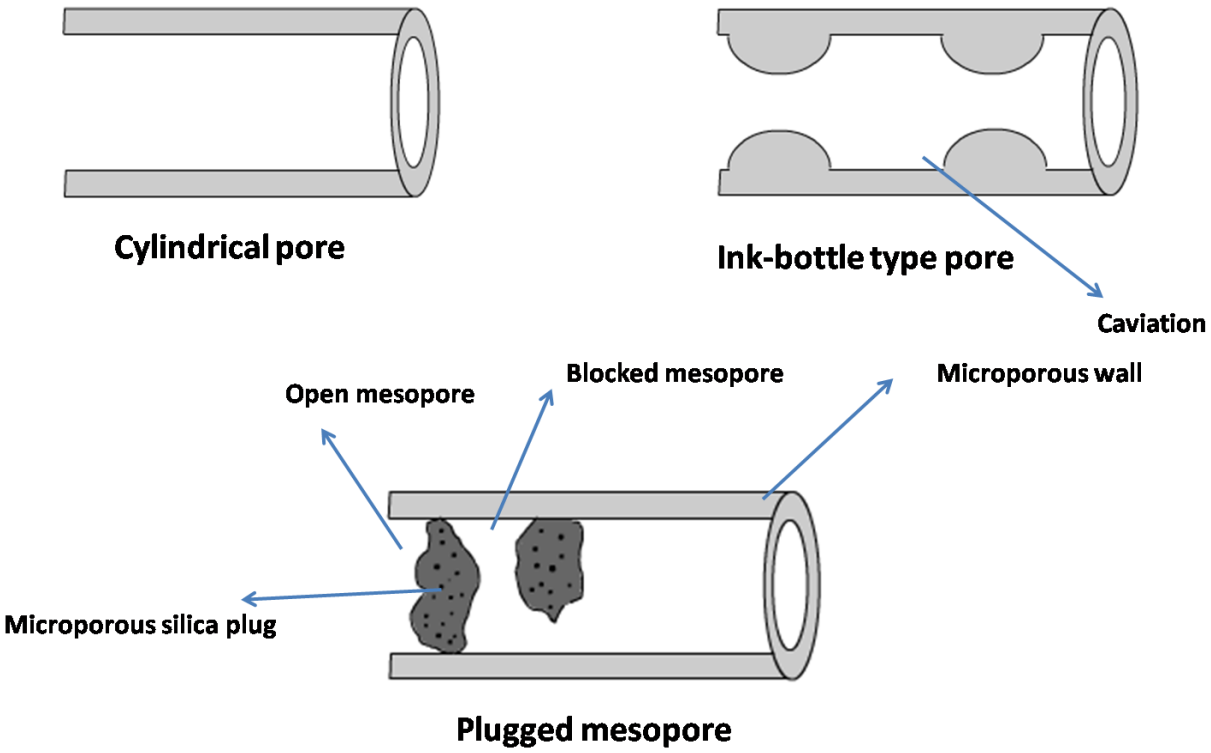

Figure 3.4.6: The schematic representation of pore types.

The sulphate ion has no direct effect on the assembly of CTABr molecules into the pluronic micelles. However, the number of CTABr in a pluronic micelles change due to change of the size of pluronic micelles. The CTABr molecule has a positively charged head group and each head group has an effective head group area. This effective head group area is the most important parameter and determines the number of CTABr in a pluronic micelle. Simply, when the micelle radius increased two times, the number of CTABr molecules that can be accommodated, increases four times, because the surface area of the micelle increases four times ($4\times\pi\times r^2$). Therefore, we may assume that the number of CTABr molecules increases in the pluronic micelles with increasing SO_4^{2-} ion concentration in the solution at the beginning of synthesis process. When the solutions with low CTABr/P123 mole ratio are used in the CTABr-P123-SO_4^{2-} system, an important amount of pluronic

surfactant remains as either in free or micellar form in the solution. As stated before in the CTABr-P123-SO_4^{2-} system the micelle number decreases and excess silica is also present in reaction medium with free P123 molecules. Therefore, some of the free P123 molecules are covered by silica monomers and are placed in the pore structure, which are known as plugs [135,136]. These nonporous or microporous plugs settle in the pore structure and show a pore blocking effect. This phenomenon can be observed in the N_2 adsorption-desorption isotherms. These plugs can be either non-porous or microporous [135]. When the plugs exist in the pore structure they can be realized from desorption brunch of the isotherm. They appear as a little step at lower P/P_o than the first larger step. **Figure 3.4.5** shows the N_2 adsorption-desorption isotherms of the mesoporous particles obtained from the CTABr-P123-SO_4^{2-} system. At low CTABr concentrations (CTABr/P123 mole ratio of 3.0) and in the presence of SO_4^{2-}, a very sharp step is observed in the desorption brunch of the isotherm. Different from the ink-bottle type pores, it is possible to calculate the size of the cavities that is formed by the plugs from the position of desorption brunch [135]. The plugs and ink-bottle type pores are illustrated in **Figure 3.4.6**. When the CTABr concentration is increased (CTABr/P123 mole ratio of 4.0) the pluging gets smaller, which can also be realized from the desorption brunch. The step originating from the plugs gets smoother since there are more CTABr molecules to form more CTABr-P123 micelles. Since the excess P123 molecules remains in the formed particles, no difference in FTIR and Raman spectra is observed. When the CTABr/P123 mole ratio is 6.0, no plug formation is observed, however the pore structure turns in to ink-bottle type pores. That means pore structure is not cylindrical anymore and it has wide and narrow sections.

3.4.2. The effect of Nitrate

As it was investigated in Chapter 1, the NO_3^- ion has no significant effect on the micellization of pluronic surfactants. Note that a hydrotropic anion (like SCN^-) increases the pluronic surfactant solubility so as the CMC and CMT. However, there is an inverse relationship between the CTABr and the hydrotropic anions of the Hofmeister series. In this investigation, we have used the NO_3^- ion because in the presence of a more hydrotropic anion, the CTABr is insoluble. Remember that the NO_3^- ion is a more lyotropic anion than SCN^- (see **Figure 1.10**).

The nitrate salts have been generally employed in the preparation of liquid crystalline mesophases, silica films (liquid crystalline templating) and mesostructured metal sulfides [118,145,146]. Compared to our system, in all above listed publications the synthesis environment is more concentrated, in terms of both nitrate and surfactant. In concentrated environment, the role of nitrate ion as a hydrotropic anion is mainly to occupy poly (propylene oxide) – poly (ethylene oxide) interface and making the interface more hydrophilic [5,146]. By changing the hydrophilic-hydrophobic balance of the micelle, different mesostructured liquid crystals and silica films have been synthesized [118,145]. In our system, the nitrates are in the interface, but the interface is already hydrated. Therefore the role of nitrate is quite different in our system. It keeps the CTABr molecules at the interface and by charge blocking effect of nitrate; it increases the amount of CTABr in pluronic micelles.

When the nitrate salt is used, it was observed that the pluronic micelles uptake more CTA^+ cations. The amount of CTA^+ in the micelle is a function of both the concentration of CTABr and NO_3^- ion.When the CTABr amount is increased in a micelle, the number of the pluronic surfactant decreases and the micelle size

decreases as discussed in the introduction part. Therefore, in the presence of nitrate ion the unitcell of the silica particles decreases (**Figure 3.4.7** and **Table 3.4.2**). At CTABr/P123 mole ratio of 3.0, the position of first diffraction line (100) shits to higher angles indicating a decrease in unit cell (from 8.8 to 8.1 nm) in the presence of 0.5 M nitrate. The unit cell change is about 9% and the surface area drop is about 42% (from 690.3 to 399.4 m^2/g), see **Table 3.4.2**. However, the XRD pattern still shows an ordered mesostructure with 2 D hexagonal mesostructure. The (110) and (200) planes are also well resolved in this composition. A further increase of the nitrate ion concentration to 1.0 M does not change the position of the first diffraction line (100), however the intensity is decreased drastically. In addition, the 2^{nd} and 3^{rd} diffracton lines ((110) and (200)) are not visible, indicating a decrease in order. At CTABr/P123 mole ratio of 6.0, the change in the position of the first diffraction line (100) is about 0.4^o, 2Θ, which indicates shrinkage of the unit cell by 22% (from 8.4 to 6.5 nm) at both nitrate concentrations, where the surface area drop is about 23% at 0.5 M nitrate concentration (from 722.7 to 555.1 m^2/g) and 16% at 1.0 M nitrate concentration (from 722.7 to 609.4 m^2/g). At both nitrate concentrations (0.5 and 1.0 M), the change in the position of the first diffraction line is the same. Howerver, at 6.0 CTABr/P123 mole ratio, the mesoporous particles are still ordered and three diffraction lines are intense enough to index to (100), (110) and (200) planes of the 2D hexagonal mesostructure.

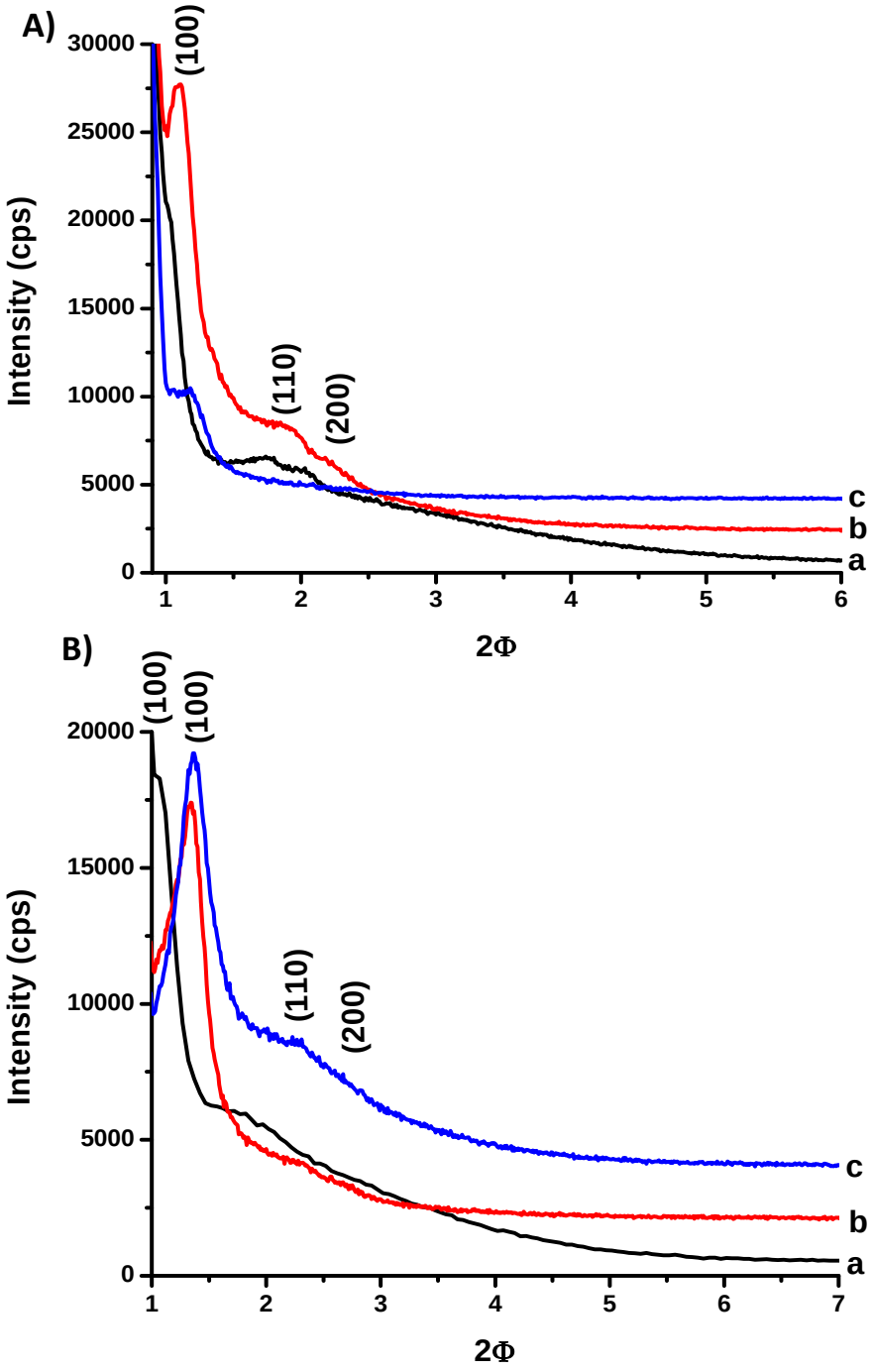

Figure 3.4.7: The PXRD patterns of the mesostructured silica obtained from the CTABr-P123-NO_3^- systems at different NO_3^- ion concentrations and CTABr/P123 mole ratios. A) The CTABr/P123 mole ratio of 3.0 and the nitrate ion concentration of (a) 0.0 M, (b) 0.5 M, and (c) 1.0 M, and B) The CTABr/P123 mole ratio of 6.0 and the nitrate ion concentration of (a) 0.0 M, (b) 0.5 M, and (c) 1.0 M .

At low CTABr concentration (CTABr/P123 mole ratio of 3.0), there is always an uncomplexed (excess) P123 molecules or species in the media. These species assemble with the silica species to form a non-porous or microporous silica. Therefore, the order of particles decreases, especially at high nitrate concentrations (1.0 M and above). The non-porous or microporous particles cause a sarp decrease in the surface area see **Table 3.4.2**. On the other hand, if an excess CTABr is present in the reaction media (CTABr/P123 mole ratio of 6.0), there is always enough CTABr to maintain the cooparative micellization, therefore highly ordered particles are formed with a smaller unit cell and with an increased surface area.

CTAB/P123 mole ratio	**$NaNO_3$ amount (M)**	**BET surface area (m^2/g)**	**d100 (nm)**	**BJH pore size distribution[a] (2r)**	**Wall thickness t[b] (nm)**
3:1	**0**	**690**	**8.8**	**5.9**	**4.3**
	0.5	**399**	**8.1**	**5.9**	**3.8**
	1	**112**	**7.5**	**5.6**	**3.1**
6:1	**0**	**723**	**8.4**	**4.6**	**4.7**
	0.5	**555**	**6.5**	**4.5**	**3.0**
	1	**609**	**6.5**	**4.2**	**3.2**

[a] Pore diameter is calculated from the adsorption branch of the isotherm by BJH method.

[b] The wall thickness t is obtained by deducing the pore diameter (2r) from the unitcell a_o ($a_o = (2/\sqrt{3})d_{100}$), namely, $t = a_o$ 2-r.

Table 3.4.2: The structural parameters of the CTABr-P123-NO_3^- system in different CTABr-P123 mole ratios and in different NO_3^-concentration.

When available CTABr in the reaction medium is consumed at early stages of the reaction at low CTABr concentrations, both kind of particles smoother and disorderd ones, are observed in the SEM images (**Figure 3.4.8**). However, at high CTABr concentrations (CTABr/P123 mole ratio of 6.0), all the particles have distinct morphology. Mainly spherical particles are formed at low NO_3^- ion concentrations (0.5 M) and wormlike particles at high NO_3^- ion concentrations (1.0 M). Decreasing CTABr solubility by NO_3^- anion probably causes the formation of elongated particles that contain excessive amount of CTA^+ together with nitrate anions rather than the pluronic molecules (see text later). Moreover, the TEM images correlate with the formation of highly ordered pore structure in the presence of excess CTABr and NO_3^- anion, (**Figure 3.4.9**). The TEM image shows a long range order and unit cell values measured from the images (6.6 nm) is consistent with the calculated d-spacing values from the XRD patterns.

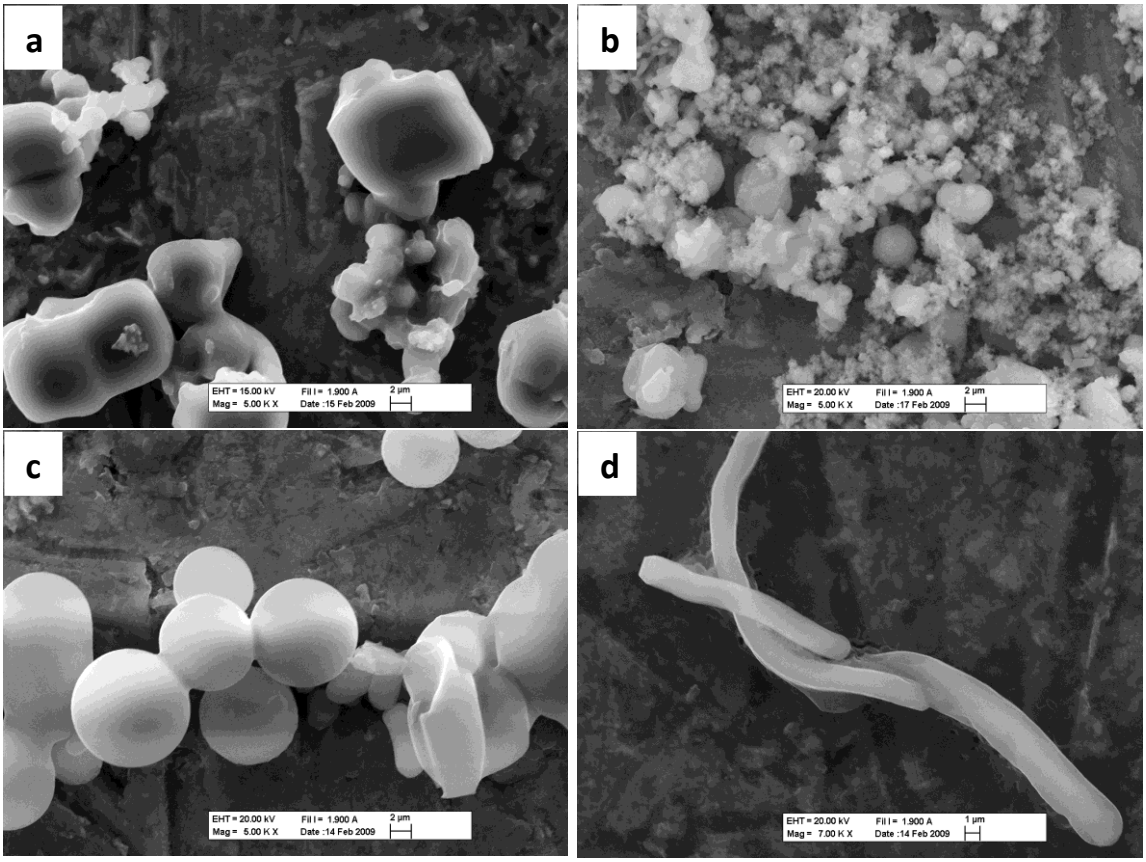

Figure 3.4.8: The SEM images of the mesoporous silica particles obtained from the CTABr-P123-NO_3^- system; the CTABr/P123 mole ratio of 3.0 and the NO_3^- ion concentration of (a) 0.5M and (b) 1.0 M and the CTABr/P123 mole ratio of 4.0 and the NO_3^- ion concentration of (c) 0.5M and (d) 1.0 M.

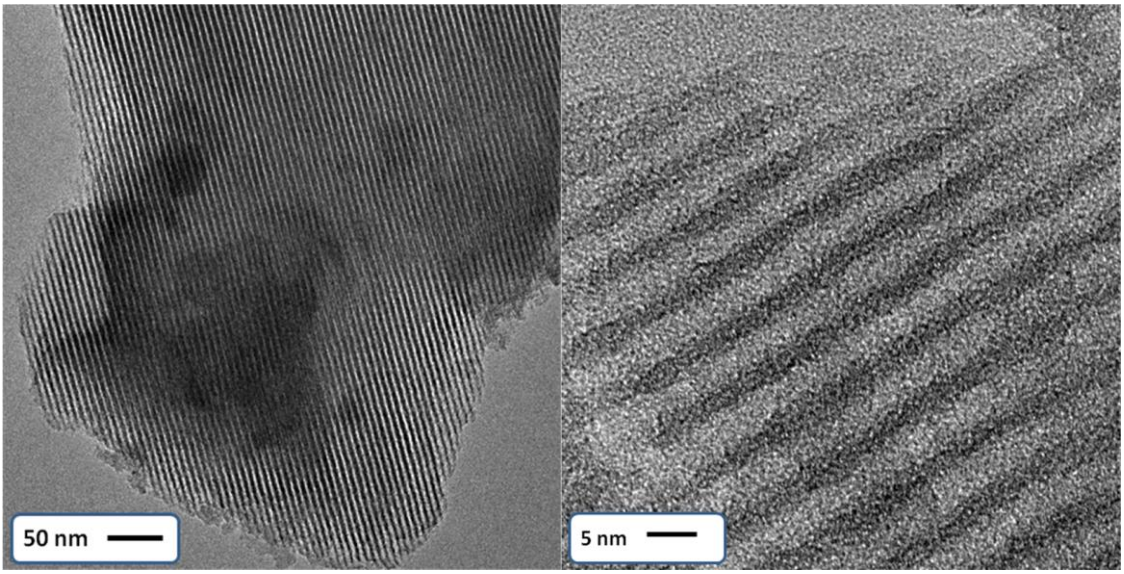

Figure 3.4.9: The TEM images of the mesostructured silica obtained from the CTABr-Pluronic-NO_3^- system with a CTABr/P123 mole ratio of 6.0 and the NO_3^- ion concentration of 1.0 M.

The increase in the CTABr amount in the mesostructured particles upon NO_3^- addition can also be determined spectroscopically. **Figure 3.4.10** shows the FTIR spectra of the particles from CTABr-P123-NO_3^- system. At low CTABr concentrations (CTABr/P123 mole ratio of 3.0), the spectrum dose not show any difference until reaching to 1.0 M NO_3^- concentration in which the obtained particles contains mainly CTABr molecule rather than P123. This can be understood from the progression of C-H symmetric and antisymmetric stretching modes of the alkyl chains, which are observed at 2850 and 2885 cm^{-1}, respectively (see **Table 3.2.2**). Low absorbance of the signals originating from P123 in the FTIR spectra indicate that at high NO_3^- concentrations, the P123 molecules are completely solvated out from the micelle and the P123 molecules remain as free surfactants in the solution, where the resulting material has significant amount of non-porous silica as stated before. The non-porous silica can be also realized from the very low surface area and absence of the micropores. If the micropores exist, that must originate from the assembly of the

P123 molecules and the silica species in the media. However, if there is enough CTABr in the media (like in case of CTABr/P123 mole ratio of 6.0), most of the P123 molecules are incorporated into the micelles, where the intensity of the P123 signals do not change with increasing NO_3^- ion in the medium. However, the CTABr signals increases. Most of the P123 molecules are used to form micelles with CTABr and little amount of P123 molecules remain in the reaction medium. Therefore, the silica particles have a higher surface area (**Table 3.4.2**). The mesoporous particles obtained under these conditions are result of the CTABr-P123 micelles and silica assembly. Because the pore size and wall thickness are high for a CTABr only systems and low for a P123 only systems [4,45,76,147]. Even in 0.5 M NO_3^- solutions, the spectrum shows a high intensity at C-H symmetric and asymmetric stretching of methylene groups of CTABr. Similar conclusions can also be obtained from the Raman spectra of the silica particles obtained from the CTABr-P123-NO_3^- system (**Figure 3.4.11**). The C-H symmetric stretching of methylene appears as a shoulder next to symmetric C-H stretching of methylene groups of the P123 (2870 cm^{-1}) with increasing NO_3^- concentration. In addition, the C-H asymmetric stretching mode of the methylene group of CTABr appears at 2885 cm^{-1} and overlaps as a broad peak with the methyl symmetric C-H stretching peak (2900 cm^{-1}) of the poly (propylene oxide) group. Especially, at high NO_3^- and CTABr concentrations, the spectrum looks very smilar to the spectrum of the particles obtained from CTABr only system. **Figure 3.4.12** schematically shows the effect of NO_3^- on the assembly in the CTABr and CTABr-P123 systems.

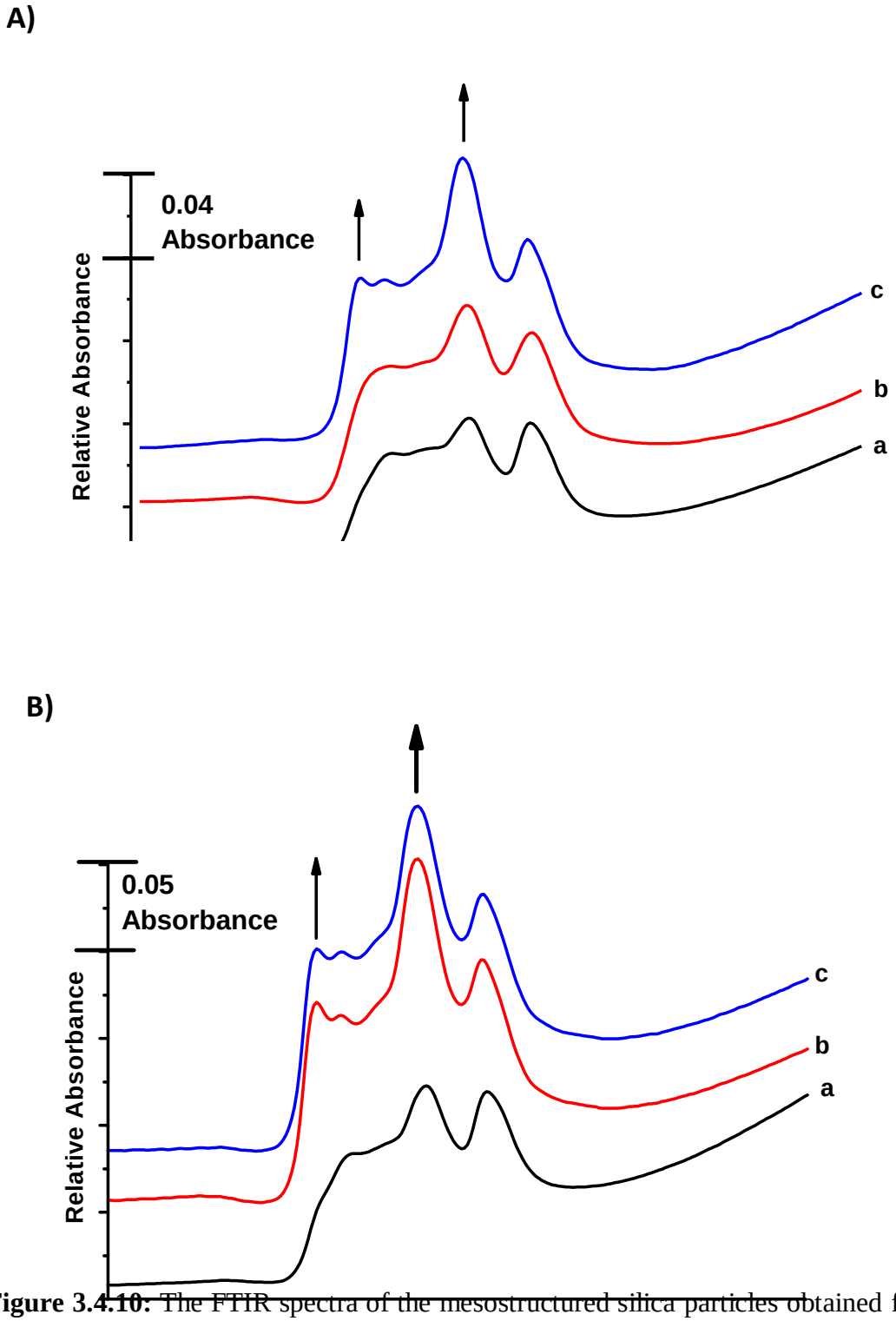

Figure 3.4.10: The FTIR spectra of the mesostructured silica particles obtained from the CTABr-P123-NO_3^- systems with different NO_3^- ion concentrations and CTABr/P123 mole ratios; A) The CTABr/P123 mole ratio of 3.0 and the NO_3^- concentrations of (a) 0.0 M, (b) 0.5 M and(c) 1.0 M; B) The CTABr/P123 mole ratio of 6.0, and the NO_3^- concentrations of (a) 0.0 M, (b) 0.5 M and (c) 1.0 M.

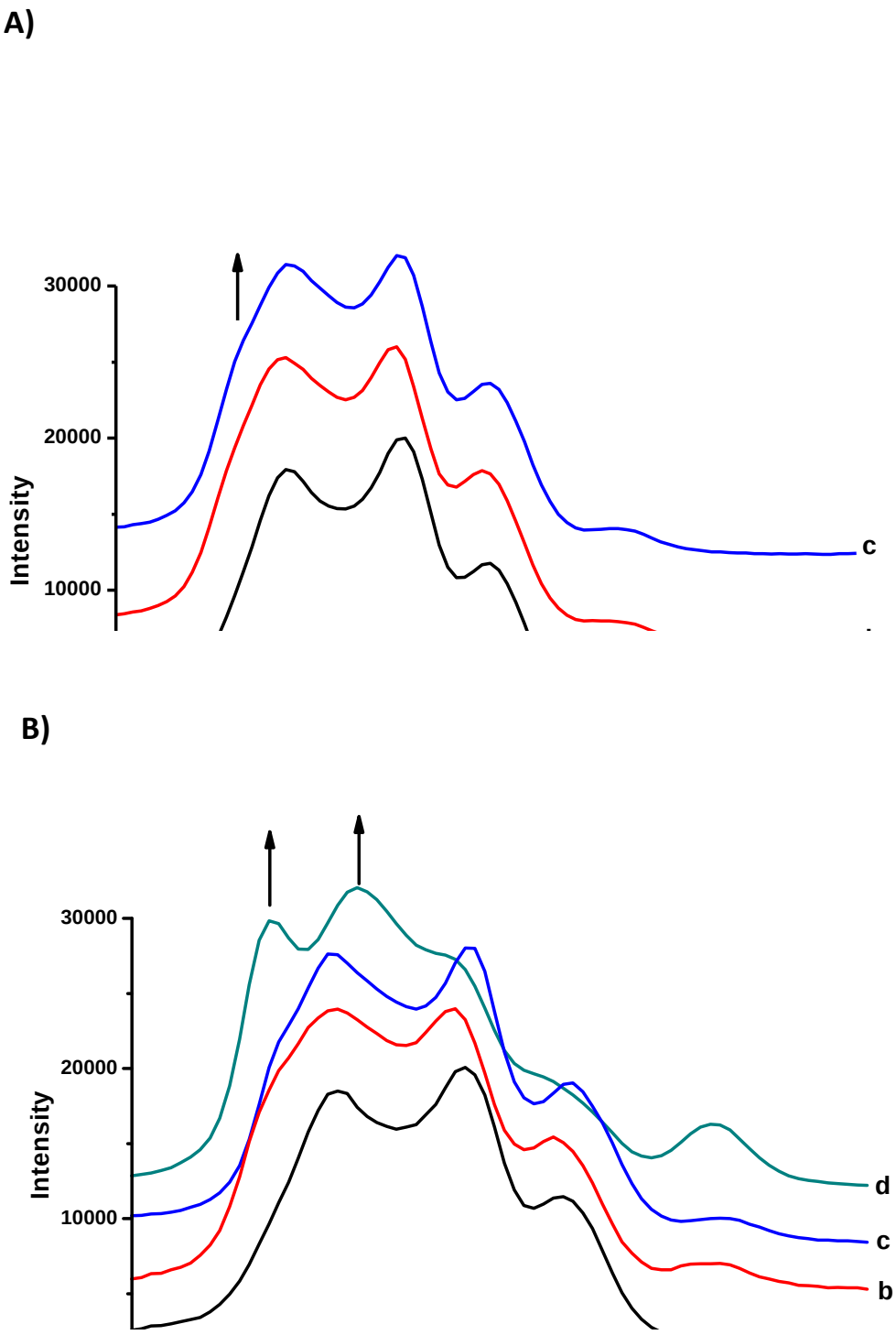

Figure 3.4.11: The Raman spectra of the mesostructured silica particles obtained from the CTABr-P123-NO_3^- systems with different NO_3^- ion concentrations and CTABr/P123 mole ratios; A) The CTABr/P123 mole ratio of 3.0 and the NO_3^- ion concentrations of (a) 0.0 M, (b) 0.5 M, and (c) 1.0 M; B) The CTABr/P123 mole ratio of 6.o the NO_3^- ion concentrations of (a) 0.0 M, (b) 0.5 M, and (c) 1.0 M and (d) the CTABr-NO_3^- systems.

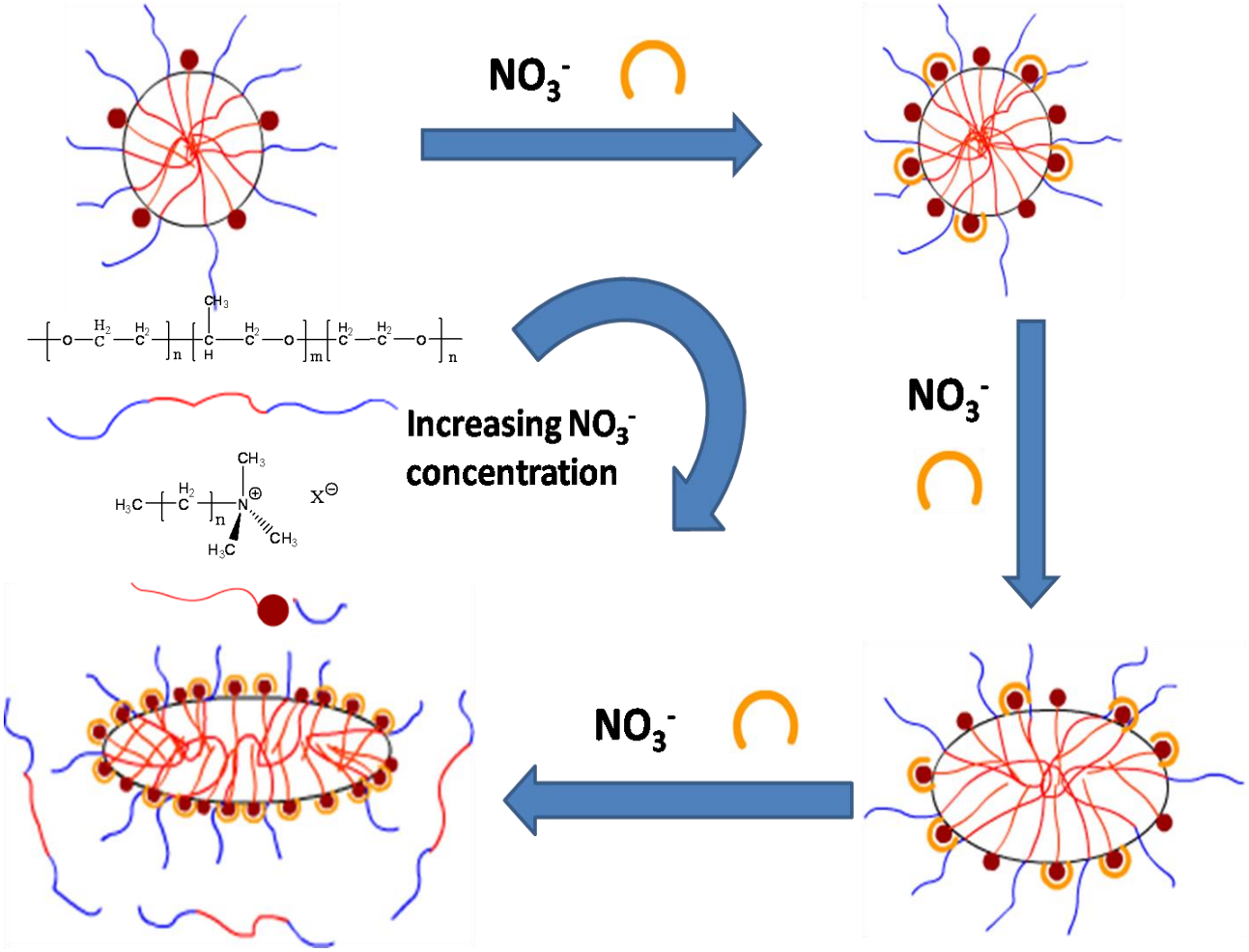

Figure 3.4.12: The effect of NO_3^- on the CTABr-P123 micelles.

Role of the NO_3^- ions on the assembly process is very important, such that one can control the amout of CTABr molecules in mesostructured particles using this anion in the synthesis media. Note that under our synthesis conditions, it is not possible to synthesize particles without the pluronics. In the absence of pluronics, the reaction results a gel formation. Drying this gel gives completely disordered white powder. Moreover, it is not possible to dissolve CTABr in above 2.0 M NO_3^- solutions. These can be considered as a direct evidence of the effect of nitrate ion on the CTABr assembly. However, it is possible to synthesize mesoporous particles using CTABr-NO_3^- couple at lower nitrate ion concentration. In these experiments, the CTABr amount was varied between 1.26×10^{-3} mol and 5.04×10^{-3} mol. **Figure**

3.4.13 shows the SEM, and TEM images and the PXRD pattern of the particles synthesized using CTABr-NO_3^- couple. The particles are higly ordered and have mainly wormlike morphology. Different from the particles obtained from the CTABr-P123 system, the mesopores are curling with a smaller repeating features, see the TEM image in **Figure 3.4.13**, compared to the TEM images of particles obtained from the CTABr-P123 system, in which the mesopores run smoothly over several micrometers with a larger pores and wall thickness.

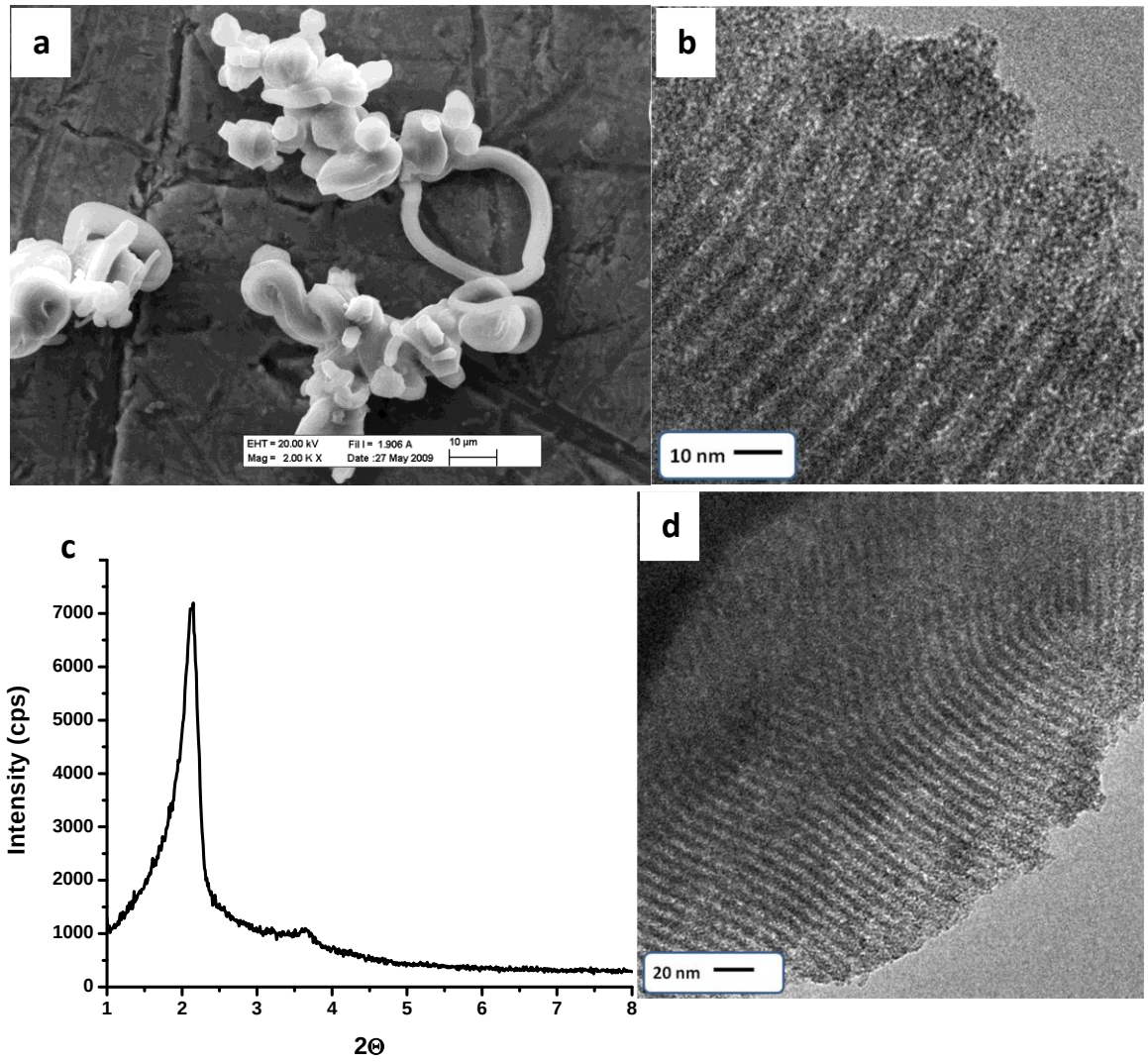

Figure 3.4.13: (a) the SEM image, (b) and (d) the TEM images, and (c) the PXRD pattern of the particles synthesized using CTAB-NO_3^- couple under 0.5M NO_3^- and 5.0 $\times 10^{-4}$ M CTABr.

An evidence for the incorporation of nitrate ions into the pores together with CTA^+ cation is the high stability of nitrate against excessive washing steps. Washing tens of times with water can not remove the nitrate ions from the particles. However, it is well known that nitrate salts in the pores can be washed out very easily. It means that the charge balancing anion of the CTA^+ is nitrate ion in the channel space of the mesostructured silica particles.

When the CTABr solubility is decreased by using nitrate, the ultimate point in the surfactant assembly is the bilayer assembly before the Cloudy Point (**Figure 1.11**). The bilayer assembly of CTABr can be obtained by using either high concentrations of CTABr, nitrate or both. This type of assembly is the reason of vesicle formation. **Figure 3.4.14** shows the TEM image of formed silica vesicles from a CTAB-NO_3^- couple.

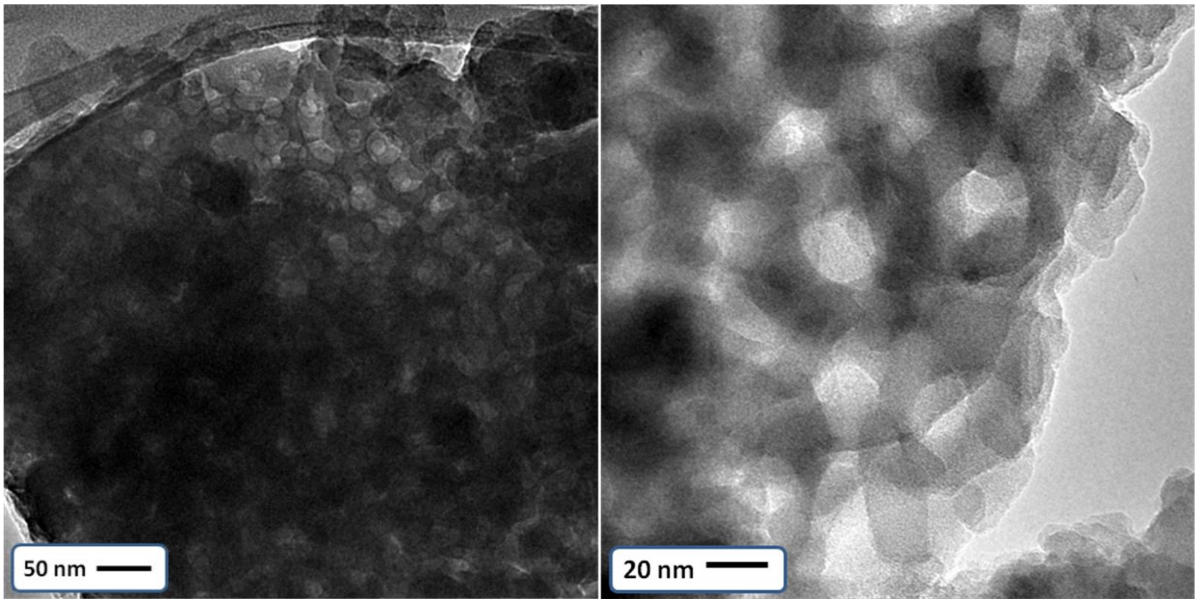

Figure 3.4.14: The TEM image of particles synthesized with CTABr-NO_3^- system. 0.5M NO_3^- and 5.0 $\times 10^{-4}$ M CTABr. (Scale bars are 50 and 20 nm, respectively)

3.4.3. The effect of Chloride Ion:

In the Hofmeister series, Cl^- anion is in between SO_4^{2-} and NO_3^-. Therefore the effect of Cl^- must be between SO_4^{2-} and NO_3^- ions in terms of assembly of both P123 and CTABr. It affects the aggregation of these surfactants by decreasing the solubility of both P123 and CTABr. However, it is not as effective as SO_4^{2-} for decreasing the solubility of P123 or NO_3^- ion for decreasing the solubility of CTABr. **Figure 3.4.15** shows the PXRD patterns of calcined samples, obtained from the CTABr-P123-Cl^- systems. At a CTABr/P123 mole ratio of 3.0 and 0.5 M chloride ion concentration, the diffraction pattern shows three distinct diffraction lines, which can be indexed to (100), (110) and (200) planes of 2D hexagonal structure. When compared to chloride free system, the diffraction lines shifts to higher 2Θ values (from 1.0^o to 1.2^o, 2Θ) and unitcell decreases from 8.4 to 6.8 nm (see **Table 3.4.3**). Increasing the Cl^- ion concentration to 1.0 M causes a further shift of the diffraction lines and the unit cell parameter a decreases to 6.5 nm. However, the 2^{nd} and 3^{rd} diffraction lines ((110) and (200)) are not well resolved and appear together as a broad peak, indicating a decrease in the order of the channels in the silica particles. On the other hand, at high CTABr/P123 mole ratio (6.0), existence of chloride ion causes a decrease in meso-order. Besides decreasing intensity of the first diffraction line (100); the (110) and (200) diffraction lines disappear. Moreover, the unitcell shifts to 7.4 and 6.9 nm for the 0.5 M and 1.0 M chloride ion concentrations, respectively (see **Table 3.4.3**).

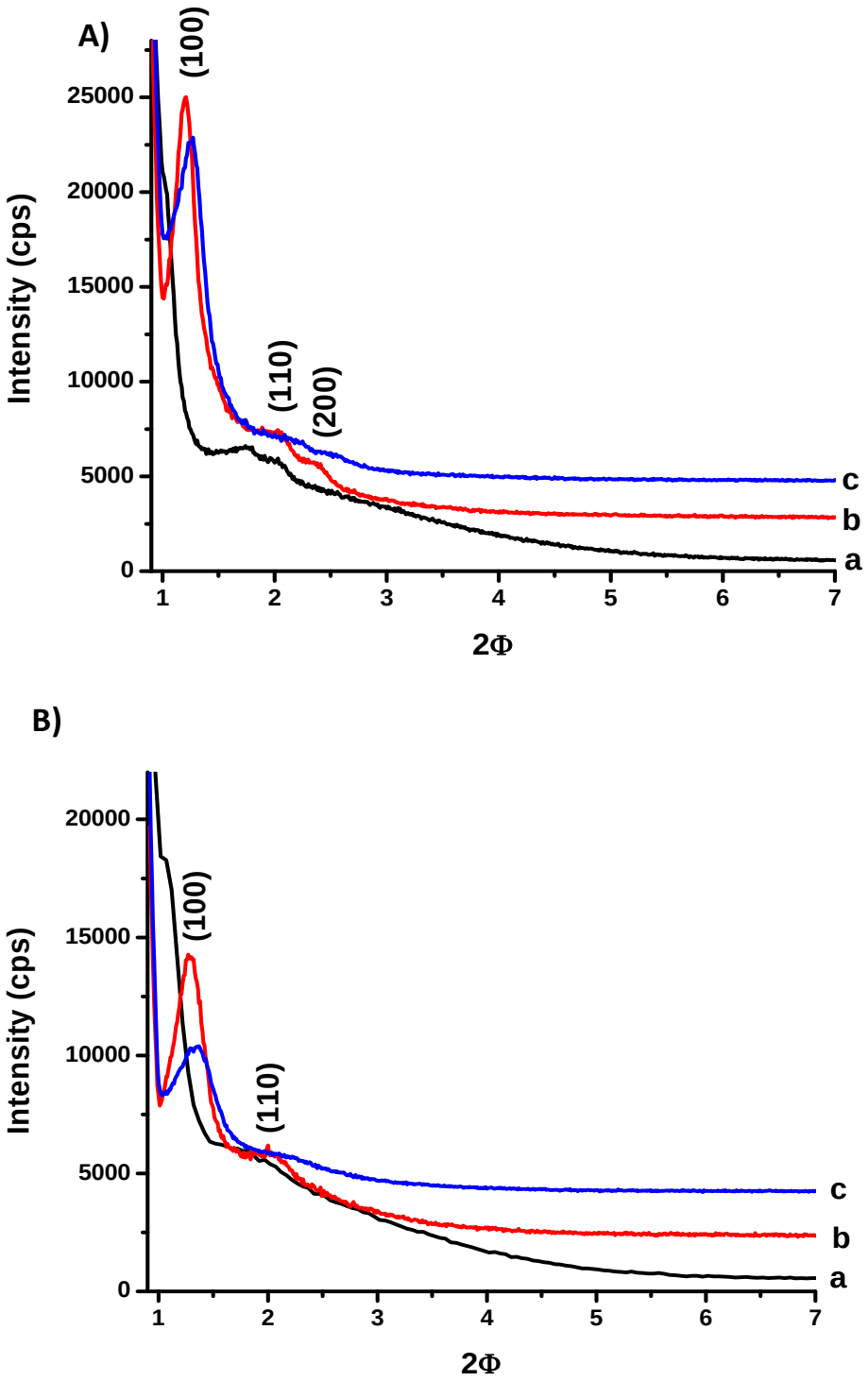

Figure 3.4.15: The PXRD patterns of the mesostructured silica obtained from the CTABr-P123-Cl^- systems at different Cl^- concentrations and CTABr/P123 mole ratios; A) The CTABr/P123 mole ratio of 3.0 and the Cl^- ion concentration of (a) 0.0 M, (b) 0.5 M, and (c) 1.0 M; B) The CTABr/P123 mole ratio of 6.0 and Cl^- ion concentration of (a) 0.0 M, (b) 0.5 M, and (c) 1.0 M.

For low CTABr concentrations, the Cl^- ion (0.5 M) increases the order of formed particles with a decrease in the unit cell. At low CTABr concentrations, the effect of the Cl^- ion is very smilar to that of SO_4^{2-} ion. Decreasing of the unit cell is an indicator for increasing of the number of CTABr molecules incorporated. However, the main effect of the Cl^- ion at low concentrations is on P123 (see text). At higher concentrations (Cl^- concentration of 1.0 M), the effect is mainly on CTABr. Remember that when the number of CTABr increases in a micelle, the number of pluronic surfactant decreases so as the order of the formed particles. The concentration dependent effect of the Cl^- anion on CTABr increases with increasing the amount of CTABr molecules. Therefore, the effect of Cl^- on the CTABr-P123-Cl^- system starts to appear at lower Cl^- concentrations for higher CTABr/P123 mole ratios (6.0). Eventually, at higher CTABr/P123 mole ratios (6.0), the unit cell and order decrease are observed (Cl^- concentration is 0.5 M). Changes in the structural parameters in the CTABr-P123-Cl^- system are a combination of the effects of SO_4^{2-} and NO_3^- (**Table 3.4.3**). Similar explanations can be made for the decrease in surface area in the presence of Cl^- ion, as in the NO_3^- case. However, the decrease is not as drastic. Because the Cl^- ion is not as effective as NO_3^- in terms of decreasing CTABr solubility and its solubility decreasing effect on P123 helps CTABr molecules to stay in the micelle. To sum up, at low CTABr concentrations the effect of Cl^- ion is mainly on decreasing solubility of P123, but at high CTABr concentrations the effect of Cl^- ion is mainly on CTABr rather than P123. It increases the number of CTABr molecules in the micelle. That necessarly means a decrease in the number of P123 molecules in the micelle. Therefore, the decrease in the pore order of the particles is the highest at high CTABr and Cl^- concentrations. The same conclusion can be made by looking the pore size distributions, for low CTABr concentrations. It does not

change too much however, a decrease is observed for high CTABr concentrations in the presence of Cl^- ion.

CTAB/P123 mole ratio	NaCl amount (M)	BET surface area (m^2/g)	d100 (nm)	BJH pore size distribution[a] (2r)	Wall thickness t[b] (nm)
6:1	0	690	8.8	5.9	4.3
	0.5	454	7.4	4.5	4.0
	1	196	6.9	4.2	3.8
3:1	0	723	8.4	4.6	4.7
	0.5	354	6.8	4.8	3.0
	1	185	6.5	4.9	2.6

[a] Pore diameter is calculated from the adsorption branch of the isotherm by BJH method.

[b] The wall thickness t is obtained by deducing the pore diameter (2r) from the unitcell a_o ($a_o = (2/\sqrt{3})d_{100}$), namely, $t = a_o$ 2-r.

Table 3.4.3: The structural parameters of the silica particles obtained from the CTABr-P123-Cl^- system at two different CTABr/P123 mole ratios and 3 different Cl^- concentrations.

The Cl^- anion has no effect on the morphology at low concentrations of both CTABr and Cl^- (**Figure 3.4.16**). The particles are a mixture of spheres and wormlike particles. In addition, these particles are highly ordered and porous; see the TEM images in **Figure 3.4.16**. Despite the particles are highly porous (**Figure 3.4.16-e**), not all of them show an ordered structure (**Figure 3.4.16-e**). However, increasing the Cl^- anion concentration, it starts to influence the CTABr molecules and no distinct morphology was obtained for these particles. Notice that a similar effect is also observed for the surface area and diffraction characteristic of these obtained particles. At low CATBr/P123 mole ratio (3.0) and low chloride ion concentration (0.5 M); the morphology is a mixture of spherical and wormlike particles. At 1.0 M chloride ion concentration, no distinct morphology was obtained. At high CTABr/P123 mole ratios, all particles have a distinct morphology at two different chloride ion concentrations (0.5 and 1.0 M). At 0.5 M chloride, the particles are spherical but the surface of these particles are cornered. When the concentration is increased to 1.0 M, the particles are perfectly spherical with some crystalline features on the surface of these particles. The morphology changes to cornered spheres for the CTABr/P123 mole ratio of 6.0 and Cl^- ion concentration of 0.5 M. Remember that same morphology is obtained for particles synthesized with CTABr-P123-SO_4^{2-} system. This is an evidence for similar effects of the Cl^- and SO_4^{2-} anions at low concentrations. The particles are spherical at both high CTABr/P123 mole ratio (6.0) and Cl^- ion concentration (1.0 M). However, some cornered features are observed on some of the spheres. The higher magnifications and EDX measurements show that these are not salt crystals but they look more like crsytalline particles obtained, in the CTABr-F127 system (see also **Figure 3.3.1**).

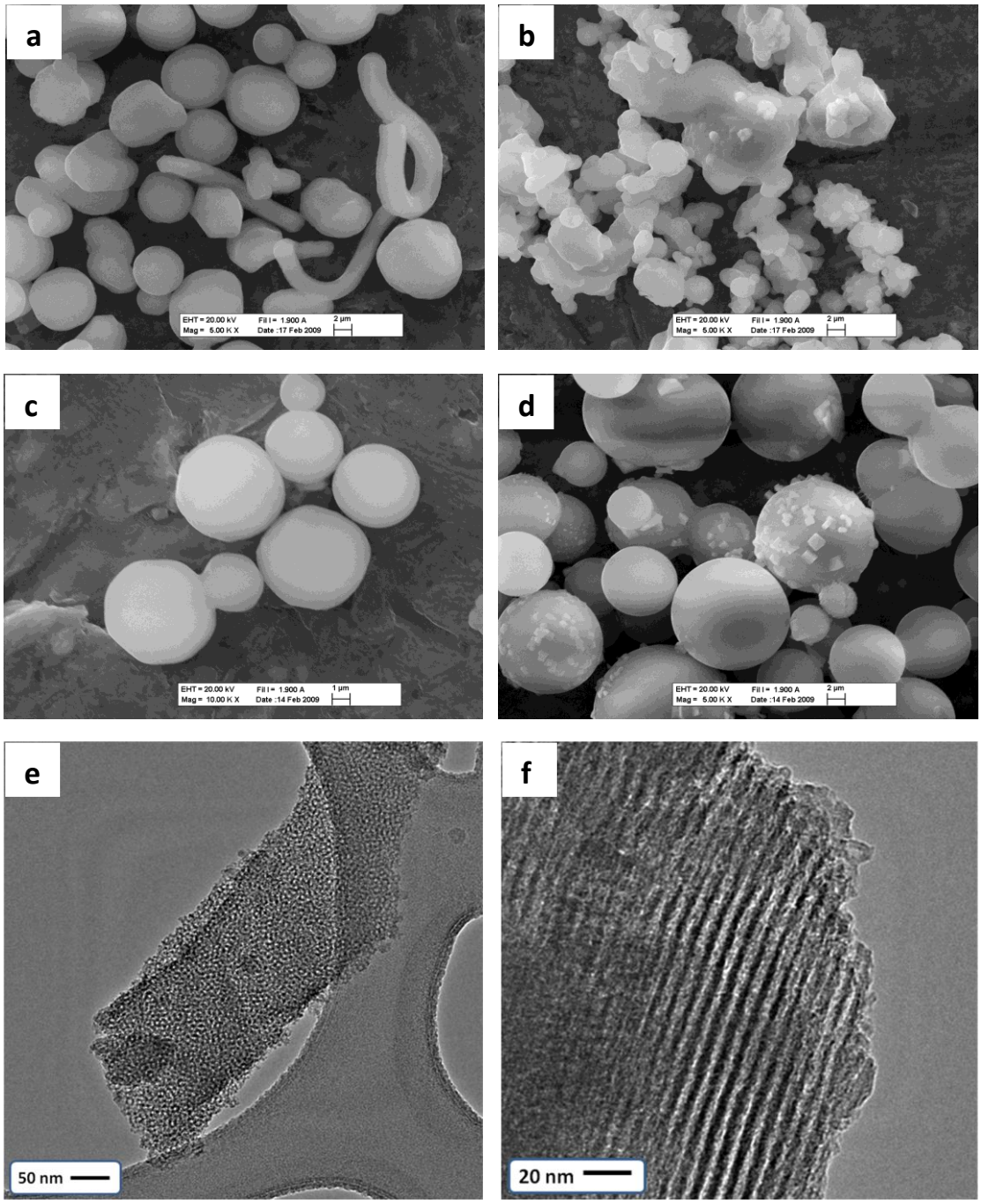

Figure 3.4.16: The SEM images of the particles obtained from the CTABr-P123-Cl^- system; for the CTABr/P123 mole ratio of 3.0 and the Cl^- ion concentration of (a) 0.5M and (b) 1.0 M and the CTABr/P123 mole ratio of 6.0 and the Cl^- ion concentration of (c) 0.5M and (d) 1.0 M. (e) and (f) are the TEM images of the particles obtained from the CTABr-P123-Cl^- system; for the CTABr/P123 mole ratio of 3.0 and Cl^- concentration of 0.5 M.

As in the nitrate case, the amount of Cl^- ion can also influence the number of CTABr in the P123-CTABr micelles, so the mesoporous particles. The amount of CTABr can be determined spectroscopically in the presence of Cl^- ion (**Figure 3.4.17** and **Figure 3.4.18**). Different form the NO_3^- ion, the Cl^- ion affects the amount of CTABr in the mesostructured particles at higher concentrations (1.0 M) at low CTABr/P123 mole ratios. Remember that the NO_3^- ion has a dominating effect even at low concentrations (0.5 M) and at low CTABr/P123 mole ratios. However, the effect of Cl^- ion at high CTABr/P123 mole ratios (6.0) is very similar to NO_3^- ions. The asymmetric C-H stretching peak at 2850 cm^{-1} in the FTIR spectrum and 2846 cm^{-1} in the Raman spectrum of methyl groups appear as a shoulder and increases in intensity. Notice also that the other signal of CTABr (C-H antisymmetric stretching of methylene group) also increases in intensity. However, the frequency of this signal is very close to antisymmetric C-H stretching mode of poly (propylene oxide) (2920 cm^{-1} and 2933 cm^{-1}, respectively) therefore, only an intensity increase is observed in the FTIR spectra, but in the Raman spectra a broad signal appears with increasing CTABr amount.

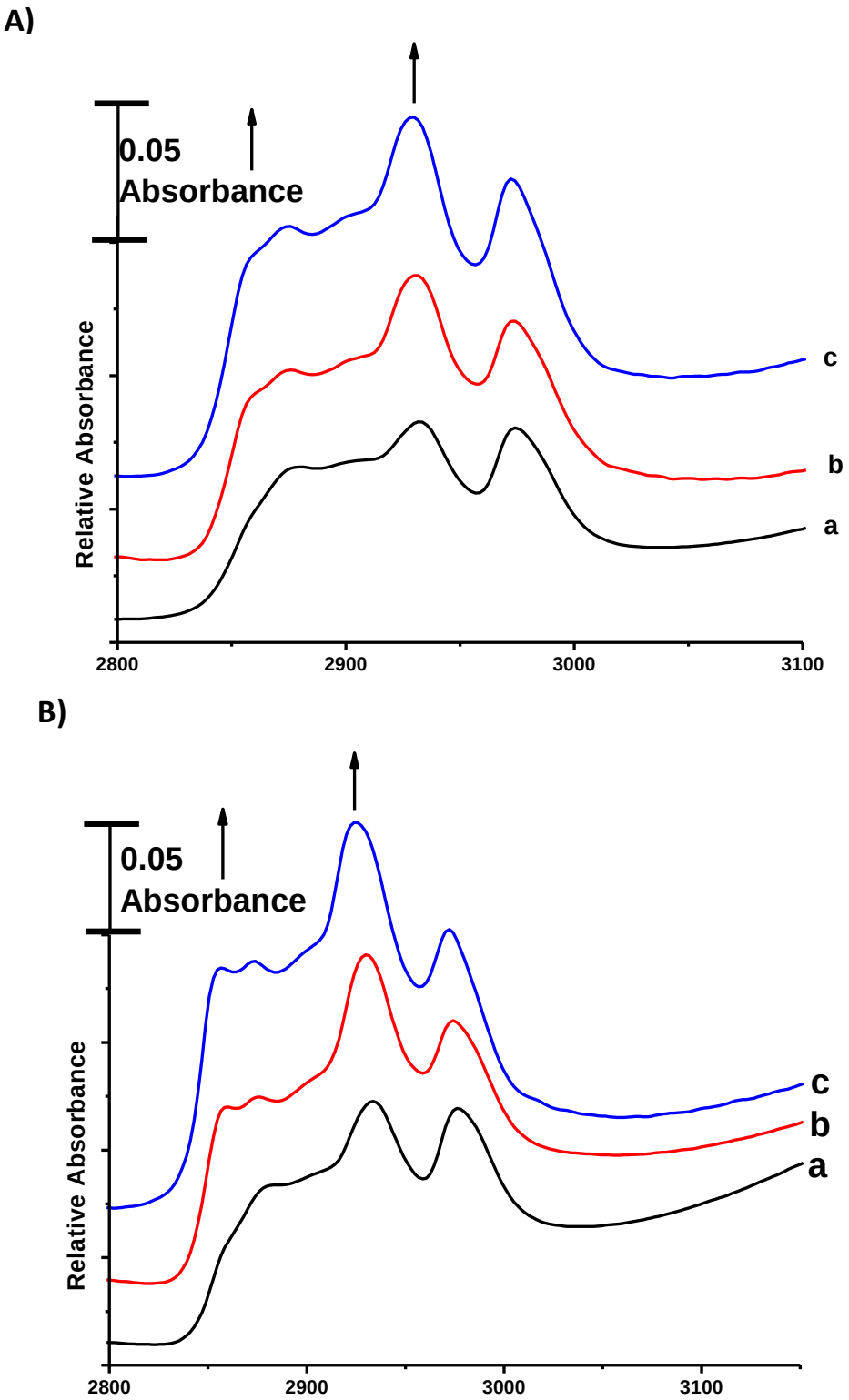

Figure 3.4.17: The FTIR spectra of the mesostructured silica particles obtained from the CTABr-P123-Cl^- systems with different Cl^- ion concentrations and the CTABr/P123 mole ratios; A) The CTABr/P123 mole ratio of 3.0 and Cl^- ion concentration of (a) 0.0 M, (b) 0.5 M, and (c) 1.0 M Cl^-; B) The CTABr/P123 mole ratio of 6.0 and the Cl^- ion concentration of (a) 0.0 M, (b) 0.5 M ,and (c) 1.0 M**.**

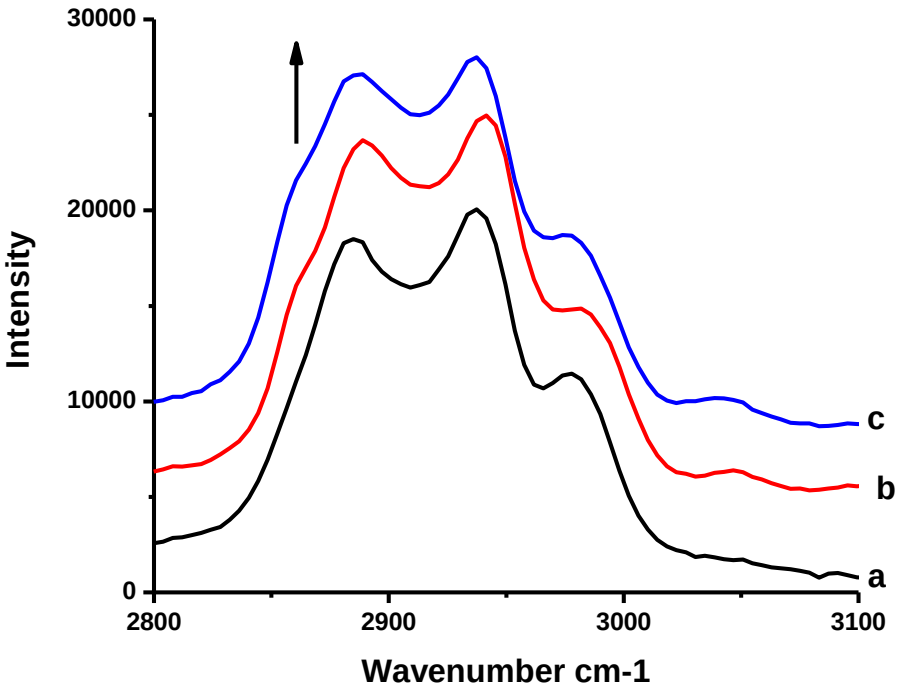

Figure 3.4.18: The Raman spectra of the mesostructured silica particles obtained from the CTABr-P123-Cl^- systems at different Cl^- ion concentrations, the CTABr/P123 mole ratio of 6.0 and the Cl^- ion concentration of (a) 0.0 M, (b) 0.5 M, and (c) 1.0 M Cl^-.

In the CTABr-P123-Cl^- system, if there is enough CTABr in the reaction media, all the particles show a type IV isotherm, which is characteristic for mesoporous materials with regular cylindrical pore size distribution except for high chloride ion concentration (1M) (see **Figure 3.4.19**). When the Cl^- ion concentration reaches 1.0 M, it starts to affect the CTABr solubility and the micelle starts to take more CTABr molecules. Increasing CTABr amount decomposes the micelles, where more disordered particles are formed. Moreover, the N_2 desorption curves of these particles show type III of hysteresis loop, which means the pore structure is slit like which can be realized from type III hysteresis loop, see **Figure 3.4.19-c,f** . This might also indicate a vesicular type assembly with a small amount of cylindrical pores. Note also that at high NO_3^- ion concentrations in the CTABr system, vesicular type

assembly has been encountered (**Figure 3.4.14**). In addition, type III hysteresis desorption brunch is also observed in high nitrate concentrations (not shown).

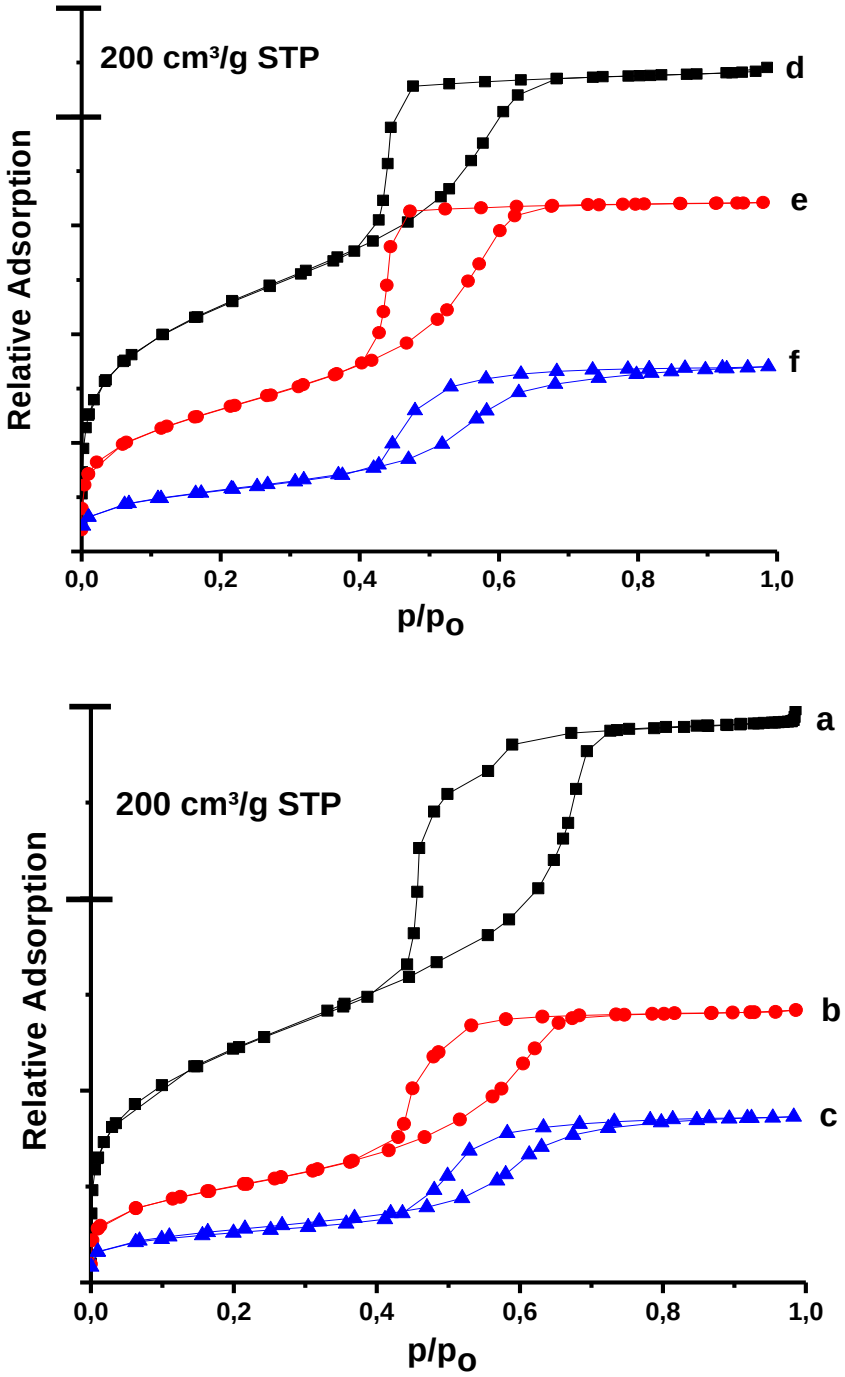

Figure 3.4.19: The N_2 adsorption-desorption isotherm of the mesoporous silica particles obtained from the CTABr-P123-Cl^- system. For the CTABr/P123 mole ratio of 3:.0 and the Cl^- ion concentration of (a) 0.0, (b) 0.5 M, and (c) 1.0 M and for the CTABr/P123 mole ratio of 6.0 and the Cl^- ion concentration of (d) 0.0, (e) 0.5 M, and (f) 1.0 M.

3.4.4. The effect of Benzene:

Dye solubilizing capacity of hydrophobic core of a micelle can also be used in order to control the structural properties of mesoporous silica particles. In the first chapter, the methyl orange is used as a probe molecule to determine micellization properties of P85. The dye concentration was around 10^{-6} M, which is very low to change the micellization of the pluronic surfactants. However, in this part, the benzene concentration is around 10^{-3} M. Benzene is almost insoluble in water, but soluble in aquous P123 solution to some extent. In all synthesis conditions in this thesis, the CTABr-P123-Benzene system formed clear solutions. When benzene penetrates into the core of CTAB-P123 micelles, it dries the core and enlarges the micelle size. As stated before in the CTABr-P123-SO_4^{2-} system, a dehydrated core means more ordered particles. In the CTABr-P123-SO_4^{2-} system, dehydrated core has been achieved by increasing micelle aggregation number; however in the CTABr-P123-Benzene system dry core is achieved by adding hydrophobic species into the core of the micelle. **Figure 3.4.20** shows the PXRD patterns of the as-synthesized particles using the CTABr-P123-Benzene system. At low CTABr/P123 mole ratios (3.0), Benzene forms more ordered particles than at higher CTABr/P123 mole ratios (6.0). Besides (100) plane, the other higher order diffraction lines ((110) and (200)) also have higher intensitiy and are well resolved at 3.0 mole ratio (CTABr/P123), when compared to 6.0 mole ratio. At 4.0 mole ratio (CTABr/P123), the samples show an intermediate behaviour between 3.0 and 6.0 mole ratios. This phenomenon can be explained by looking at the role of CTABr in the assembly of pluronic surfactants (**Figure 3.4.21**). At CTABr free or low CTABr concentrations, an increase in hydrophobic character of the micelle results with a geometry change from spherical micelle to elongated micelle. When hydrophobic molecules enter the core of a micelle

they cause a core expansion and a more effective packing is preferred after a size increase. However, at high CTABr concentrations, the geometry change was suppressed by positively charged head group repulsion. The positively charged head groups of CTABr are accommodated in core-corona interface, where the effective head group area is the highest in spherical packing. Therefore, a higher CTABr content in micelle forces surfactants to pack in a spherical geometry. On the other hand, interestingly benzene solubility is independent of CTABr amount but the existence of CTABr changes the order and morphology of the particles (see text). In other words, the limit in benzene solubility in CTABr-P123-Benzene system only depends on the P123 amount.

In our synthesis conditions, maximum amount of benzene that forms a clear solution in CTABr-P123-Benzene system at room temperature is around 5 ml for a 100 ml bench (5.65×10^{-3} M). A further increase in benzene amount forms a slurry solution, but even to these solutions, TMOS was added and the original procedure was continued. The resulting materials from these slurry solutions are higly mesoporous but poorly ordered (see **Table 3.4.4**). This amount of benzene (5.65×10^{-3} M) might be still soluble since at higher temperatures the hydrophobicity of pluronic surfactant micelles increases and probably solublizing capacity of hydrophobic contents also increases. That means a clear solution might be obtained at higher temperatures (further steps of the reaction). However, even at higher temperatures benzene has a solubility limit. The highest amount of benzene that can be used in order to obtain mesoporous materials is about 8 ml (9.04×10^{-3} M). Above this benzene concentrations; the particles are disordered and no distinct morphology was obtained (not shown).

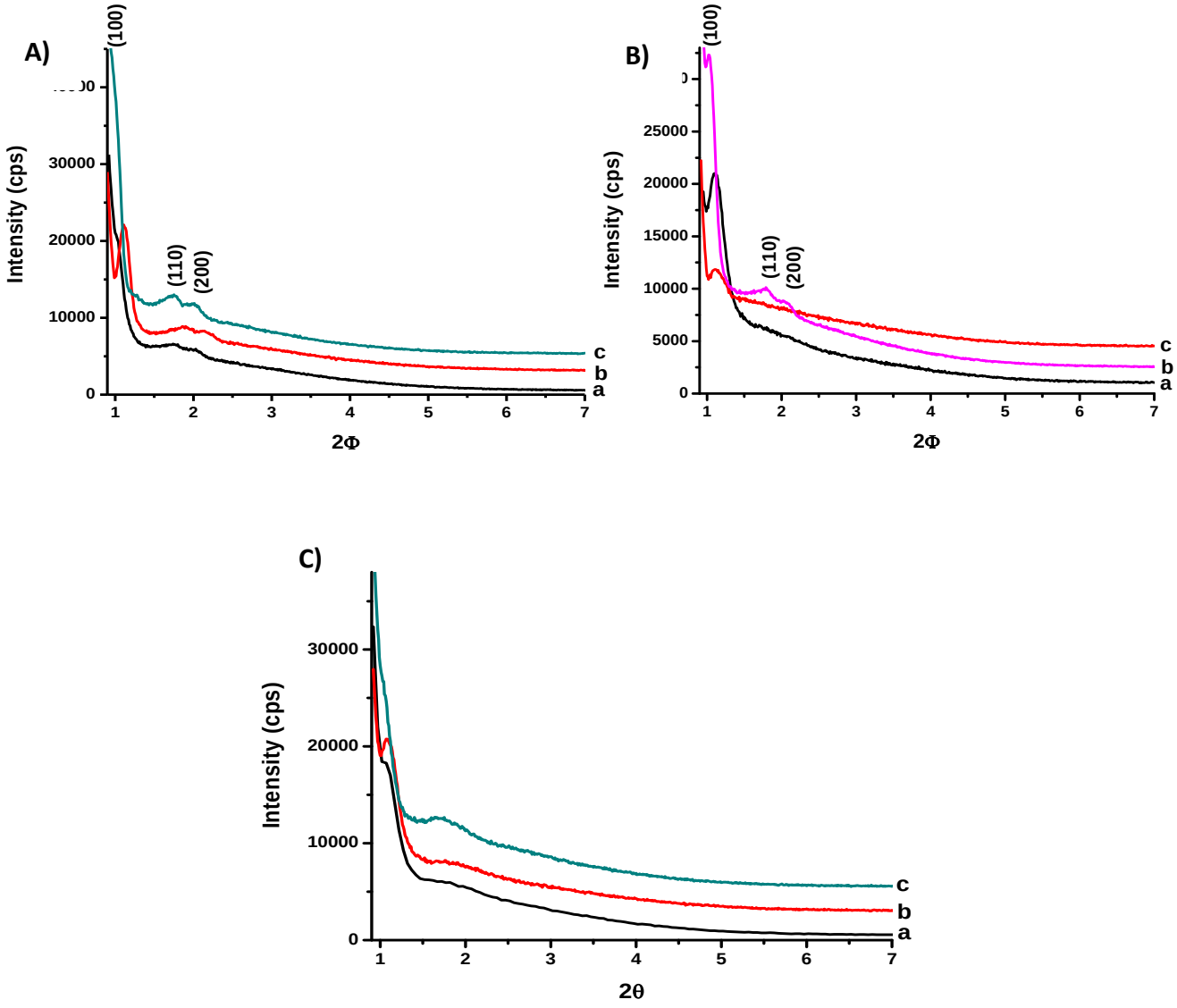

Figure 3.4.20: The PXRD patterns of the mesostructured silica particles obtained from the CTABr-P123-Benzene systems at different benzene concentrations and CTABr/P123 mole ratios. A) The CTABr/P123 mole ratio of 3.0 and (a) 0.0 M, (b) 1.1×10^{-3} M and (c) 3.4×10^{-3} M benzene. B) The CTABr/P123 mole ratio of 4.0 (a) 0.0 M, (b) 1.7×10^{-3} M and (c) 3.4×10^{-3} M benzene. C) The CTABr/P123 mole ratio of 6.0 (a) 0.0 M, (b) 1.1×10^{-3} M and (c) 3.4×10^{-3} M benzene.

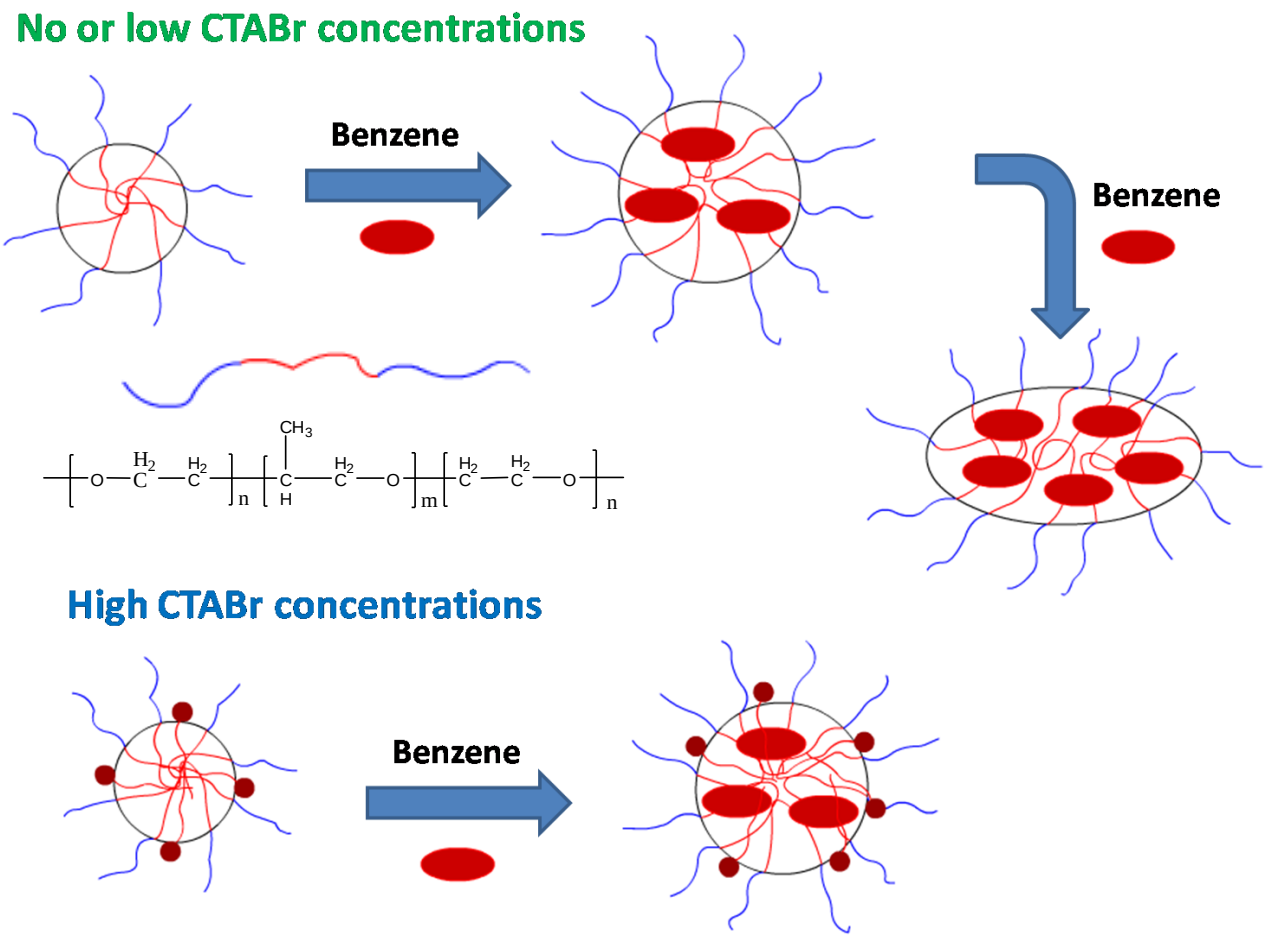

Figure 3.4.21: The schematic description of CTABr-P123-Benzene micellization in different CTABr concentrations.

The effect of benzene on the morphology can be classified in three groups. The first one is at low CTABr/P123 mole ratios, the second one is at high CTABr/P123 mole ratios and the last one is at intermediate concentrations. At high CTABr/P123 concentrations (6.0), benzene has no observable effect on the morphology (not shown) and in the diffraction patterns (see **Figure 3.4.20**). **Figure 3.4.22** shows the SEM images of the samples obtained from the CTABr-P123-Benzene system at low CTABr/P123 mole ratios (3.0). Note that in the absence of

benzene a mixture of spheres and wormlike partices are obtained. By increasing benzene concentration (1.1×10^{-3}M) all the particles are predominantly wormlike. As discussed in the previous paragraphs, the meso-order also increases (from the PXRD patterns) in these elongated particles. A further increase in benzene amount not only increases the order of the particles but also some elongated crystalline particles are also observed (**Figure 3.4.22-c,d**). The side wiev of the crystalline particles are perfectly hexagonal (**Figure 3.4.22-c inlet image**). This observation is consistent with a 2D hexagonal mesostructure determined from the PXRD patterns. Note also that these elongated particles are bifringent under polarized optical microscope indicating a 2D hexagonal mesostructure (not shown). Elongated particles are result of a stronger hydrophobic interaction in the benzene containing cores of the micelles, therefore an order increase and a morphology change are observed in CTABr-P123-Benzene system. Suprisingly, at 3.4×10^{-3} M and higher benzene concentrations, the number of spherical particles increases and a mixture of spherical and wormlike particles are obtained (**Figure 3.4.22-d**). The most reliable explanation is the effect of benzene as a solvent. When it is used in excess, it is no more acting as an additive but it is a co-solvent. By taking into consideration that benzene is a much better solvent than water for pluronic surfactants, therefore a decrease (from PXRD patterns, not shown) of the meso-order and morphology change is not a surprise.

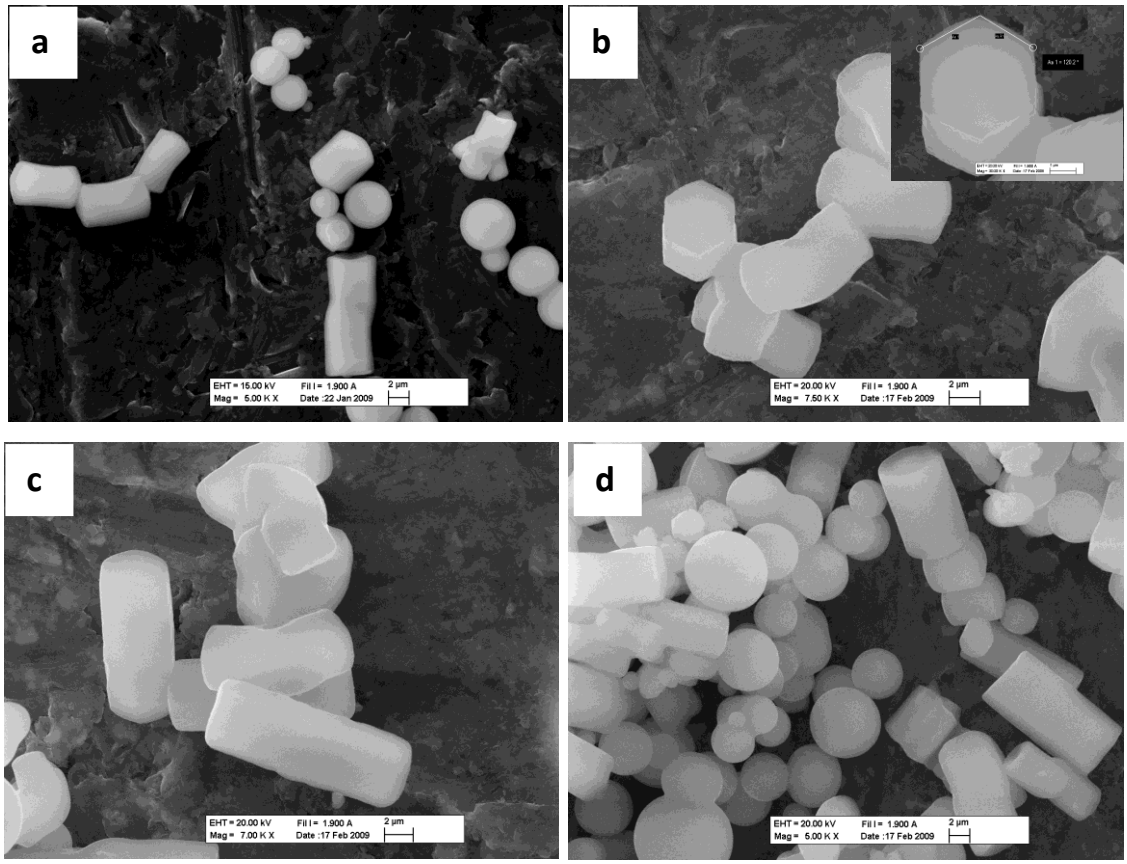

Figure 3.4.22: The SEM images of the CTABr-P123-Benzene system; for the CTABr/P123 mole ratio of 3.0 and the Benzene concentration of (a) 0.0 M, (b) 1.1×10^{-3} M (c) 2.3×10^{-3} M and (d) 3.4×10^{-3} M.

The CTABr/P123 mole ratio of 4.0 can be accepted as an intermediate concentration for the CTABr-P123-Benzene system. At this mole ratio, benzene causes formation of various morphologies from the same synthesis pot (**Figure 3.4.23**). At 1.7×10^{-3} and 3.4×10^{-3} M concentrations, the observed morphologies are sphere, wormlike, crystal like, coin type, gyroid, bagel and gyroscope type. To the best of our knowledge the gyroscope type particles have not been observed yet. In general the particles, at this CTABr/P123 mole ratio of 4.0, are shorther in length and more oval when compared to the particles synthesized at 3.0 mole ratio in the CTABr-P123-Benzene system. When the benzene concentration is above ~5.0×10^{-3}

M, disordered particles start to form and its amount increase with increasing benzene concentration (see **Figure 3.4.23-c,d**). Note that these particles are completely disordered.

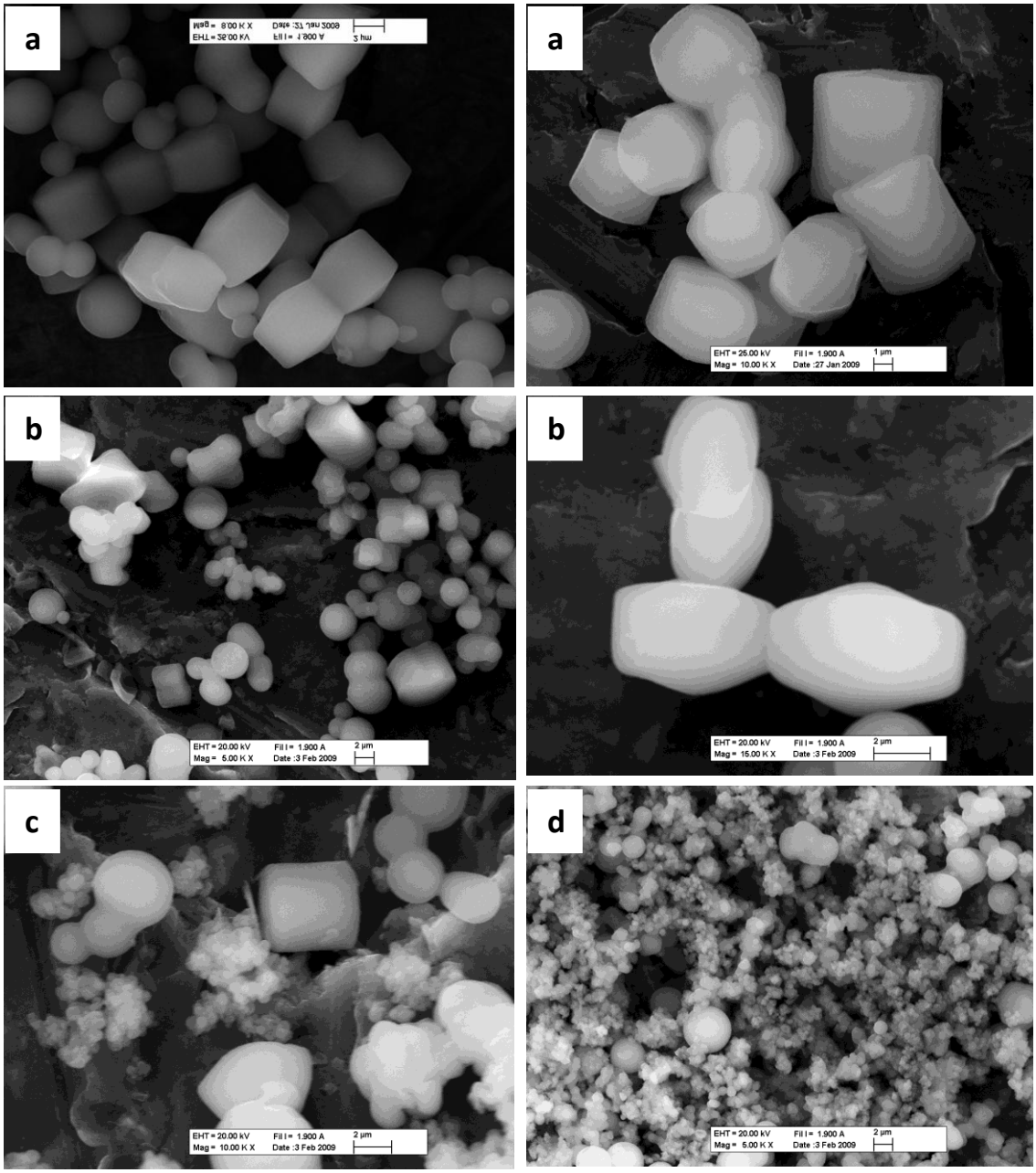

Figure 3.4.22: The SEM images of the CTABr-P123-Benzene system; for the CTABr/P123 mole ratio of 4.0 and the Benzene concentration of (a) 1.7×10^{-3} M, (b) 3.4×10^{-3} M, (c) 5.7×10^{-3} M and (d) 9.0 M $\times10^{-3}$.

The TEM images also support that higly ordered 2D hexagonal particles are formed from the CTABr-P123-Benzene system (**Figure 3.4.23**). The top part of the TEM image in **Figure 3.4.23-a** is a perfect illustration of the hexagonal ordering. The pore channels of these particles are straight and continue through the particle (**Figure 3.4.23-b).**

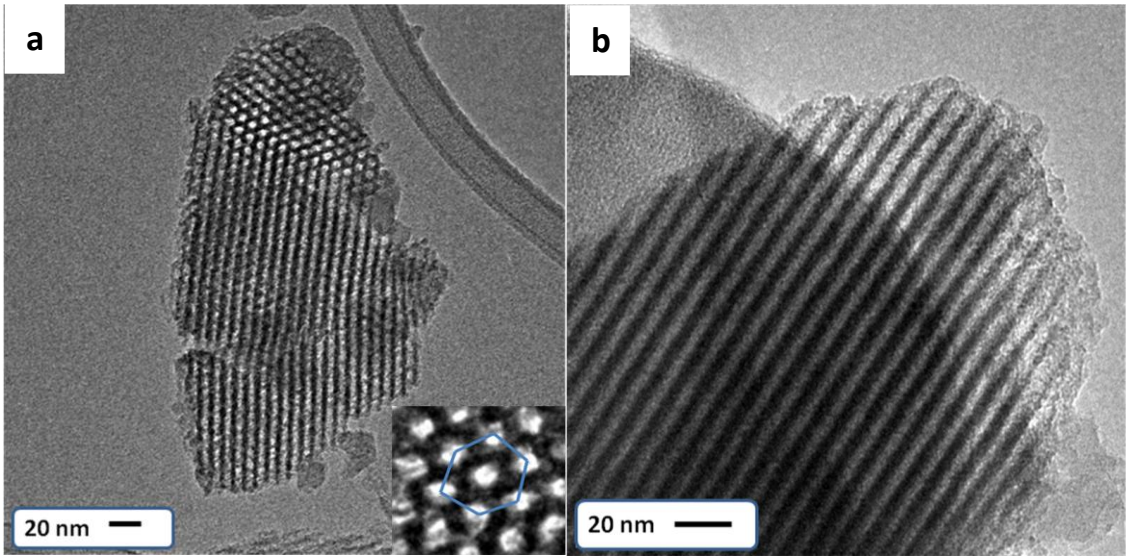

Figure 3.4.23: The TEM images of the samples obtained from the CTABr-P123-Benzene system; for the CTABr/P123 mole ratio of 4.0 and the Benzene concentration of 1.7×10^{-3} M. The inset in a is a magnified upper part of the image to show hexagonal packing.

The most characteristic property of the organic additives is their role as pore swelling agent. Therefore, an increase in the pore size distribution is observed for the CTABr-P123-Benzene system depending on the CTABr and benzene concentrations (see **Table 3.4.4**). In our system at low CTABr (CTABr/P123 mole ratios of 3.0 and 4.0) concentrations, the wall thickness decreases with increasing benzene, which can be attributed to a decreased repulsion between the benzene containing micelles or

increased hydrophobic interaction in the micelles (**Table 3.4.4**). The wall thickness does not change and a pore size expansion is observed for only high benzene concentrations at high CTABr concentrations (CTABr/P123 mole ratios of 6.0). Because, higher amounts of CTABr molecules in the micelle prevents a decrease at repulsive forces (because of charge repulsion) in the benzene containing micelles.

CTAB/P123 mole ratio	Benzene Amount ($*10^{-3}$ M)	BET surface area (m^2/g)	d100 (nm)	BJH pore size distribution[a] (2r)	Wall thickness t[b] (nm)
3:1	0	690.3	8.8	5.9	4.3
	1.13	665.4	7.9	5.5	3.7
	2.26	756.4	7.9	5.7	3.5
	3.39	696.4	8.8	6.6	3.5
4:1	0	685.3	7.9	4.1	5.0
	1.70	687.5	7.9	5.4	3.7
	3.39	645.4	7.9	5.4	3.7
	5.65	690.4	---------	6.9	----------
	9.04	717.5	---------	6.7	----------
6:1	0	722.7	8.4	4.6	4.7
	1.13	619.0	8.1	4.7	4.6
	2.26	665.0	8.5	4.9	4.8
	3.39	643.2	8.9	5.6	4.7

[a] Pore diameter is calculated from the adsorption branch of the isotherm by BJH method.

[b] The wall thickness t is obtained by deducing the pore diameter (2r) from the unitcell a_o ($a_o = (2/\sqrt{3})d_{100}$), namely, t= a_o 2-r.

Table 3.4.4: The structural parameters of the CTABr-P123-Benzene system at different CTABr/P123 mole ratios and in different Benzene concentration.

3.5. The Catalytic Effect of Flouride Ion in the Synthesis of Mesoporous Silica:

The effect of flouride ion on the micellization of pluronic surfactants has been discussed in **chapter 1**. It decreases the pluronic surfactant solubility by means of the CMC and CMT. On the ther hand, in the CTABr-P123-F^- system, the role of F^- ion is more than controlling the micellization of P123. flouride ion is also a catalyst for both hydrolysis and condensation reactions of silica species [89]. Many mesoporous silica materials have been synthesized using flouride ion, in order to improve the micellization and to increase the reaction rate [86-88,92,93]. In the CTABr-P123-F^- system, the used concentration interval is too low to affect the micellization of P123 ($\sim 10^{-2}$ M). Notice that the concentration range of F^- ion is almost ten times smaller than the minimum concentration (0.1 M) investigated in the micellization experiments (see **Figure 3.18**). The role of the flouride ion in the CTABr-P123-F^- system, is to speed up the silica polymerization. Since the hydrolysis of TMOS is already very fast (~10 s in dilute solutions (0.1 M)), the effect of the flouride ion on the CTABr-P123-F^- system is only on the condensation of silica. In the absence of flouride ion (the CTABr-P123 system), the reaction takes place in five days at 95^oC, but the synthesis time is less than 20 min in the CTABr-P123-F^- system. Moreover, the particle size distribution is uniform when compared to flouride ion free system and the surface area of the particles is also higher in the CTABr-P123-F^- system (see text).

Figure 3.5.1 shows the PXRD patterns of as-synthesized powder samples from the CTABr-P123-F^- system in different reaction times. The reactions were stopped at different times by adding excessive amount of water (more than 300 ml) to

the solution and washing the sample after filtration in order to decrease the Flouride ion concentration. Note that in the absence of flouride ion and at low pH values (pH = 1), the polymerization of silica is very slow at room temperature. The intensity of first diffraction line (100) was taken as the reference point. The intensity and shape of the diffraction line reaches its final form in ten minutes and further reaction time does not improve the diffraction pattern. This shows that the ordered mesoporous particles are formed in ten minutes. Moreover, the SEM images of the particles supports the same argument, they show no difference after ten minutes of the synthesis, **Figure 3.5.2**. All the particles are spherical in geometry and the size of the spherical particles does not change after ten minutes (**Figure 3.5.3**).

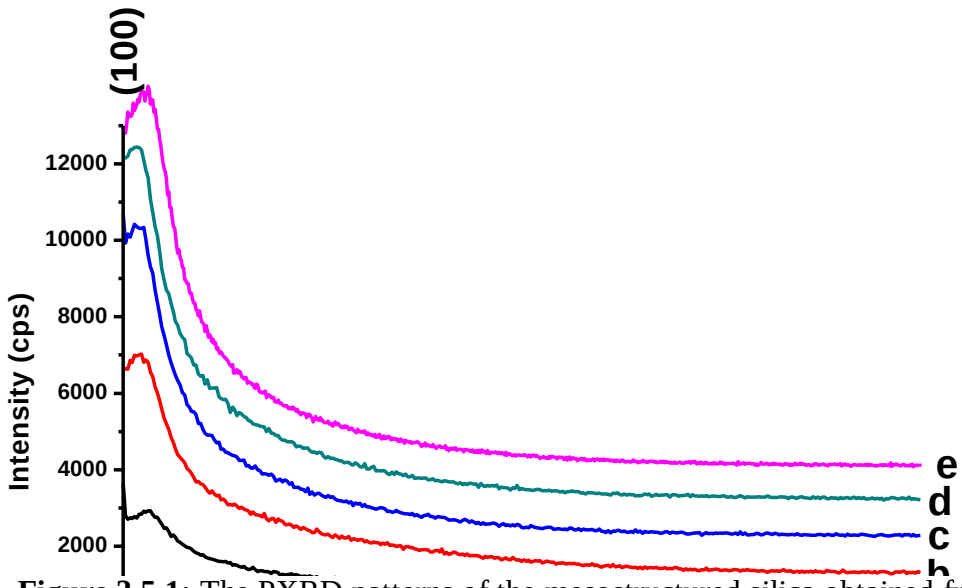

Figure 3.5.1: The PXRD patterns of the mesostructured silica obtained from CTABr-P123-F^- systems at different synthesis times; the CTABr/P123 mole ratio of 5.0 (P123 concentration is 1.74×10^{-3} M) and the F^- ion concentration is 2×10^{-2} M: (a) 3.0 min, (b) 5.0 min, (c) 10 min, (d) 20 min and (e) 40 min.

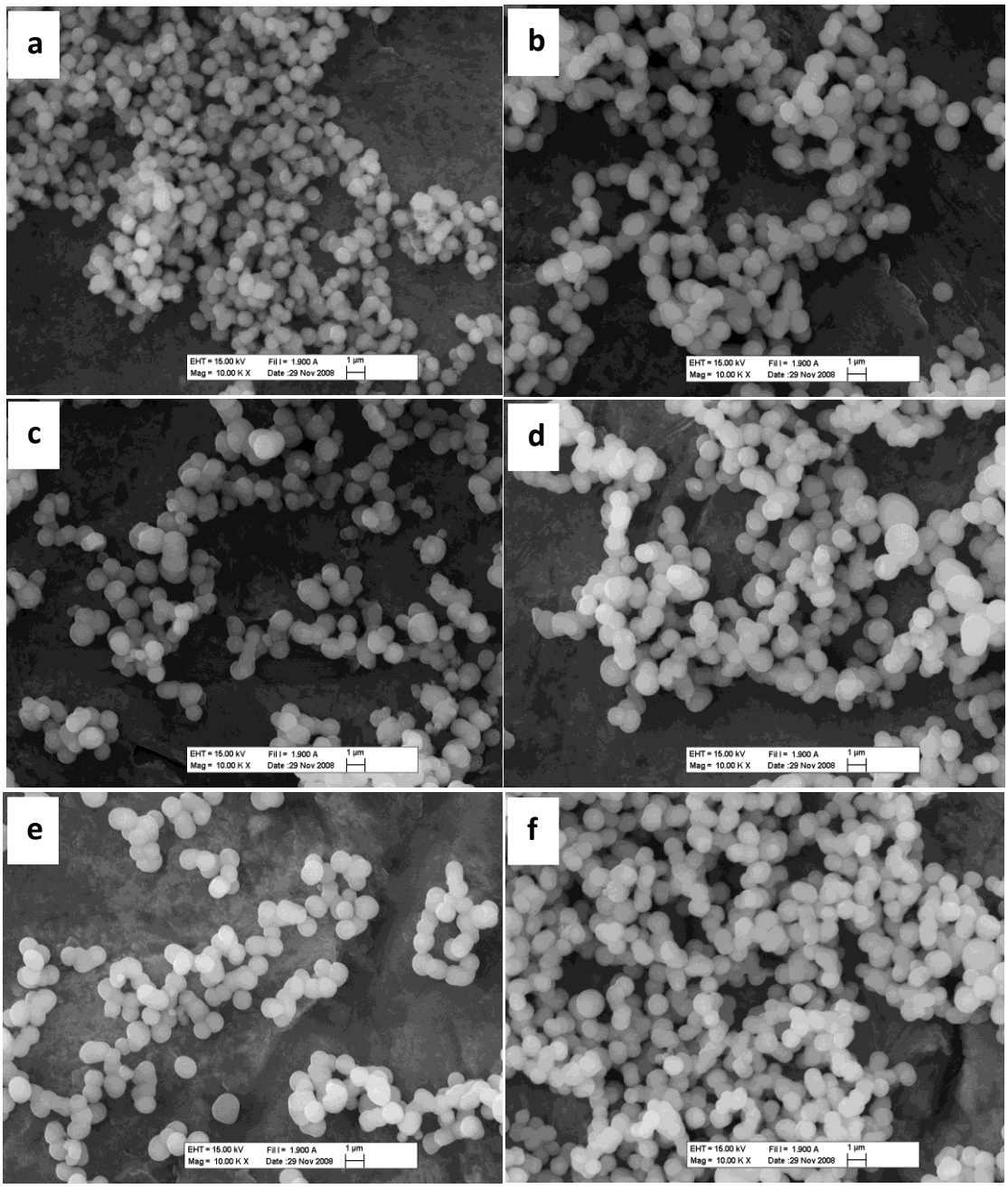

Figure 3.5.2: The SEM images of the mesostructured silica particles obtained from the CTABr-P123-F- systems at different synthesis times; the CTABr/P123 mole ratio of 5.0 (P123 concentration is 1.74×10-3 M) and the F^- ion concentration is 2×10^{-2} M: (a) 3.0 min, (b) 5.0 min, (c) 10 min, (d) 20 min and (e) 40 min.

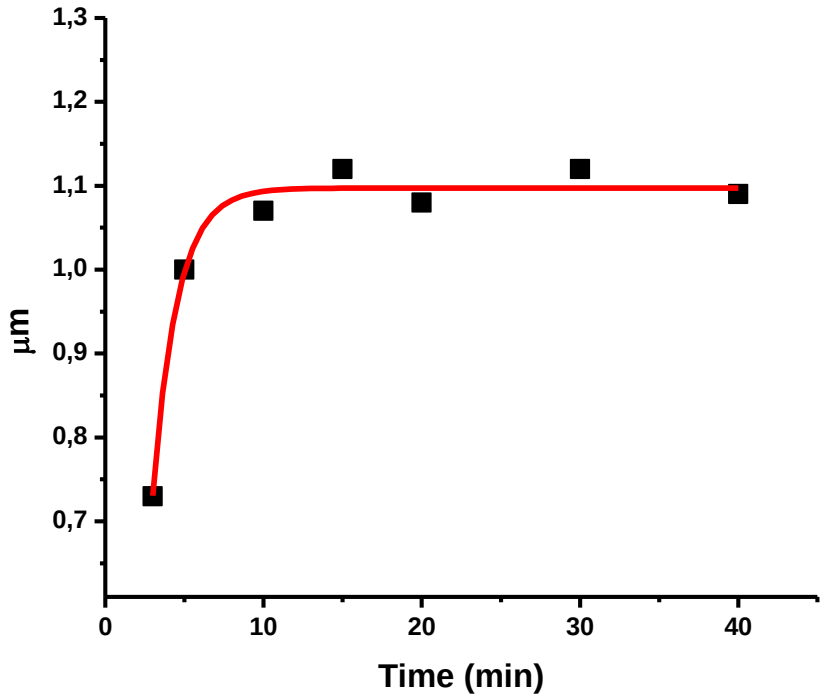

Figure 3.5.3: The Average Particle Size of the mesostructured silica particles obtained from the CTABr-P123-F^- system at different synthesis times; the CTABr/P123 mole ratio of 5.0 (P123 concentration is 1.74×10^{-3} M) and the F^- ion concentration is 2×10^{-2} M: (a) 3.0 min, (b) 5.0 min, (c) 10 min, (d) 20 min, and (e) 40 min. The average particle size is calculated by counting 100 particles.

All the reactions were started at RT. Despite the temperature increases up to 35 ^oC after fourty minutes during the sonication of a reaction mixture, the temperature change is less than 5^oC in twenty minutes. Note that mesoporous particles are formed in less than 20 min, so the effect of temperature change is neglegible. Moreover, a change in the starting temperature of the reaction has a remarkable effect on the morphology and pore structure of mesoporous particles (see text later), however a 5^oC change in temperature during the reaction does not cause any change on these particles. Therefore, the CTABr-P123-F^- system serves a new and fast method in synthesis of monodispersed mesoporous spherical silica particles. To the best of our

knowledge, this is the fastest method in the literature for the synthesis particles in the CTABr-P123 system, known as SBA-15. **Figure 3.5.4** shows the SEM images and size distributions of the particles synthesized in two different systems CTABr-P123-F^- and CTABr-P123. The particles synthesized using the CTABr-P123-F^- system has more uniform size distribution than the particles from the CTABr-P123 system. In both systems, particles are spherical in shape.

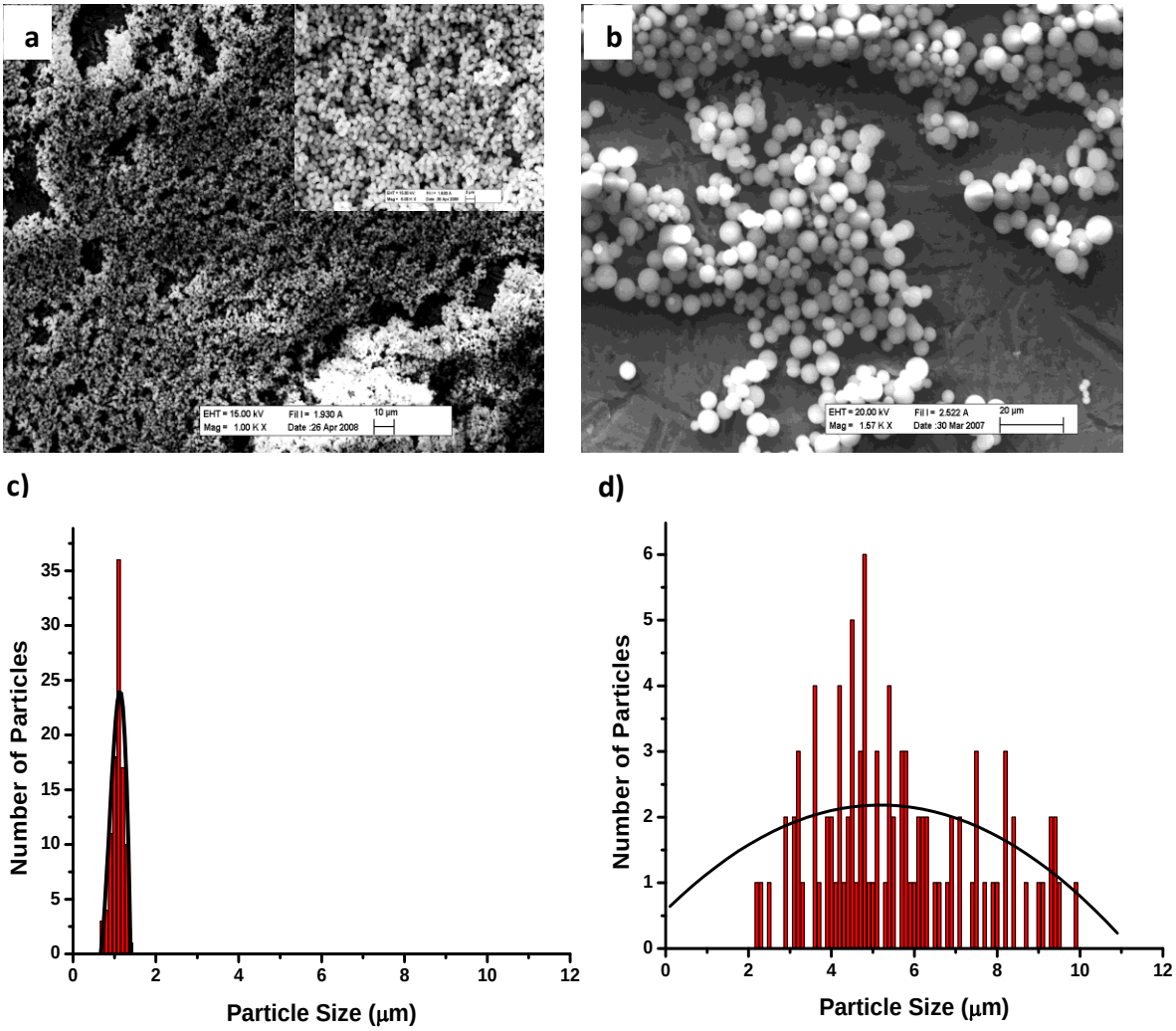

Figure 3.5.4: The SEM images and particle size distributions of the mesostructured silica obtained from the CTABr-P123-F^- system (F^- concentration is 2×10^{-2} M) (a) the SEM image scale bar is 10μm (the inset is a magnified image, where the scale bar is 3μm) and (c) particle size distribution and the CTABr-P123 system; (b) the SEM image (scale bar is 20μm) and (d) particle size distribution. The CTABr/P123 mole ratio is 5.0 (in both systems)**.**

The particles, in the CTABr-P123-F^- system, were synthesized in an ultrasonic bath. The ultrasound has both chemical and physical effects. The physical effects have also chemical consequences, which are enhanced mass transport, emulsification, thermal heating and macroscopic smoothing [149-151]. The ultrasound is generally used in accelerating chemical reactions in liquid-solid heterogeneous systems, sonochemical modification, polymer degradation, heterogenous catalysis, biomaterial preparation, nanostructured materials like cadmium selenide and metal oxide nano-wires etc. [148-152]. All of the above mentioned effects of ultrasound are a result of cavity formation. High intensity ultrasound causes acoustic cavity formation and collapse of these cavities causes local heating (up to 6000 C^o), high pressure (up to 1000 atm) and accelerated mass transport around the cavities [148,149]. A wide range of ultrasonic equipment is available commercially (20-100 kHz) and the most powerful ones have higher frequency than 10MHz [149,153]. However, the ultrasonic cleaners have generally lower frequency (< 70 Hz) [148,150].

In the synthesis of mesostructured silica particles, ultrasound radiation has been employed first time by Gedanken et al. in order to synthesise MCM-41 type mesoporous materials [154]. With the help of an ultrasound, they have achieved the synthesis in a very short time and obtained thicker interwalls. The used equipment had 100 Watt/cm^2 ultrasound intensity and 20 kHz frequency. In the CTABr-P123-F^- system, the used ultrasound radiation has only 50 Hz frequency. When compared to the system of Gedanken our ultrasound radiation is much weaker. On the other hand, it is also possible to observe cavity formation so as the similar effects (such as degassing, emulsifying, dispersion, erosion, sonoluminisance, cleaning of the surface

of solids) with a low frequency ultrasound [150]. Different from the high frequncey ultrasound, low frequency ultrasound polishes the surface of microscopic particles; nevertheless the effect is formation of rough surface in the former [150]. The ultrasound radiation has caused a smoother surface and more ordered pore structure in the CTABr-P123-F^- system (see text).

3.5.1. The Effect of CTABr Concentration and Ultrasound Radiation on the Formation of Mesoporous Silica Particles:

The cooparative assembly of CTABr and P123 is the key factor in the formation of mesoporous particles in the CTABr-P123 system. The CTABr improves the micellization of P123, supplies positive charge to the micelles and helps micelles to assemble in an ordered way. The same contributions of CTABr can also be listed for CTABr-P123-F^- system. Since the silica polymerization is accelerated by F^- ion, a decrease at assembly rate by increasing positive charge on the CTABr-P123 micelles is observed by increasing CTABr concentration. **Figure 3.5.5** shows the Turbidty Point (TP) times as a function of CTABr concentration in the CTABr-P123-F^- system. The TP is determined for the P123 concentration of 1.74×10^{-3}M and F^- ion concentration of 2.4×10^{-3} M. Note that the TP also depends on the P123 and F^- ion concentrations, but their effect will be discussed later. Therefore, in order to observe the effect of CTABr on the TP and mesostructured particles, the P123 and the F^- ion concentrations are kept constant for these experiments. The TP is consisting of two regions (Region I and Region II) and both regions show a linear dependance to the CTABr concentration. The slope of the Region I is smaller than the slope of the Region II, indicating a change in the micellar form after a certain CTABr concentration. Note that an increase in the pluronic surfactant concentration enlarges Region I.

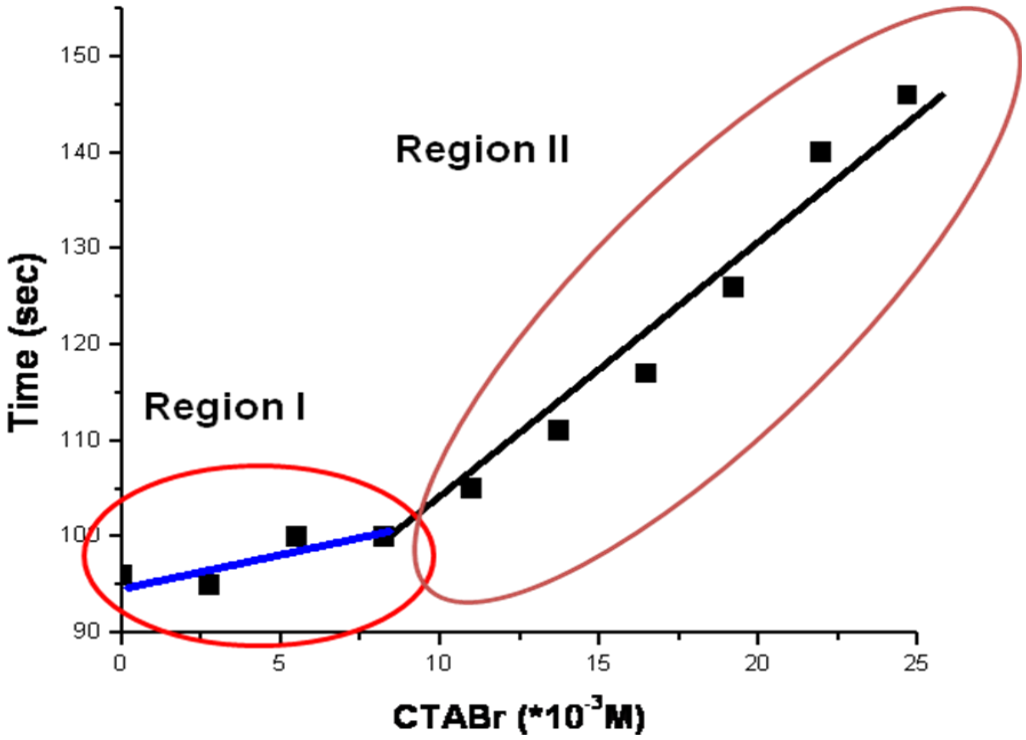

Figure 3.5.5: The TP points of the particles obtained from CTABr-P123-F^- system; P123 concentration is 1.74×10^{-3}M, TMOS concentration is 0.16 M and F^- concentration is 2.4×10^{-3} M.

The linear trend in Region I can be attributed to increasing number of CTABr molecules in CTABr-P123 micelles. When the CTABr molecules increase in number, the CTABr-P123 micelles will be more positively charged. Since the silica particles are also positively charged at pH 1, the assembly of positively charged silica monomers with positively charged CTABr-P123 micelles gets slower. Strating with Region II, the slope increases suddenly, indicating a change in the CTABr-P123 micelles. The most reasonable explanation is a sudden decrease at the number of the P123 molecules in the CTABr-P123 micelles. Since, in pluronic-CTABr system increasing CTABr concentration breaks down the pluronic micelles and then forms their own micelles after a certain concentration (see **Section 1.4.3**). Therefore, high CTABr concentration might cause disappearance of the CTABr-P123 micelles and formation of CTABr micelles. In this region the micelles consist of only CTABr

molecules, therefore the slope is steeper and the P123 molecules float as free surfactant in the solution. The PXRD patterns of the mesostructured particles from the CTABr-P123-F^- system also supports this argument (**Figure 3.5.6**). At relatively low CTABr concentrations (in concentration range of Region I), the particles have a broad, but intense diffraction line due to (100) planes. The (110) and (200) planes can not be resolved since they are under the first broad diffraction line. A broad diffraction line might originate from a structural disorder or is due to a decreased in particle size (see texts later). At higher CTABr concentrations (Region II), the particles show a broad diffraction line with a very low intensity. Moreover, the first diffractin line shifts to higher angles (2Θ) with increasing the CTABr concentrations. These observations also support that at high CTABr concentrations, the micelles are formed mainly by the CTABr molecules rather than CTABr-P123 couple.

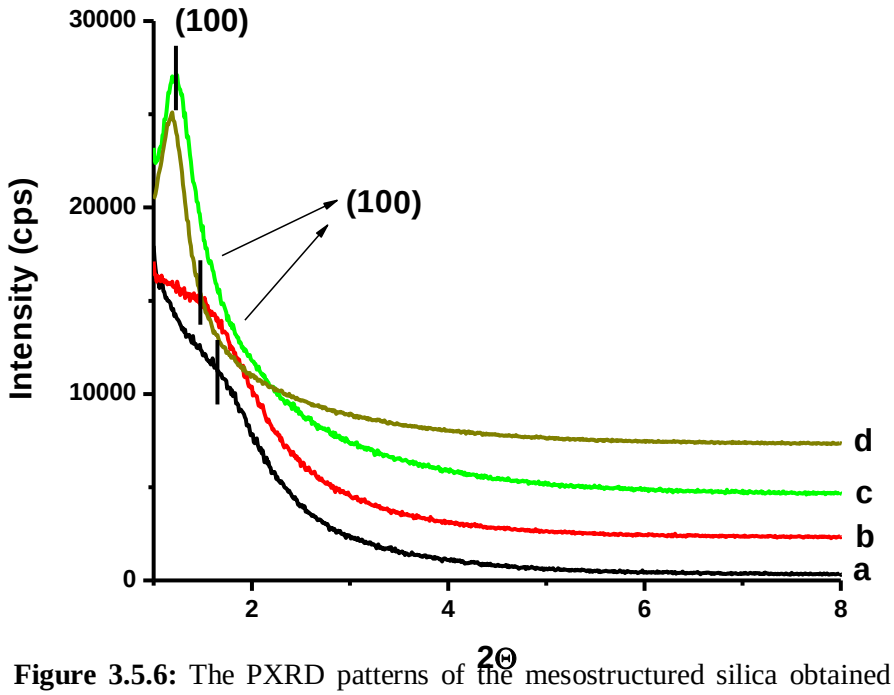

Figure 3.5.6: The PXRD patterns of the mesostructured silica obtained from the CTABr-P123-F^- systems with CTABr concentration of (a) 4.6×10^{-2} M, (b) 3.0×10^{-2} M, (c) 1.3×10^{-2} M and (d) 0.9×10^{-2} M. The P123 concentration is 1.74×10^{-3}M, the TMOS concentration is 0.16 M and the F^- ion concentration is 2.4×10^{-3} M.

All the particles are mainly spherical in shape, which are synthesized from the CTABr-P123-F^- system. On the other hand, mixing type has a significant impact on the shape and surface morphology of formed particles. **Figure 3.5.7** shows the SEM images of particles synthesized from the CTABr-P123-F^- system with different CTABr concentrations in two different mixing methods (sonication and stirring). Regardless of the CTABr concentration, the particles synthesized with stirring are aggregated spherical particles. These aggregated particles are not perfectly spherical and most of them are sticked to each other and connections are covered by silica particles. On the other hand, the particles synthesized under constant ultrasonic radiation are spherical and their surface morphology is smoother, in addition the particle size depends on the CTABr concentration. The particles synthesized at lower CTABr concentrations have lower average particle size (not shown). Remember that increasing CTABr concentration decreases the TP so the rate of assembly of the silica species with the micelles (see **Figure 3.5.5**). When the CTABr concentration is high enough (Region II), the spherical particles are covered by some features (CTABr concentration is 4.6×10^{-2} M). These features are formed most probably by polymerization of silica around the free P123 molecules and settling of these microscopic aggregates on the sureface of the spherical particles. The most remarkable difference between the particles synthesized under constant stirring and sonication is the smoothness of the spherical particles synthesized under constant ultrasonic radiation. As mentioned before ultrasonic radiation causes a mechanical removal of the surface materials resulting with a smooth surface morphology of the spherical particles. Moreover, the particles synthesized under constant ultrasonic radiation are more ordered when compared to the particles synthesized under constant stirrinig, especially at high CTABr concentrations.

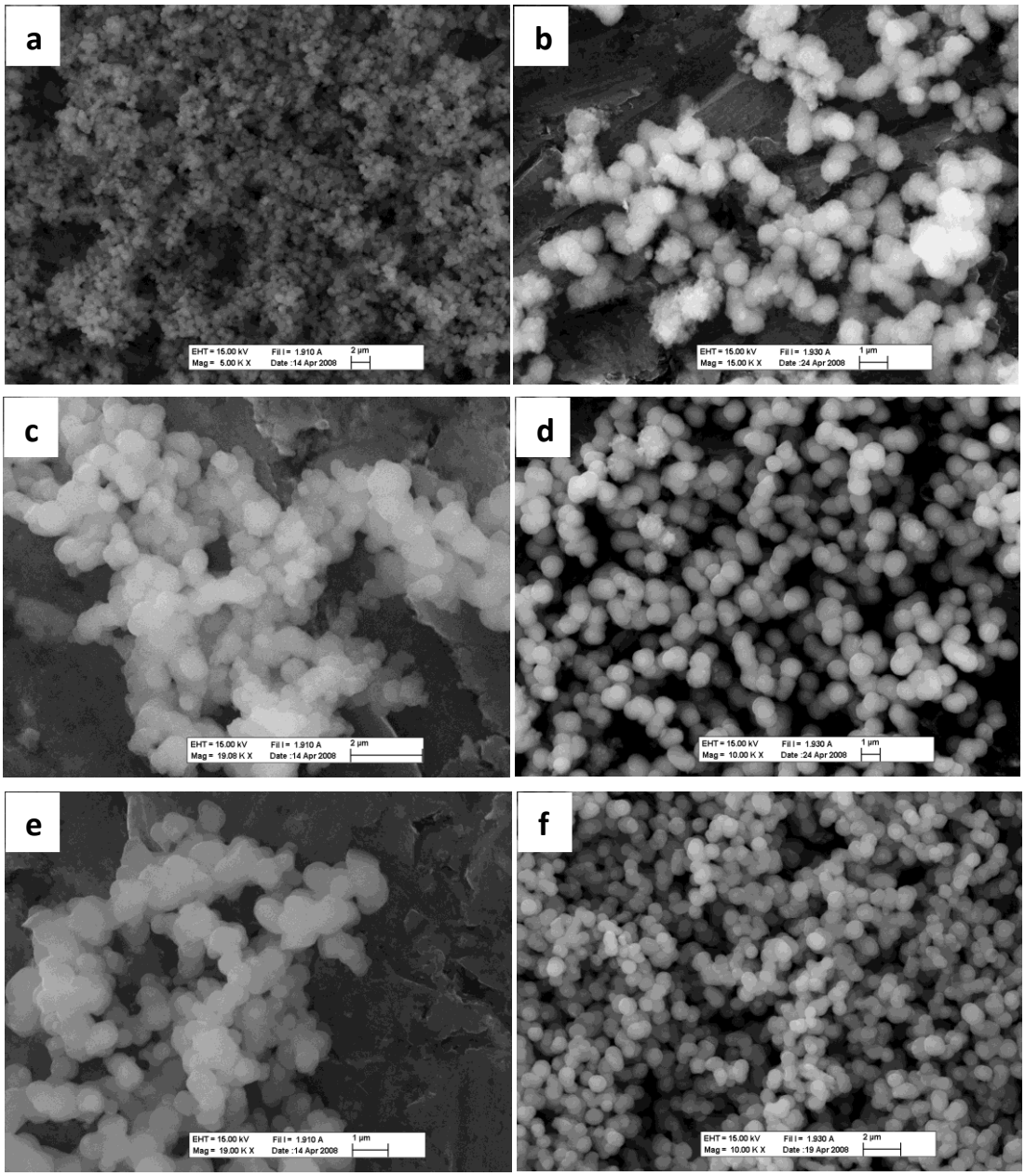

Figure 3.5.7: The SEM images of the mesostructured silica obtained from CTABr-P123-F^- systems synthesized under constant stirring (M) or sonication (S) with CTABr concentration of a) 4.6×10^{-2} M (M), b) 4.6×10^{-2} M (S), c) 3.0×10^{-2} M (M), d) 3.0×10^{-2} M (S), e) 0.9×10^{-2} M (M) and f) 0.9×10^{-2} M (S) . The P123 concentration is 1.74×10^{-3}M, TMOS concentration is 0.16 M and the F^- ion concentration is 2.4×10^{-3} M.

3.5.2. The Effect of Flouride Ion Concentration on the Formation of Mesoporous Silica Particles:

The role of flouride ion as a catalyst is to speed up the synthesis process even at very low flouride ion concentrations. An increase in the silica polymerization rate has remarkable consequencies on the silica particles. **Figure 3.5.8** shows the Turbidity Point (TP) time as a function of the F^- ion concentration, where the CTABr/P123 mole ratio is 5.0. The TP data can be fit to first order exponential decay and reaches to a plateau for F^- ion concentration of 2×10^{-2} M, above this concentration the TP does not change.

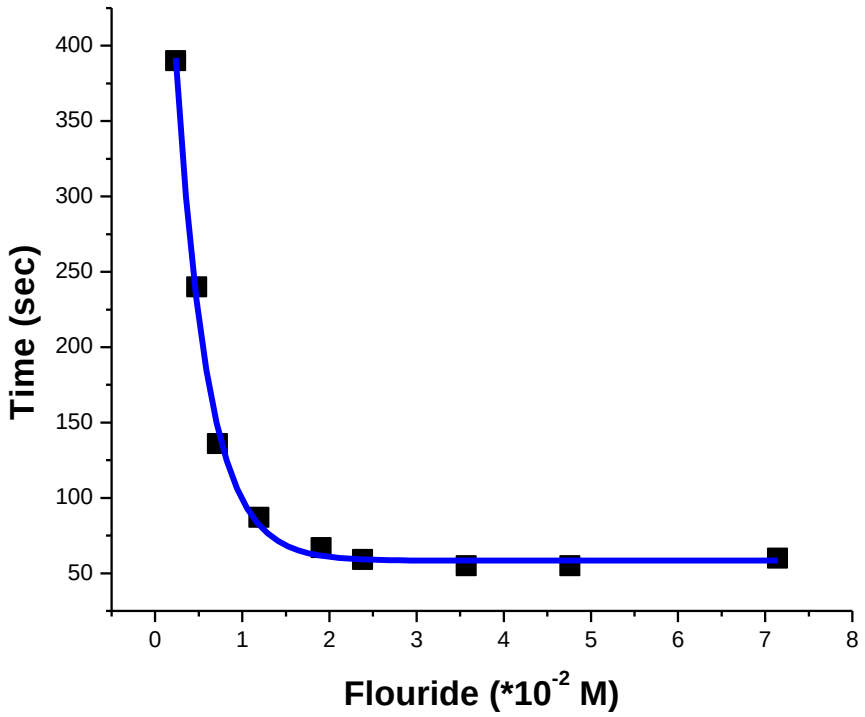

Figure 3.5.8: The TP points of the particles obtained from CTABr-P123-F^- system at various F^- concentrations; P123 concentration is 1.74×10^{-3}M, TMOS concentration is 0.16 M and CTABr concentration is 9.0×10^{-3} M.

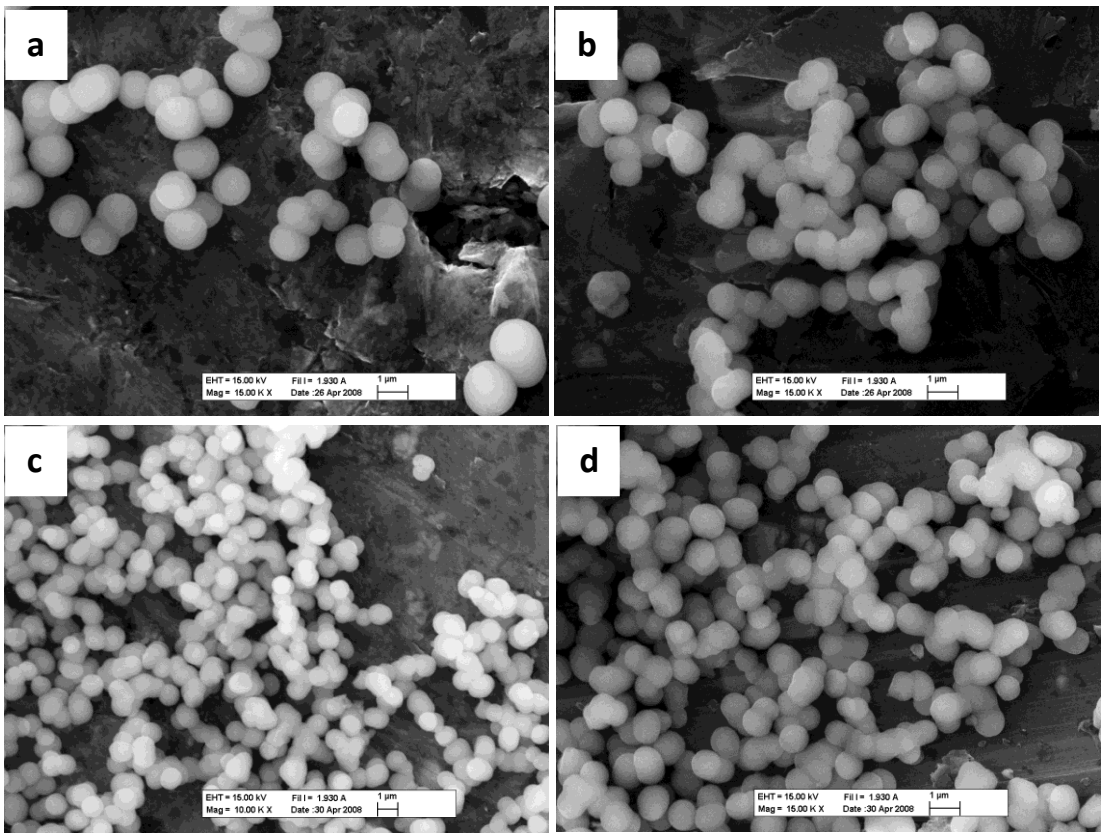

Figure 3.5.9: The SEM images of the mesostructured silica obtained from the CTABr-P123-F^- systems synthesized under constant sonication, the CTABr/P123 mole ratio of 5.0 and the F^- ion concentration of (a) 1.1×10^{-2} M, (b) 1.5×10^{-2} M, (c) 2.0×10^{-2} M and (d) 2.5×10^{-2} M.

An increase in the rate of silica polymerization, with the help of increasing the flouride ion concentration, results in monodispersed spherical particles, having different size distributions depending on the flouride ion concentration. **Figure 3.5.9** show the SEM images of the particles obtained from the CTABr-P123-F^- system at various F^- ion concentrations. Despite the particles are mainly spherical in shape and monodispersed at all F^- ion concentrations, only at low concentrations morphology of the particles is perfectly spherical. It is observed that the particles are not perfectly spherical, like in the CTABr-P123 system (not shown). Moreover, all particles have smooth surface. **Figure 3.5.10** the particle size distributions of the particles from CTABr-P123-F^- system at various F^- ion concentrations. The error bars in the figure

indicates the particle size range at various F^- ion concentrations. The particles get smaller in size with increasing F^- ion concentration. In the absence of F^- ion, the particles have larger average particle size and a wide size distribution. On the other hand, the particles synthesized from the CTABr-P123-F^- system have much smaller particle sizes with a narrow size distribution. Note that the average particle size, in **Figure 3.5.10,** can be fit to the first order exponential decay. This shows a direct relation between the rate of reaction and particle size distribution of the formed particles.

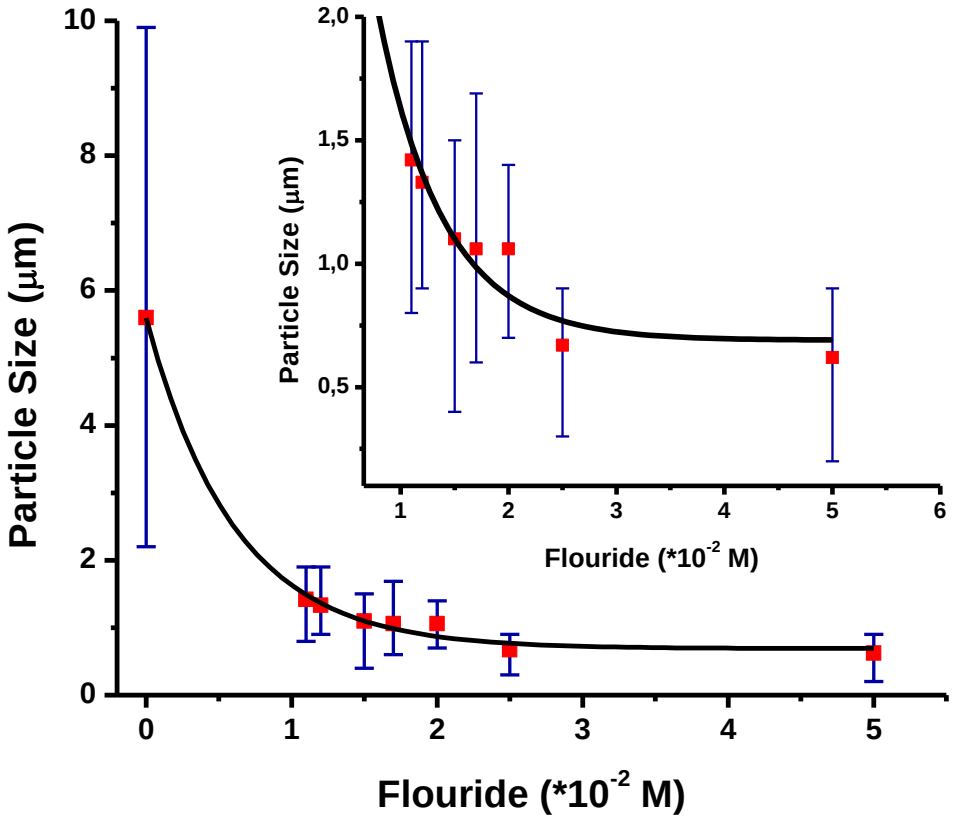

Figure 3.5.10: The average particle size of the particles obtained from the CTABr-P123-F^- system at various F^- ion concentrations; P123 concentration is 1.74×10^{-3}M, TMOS concentration is 0.16 M and CTABr concentration is 9.0×10^{-3} M.

Table 3.5.1 gives a more detailed picture of the relation between the particle size distribution and monodispersity with respect to the F^- ion concentration in the CTABr-P123-F^- system . Besides average particle size dependence of various F^- ion concentrations, the difference between the smallest and largest particles get smaller with increasing F^- ion concentration. The F^- ion concentration is effective up to 2.5×10^{-2} M and further increase of the F^- ion concentration in the synthesis media does not change the particle size and monodispersity. Recall that the TP also does not change above this F^- ion concentration.

NaF concentration (*10^{-3} M)	Turbidity Point (TP) (s)	Average Particle Size[b] (ųm)	Minumum Particle Size(ųm)	Maximum Particle Size (ųm)
11.0	**200**	**1.4**	**0.8**	**1.9**
12.0	**170**	**1.3**	**0.9**	**1.9**
15.0	**140**	**1.1**	**0.5**	**1.6**
17.0	**120**	**1.1**	**0.6**	**1.7**
20.0	**100**	**1.0**	**0.7**	**1.4**
24.8	**80**	**0.7**	**0.3**	**0.9**
49.6	**60**	**0.6**	**0.2**	**0.9**
0[a]	**----------**	**5.6**	**2.2**	**9.9**

[a] particle sobtaine from CTABr-P123 system with CTABr/P123 mole ratio of 5:1.

[b] average particles are calculated by measuring sizes of a hundred particles and taking average of these particles.

Table 3.5.1: The particle size distributions of the particles obtained from the CTABr-P123-F^- system at various F^- ion concentrations and CTABr/P123 mole ratio of 5.0.

Particles synthesized from the CTABr-P123-F^- system show only one intense diffraction line regardless of the F^- ion concentration, **Figure 3.5.11**. The unitcell values are constant and not sensitive to the F^- ion concentration. The line shape and intensity of the diffraction line also shows no difference, which can be interpreted as

F^- ion has no effect on the meso-order of the particles. Remember that the F^- ion concentration range is too low to change the micellization of the P123.

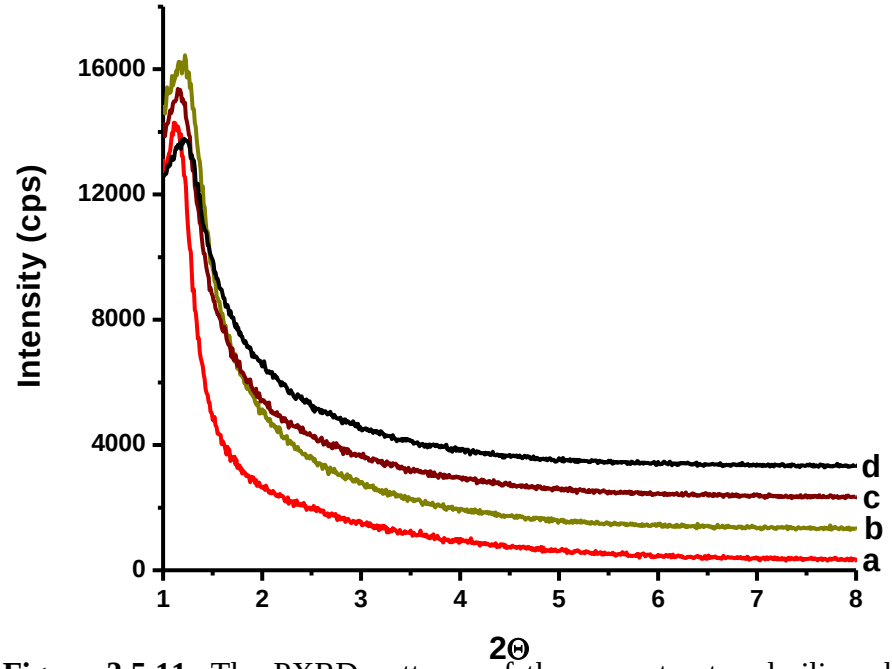

Figure 3.5.11: The PXRD patterns of the mesostructured silica obtained from the CTABr-P123-F^- systems with a CTABr/P123 mole ratio of 5.0 and the F^- ion concentration of (a) 1.1×10^{-2} M, (b) 2.0×10^{-2} M, (c) 2.5×10^{-2} M and (d) 5.0×10^{-2} M.

Despite the fact that the F^- ion only changes the rate of silica polymerization and does not have any effect on the XRD patterns (**Figure 3.5.11**), nevertheless the pore structure of the particles shows difference. **Figure 3.5.12** shows the N_2 adsorption-desorption isotherms of particles from the CTABr-P123-F^- system at different F^- ion concentrations. All the samples have type IV isotherm, which is characteristic for mesoporous materials. The only difference, in the isotherms, appears in the desorption branches of the isotherms. At low F^- ion concentrations (between 1.1×10^{-2} and 1.5×10^{-2} M) desorption brunch does not show any hysteresis, but at higher F^- ion concentrations (between 2.0×10^{-2} and 5.0×10^{-2} M) a hysteresis loop starts to appear. It is known that the adsorption brunch is controlled by the size

of the pore and the desorption brunch is controlled by the size of the interconnecting channels for ink-bottle type of mesopores (so called necks) [155]. When the particles are synthesized at low temperature (like in the CTABr-P123-F^- system) the pore structure is most probably ink-bottle type because of low hydrophobic interaction and repulsion between hydrated poly (ethylene oxide) shells at RT. Therefore, a change in hysteresis loops indicates a change in pore structure with increasing flouride ion concentration. For the ink-bottle type pore structure the hysteresis is not observed if the mesopore is not accessable from both ends [156]. To sum up, at low F^- ion concentrations the ink-bottle type pore structure is close ended but at higher F^- ion concentrations despite the fact that the pore structure is still ink-bottle type, the pores are open ended.

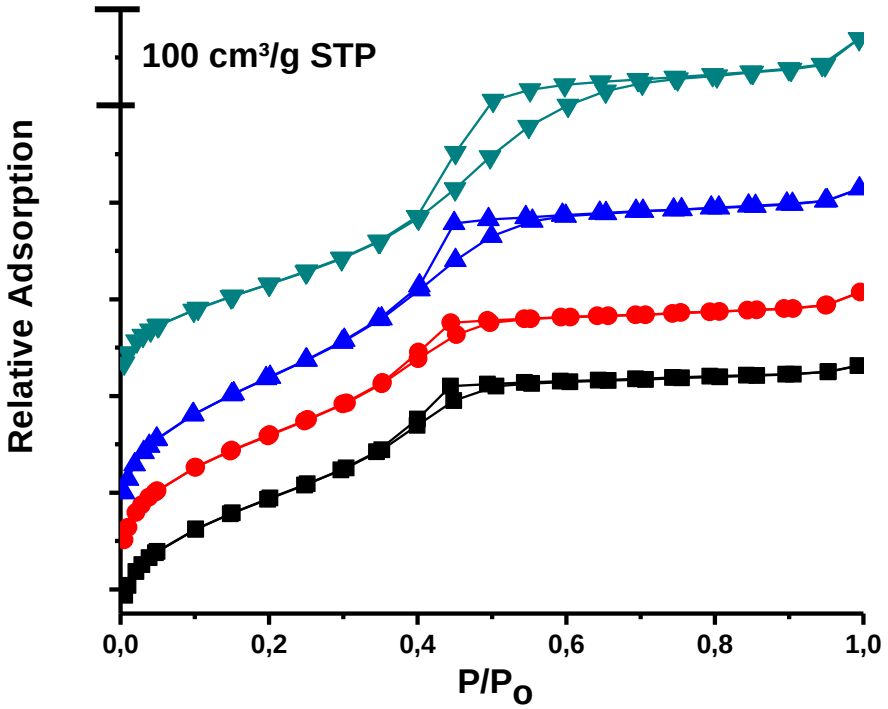

Figure 3.2.12: The N_2 adsorption-desorption isotherms at 77K of the samples obtained from the CTAB-P123-F^- system with a CTABr/P123 mole ratio of 5.0 and the F- ion concentrations of, ■ 1.1×10^{-2} M, ● 1.5×10^{-2} M, ▲ 2.0×10^{-2} M and ▼5.0×10^{-2} M.

Different from the other CTABr-P123-X (X = SO_4^{2-}, NO_3^-, Cl^- and Benzene) systems, the CTABr-P123-F^- system does not show any difference on the structural properties, like pore size, unit cell, wall thickness etc. **Table 3.5.2** shows the structural parameters of the silica particles obtained from the CTABr-P123-F^- system at different F^- ion concentrations. The structural parameters are almost the same as the particles synthesized with CTABr-P123 system. The particles, synthesized using the CTABr-P123-F^- system, have higher surface area than the particles synthesized using the CTABr-P123-X (X = SO_4^{2-}, NO_3^-, Cl^- and Benzene) systems and the BET surface area can be as high as 810 m^2/g. (see **Table 3.5.2**). Therefore, it can be concluded that flouride ion has no effect on the micellization of the P123 and CTABr at used concentration range; it only accelerates the silica polymerization and enables one to synthesize monodispersed, mesoporous silica particles at RT and in very short short time.

NaF concentration (*10^{-3} M)	BET surface area (m^2/g)	d100 (nm)	BJH pore size distribution[b] (2r)	Wall thickness[c] t (nm)
11.0	**703**	**7.8**	**3.4**	**5.6**
12.0	**652**	**7.9**	**3.4**	**5.7**
15.0	**755**	**7.6**	**3.4**	**5.4**
17.0	**712**	**7.8**	**3.4**	**5.6**
20.0	**809**	**7.4**	**3.4**	**5.1**
24.8	**730**	**7.6**	**3.5**	**5.3**
49.6	**552**	**7.3**	**3.5**	**4.9**
0[a]	**698**	**8.0**	**3.4**	**5.8**

[a] particles obtaine from CTABr-P123 system with CTABr/P123 mole ratio of 5:1.

[b] Pore diameter is calculated from the desorption branch of the isotherm by BJH method.

[c] The wall thickness t is obtained by deducing the pore diameter (2r) from the unitcell a_o ($a_o = (2/\sqrt{3})d_{100}$), namely, t= a_o 2-r.

Table 3.5.2: The structural parameters of the silica particles obtained from the CTABr-P123-F^- system at CTABr/P123 mole ratio of 5.0 and 7 different F^- ion concentrations.

3.5.3. The Effect of P123 Concentration on the Formation of Mesoporous Silica Particles:

The Turbidity Point (TP) is the point that indicates the rate of the silica polymerization around the CTABr-P123 micelles in the existence of a catalyst (F^-). Like CTABr, P123 also affects the TP and the formed particles. Concentration of P123 is also important in the assembly process in the CTABr-P123 micelles and in the TP. Increasing P123 concentration might cause changes in the number of micelles, aggregation number, content of the CTABr-P123 micelles and the formation of aggregates of the pluronic surfactant in the solution, when it is used in high concentrations.

Figure 3.5.13 shows the TP time as a function of P123 concentrations. The TP data can be fitted to first order exponential growth. The TP times increases exponentially with increasing P123 concentration. At lower P123 concentrations (below 1.5×10^{-3} M), an increase in the P123 concentration increases the number of micelles, but decreases CTABr concent of a CTABr-P123 micelle, therefore the TP point decreases slightly in this range (see **Section 3.5.1**). At higher P123 concentrations (above 1.5×10^{-3} M), P123 is the main content of the formed micelles and P123 is starting to reach its CP, so the P123 aggregates start to form in the solution. The formation of excessive amount of the P123 micelles and aggregates decreases the TP. Because the surface area of the P123 aggregates are smaller than the surface area of the P123 in its micellar form. It is known that the silica species have a stronger interaction with the hydrated poly (ethylene oxide) groups and a decrease in the surface area of the P123 aggregates causes a decrease in the TP.

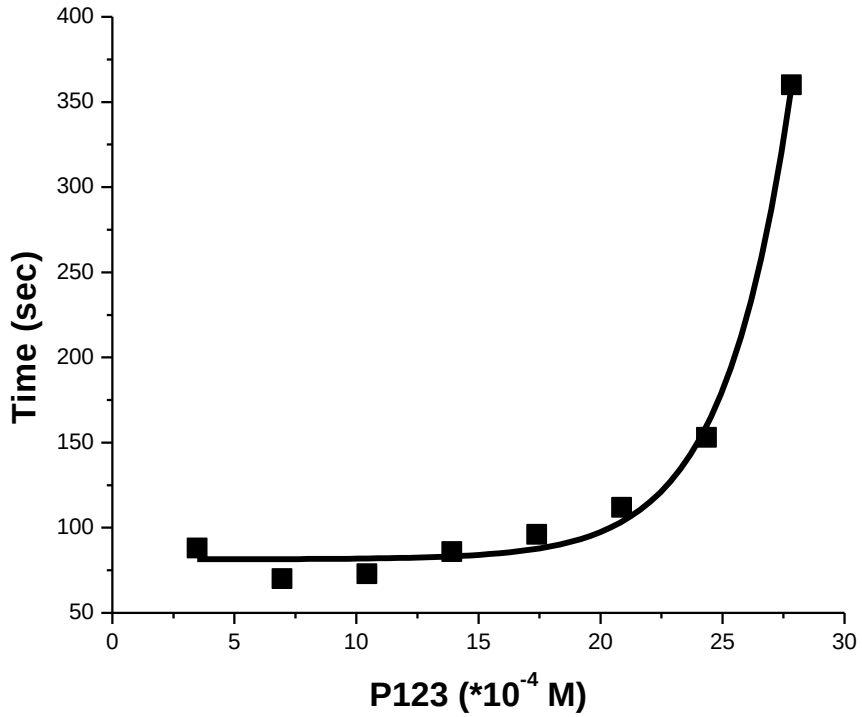

Figure 3.5.13: The TP of the particles obtained from the CTABr-P123-F^- system at various P123 concentrations; F^- ion concentration is 2.4×10^{-2}M, TMOS concentration is 0.16 M and CTABr concentration is 9.0×10^{-3} M.

The significant change at the TP, depending on the P123 concentration, is also correlated with the SEM images of the particles. **Figure 3.5.14** show the SEM images of the particles from the CTABr-P123-F^- system at various P123 concentrations. At low P123 concentrations (between 1.1×10^{-3} and 2.0×10^{-3} M), the particles are monodispersed and the average particle size is around 1.0 μm. At higher P123 concentration, 2.3×10^{-3} M, the sample contains perfectly spherical particles with smooth surface and nonuniform size distiribution; the other group of particles are uniform spherical particles. Above this P123 concentration (>2.3×10^{-3} M), only obtained morphology is perfectly spherical particle with smooth surface and nonuniform size distribution. Note that at high P123 concentrations in which a nonuniform size distribution is obtained, the TP is also high (200 s). When the

reaction rate is high (for low P123 concentrations) the particles are monodispersed and with increasing P123 concentration the size distribution of particles gets wider. Most probably when the P123 concentration is high enough (above 2.3×10^{-3} M), the assembly process goes through a different mechanism. This claim can also be supported by the PXRD and N_2 adsorption –desorption measurements (see texts later).

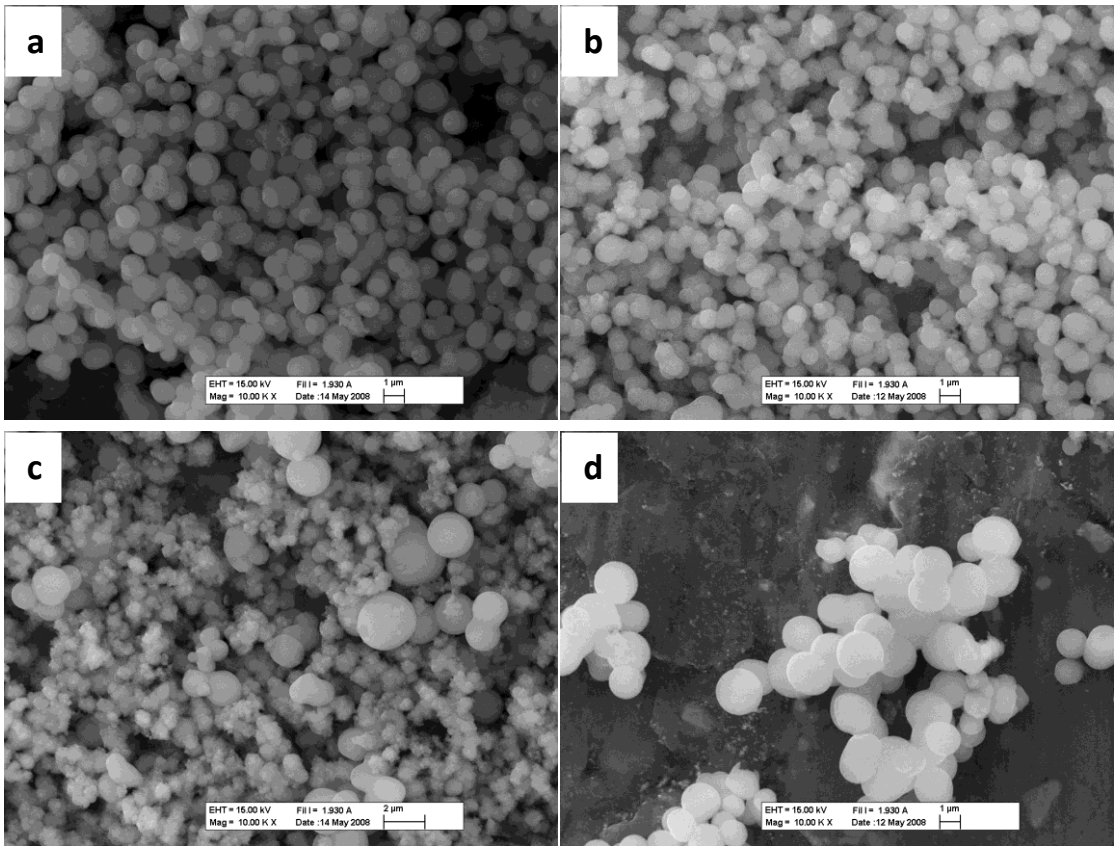

Figure 3.5.14: The SEM images of the mesostructured silica obtained from the CTABr-P123-F^- systems synthesized under constant sonication, F^- ion concentration of 2.4×10^{-2}M and various P123 concentrations of (a) 1.1×10^{-3} M, (b) 2.0×10^{-3} M, (c) 2.3×10^{-3} M, and (d) 2.6×10^{-3} M.

The change in the formation mechanism, with increasing P123 concentration, is clear on the PXRD patterns. **Figure 3.5.15** shows the PXRD patterns of particles synthesized using the CTABr-P123-F^- system at various P123 concentrations. At low P123 concentrations (1.1 $\times 10^{-3}$ M), the first (also the only observed diffraction line) diffraction line is observed at higher angles indicating a smaller unit cell. The diffraction line is broader when compared to particles synthesized at higher P123 concentrations. A broad diffraction line is a result of smaller particle size. It is a well known fact that smaller particles have broader diffraction line. Above this concentration (1.1 $\times 10^{-3}$ M) the diffraction line gets sharper and shifts to smaller angles. With a further increase of the P123 concentration to 2.6 $\times 10^{-3}$ M, the particles becomes less ordered, compare the XRD patterns a through e in **Figure 3.5.15**.

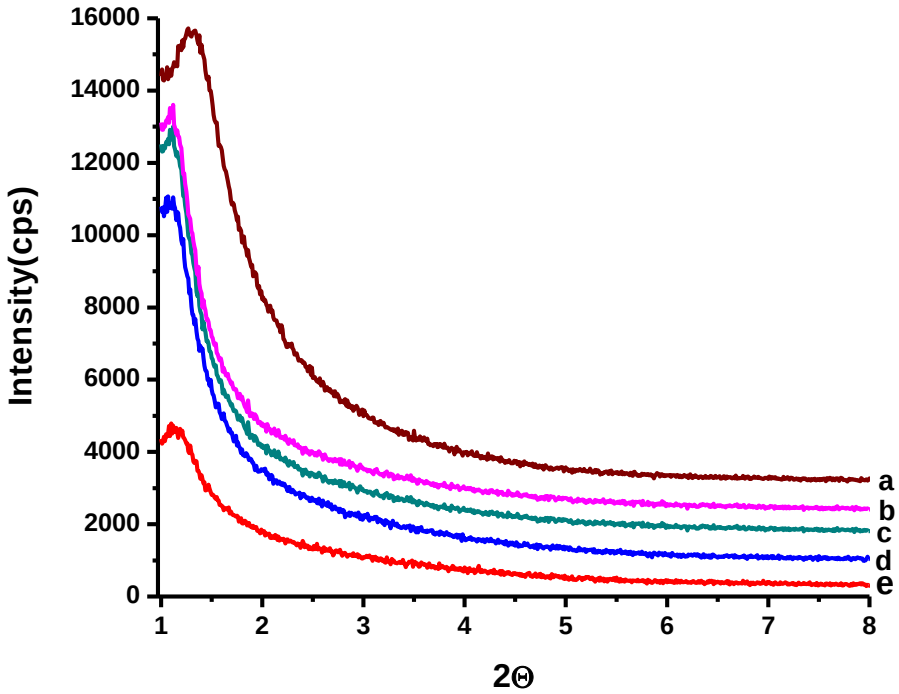

Figure 3.5.15: The PXRD patterns of the mesostructured silica obtained from the CTABr-P123-F^- systems synthesized under constant sonication, the F^- ion concentration of 2.4×10^{-2}M and various P123 concentrations of (a) 1.1×10^{-3} M (b) 2.0×10^{-3} M, (c) 2.3×10^{-3} M, (d) 2.4×10^{-3} M and (e) 2.6×10^{-3} M.

The N_2 adsorption-desorption isotherms are also consistent with the changes in the SEM images and XRD patterns with increasing P123 concentrations, **Figure 3.5.16**. First of all, the particles regardless of the P123 concentrations show characteristic mesopore adsorption branches (Type IV). At low P123 concentrations (1.1×10^{-3} M), desorption branch shows type III hysteresis loop indicating a slit like pore structure. For P123 concentration of 2.0×10^{-3} M, the hysteresis loop starts to disappear but contains a small type III hysteresis loop. A further increase of the P123 concentration results with a desorption branch, which looks like a twin of the adsorption branch. As stated above this type of adsorption branch indicates a closed ended ink-bottle type pore structure.

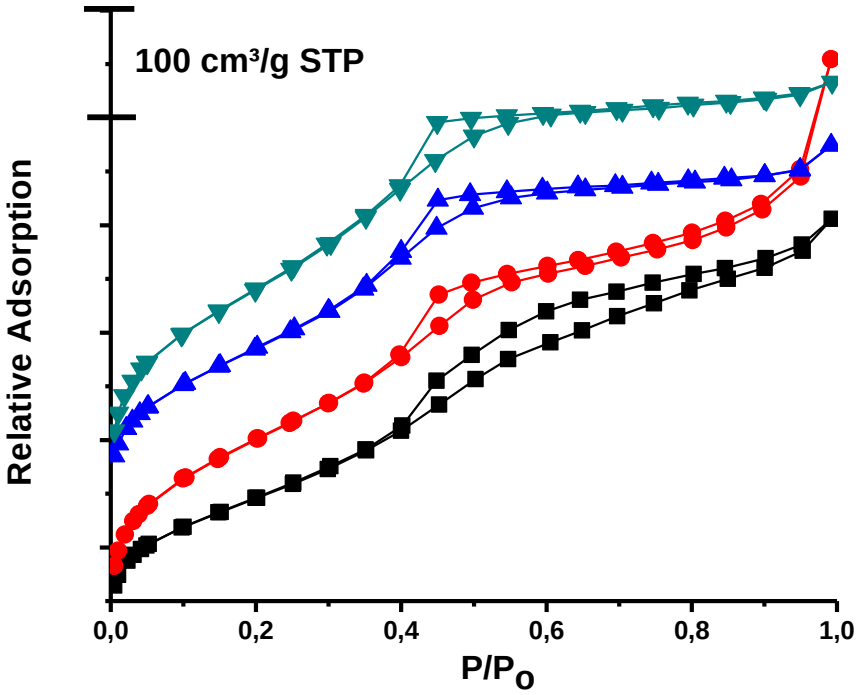

Figure 3.2.16: The N_2 adsorption-desorption isotherms at 77K of the particles obtained from the CTAB-P123-F^- system synthesized under constant sonication, F- concentration of 2.4×10^{-2}M and various P123 concentrations of ■ 1.1×10^{-3} M, ● 2.0×10^{-3} M, ▲ 2.3×10^{-3} M and ▼2.6×10^{-3} M.

The structural properties of the particles from CTABr-P123-F^- system show the origin of the changes in the XRD patterns at various P123 concentrations, which are adapted from the N_2 adsorption- desorption isotherms (**Table 3.5.3**). Regardless of pore structure of the particles, the BJH pore size distribution is 3.4 nm for all particles and do not change with changing P123 concentration. However, at low P123 concentrations (1.1×10^{-3} M) the wall thickness is almost 1.4 nm smaller than the particles synthesized at higher P123 concentrations. In addition, a thinner wall thickness at 1.1×10^{-3} M P123 concentration could explain the high surface area for this sample (885.0 m^2/g). Note that this surface area is the highest among the particles synthesized in this work.

P123 concentration (*10^{-3} M)	**BET surface area (m^2/g)**	**d100 (nm)**	**BJH pore size distribution[a] (2r)**	**Wall thickness[b] t (nm)**
2.56	**552**	**7.8**	**3.4**	**5.6**
2.40	**798**	**8.0**	**3.4**	**5.8**
2.28	**798**	**8.0**	**3.4**	**5.8**
2.00	**692**	**8.0**	**3.4**	**5.8**
1.14	**885**	**6.8**	**3.4**	**4.4**

[a] Pore diameter is calculated from the desorption branch of the isotherm by BJH method.

[b] The wall thickness t is obtained by deducing the pore diameter (2r) from the unitcell a_o ($a_o = (2/\sqrt{3})d_{100}$), namely, t= a_o 2-r.

Table 3.5.3: The structural parameters of the silica particles obtained from the CTABr-P123-F^- system at F^- ion concentration of 2.4×10^{-2}M.

3.5.4. The Effect of Synthesis Temperature on the Mesoporous Silica Particles in the CTABr-P123-F^- System:

So far all particles from CTABr-P123-F^- system were synthesized at RT. When the synthesis is conducted at higher temperatures, the resulting particles show different morphological and structural properties. The synthesis temperature is carefully adjusted to higher values by a temperature controlled ultrasonic bath, where the reactions were started 20 minutes after the reaction mixture reached to a thermal equilibrium in the ultrasonic bath.

Micellization of P123 changes drastically with increasing temperature. When the synthesis is conducted at higher temperatures, the solubility of P123 decreases and hydrophobic interaction between the micelles increase. As discussed in previous chapter, any factor decreasing surfactant solubility decreases the CMC and CMT, increases the micelle size and the order of the particles. **Figure 3.5.17** shows the PXRD patterns of the particles synthesized using the CTABr-P123-F^- system at different synthesis temperatures. With increasing synthesis temperature, the intensity of the first diffraction line (100) increases and shifts to lower angles. The first diffraction line of the particles synthesized at 55 and 65^oC could not be observed since they are below 1$^o(2\Theta)$. Their position is determined from the second diffraction line (which is indexed to (110)). Note that with increasing synthesis temperature; first the diffraction line (100) shifts to smaller angles indicating an increase in the unit cell. In addition, the second (110) and third (200) diffraction lines are also observed as a shoulder at 35^oC. Then the intensity of the diffraction line increase and shifts to smaller angles at higher temperatures (45 and 65^oC). The increase of the unitcell can be attributed to expansion of the micelle size with increasing temperature (see later).

Note that when the reaction was initiated below 25C^{o}, the resulting particles are disordered and do not have any distinct morphology. Therefore, if one wants to obtain an ordered mesoporous particles with spherical morphology, temperature has to be adjusted carefully before starting the synthesis procedure.

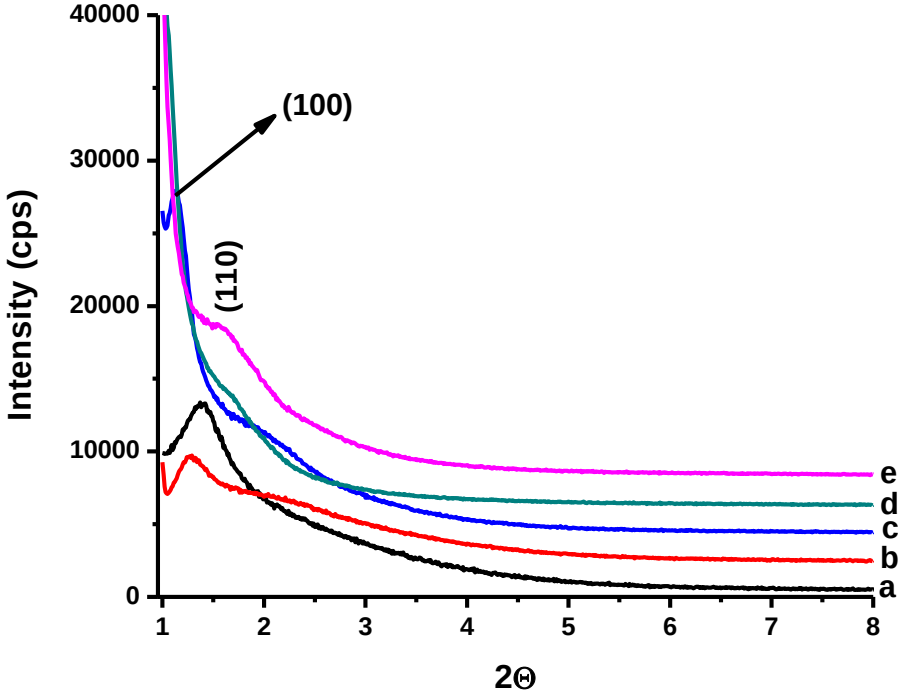

Figure 3.5.17: The PXRD patterns of the mesostructured silica obtained from the CTABr-P123-F^{-} systems synthesized under constant sonication, F^{-} ion concentration of 2.4×10^{-2}M, CTABr/P123 mole ratio of 5.0 and with various synthesis temperatures of (a) 25, (b) 35, (c) 45 (d)55 and (e) 65 (^{o}C).

The synthesis temperature also affects the shape and surface morphology of the particles. **Figure 3.5.18** shows the SEM images of the particles from CTABr-P123-F^{-} system synthesized at different temperatures. All the particles are spherical, monodispersed and have a smooth surface morphology at RT. When the temperature of the synthesis media is raised to 35^{o}C, a mixture of two different particles with different sizes and surface morphology are obtained. Some particles look like the

ones synthesized at RT and the other ones are again spherical but smaller in size and have a rough surface morphology. Above 35^{o}C, all the particles are smaller, spherical with a rough surface morphology (like second type of particles synthesized at 35C^{o}). A size decrease with increasing synthesis temperature might be attributed to the increasing rate of silica polymerization at higher temperatures.

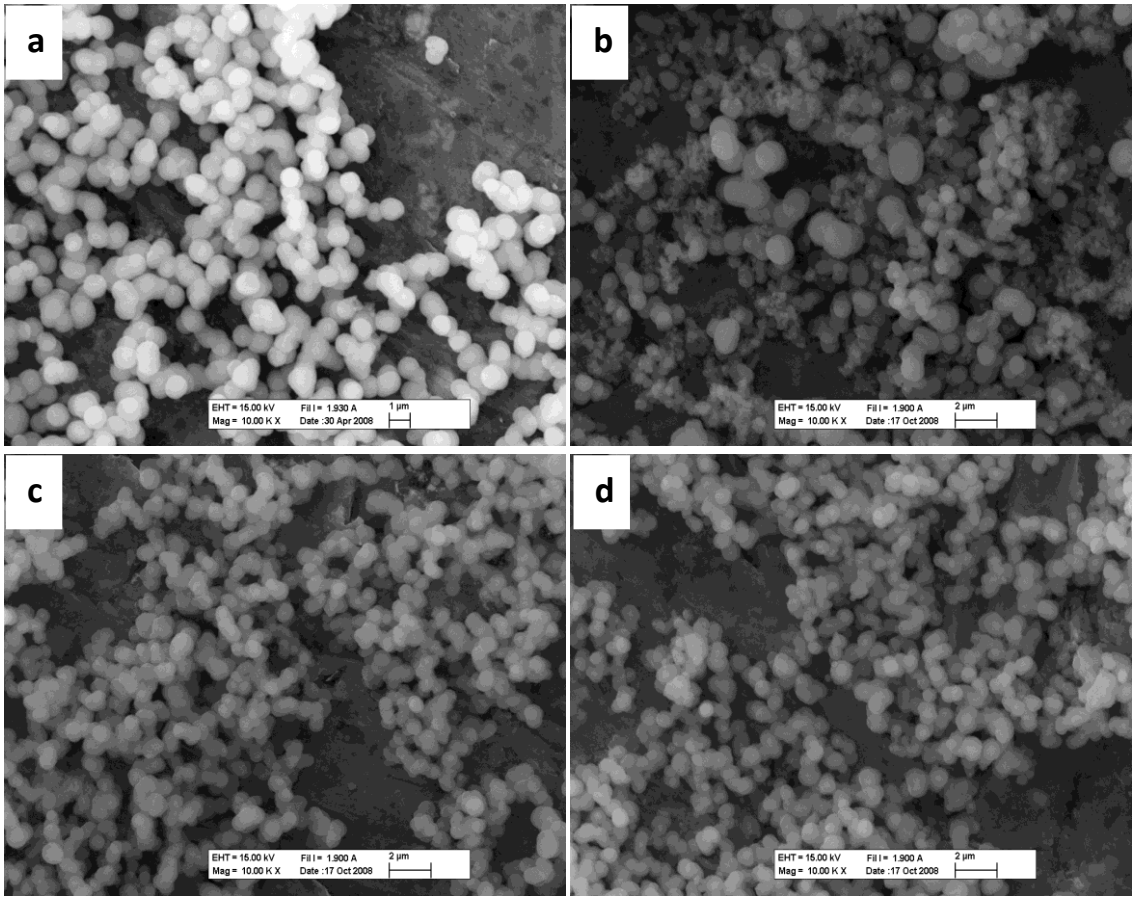

Figure 3.5.18: The SEM images of the mesostructured silica obtained from the CTABr-P123-F^- systems synthesized under constant sonication, F^- ion concentration of 2.4×10^{-2} M, CTABr/P123 mole ratio of 5.0 and with various synthesis temperatures of (a) 25, (b) 35, (c) 45 and (d) 55 (^{o}C).

Increasing the synthesis temperature causes a decrease in the P123 solubility by dehydration of both poly (propylene oxide) and poly (ethylene oxide) groups. As stated in the previous chapter, this may increase the micelle size, so the pore size of the mesoporous particles (**Figure 3.5.19**). Increasing the synthesis temperature, starting from 25C^{o}, gradually increases the pore size of the particles, up to 65C^{o} (see **Figure 3.5.19**). **Figure 3.5.20** shows the TEM images of the samples synthesized from the CTABr-P123-F^{-} system at two different temperatures (25 and 65^{o}C). The measured unitcell values and pore sizes are consistent with the BJH pore size measurements and PXRD patterns for the particles synthesized at 65^{o}C. The particles synthesized at 25^{o}C are also highly porous but it was not possible to take the TEM image of a single pore structure because investigated samples burned (were damaged) in very short times under electron beam.

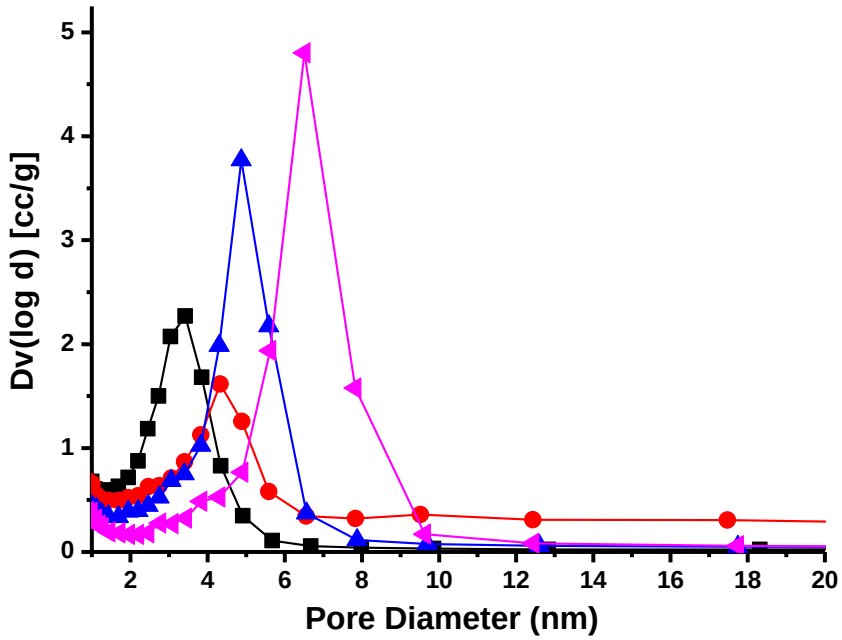

Figure 3.5.19: The BJH Desorption pore size distribution of the particles synthesized from the CTAB-P123-F^- system under a constant sonication, The F^- ion concentration of 2.4×10^{-2}M, CTABr/P123 mole ratio of 5.0 and synthesis temperatures of ■ 25, ● 35, ▲ 45 and ▼65 (^oC).

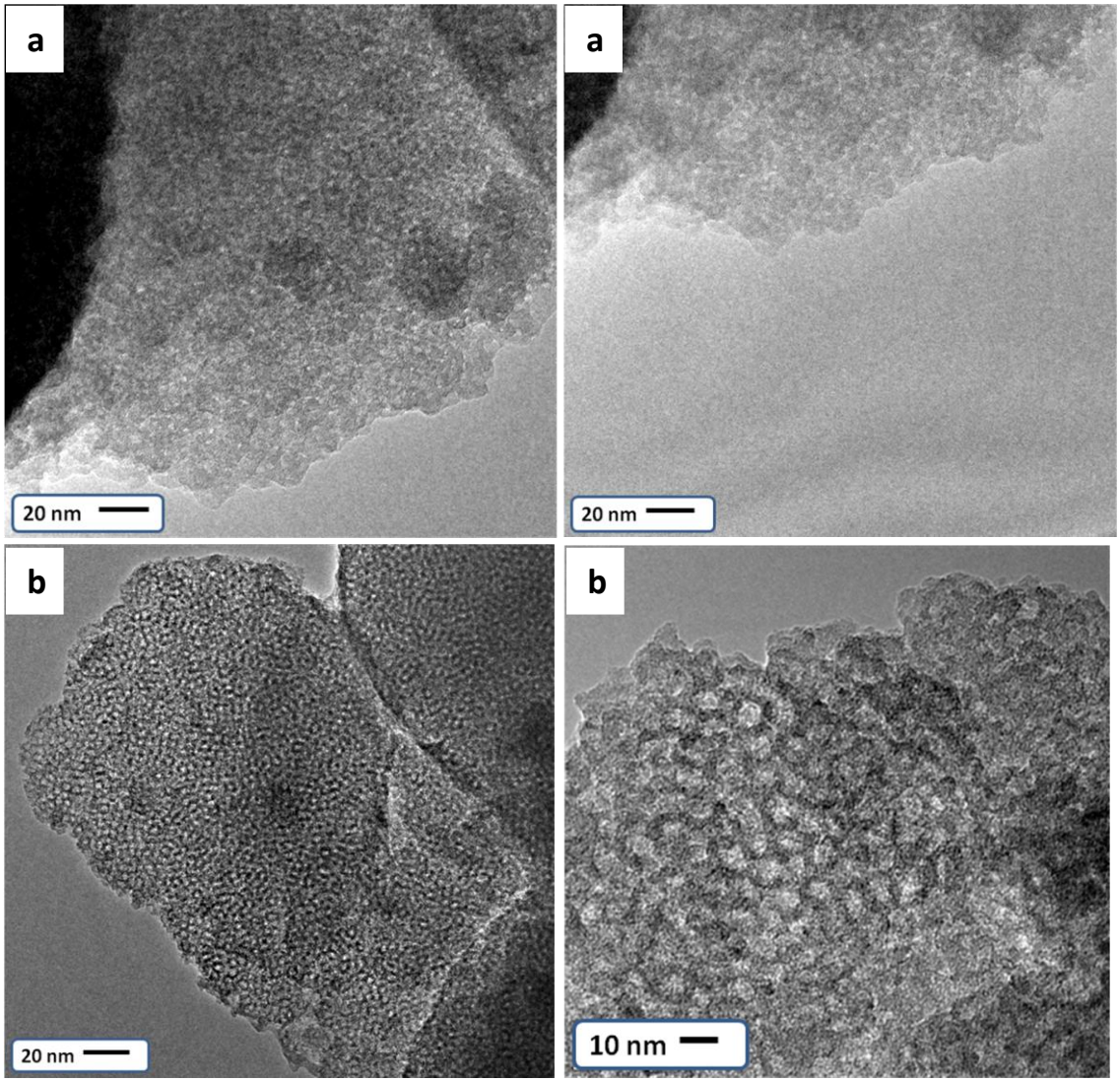

Figure 3.5.20: The TEM images of the mesostructured silica obtained from the CTABr-P123-F^- systems, synthesized under a constant sonication, the F^- ion concentration of 2.4×10^{-2}M, CTABr/P123 mole ratio of 5.0 and two different synthesis temperatures of (a) 25 and (b) 65 (^oC).

The temperature increase does not only change the pore size of the particles but also changes the pore structure of resulting material. **Figure 3.5.21** shows the N_2 adsorption-desorption isotherms of the particles obtained from the CTABr-P123-F^- system, synthesized at different temperatures. All adsorption isotherms are of type IV indicating a mesoporous structure. Desorption branch of the particles synthesized at

25°C shows no hysteresis branch. As stated before this indicates a close ended ink-bottle type pore system. The desorption branch starts to show hysteresis starting at 35°C with increasing temperature of the reaction media. Recall that this temperature is a transition temperature in which the morphology and diffraction patterns start to change (see **Figure 3.5.17** and **Figure 3.5.18**). Above 35°C, the desorption branch shows type I hysteresis loop, which is characteristic for open ended cylindrical pore structure. That means particles have a more ordered and cylindrical pore structure with increasing synthesis temperature. Because the micelles formed with decreased solubility of P123 molecules have stronger hydrophobic interaction during the assembly process.

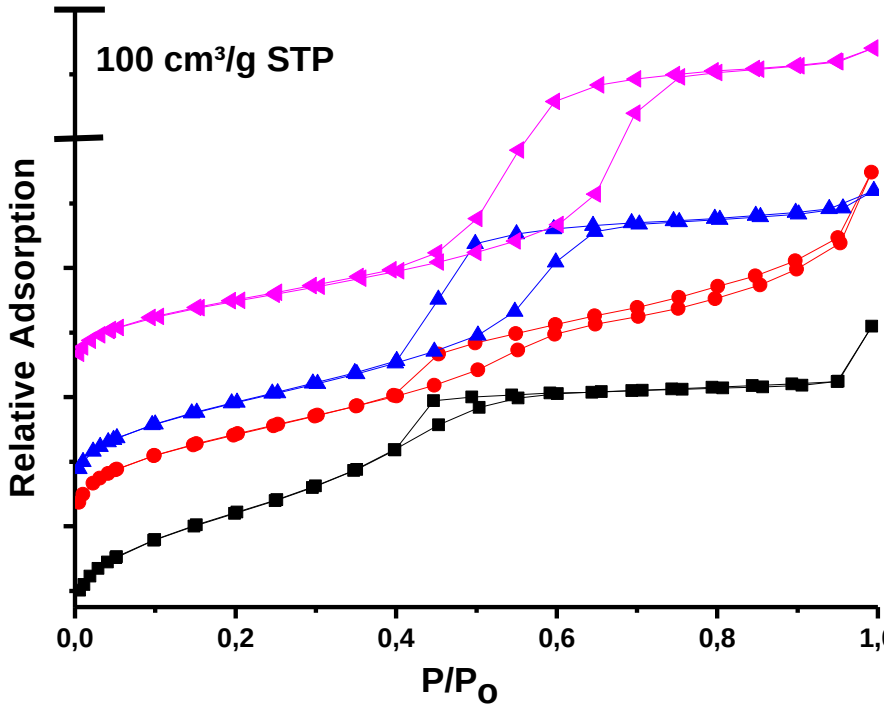

Figure 3.5.21: The N_2 adsorption-desorption isotherms at 77K for the particles from the CTAB-P123-F^- system synthesized under a constant sonication, the F^- ion concentration of 2.4×10^{-2}M, CTABr/P123 mole ratio of 5.0 and at various synthesis temperatures of ■ 25, ● 35, ▲ 45 and ▼65 (°C).

A decrease in the surfactant solubility with a temperature increase also increases micelle aggregation number with a micelle size expansion (pore size expansion). Accordingly the number of micelles in the solution decreases and a significant amount of nonporous silica is also formed by the excess silica in the solution. Therefore, as in the CTABr-P123-SO_4^{2-} system, surface area decreases with increasing temperature (**Table 3.5.4**). The wall thickness decreases around 1 nm, because the shell of the micelle becomes dehydrated with increasing temperature. Remember that the wall thickness is the sum of shell thickness and intermicellar distance.

Synthesis Tmeperature (C^o)	**BET surface area (m^2/g)**	**d100 (nm)**	**BJH pore size distribution[a] (2r)**	**Wall thickness[b] t (nm)**
25	**809**	**7.4**	**3.4**	**5.3**
35	**697**	**7.0**	**4.3**	**3.8**
45	**693**	**7.9**	**4.8**	**4.3**
55	**372**	**8.7[c]**	**6.5**	**3.5**
65	**537**	**9.1[c]**	**6.6**	**3.9**

[a] Pore diameter is calculated from the desorption branch of the isotherm by BJH method.

[b] The wall thickness t is obtained by deducing the pore diameter (2r) from the unitcell a_o ($a_o = (2/\sqrt{3})d_{100}$), namely, t= a_o 2-r.

[c] d (100) spacing is calculated from the position of the (110) plane.

Table 3.5.4: The structural parameters of the silica particles obtained from the CTABr-P123-F^- system with F^- ion concentration of 2.4×10^{-2}M, CTABr/P123 mole ratio of 5.0 and at five different synthesis temperatures.

The same experiments were also conducted for CTABr-P103-F^- and the CTABr-P65-F^- systems.The turbidity point experiments show the same trend as the CTABr-P123-F^- system. A linear dependence of the TP with CTABr concentration, first order exponential growth with increasing flouride ion concentration and exponential decay with increasing pluronic surfactant (P65 and P103) concentration relations are also observed in these systems.

The particles synthesized from the CTABr-P65-F^- system do not show any diffraction line unless the synthesis is conducted at high temperatures. However, the particles synthesized from the CTABr-P103-F^- system show one broad diffraction line at RT synthesis. Besides external factors (additives and temperature), the order of the particles depend on the hydrophobic-hydrophilic character of the surfactant. As stated in introduction part, the hydrophobic character of the pluronic surfactants follow the following order P65<P103<P123.

The particles synthesized form the CTABr-P103-F^- and CTABr-P65-F^- systems are monodispersed and have spherical geometry with smooth surface morphology (see **Figure 3.5.22**).

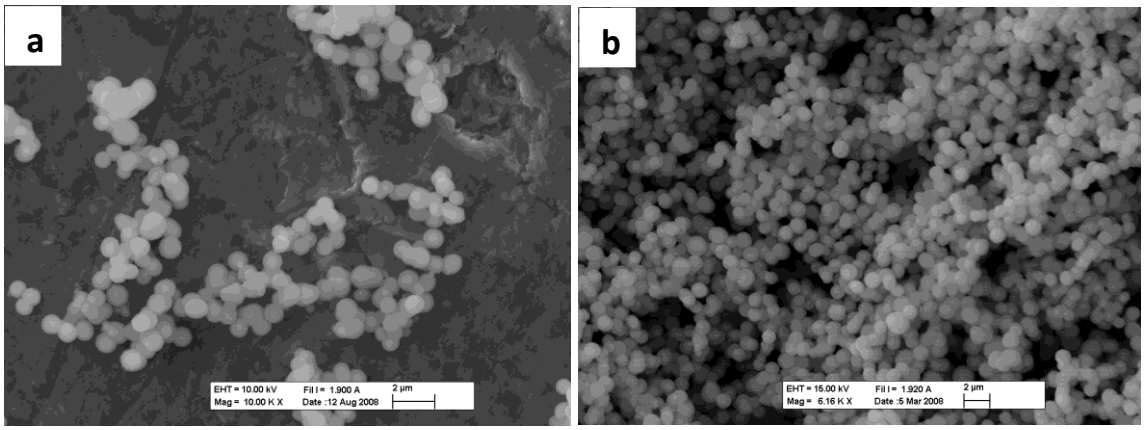

Figure 3.5.22: The SEM image of the mesostructured silica obtained from (a) the CTABr-P103-F^- system synthesized under constant sonication, F- concentration of 2.4×10^{-2}M, CTABr/P123 mole ratio of 6.0 and (b) the CTABr-P65-F^- system synthesized under constant sonication, F^- ion concentration of 2.4×10^{-2}M, CTABr/P123 mole ratio of 4.0.

4. Conclusion:

In this thesis, mesoporous silica particles, using the CTABr-PX-Y (where X is 65, 85, 103, and 123, PX is F127, and Y= F^-, SO_4^{2-}, Cl^-, NO_3^-, and benzene) systems, have been synthesized in various morphological and structural forms. The effect of additives, concentration of CTABr and pluronic surfactant type on the CTABr-Pluronic micelles, assembly properties of these micelles and the morphology of the final products were investigated.

In the first part of the thesis, the effect of CTABr on the CTABr-P123 system as a co-surfactant has been studied. The P123 molecules are far above its CP and insoluble in water at our reaction conditions (95^oC). The role of CTABr is to break P123 aggregates into micelles and form micelles together with P123. Moreover, the CTABr molecules supply positive charge to the core of the micelles and positively charged silica species assemble at the corona part of the micelle. The CTABr molecules increase the solubility of the pluronic surfactant. However, there is a limit of CTABr in each CTABr-PX system, the excess CTABr molecules go to air-water interface and form mesostructured silica films. By controlling the CTABr amount in the micelles, it is possible to synthesize mesoporous silica particles with different morphologies (sphere and wormlike etc.) and pore structures.

In spite of the fact that the CTABr molecules are necessary in order to obtain ordered particles with distinct morphology, the hydrophobic character of the pluronic surfactant determines the mesostructure type and morphology of the particles. The hydrophilic surfactants (F127) forms crystal like particles with a cubic mesostructure, on the other hand, relatively hydrophobic surfactants (P103 and P123) form elongated particles at low CTABr concentrations and spherical particles at high CTABr

concentrations. The surfactants, having a more hydrophilic character like P65 and P85, form elongated particles at low CTABr concentrations and spherical particles at higher CTABr concentrations, but they require lower concentrations of CTABr to form spherical particles than the more hydrophobic surfactants, like P103 and P123. One way of controlling the particle morphology is to control the PPO and PEO blocks of the pluronics.

Anions from the Hoffmeister series causes a drastic change in the micellization of both pluronic surfactants and CTABr. The lyotropic anions decreases the solubility of the pluronic surfactants, on the other hand hydrotropic anions increases the solubility of pluronic surfactants. Different from the pluronic surfactants, the hydrotropic anions decreases the solubility of CTABr and enhances the micellization of CTABr. Therefore, it is possible to control micellization of the pluronic surfactants and CTABr by using these ions in the synthesis medium.

When the lyotropic anions (such as SO_4^{2-} ion) are used in the CTABr-P123 system, better ordered and elongated particles are obtained with larger pore size. However, the hydrotropic anions (like NO_3^-) decrease the CTABr solubility and so it is possible to control the amount of CTABr in the CTABr-P123 micelles. When more CTABr molecules are incorporated to the micelles, the micelle size decreases so as the pore size of the particles. Water insoluble organic additives (benzene and cyclohexane) can be dissolved in pluronic surfactant solutions, in the core of micelles. Penetration of the benzene molecules into the core of the micelles dehydrates the core-corona interface of the micelles. The hydrophobic interaction is enhanced in the micelles and more ordered particles with enlarged mesopores are obtained in the presence of benzene in the reaction media.

The F^- ion has a dual role in the synthesis of mesoporous silica using CTABr-PX system. One is like the other lyotropic anions, it enhances the micelization of pluronics and the other is; that acts as a catalyst in the media. In this thesis, F^- ion is used as catalyst to able tosynthesize particles in very short time and at RT with the help of an ultrasonic bath. Monodispersed mesoporous silica particles have been obtained using the CTABr-P123-F^- system under a constant ultrasonic radiation with a high BET surface area. Moreover, by carefully controlling the synthesis temperature, the pore sizes can be expanded from 3.4 to 7.0 nm.

As a summary, the micellization of the pluronics have key importance in the assembly of mesoporous silica particles. The hydrophobic-hydrophilic balance in the micelles determines the shape of the micelles as a result the morphology of the final product. The hydrophobic-hydrophilic balance can be changed by changing the number of PEO, PPO blocks in the pluronic or by adding additives (such as salts and organics) or by controlling the temperature. Increasing the balance in the favor of hydrophilicity changes the particles from wormlike to spheres to crystalline morphologies.

5. References:

[1] Kresge, C. T.; Leonowicz, M. E.; Roth, W. J.; Vartuli, J. C.; Beck, J. S., Ordered mesoporous molecular-sieves synthesized by a liquid-crystal template mechanism. *Nature* **1992,** 359, (6397), 710-712.

[2] Boissiere, C.; Larbot, A.; van der Lee, A.; Kooyman, P. J.; Prouzet, E., A new synthesis of mesoporous MSU-X silica controlled by a two-step pathway. *Chemistry of Materials* **2000,** 12, (10), 2902-2913.

[3] Sayari, A.; Hamoudi, S., Periodic mesoporous silica-based organic - Inorganic nanocomposite materials. *Chemistry of Materials* **2001,** 13, (10), 3151-3168.

[4] Mizutani, M.; Yamada, Y.; Yano, K., Pore-expansion of monodisperse mesoporous silica spheres by a novel surfactant exchange method. *Chemical Communications* **2007**, (11), 1172-1174.

[5] Poyraz, A. S.; Albayrak, C.; Dag, Ö., The effect of cationic surfactant and some organic/inorganic additives on the morphology of mesostructured silica templated by pluronics. *Microporous and Mesoporous Materials* **2008,** 115, (3), 548-555.

[6] Yu, C. Z.; Tian, B. Z.; Fan, J.; Stucky, G. D.; Zhao, D. Y., Nonionic block copolymer synthesis of large-pore cubic mesoporous single crystals by use of inorganic salts. *Journal of the American Chemical Society* **2002,** 124, (17), 4556-4557.

[7] Chen, Q. R.; Sakamoto, Y.; Terasaki, O.; Che, S. A., Synthesis of silica mesoporous crystals with controlled structure and morphology using gemini surfactant. *Microporous and Mesoporous Materials* **2007,** 105, (1-2), 24-33.

[8] Leonard, A.; Blin, J. L.; Robert, M.; Jacobs, P. A.; Cheetham, A. K.; Su, B. L., Toward a better control of internal structure and external morphology of mesoporous silicas synthesized using a nonionic surfactant. *Langmuir* **2003,** 19, (13), 5484-5490.

[9] Chan, H. B. S.; Budd, P. M.; Naylor, T. D., Control of mesostructured silica particle morphology. *Journal of Materials Chemistry* **2001,** 11, (3), 951-957.

[10] Wang, B.; Chi, C.; Shan, W.; Zhang, Y. H.; Ren, N.; Yang, W. L.; Tang, Y., Chiral mesostructured silica nanofibers of MCM-41. *Angewandte Chemie-International Edition* **2006,** 45, (13), 2088-2090.

[11] Prouzet, E.; Cot, F.; Boissiere, C.; Kooyman, P. J.; Larbot, A., Nanometric hollow spheres made of MSU-X-type mesoporous silica. *Journal of Materials Chemistry* **2002,** 12, (5), 1553-1556.

[12] Yang, H.; Coombs, N.; Ozin, G. A., Morphogenesis of shapes and surface patterns in mesoporous silica. *Nature* **1997,** 386, (6626), 692-695.

[13] Yano, K.; Fukushima, Y., Particle size control of mono-dispersed super-microporous silica spheres. *Journal of Materials Chemistry* **2003,** 13, (10), 2577-2581.

[14] Biswas, K.; Ray, J. C.; Choi, J. S.; Ahn, W. S., Morphology control of MSU-1 silica particles. *Journal of Non-Crystalline Solids* **2008,** 354, (1), 1-9.

[15] Yamada, Y.; Nakamura, T.; Ishi, M.; Yano, K., Reversible control of light reflection of a colloidal crystal film fabricated from monodisperse mesoporous silica spheres. *Langmuir* **2006,** 22, (6), 2444-2446.

[16] Stein, A. In Sphere templating methods for periodic porous solids, *Microporous and Mesoporous Materials* **2001**; 44, SP Iss 227-239.

[17] Trewyn, B. G.; Giri, S.; Slowing, II; Lin, V. S. Y., Mesoporous silica nanoparticle based controlled release, drug delivery, and biosensor systems. *Chemical Communications* **2007**, (31), 3236-3245.

[18] Boissiere, C.; Martines, M. A. U.; Tokumoto, M.; Larbot, A.; Prouzet, E., Mechanisms of pore size control in MSU-X mesoporous silica. *Chemistry of Materials* **2003,** 15, (2), 509-515.

[19] Kleitz, F.; Solvyov, L. A.; Anilkumar, G. M.; Choi, S. H.; Ryoo, R., Transformation of highly ordered large pore silica mesophases (Fm3m, Im3m and p6mm) in a ternary triblock copolymer-butanol-water system. *Chemical Communications* **2004**, (13), 1536-1537.

[20] Jin, Z. W.; Wang, X. D.; Cui, X. G., A two-step synthesis of well-ordered cubic mesoporous silica materials under mildly acidic conditions. *Microporous and Mesoporous Materials* **2008,** 108, (1-3), 183-192.

[21] Che, S.; Sakamoto, Y.; Terasaki, O.; Tatsumi, T., Control of crystal morphology of SBA-1 mesoporous silica. *Chemistry of Materials* **2001,** 13, (7), 2237-+.

[22] Fan, J.; Boettcher, S. W.; Tsung, C. K.; Shi, Q.; Schierhorn, M.; Stucky, G. D., Field-directed and confined molecular assembly of mesostructured materials: Basic principles and new opportunities. *Chemistry of Materials* **2008,** 20, (3), 909-921.

[23] Kleitz, F.; Choi, S. H.; Ryoo, R., Cubic Ia3d large mesoporous silica: synthesis and replication to platinum nanowires, carbon nanorods and carbon nanotubes. *Chemical Communications* **2003**, (17), 2136-2137.

[24] Gu, J. L.; Xiong, L. M.; Shi, J. L.; Hua, Z. L.; Zhang, L. X.; Li, L., Thioether moiety functionalization of mesoporous silica films for the encapsulation of highly dispersed gold nanoparticles. *Journal of Solid State Chemistry* **2006,** 179, (4), 1060-1066.

[25] Minchev, C.; Huwe, H.; Tsoncheva, T.; Paneva, D.; Dimitrov, M.; Mitov, I.; Froba, M. In *Iron oxide modified mesoporous carbons: Physicochemical and catalytic study*, 2005; 2005; pp 333-341.

[26] Ma, Y. R.; Qi, L. M.; Ma, J. M.; Wu, Y. Q.; Liu, O.; Cheng, H. M., Large-pore mesoporous silica spheres: synthesis and application in HPLC. *Colloids and Surfaces a-Physicochemical and Engineering Aspects* **2003,** 229, (1-3), 1-8.

[27] Han, Y.; Lee, S. S.; Ying, J. Y., Spherical siliceous mesocellular foam particles for high-speed size exclusion chromatography. *Chemistry of Materials* **2007,** 19, (9), 2292-2298.

[28] Wang, S. B., Ordered mesoporous materials for drug delivery. *Microporous and Mesoporous Materials* **2009,** 117, (1-2), 1-9.

[29] Condon, J. B., Surface Area and Porosity Determinations by Physisorption. *Elsevier* **2006**.

[30] Newalkar, B. L.; Komarneni, S., Control over microporosity of ordered microporous-mesoporous silica SBA-15 framework under microwave-hydrothermal conditions: Effect of salt addition. *Chemistry of Materials* **2001,** 13, (12), 4573-4579.

[31] Imperor-Clerc, M.; Davidson, P.; Davidson, A., Existence of a microporous corona around the mesopores of silica-based SBA-15 materials templated by triblock copolymers. *Journal of the American Chemical Society* **2000,** 122, (48), 11925-11933.

[32] Jaroniec, M.; Kruk, M.; Olivier, J. P., Standard nitrogen adsorption data for characterization of nanoporous silicas. *Langmuir* **1999,** 15, (16), 5410-5413.

[33] Thommes, M.; Kohn, R.; Froba, M., Sorption and pore condensation behavior of nitrogen, argon, and krypton in mesoporous: MCM-48 silica materials. *Journal of Physical Chemistry B* **2000,** 104, (33), 7932-7943.

[34] Storck, S.; Bretinger, H.; Maier, W. F., Characterization of micro- and mesoporous solids by physisorption methods and pore-size analysis. *Applied Catalysis a-General* **1998,** 174, (1-2), 137-146.

[35] Galarneau, A.; Cambon, N.; Di Renzo, F.; Ryoo, R.; Choi, M.; Fajula, F., Microporosity and connections between pores in SBA-15 mesostructured silicas as a function of the temperature of synthesis. *New Journal of Chemistry* **2003,** 27, (1), 73-79.

[36] Galarneau, A.; Cambon, H.; Di Renzo, F.; Fajula, F., True microporosity and surface area of mesoporous SBA-15 silicas as a function of synthesis temperature. *Langmuir* **2001,** 17, (26), 8328-8335.

[37] Sonwane, C. G.; Ludovice, P. J., A note on micro- and mesopores in the walls of SBA-15 and hysteresis of adsorption isotherms. *Journal of Molecular Catalysis a-Chemical* **2005,** 238, (1-2), 135-137.

[38] Silvestre-Albero, A.; Jardim, E. O.; Bruijn, E.; Meynen, V.; Cool, P.; Sepulveda-Escribano, A.; Silvestre-Albero, J.; Rodriguez-Reinoso, F., Is There Any Microporosity in Ordered Mesoporous Silicas? *Langmuir* **2009,** 25, (2), 939-943.

[39] Miyazawa, K.; Inagaki, S., Control of the microporosity within the pore walls of ordered mesoporous silica SBA-15. *Chemical Communications* **2000**, (21), 2121-2122.

[40] Naono, H.; Hakuman, M.; Shiono, T., Analysis of nitrogen adsorption isotherms for a series of porous silicas with uniform and cylindrical pores: A new method of calculating pore size distribution of pore radius 1-2 nm. *Journal of Colloid and Interface Science* **1997,** 186, (2), 360-368.

[41] Sakaki, T., On the Harkins-Jura's Adsorption Isotherm and Its Constants. *Science* **1953,** 26, (5), 213-218.

[42] H.K.Livingston, Relation Between the Brunauer-Emmett-Teller and Harkins-Jura Isotherms. *Nature* **1948,** 162, 109-110.

[43] Zhang, W. H.; Zhang, L.; Xiu, J. H.; Shen, Z. Q.; Li, Y.; Ying, P. L.; Li, C., Pore size design of ordered mesoporous silicas by controlling micellar properties of triblock copolymer $EO_{20}PO_{70}EO_{20}$. *Microporous and Mesoporous Materials* **2006,** 89, (1-3), 179-185.

[44] Stevens, W. J. J.; Lebeau, K.; Mertens, M.; Van Tendeloo, G.; Cool, P.; Vansant, E. F., Investigation of the morphology of the mesoporous SBA-16 and SBA-15 materials. *Journal of Physical Chemistry B* **2006,** 110, (18), 9183-9187.

[45] Naik, S. P.; Elangovan, S. P.; Okubo, T.; Sokolov, I., Morphology control of mesoporous silica particles. *Journal of Physical Chemistry C* **2007,** 111, (30), 11168-11173.

[46] Yano, K.; Fukushima, Y., Synthesis of mono-dispersed mesoporous silica spheres with highly ordered hexagonal regularity using conventional alkyltrimethylammonium halide as a surfactant. *Journal of Materials Chemistry* **2004,** 14, (10), 1579-1584.

[47] Prouzet, E.; Boissiere, C.; Kim, S. S.; Pinnavaia, T. J., Roughness of mesoporous silica surfaces deduced from adsorption measurements. *Microporous and Mesoporous Materials* **2009,** 119, (1-3), 9-17.

[48] Chen, F. X.; Shen, S. C.; Xu, X. J.; Xu, R.; Kooli, F., Modification of micropore-containing SBA-3 by TEOS liquid phase deposition. *Microporous and Mesoporous Materials* **2005,** 79, (1-3), 85-91.

[49] Wan, Y.; Shi, Y. F.; Zhao, D. Y., Designed synthesis of mesoporous solids via nonionic-surfactant-templating approach. *Chemical Communications* **2007**, (9), 897-926.

[50] Garcia-Martinez, J.; Linares, N.; Sinibaldi, S.; Coronado, E.; Ribera, A., Incorporation of Pd nanoparticles in mesostructured silica. *Microporous and Mesoporous Materials* **2009,** 117, (1-2), 170-177.

[51] Tsoncheva, T.; Paneva, D.; Mitov, I.; Huwe, H.; Froba, M.; Dimitrov, M.; Minchev, C., Iron modified mesoporous carbon and silica catalysts for methanol decomposition. *Reaction Kinetics and Catalysis Letters* **2004,** 83, (2), 299-305.

[52] Sun, J. M.; Bao, X. H., Textural manipulation of mesoporous materials for hosting of metallic nanocatalysts. *Chemistry-a European Journal* **2008,** 14, (25), 7478-7488.

[53] Fellenz, N. A.; Marchetti, S. G.; Bengoa, J. F.; Mercader, R. C.; Stewart, S. J., Synthesis and magnetic characterization of magnetite particles embedded in mesoporous MCM-41. *Journal of Magnetism and Magnetic Materials* **2006,** 306, (1), 30-34.

[54] N. Andersson, R. W. C. a. P. C. A. A., One-Pot synthesis of well ordered mesoporous magnetic carriers. *Journal of Materials Chemistry* **2007**, (17), 2700-2705.

[55] Vradman, L.; Landau, M. V.; Herskowitz, M.; Ezersky, V.; Talianker, M.; Nikitenko, S.; Koltypin, Y.; Gedanken, A., High loading of short WS2 slabs inside SBA-15: promotion with nickel and performance in hydrodesulfurization and hydrogenation. *Journal of Catalysis* **2003,** 213, (2), 163-175.

[56] Hoffmann, F.; Cornelius, M.; Morell, J.; Froba, M., Silica-based mesoporous organic-inorganic hybrid materials. *Angewandte Chemie-International Edition* **2006,** 45, (20), 3216-3251.

[57] Kim, J. H.; Yoon, S. B.; Kim, J. Y.; Chae, Y. B.; Yu, J. S. In Synthesis of monodisperse silica spheres with solid core and mesoporous shell: Morphological control of mesopores. *Colloids and Surfaces a-Physicochemical and Engineering Aspects* 2008; 313, SP Iss; 77-81.

[58] Lin, V. S. Y., Veni, vidi, vici and then... vanished. *Nature Materials* **2009,** 8, 252-253.

[59] Lin, C. X.; Qiao, S. Z.; Yu, C. Z.; Ismadji, S.; Lu, G. Q., Periodic mesoporous silica and organosilica with controlled morphologies as carriers for drug release. *Microporous and Mesoporous Materials* **2009,** 117, (1-2), 213-219.

[60] Schramm, L. L., *Emulsions, Foams, and Suspensions*. *Wiley* **2005**.

[61] Song, S. W.; Hidajat, K.; Kawi, S., pH-controllable drug release using hydrogel encapsulated mesoporous silica. *Chemical Communications* **2007**, (42), 4396-4398.

[62] Garcia-Santamaria, F.; Miguez, H.; Ibisate, M.; Meseguer, F.; Lopez, C., Refractive index properties of calcined silica submicrometer spheres. *Langmuir* **2002,** 18, (5), 1942-1944.

[63] Nakashima, K.; Bahadur, P., Aggregation of water-soluble block copolymers in aqueous solutions: Recent trends. *Advances in Colloid and Interface Science* **2006,** 123, 75-96.

[64] Patel, K.; Bahadur, P.; Guo, C.; Ma, J. H.; Liu, H. Z.; Nakashima, K., Salt-induced micellization of pluronic F88 in water. *Journal of Dispersion Science and Technology* **2008,** 29, (5), 748-755.

[65] Malmsten, M.; Lindman, B., Self –Assembly in aqueous block copolymer solutions. *Macromolecules* **1992,** 25, (20), 5440-5445.

[66] Trong, L. C. P.; Djabourov, M.; Ponton, A., Mechanisms of micellization and rheology of PEO-PPO-PEO triblock copolymers with various architectures. *Journal of Colloid and Interface Science* **2008,** 328, (2), 278-287.

[67] Alexandridis, P.; Holzwarth, J. F.; Hatton, T. A., Micellization of poly (ethylene oxide) - poly (propylene oxide)- poly (ethylene oxide) triblock copolymers in aqueous solutions- thermodynamics of copolymer association. *Macromolecules* **1994,** 27, (9), 2414-2425.

[68] Jain, N. J.; George, A.; Bahadur, P., Effect of salt on the micellization of pluronic P65 in aqueous solution. *Colloids and Surfaces a-Physicochemical and Engineering Aspects* **1999,** 157, (1-3), 275-283.

[69] Senkow, S.; Mehta, S. K.; Douheret, G.; Roux, A. H.; Roux-Desgranges, G., Aqueous solutions of some amphiphilic poly(ethylene oxide)-poly(propylene oxide)-poly(ethylene oxide) triblock copolymers. A thermodynamic study over a wide concentration range at temperatures between 288.15 and 328.15 K. *Physical Chemistry Chemical Physics* **2002,** 4, (18), 4472-4480.

[70] Jain, N. J.; Aswal, V. K.; Goyal, P. S.; Bahadur, P., Salt induced micellization and micelle structures of PEO/PPO/PEO block copolymers in aqueous solution. *Colloids and Surfaces a-Physicochemical and Engineering Aspects* **2000,** 173, (1-3), 85-94.

[71] Nagarajan, R., Solubilization of hydrocarbons and resulting aggregate shape transitions in aqueous solutions of Pluronic (R) (PEO-PPO-PEO) block copolymers. *Colloids and Surfaces B-Biointerfaces* **1999,** 16, (1-4), 55-72.

[72] Qi, L. M.; Ma, J. M.; Cheng, H. M.; Zhao, Z. G., Micrometer-sized mesoporous silica spheres grown under static conditions. *Chemistry of Materials* **1998,** 10, (6), 1623-1626.

[73] Yu, C. Z.; Fan, J.; Tian, B. Z.; Zhao, D. Y., Morphology development of mesoporous materials: a colloidal phase separation mechanism. *Chemistry of Materials* **2004,** 16, (5), 889-898.

[74] Zhou, G. W.; Chen, Y. J.; Yang, J. H.; Yang, S. H., From cylindrical-channel mesoporous silica to vesicle-like silica with welldefined multilamella shells and large inter-shell mesopores. *Journal of Materials Chemistry* **2007,** 17, (27), 2839-2844.

[75] Lu, Y. F., Surfactant-templated mesoporous materials: From inorganic to hybrid to organic. *Angewandte Chemie-International Edition* **2006,** 45, (46), 7664-7667.

[76] Martines, M. A. U.; Yeong, E.; Larbot, A.; Prouzet, E., Temperature dependence in the synthesis of hexagonal MSU-3 type mesoporous silica synthesized with Pluronic P123 block copolymer. *Microporous and Mesoporous Materials* **2004,** 74, (1-3), 213-220.

[77] Forster, S.; Antonietti, M., Amphiphilic block copolymers in structure-controlled nanomaterial hybrids. *Advanced Materials* **1998,** 10, (3), 195-+.

[78] Mesa, M.; Sierra, L.; Guth, J. L., Contribution to the study of the formation mechanism of mesoporous SBA-15 and SBA-16 type silica particles in aqueous acid solutions. *Microporous and Mesoporous Materials* **2008,** 112, (1-3), 338-350.

[79] Zhou, X. F.; Qiao, S. Z.; Hao, N.; Wang, X. L.; Yu, C. Z.; Wang, L. Z.; Zhao, D. Y.; Lu, G. Q., Synthesis of ordered cubic periodic mesoporous organosilicas with ultra-large pores. *Chemistry of Materials* **2007,** 19, (7), 1870-1876.

[80] Hanrahan, J. P.; Donovan, A.; Morris, M. A.; Holmes, J. D., Synthesis and swelling of large pore diameter mesoporous silica spheres. *Journal of Materials Chemistry* **2007,** 17, (37), 3881-3887.

[81] Zhang, H.; Sun, J. M.; Ma, D.; Bao, X. H.; Klein-Hoffmann, A.; Weinberg, G.; Su, D. S.; Schlogl, R., Unusual mesoporous SBA-15 with parallel channels running along the short axis. *Journal of the American Chemical Society* **2004,** 126, (24), 7440-7441.

[82] Nagarajan, R., Solubilization of "guest" molecules into polymeric aggregates. *Polymers for Advanced Technologies* **2001,** 12, (1-2), 23-43.

[83] Bedrov, D.; Smith, G. D.; Yoon, J. Y., Structure and interactions in micellar solutions: Molecular simulations of Pluronic L64 aqueous solutions. *Langmuir* **2007,** 23, (24), 12032-12041.

[84] Liu, J.; Fan, F.; Feng, Z.; Zhang, L.; Bai, S.; Yang, Q.; Li, C., From Hollow Nanosphere to Hollow Microsphere: Mild Buffer Provides Easy Access to Tunable Silica Structure. *Journal of Physical Chemistry C* **2008,** 112, (42), 16445-16451.

[85] Baccile, N.; Teixeira, C. V.; Amenitsch, H.; Villain, F.; Linden, M.; Babonneau, F., Time-resolved in situ Raman and small-angle X-ray diffraction experiments: From silica-precursor hydrolysis to development of mesoscopic order in SBA-3 surfactant-templated silica. *Chemistry of Materials* **2008,** 20, (3), 1161-1172.

[86] Kim, J. M.; Han, Y. J.; Chmelka, B. F.; Stucky, G. D., One-step synthesis of ordered mesocomposites with non-ionic amphiphilic block copolymers: implications of isoelectric point, hydrolysis rate and fluoride. *Chemical Communications* **2000**, (24), 2437-2438.

[87] Shao, Y. F.; Wang, L. Z.; Zhang, J. L.; Anpo, M., Novel synthesis of high hydrothermal stability and long-range order MCM-48 with a convenient method. *Microporous and Mesoporous Materials* **2005,** 86, (1-3), 314-322.

[88] Li, Y.; Zhang, W. H.; Zhang, L.; Yang, Q. H.; Wei, Z. B.; Feng, Z. C.; Li, C., Direct synthesis of Al-SBA-15 mesoporous materials via hydrolysis-controlled approach. *Journal of Physical Chemistry B* **2004,** 108, (28), 9739-9744.

[89] C. Jeffrey Brinker, G. W. S., Sol-Gel Science: The Physics and Chemistry of Sol-Gel Processing. *Elsevier* **1989**.

[90] Sassi, Z.; Bureau, J. C.; Bakkali, A., Structural characterization of the organic/inorganic networks in the hybrid material (TMOS-TMSM-MMA). *Vibrational Spectroscopy* **2002,** 28, (2), 251-262.

[91] Kim, Y. H.; Hwang, M. S.; Kim, H. J.; Kim, J. Y.; Lee, Y., Infrared spectroscopy study of low-dielectric-constant fluorine-incorporated and carbon-incorporated silicon oxide films. *Journal of Applied Physics* **2001,** 90, (7), 3367-3370.

[92] Schmidt-Winkel, P.; Yang, P. D.; Margolese, D. I.; Chmelka, B. F.; Stucky, G. D., Fluoride-induced hierarchical ordering of mesoporous silica in aqueous acid-syntheses. *Advanced Materials* **1999,** 11, (4), 303-307.

[93] Bagshaw, S. A.; Bruce, I. J., Rapid calcination of high quality mesostructured MCM-41, MSU-X, and SBA-15 silicate materials: A step towards continuous processing? *Microporous and Mesoporous Materials* **2008,** 109, (1-3), 199-209.

[94] Vaz, P. D.; Nunes, C. D.; Vasconcellos-Dias, M.; Nolasco, M. M.; Ribeiro-Claro, P. J. A.; Calhorda, M. J., Vibrational study on the local structure of post-synthesis and hybrid mesoporous materials: Are there fundamental distinctions? *Chemistry-a European Journal* **2007,** 13, (28), 7874-7882.

[95] E.D. Goddard, C. A. J. H., and G.C. Benson, Heats of micelle formation of paraffin Chain Salts in water. *The Journal of Physical Chemistry* **1956,** 61, (5), 593-598.

[96] Yang, L.; Alexandridis, P.; Steytler, D. C.; Kositza, M. J.; Holzwarth, J. F., Small-angle neutron scattering investigation of the temperature-dependent aggregation behavior of the block copolymer pluronic L64 in aqueous solution. *Langmuir* **2000,** 16, (23), 8555-8561.

[97] Matsuoka, K.; Yonekawa, A.; Ishii, M.; Honda, C.; Endo, K.; Moroi, Y.; Abe, Y.; Tamura, T., Micellar size, shape and counterion binding of N-(1,1-Dihydroperfluoroalkyl)-N,N,N-trimethylammonium chloride in aqueous solutions. *Colloid and Polymer Science* **2006,** 285, (3), 323-330.

[98] Bedrov, D.; Smith, G. D.; Yoon, J. Y., Structure and interactions in micellar solutions: Molecular simulations of Pluronic L64 aqueous solutions. *Langmuir* **2007,** 23, (24), 12032-12041.

[99] Ma, J. H.; Guo, C.; Tang, Y. L.; Wang, J.; Zheng, L.; Liang, X. F.; Chen, S.; Liu, H. Z., Salt-induced micellization of a triblock copolymer in aqueous solution: A H-1 nuclear magnetic resonance spectroscopy study. *Langmuir* **2007,** 23, (6), 3075-3083.

[100] Kabanov, A. V.; Nazarova, I. R.; Astafieva, I. V.; Batrakova, E. V.; Alakhov, V. Y.; Yaroslavov, A. A.; Kabanov, V. A., Micelle formation and solubilization of fluorescent probes in poly(oxyethylene-b-oxypropylene-b-oxyethylene) (vol 28, pg 2303, 1995). *Macromolecules* **1996,** 29, (27), 8999-8999.

[101] Zhang, X. Q.; Yuan, S. L.; Wu, J., Mesoscopic simulation on phase behavior of ternary copolymeric solution in the absence and presence of shear. *Macromolecules* **2006,** 39, (19), 6631-6642.

[102] Shaheen, A.; Kaur, I.; Mahajan, R. K., Potentiometric studies of micellization behavior of cationic surfactants in the presence of glycol additives and triblock polymer (Pluronic F68), using surfactant-selective sensors based on neutral ion-pair complexes. *Industrial & Engineering Chemistry Research* **2007,** 46, (13), 4706-4709.

[103] Zhao, C. L.; Winnik, M. A.; Riess, G.; Croucher, M. D, Fluorescence probe techniques used to study micelle formation in water-soluble block copolymers. *Langmuir* **1990,** 6, (2), 514-516.

[104] Carale, T. R.; Pham, Q. T.; Blankschtein, D., Salt effect on intermicellar interactions and micellization of nonionic suffactants in aqueous-solutions. *Langmuir* **1994,** 10, (1), 109-121.

[105] Kaewsaiha, P.; Matsumoto, K.; Matsuoka, H., Sphere-to-rod transition of non-surface-active amphiphilic diblock copolymer micelles: A small-angle neutron scattering study. *Langmuir* **2007,** 23, (18), 9162-9169.

[106] Termonia, Y., Sphere-to-cylinder transition in dilute solutions of diblock copolymers. *Journal of Polymer Science Part B-Polymer Physics* **2002,** 40, (9), 890-895.

[107] Patel, K.; Bahadur, P.; Guo, C.; Ma, J. H.; Liu, H. Z.; Yamashita, Y.; Khanal, A.; Nakashima, K., Salt induced micellization of very hydrophilic PEO-PPO-PEO block copolymers in aqueous solutions. *European Polymer Journal* **2007,** 43, (5), 1699-1708.

[108] Antonietti, M.; Forster, S., Vesicles and liposomes: A self-assembly principle beyond lipids. *Advanced Materials* **2003,** 15, (16), 1323-1333.

[109] Wang, H. N.; Wang, Y. H.; Zhou, X.; Zhou, L.; Tang, J.; Lei, J.; Yu, C., Siliceous unilamellar vesicles and foams by using block-copolymer cooperative vesicle templating. *Advanced Functional Materials* **2007,** 17, (4), 613-617.

[110] Segota, S.; Tezak, D., Spontaneous formation of vesicles. *Advances in Colloid and Interface Science* **2006,** 121, (1-3), 51-75.

[111] Svenson, S., Self-assembly and self-organization: Important processes, but can we predict them? *Journal of Dispersion Science and Technology* **2004,** 25, (2), 101-118.

[112] Engberts, J.; Kevelam, J., Formation and stability of micelles and vesicles. *Current Opinion in Colloid & Interface Science* **1996,** 1, (6), 779-789.

[113] Kunz, W.; Henle, J.; Ninham, B. W., 'Zur Lehre von der Wirkung der Salze' (about the science of the effect of salts): Franz Hofmeister's historical papers. *Current Opinion in Colloid & Interface Science* **2004,** 9, (1-2), 19-37.

[114] Cacace, M. G.; Landau, E. M.; Ramsden, J. J., The Hofmeister series: salt and solvent effects on interfacial phenomena. *Quarterly Reviews of Biophysics* **1997,** 30, (3), 241-277.

[115] Forster, S.; Zisenis, M.; Wenz, E.; Antonietti, M., Micellization of strongly segregated block copolymers. *Journal of Chemical Physics* **1996,** 104, (24), 9956-9970.

[116] Goldmints, I.; vonGottberg, F. K.; Smith, K. A.; Hatton, T. A., Small-angle neutron scattering study of PEO-PPO-PEO micelle structure in the unimer-to-micelle transition region. *Langmuir* **1997,** 13, (14), 3659-3664.

[117] Bharatiya, B.; Ghosh, G.; Bahadur, P.; Mata, J., The effects of salts and ionic surfactants on the micellar structure of tri-block copolymer PEO-PPO-PEO in aqueous solution. *Journal of Dispersion Science and Technology* **2008,** 29, (5), 696-701.

[118] Albayrak, C.; Gulten, G.; Dag, O., Phase separation in liquid crystalline mesophases of $[Co(H_2O)_6]X_2$: P65 systems (X = NO_3^-, Cl^-, or ClO_4^-). *Langmuir* **2007,** 23, (2), 855-860.

[119] Ma, J. H.; Wang, Y.; Guo, C.; Liu, H. Z.; Tang, Y. L.; Bahadur, P., Oil-induced aggregation of block copolymer in aqueous solution. *Journal of Physical Chemistry B* **2007,** 111, (38), 11140-11148.

[120] da Silva, R. C.; Olofsson, G.; Schillen, K.; Loh, W., Influence of ionic surfactants on the aggregation of poly(ethylene oxide)-poly(propylene oxide)-poly(ethylene oxide) block copolymers studied by differential scanning and isothermal titration calorimetry. *Journal of Physical Chemistry B* **2002,** 106, (6), 1239-1246.

[121] Mata, J.; Varade, D.; Bahadur, P., Aggregation behavior of quaternary salt based cationic surfactants. *Thermochimica Acta* **2005,** 428, (1-2), 147-155.

[122] del Burgo, P.; Aicart, E.; Junquera, E., Mixed vesicles and mixed micelles of the cationic-cationic surfactant system: Didecyldimethylammonium bromide/dodecylethyldimethylammonium bromide/water. *Colloids and Surfaces a-Physicochemical and Engineering Aspects* **2007,** 292, (2-3), 165-172.

[123] Subramanian, V.; Ducker, W. A., Counterion effects on adsorbed micellar shape: Experimental study of the role of polarizability and charge. *Langmuir* **2000,** 16, (10), 4447-4454.

[124] Aswal, V. K.; Goyal, P. S., Role of different counterions and size of micelle in concentration dependence micellar structure of ionic surfactants. *Chemical Physics Letters* **2003,** 368, (1-2), 59-65.

[125] Li, Y.; Xu, R.; Bloor, D. M.; Holzwarth, J. F.; Wyn-Jones, E., The binding of sodium dodecyl sulfate to the ABA block copolymer pluronic F127 ($EO_{97}PO_{69}EO_{97}$): An electromotive force, microcalorimetry, and light scattering investigation. *Langmuir* **2000,** 16, (26), 10515-10520.

[126] Ganguly, R.; Aswal, V. K.; Hassan, P. A.; Gopalakrishnan, I. K.; Kulshreshtha, S. K., Effect of SDS on the self-assembly behavior of the PEO-PPO-PEO triblock copolymer $(EO)_{(20)}(PO)_{(70)}(EO)_{(20)}$. *Journal of Physical Chemistry B* **2006,** 110, (20), 9843-9849.

[127] Li, Y.; Xu, R.; Couderc, S.; Bloor, D. M.; Holzwarth, J. F.; Wyn-Jones, E., Binding of tetradecyltrimethylammonium bromide to the ABA block copolymer pluronic F127 (EO_{97} PO_{69} EO_{97}): Electromotive force, microcalorimetry, and light scattering studies. *Langmuir* **2001,** 17, (19), 5742-5747.

[128] Jansson, J.; Schillen, K.; Nilsson, M.; Soderman, O.; Fritz, G.; Bergmann, A.; Glatter, O., Small-angle X-ray scattering, light scattering, and NMR study of PEO-PPO-PEO triblock copolymer/cationic surfactant complexes in aqueous solution. *Journal of Physical Chemistry B* **2005,** 109, (15), 7073-7083.

[129] Jansson, J.; Schillen, K.; Olofsson, G.; da Silva, R. C.; Loh, W., The interaction between PEO-PPO-PEO triblock copolymers and ionic surfactants in aqueous solution studied using light scattering and calorimetry. *Journal of Physical Chemistry B* **2004,** 108, (1), 82-92.

[130] Zhang, Y.; Lam, Y. M. In Study of mixed micelles and interaction parameters for polymeric nonionic and normal surfactants. *Journal of Nanoscience and Nanotechnology* 2006; 6, (12), 3877-3881.

[131] Thomas, A.; Schierhorn, M.; Wu, Y. Y.; Stucky, G., Assembly of spherical micelles in 2D physical confinements and their replication into mesoporous silica nanorods. *Journal of Materials Chemistry* **2007,** 17, (43), 4558-4562.

[132] Flodstrom, K.; Wennerstrom, H.; Alfredsson, V., Mechanism of mesoporous silica formation. A time-resolved NMR and TEM study of silica-block copolymer aggregation. *Langmuir* **2004,** 20, (3), 680-688.

[133] Mesa, M.; Sierra, L.; Guth, J. L., Contribution to the study of the formation mechanism of mesoporous silica type SBA-3. *Microporous and Mesoporous Materials* **2007,** 102, (1-3), 70-79.

[134] Oakes, J.; Gratton, P., Kinetic investigations of the oxidation of Methyl Orange and substituted arylazonaphthol dyes by peracids in aqueous solution. *Journal of the Chemical Society-Perkin Transactions 2* **1998**, (12), 2563-2568.

[135] Van Der Voort, P.; Ravikovitch, P. I.; De Jong, K. P.; Benjelloun, M.; Van Bavel, E.; Janssen, A. H.; Neimark, A. V.; Weckhuysen, B. M.; Vansant, E. F., A new templated ordered structure with combined micro- and mesopores and internal silica nanocapsules. *Journal of Physical Chemistry B* **2002,** 106, (23), 5873-5877.

[136] Thommes, M.; Smarsly, B.; Groenewolt, M.; Ravikovitch, P. I.; Neimark, A. V., Adsorption hysteresis of nitrogen and argon in pore networks and characterization of novel micro- and mesoporous silicas. *Langmuir* **2006,** 22, (2), 756-764.

[137] Ravikovitch, P. I.; Neimark, A. V., Experimental confirmation of different mechanisms of evaporation from ink-bottle type pores: Equilibrium, pore blocking, and cavitation. *Langmuir* **2002,** 18, (25), 9830-9837.

[138] Guo, C.; Wang, J.; Liu, H. Z.; Chen, J. Y., Hydration and conformation of temperature-dependent micellization of PEO-PPO-PEO block copolymers in aqueous solutions by FT-Raman. *Langmuir* **1999,** 15, (8), 2703-2708.

[139] Yang, B.; Guo, C.; Chen, S.; Ma, J. H.; Wang, J.; Liang, X. F.; Zheng, L.; Liu, H. Z., Effect of acid on the aggregation of poly(ethylene oxide)-poly(propylene oxide)-poly(ethylene oxide) block copolymers. *Journal of Physical Chemistry B* **2006,** 110, (46), 23068-23074.

[140] Kung, K. H. S.; Hayes, K. F., Fourier-transform Infrared Spectroscopic study of the adsorption of cetyltrimethylammonium bromide and cetylpyridinium chloride on silica. *Langmuir* **1993,** 9, (1), 263-267.

[141] Sun, S. C.; Birke, R. L.; Lombardi, J. R., Surface-Enhanced Raman-Spectroscopy of surfactants on silver electrodes. *Journal of Physical Chemistry* **1990,** 94, (5), 2005-2010.

[142] Zhu, J. X.; He, H. P.; Zhu, L. Z.; Wen, X. Y.; Deng, F., Characterization of organic phases in the interlayer of montmorillonite using FTIR and C-13 NMR. *Journal of Colloid and Interface Science* **2005,** 286, (1), 239-244.

[143] Su, Y. L.; Wang, J.; Liu, H. Z., FTIR spectroscopic study on effects of temperature and polymer composition on the structural properties of PEO-PPO-PEO block copolymer micelles. *Langmuir* **2002,** 18, (14), 5370-5374.

[144] Mesa, M.; Sierra, L.; Patarin, J.; Guth, J. L., Morphology and porosity characteristics control of SBA-16 mesoporous silica. Effect of the triblock surfactant Pluronic F127 degradation during the synthesis. *Solid State Sciences* **2005,** 7, (8), 990-997.

[145] Demirörs, A. F.; Arslan, M.; Dag, Ö., The effect of anions of transition metal salts on the structure of modified mesostructured silica films and monoliths. *Microporous and Mesoporous Materials* **2007,** 98, (1-3), 249-257.

[146] Dag, Ö.; Alayoglu, S.; Tura, C.; Çelik, Ö., Lyotropic liquid-crystalline phase of oligo(ethylene oxide) surfactant/transition metal salt and the synthesis of mesostructured cadmium sulfide. *Chemistry of Materials* **2003,** 15, (14), 2711-2717.

[147] Yamada, T.; Zhou, H. S.; Asai, K.; Honma, I., Pore size controlled mesoporous silicate powder prepared by triblock copolymer templates. *Materials Letters* **2002,** 56, (1-2), 93-96.

[148] Suslick, K. S.; Price, G. J., Applications of ultrasound to materials chemistry. *Annual Review of Materials Science* **1999,** 29, 295-326.

[149] Price, G. J., Curent Trends in Sonochemistry. *Royal Society of Chemistry* **1992**.

[150] Margulis, M. A., Sonochemistry and Caviation. *Gordon and Breach Science Publishers SA* **1995**.

[151] Mastai, Y.; Polsky, R.; Koltypin, Y.; Gedanken, A.; Hodes, G., Pulsed sonoelectrochemical synthesis of cadmium selenide nanoparticles. *Journal of the American Chemical Society* **1999,** 121, (43), 10047-10052.

[152] Tian, B. Z.; Liu, X. Y.; Yang, H. F.; Xie, S. H.; Yu, C. Z.; Tu, B.; Zhao, D. Y., General synthesis of ordered crystallized metal oxide nanoarrays replicated by microwave-digested mesoporous silica. *Advanced Materials* **2003,** 15, (16), 1370-+.

[153] Lorimer, T. J. M. a. J. P., Sonochemistry theory, applications and uses of ultrasound in chemistry. *Ellis Horwood Limited* **1988**.

[154] Tang, X. H.; Liu, S. W.; Wang, Y. Q.; Huang, W. P.; Sominski, E.; Palchik, O.; Koltypin, Y.; Gedanken, A., Rapid synthesis of high quality MCM-41 silica with ultrasound radiation. *Chemical Communications* **2000**, (21), 2119-2120.

[155] Ravikovitch, P. I.; Neimark, A. V., Experimental confirmation of different mechanisms of evaporation from ink-bottle type pores: Equilibrium, pore blocking, and cavitation. *Langmuir* **2002,** 18, (25), 9830-9837.

[156] Libby, B.; Monson, P. A., Adsorption/desorption hysteresis in inkbottle pores: A density functional theory and Monte Carlo simulation study. *Langmuir* **2004,** 20, (10), 4289-4294.